

University of Louisville

## ThinkIR: The University of Louisville's Institutional Repository

---

Electronic Theses and Dissertations

---

12-2021

### Preclinical development of Avaren-Fc: a novel lectin-Fc fusion protein targeting cancer-associated high-mannose glycans.

Matthew William Dent  
*University of Louisville*

Follow this and additional works at: <https://ir.library.louisville.edu/etd>



Part of the [Biotechnology Commons](#)

---

#### Recommended Citation

Dent, Matthew William, "Preclinical development of Avaren-Fc: a novel lectin-Fc fusion protein targeting cancer-associated high-mannose glycans." (2021). *Electronic Theses and Dissertations*. Paper 3789. Retrieved from <https://ir.library.louisville.edu/etd/3789>

This Doctoral Dissertation is brought to you for free and open access by ThinkIR: The University of Louisville's Institutional Repository. It has been accepted for inclusion in Electronic Theses and Dissertations by an authorized administrator of ThinkIR: The University of Louisville's Institutional Repository. This title appears here courtesy of the author, who has retained all other copyrights. For more information, please contact [thinkir@louisville.edu](mailto:thinkir@louisville.edu).

PRECLINICAL DEVELOPMENT OF AVAREN-FC: A NOVEL LECTIN-FC  
FUSION PROTEIN TARGETING CANCER-ASSOCIATED HIGH-MANNOSE  
GLYCANS

By

Matthew William Dent  
B.S., Arizona State University, 2014  
M.Sc., University of East Anglia, 2015  
M.S., University of Louisville, 2019

A Dissertation  
Submitted to the Faculty of the  
School of Medicine of the University of Louisville  
In partial fulfillment of the Requirements for the Degree of

Doctor of Philosophy in Pharmacology and Toxicology

Department of Pharmacology and Toxicology  
University of Louisville School of Medicine  
Louisville, Kentucky

December 2021

Copyright 2021 by Matthew William Dent

All rights reserved



PRECLINICAL DEVELOPMENT OF AVAREN-FC: A NOVEL LECTIN-FC  
FUSION PROTEIN TARGETING CANCER-ASSOCIATED HIGH-MANNOSE  
GLYCANS

By

Matthew William Dent  
B.S., Arizona State University, 2014  
M.Sc., University of East Anglia, 2015  
M.S., University of Louisville, 2019

A Dissertation approved on

November 17, 2021

By the following dissertation committee:

---

Dr. Nobuyuki Matoba

---

Dr. Kenneth Palmer

---

Dr. Sucheta Telang

---

Dr. Jun Yan

---

Dr. Donald Miller

## DEDICATION

This dissertation is dedicated to:

My parents

Dr. Jason C. Dent and Kimberly A. Dent

Who have unquestioningly supported and motivated me in my educational pursuits

My brothers

Alec C. Dent and Sean D. Dent

Who have always been my best friends

My mentor

Dr. Nobuyuki Matoba

Whose mentorship and wisdom I can only hope to emulate one day

And most importantly, to my dear wife

Milena Mazalovska

Who made all of this possible

And to my son

Maksim J. Dent

Who made it all worth it

七転び八起き

## ACKNOWLEDGMENTS

There is no shortage of people to whom I owe my gratitude, and no list could ever be comprehensive. I would first like to thank my mentor, Dr. Nobuyuki Matoba, who has given me a gift of wisdom and knowledge that can never be repaid. I would also like to thank my committee members, Dr. Kenneth Palmer, Dr. Jun Yan, Dr. Donald Miller, and Dr. Sucheta Telang, who have helped provide me with the crucial guidance necessary to continue as a scientist. To the class of 2016, and all of the other wonderful people I've come to call my friends here in Louisville: I can never thank you enough. You have made living in the south bearable. To my family, I am truly blessed to have had your unconditional support throughout my entire life. I am thankful for all of my grandparents, who have always been there to help raise me and teach me important lessons about how to live life and experience the world. To my brothers, Alec and Sean, you guys are the funniest, coolest, smartest, most humble people I know and often remind me of what I want to be in the future. To my parents, Jason and Kim, I will never be able to thank you enough for having given me everything that I could ever want in my life, both materially and emotionally. Most importantly, I want to express my heartfelt gratitude to my wife, Milena, who had to endure a pregnancy and the first months of our child's life alone in another country and still had the fortitude to stand by my side and see me through this. There are no words to describe how thankful I am for all you sacrificed for us. To Maksim, my handsome little fella, your entrance into this world made all of this struggle worth it.

## ABSTRACT

### PRECLINICAL DEVELOPMENT OF AVAREN-FC: A NOVEL LECTIN-FC FUSION PROTEIN TARGETING CANCER-ASSOCIATED HIGH-MANNOSE GLYCANS

Matthew William Dent

November 17, 2021

This dissertation explores the anticancer activity of Avaren-Fc (AvFc), a novel lectin-Fc fusion protein or “lectibody” targeting cancer and virus-associated high-mannose glycans. Previously, we have shown that AvFc recognizes a broad selection of established cancer cell lines from a wide array of tissue types, can potently induce antibody-dependent cell-mediated cytotoxicity (ADCC) against them, and exhibits anti-cancer activity *in vivo*. However, the exact mechanism of action remains elusive. We hypothesized that the primary mechanism of action is through Fc-mediated effector functions, and the purpose of this dissertation is to explore this question through the use of Fc variants that either increase or decrease ADCC activity relative to the WT molecule using the B16F10 murine melanoma model.

Chapters 1 and 2 give a comprehensive overview of glycosylation and its role in cancer and disease, the molecule AvFc, the mechanism of action of the various Fc-mediated effector functions, and the current status of plant-made cancer biologics. Chapter 4 discusses the efficacy of AvFc in a human liver chimeric mouse model of HCV

infection, which helped not only to establish AvFc's activity *in vivo* but also demonstrated its safety and feasibility as a drug candidate. The bulk of the data obtained regarding the anticancer activity of AvFc are contained in Chapter 5, which establishes that Fc-mediated functions are the primary mechanisms of action and that AvFc administration is associated with the recruitment of Fc $\gamma$ R-bearing cells to the tumor microenvironment. Interestingly, these studies also indicated that the presence of pre-existing immunity in the presence of anti-drug antibodies to AvFc did not obviate its activity *in vivo*. Further exploration of the anticancer activity of AvFc is detailed in Chapter 6, which discusses the use of AvFc as a therapeutic for ovarian cancer (OVCA) and details its *in vitro* and *in vivo* activities. The results presented herein provide evidence to suggest that cancer-associated high-mannose glycans may be a viable pharmacological target and that AvFc is a unique and potent first-in-class agent with significant anticancer capabilities through recognition of this glycobiomarker, warranting its further development as a therapeutic against cancers with limited therapeutic options such as OVCA.

## TABLE OF CONTENTS

DEDICATION .....	iii
ABSTRACT .....	v
LIST OF FIGURES .....	ix
LIST OF TABLES .....	xii
CHAPTER 1: BACKGROUND .....	1
1.1: Glycoconjugates .....	1
1.2: N-glycosylation of proteins .....	4
1.2.1: Synthesis of the dolichol-phosphate precursor .....	7
1.2.2: Initial glycan processing and quality control of protein folding .....	9
1.2.3: Processing of hybrid and complex glycans .....	11
1.3: N-glycosylation and disease .....	19
1.3.1: N-glycosylation of viral glycoproteins .....	19
1.3.2: Aberrant N-glycosylation in cancer .....	21
1.4: Avaren-Fc, a novel high-mannose-binding agent .....	27
1.4.1: Design and antiviral activity .....	31
1.4.2: Anti-cancer activity and possible mechanism of action .....	32
1.5: Antibody-mediated immune effector functions in cancer .....	33
1.5.1: The classical complement pathway .....	34
1.5.2: Antibody-dependent phagocytosis .....	36
1.5.3: Antibody-dependent cell-mediated cytotoxicity .....	38
CHAPTER 2: CANCER BIOLOGICS MADE IN PLANTS .....	42
2.1: Introduction .....	42
2.2: Cancer vaccines and immunotherapy .....	43
2.3: Drug delivery and imaging .....	47
2.4: Anti-cancer lectins .....	49
2.5: Conclusions .....	51
CHAPTER 3: METHODS AND MATERIALS .....	53
CHAPTER 4: SAFETY AND EFFICACY OF AVAREN-FC LECTIBODY TARGETING HCV HIGH-MANNOSE GLYCANS IN A HUMAN LIVER CHIMERIC MOUSE MODEL .....	76
4.1: Introduction .....	76
4.2: Results .....	78
4.2.1: AvFc exhibits broad anti-HCV activity <i>in vitro</i> .....	78

4.2.2: Formulation of AvFc into a biocompatible buffer for <i>in vivo</i> studies .....	82
4.2.3: Pharmacological and toxicological analysis of AvFc in mice .....	87
4.2.4: AvFc protects against HCV infection <i>in vivo</i> .....	94
4.3: Discussion .....	97
CHAPTER 5: THE ANTI-CANCER POTENTIAL OF AVAREN-FC AND ITS MECHANISM OF ACTION .....	102
5.1: Introduction .....	102
5.2: Results .....	105
5.2.1: Analysis of C <sub>H2</sub> N-glycans of AvFc .....	105
5.2.2: Expression, purity, and binding activity of AvFc variants .....	110
5.2.3: AvFc <sup>AXF</sup> exhibits higher affinity to FcγRs from humans and mice .....	114
5.2.4: AvFc binding to B16F10 cells induces ADCC but not direct cytotoxicity ..	118
5.2.5: Fc-mediated effector functions are required for AvFc's activity in the B16F10 flank tumor model .....	122
5.2.6: Protection against metastatic B16F10 challenge by AvFc requires high-mannose binding .....	125
5.2.7: Impact of pretreatment of mice with AvFc on its anticancer activity <i>in vivo</i> . .....	127
5.2.8: Flow cytometry analysis of B16F10 tumor-infiltrating immune cells .....	131
5.3: Discussion .....	148
CHAPTER 6: DEVELOPMENT OF AVAREN-FC AS AN IMMUNOTHERAPEUTIC AGAINST OVARIAN CANCER .....	161
6.1: Introduction .....	161
6.2: Results .....	164
6.2.1: AvFc recognizes human ovarian cancer tissues and cell lines and induces ADCC .....	164
6.2.2: Establishment of the ID8-luciferase challenge model .....	168
6.2.3: Proteomics analysis of AvFc binding partners on ovarian cancer cells .....	173
6.3: Discussion .....	178
CHAPTER 7: SUMMARY AND FUTURE DIRECTIONS.....	185
7.1: Summary .....	185
7.2: Lectikines and other conjugates .....	188
7.3: Receptor targeting activities and their contribution to the mechanism of action.	193
7.4: Further assessment of the immunogenicity and immunotoxicity of Avaren-Fc ..	196
7.5: Conclusion.....	206
REFERENCES .....	208
CURRICULUM VITAE .....	233

## LIST OF FIGURES

Figure 1. The major classes of N-glycans.....	6
Figure 2. Synthesis of the dolichol-phosphate precursor.....	8
Figure 3. Simplified diagram of protein quality control in the ER.....	10
Figure 4. General outline of N-glycosylation in mammals.....	16
Figure 5. General outline of N-glycosylation in plants.....	18
Figure 6. Structure of poly-LacNAc and generation of branched, bisected, and fucosylated N-glycans.....	23
Figure 7. The predicted 3D structure of Avaren-Fc.....	30
Figure 8. Simplified diagram of various Fc-mediated effector functions.....	41
Figure 9. <i>In vitro</i> HCV inhibition assays.....	80
Figure 10. Stability of AvFc in various buffers.....	83
Figure 11. Liquid formulation development for AvFc.....	85
Figure 12. Pharmacokinetics of AvFc in Mice.....	89
Figure 13. Characterization of the non-sugar-binding mutant AvFc <sup>lec-</sup> .....	90
Figure 14. Toxicological analysis of systemically administered AvFc in the PXB® human liver chimeric mouse model.....	91
Figure 15. Histopathological examination of PXB mouse liver tissues.....	93
Figure 16. The protective effect of AvFc against HCV challenge in PXB mice.....	95
Figure 17. Glycan analysis by HPLC.....	107
Figure 18. Purity and binding activity of AvFc variants.....	112

Figure 19. Representative sensorgrams of AvFc variant binding to FcγRs.....	116
Figure 20. Induction of ADCC but not cytotoxicity by AvFc. ....	120
Figure 21. Activity of AvFc in the B16F10 flank tumor model. ....	123
Figure 22. Activity of AvFc <sup>ΔXF</sup> in the B16F10 melanoma metastasis model.....	126
Figure 23. Impact of pretreatment on the anticancer activity of AvFc <i>in vivo</i> . ....	129
Figure 24. NK cell gating strategy.....	134
Figure 25. CD4 T cell gating strategy.....	135
Figure 26. CD8 T cell gating strategy.....	136
Figure 27. Comparison of NK and T cell subsets within B16F10 tumors.....	137
Figure 28. Dendritic cell gating strategy.....	139
Figure 29. Gating strategy for DC activation and costimulatory markers.....	140
Figure 30. Comparison of classical dendritic cell subsets within B16F10 tumors. ....	141
Figure 31. Neutrophil gating strategy. ....	143
Figure 32. Classical monocyte/macrophage gating strategy.....	144
Figure 33. Non-classical monocyte gating strategy.....	145
Figure 34. Comparison of neutrophil, macrophage, and monocyte populations within B16F10 tumors.....	146
Figure 35. Pharmacokinetic analysis of AvFc <sup>WT</sup> .....	151
Figure 36. Impact of ADAs and anti-tumor antibodies on ADCC activity. ....	158
Figure 37. Recognition of human OVCA tissues by AvFc with immunohistochemistry. .....	166
Figure 38. AvFc binds to many OVCA cell lines and induces ADCC.....	167
Figure 39. ID8-luciferase challenge model with 2x10 <sup>6</sup> cells/animal.....	170

Figure 40. ID8-luciferase challenge model with  $1 \times 10^6$  cells/animal..... 172

Figure 41. Summary of lectikine approaches using AvFc- or Avaren-cytokine fusions.192

## LIST OF TABLES

Table 1. Definition and description of AvFc variants used in these studies.....	58
Table 2. IC50 values for AvFc and Avaren against HCVcc.....	80
Table 3. Buffers used in the initial screening of AvFc preformulation analysis. ....	84
Table 4. Histopathology of chimeric mouse liver tissue.....	92
Table 5. C <sub>H2</sub> glycan analysis of AvFc variants by LC-MS. ....	108
Table 6. Representative example of SPR kinetic data. ....	117
Table 7. Summary of cell-surface markers used in B16F10 tumor immunophenotyping. .....	133
Table 8. Identification of putative cell-surface binding partners of AvFc on human and murine OVCA cell lines.....	177
Table 9. Identification of putative cell-surface binding partners of AvFc on lung and blood cancer cell lines.....	183
Table 10. Pichler classification of adverse reactions to biologics. ....	199

## CHAPTER 1: BACKGROUND

### 1.1: Glycoconjugates

Glycosylation, the enzymatic formation of glycosidic linkages between oligomeric carbohydrate chains called glycans to biological macromolecules, is one of the fundamental biochemical modifications and a key pathophysiological regulatory mechanism [1]. The various glycoconjugates are defined by the monosaccharide composition of the glycan moiety, the class of macromolecule (protein, lipid, or other saccharides) they are linked to, and the nature of that linkage. Glycans are built through the sequential action of glycosyltransferase enzymes, which are localized to multiple organelle compartments and catalyze the formation of glycosidic bonds between activated nucleotide monosaccharide donors and the acceptor sugars. The sum of the glycans on the cell surface make up a structure known as the glycocalyx, which not only creates a protective barrier but plays a significant role in protein structure and quality control, cell-cell signaling, and adhesion both between cells and between cells and the extracellular matrices. Glycans can also act as ligands for a class of proteins called lectins that are expressed on a number of tissues, especially those of the immune system in vertebrates. Each of these classes of glycoconjugates have distinct functions in the cell, and defects in the glycome in humans are linked to a remarkable number of diseases [2]. While glycosylation occurs in one form or another across the tree of life, such as in bacterial and archaeal cell wall synthesis, the focus of this dissertation will be on metazoan (animal) glycosylation, in particular the glycosylation of proteins performed by

mammals, as well as some brief discussion of the glycosylation of recombinant proteins in plants.

One of the major classes of glycoconjugates are the glycoproteins. The attachment of glycan structures to proteins is one of the fundamental post-translational modifications and occurs on proteins that are processed in the endomembrane system [1]. There are two major forms of protein glycosylation: asparagine or N-linked glycosylation and serine or threonine-linked glycosylation, called O-glycosylation. The resulting glycans are therefore referred to as N-glycans and O-glycans glycans, respectively. N- and O-glycans significantly impact the structure and function of mature proteins and are extremely important to ensure quality control and folding during translation. The composition of these glycans varies significantly between species, cell types, and even proteins. Significant changes in N- and O-glycosylation patterns may be useful biomarkers to identify different disease states, and defects in these pathways are known to cause several human diseases [2]. A more detailed discussion of N-linked glycosylation follows in section 1.2.

O-glycosylation is a common glycoprotein modification that occurs at the OH-groups of serine and threonine residues. Almost all O-glycans have one of four major core structures that can be extended to give linear or branched chains, and structures are built one sugar at a time by enzymes called glycosyltransferases [3]. Each of the 4 cores begins with  $\alpha$ 1,3-linked N-acetylgalactosamine (GalNAc), which is then linked to either a Gal or GlcNAc sugar by a  $\beta$ 1,3-linkage. Cores 2 and 4 also contain an additional GlcNAc residue attached by a  $\beta$ 1,6-linkage [4]. Extension of these cores occurs in the Golgi apparatus, where the biosynthetic glycosyltransferases are embedded into the membrane

facing the Golgi lumen and interact with proteins as they are trafficked through the endomembrane system [5]. Unlike N-glycans, O-glycans only rarely contain mannose (Man), glucose (Glc), or xylose (Xyl) but may contain GalNAc, Gal, fucose (Fuc), and sialic acids [4]. The expression and activity levels as well as the localization of these enzymes determine the range of O-glycans that can be synthesized, creating tremendous inter-species and even inter-tissue or cell heterogeneity. The functions of O-glycans vary widely. The most well-known class of proteins containing O-glycans are the mucins, which can contain hundreds of these glycans attached to a protein scaffold with high molecular weight. The hydrophilic nature of O-glycans and their negative charge promotes the binding and sequestration of water and salts, allowing mucins to form viscous gels that line the mucosal epithelial surfaces of the body [6, 7]. These mucous layers provide a physical and chemical barrier to outside agents and pathogens in addition to keeping surfaces hydrated. Some mucins, like the P-selectin glycoprotein ligand 1 (PSGL-1) are membrane bound and act as ligands for lectin receptors such as the selectins and galectins [8]. Other O-glycan-containing proteins are the targets of selectins and galectins expressed on the surface of cells of the immune system, and function in immune cell trafficking throughout the body as well as signal transduction [9]. O-glycans also make up the ABO and Lewis blood group antigens, and loss of some glycosyltransferases such as GALNT3 and GALNT2 are associated with the tumoral calcinosis and cardiovascular disease [10-12]. While O-glycans are important for the structure and function of many proteins, arguably the more important post-translational modification for recombinantly produced therapeutic proteins is N-glycosylation, which will be discussed further.

## 1.2: N-glycosylation of proteins

Asparagine-linked, or N-linked, glycosylation is an important post-translational modification that plays a significant role in the control of protein folding as well as the structure and function of mature proteins. Like O-glycosylation, N-glycosylation occurs on secreted and membrane-bound proteins that are trafficked into the ER for processing through the endomembrane system. Unlike O-glycans, which can in theory be applied to any serine or threonine residue, the minimal sequence to which these glycans can be attached is Asn-X-Ser/Thr-X, where X can be any amino acid except for proline [1]. Also unlike O-glycans, which are built sugar-by-sugar, N-glycans are first assembled separately into a large precursor glycan structure attached to dolichol phosphate in the ER membrane prior to their attachment to the protein, at which point they are trimmed and extended by a number of glucosidases and glycosyltransferases expressed in the luminal space of the ER and Golgi apparatus. This “*en bloc*” transfer of large N-glycans can be limited by the structure of the nascent protein itself, and as such while  $\approx 70\%$  of all proteins contain the N-X-S/T-X sequon only an estimated 70% of the sites are actually occupied by one [1]. All N-glycans share a common core structure with the sequence  $\text{Man}\alpha 1-3(\text{Man}\alpha 1-6)\text{Man}\beta 1-4\text{GlcNAc}\beta 1-4\text{GlcNAc}\beta 1-\text{Asn}$  (Figure 1) and different types of N-glycans are then defined based on the extension of this core. The three major types of N-glycans are: high-mannose glycans, which have between 2 and 6 additional mannose sugars that extend both arms of the trimannose core, complex glycans, where both the  $\alpha 3$ - and  $\alpha 6$ -mannose arms contain polysaccharide chains initiated with  $\beta 1,2$ -GlcNAc, and hybrid glycans, where the  $\alpha 3$  arm is extended with  $\beta 1,2$ -GlcNAc while the

other contains additional mannose residues. In addition, multiple GlcNAc residues can extend from the core creating multi-antennary and bisecting structures, which can be further built upon to create large multi-branched glycans (Figure 6). There is significant glycan-site heterogeneity, and the presence of an N-glycosylation sequon does not guarantee either the presence of a glycan or a particular glycan structure, and as such the same site on multiple proteins may be occupied by different glycan structures in a rather stochastic fashion. As with O-glycans, the expression and localization of the various glycosyltransferases as well as the availability of substrate define the range of glycans that can be generated, and this can vary tremendously between species and in different disease states [1, 2, 13, 14].

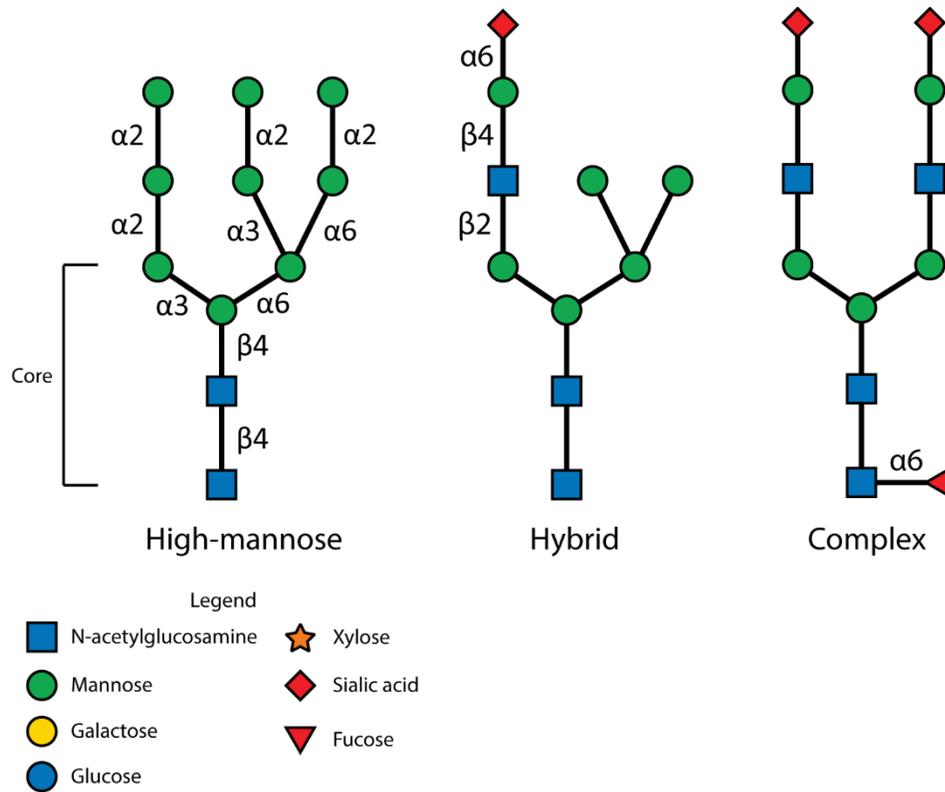


**Figure 1. The major classes of N-glycans.**

N-glycans can be divided into 3 major classes: high-mannose, complex, and hybrid.

High-mannose glycans contain between 5 and 9 mannose sugars (including the trimannose core). Complex glycans, on the other hand, have both the  $\alpha$ 3- and  $\alpha$ 6-mannose arms extended by GlcNAc. Hybrid glycans have the  $\alpha$ 3-mannose arm extended by GlcNAc while the other contains mannose. The core glycan structure can also be extended by multiple GlcNAc residues to create large multi-antennary and bisecting structures (see Figure 6).

### 1.2.1: Synthesis of the dolichol-phosphate precursor

The biosynthesis of N-glycans takes place in two phases and primarily occurs within the ER and Golgi apparatus of eukaryotic cells. The first phase, which is well conserved among eukaryotes, is the generation of the dolichol-phosphate-linked (Dol-P) glycan precursor structure (Figure 2). Dolichol is a polyisoprenol lipid made up of repeating five-carbon isoprene units, as many as 19 in mammals, that is found on both the inner and outer ER membrane. Phosphorylated dolichol (Dol-P), which is generated by dolichol kinase (DOLK), is acted upon by the glycosyltransferase ALG7, which catalyzes the addition of a single GlcNAc-1-phosphate and forms Dol-P-P-GlcNAc [15]. This structure is expanded upon with a second GlcNAc and 5 Man residues by subsequent cytoplasmic glycosyltransferases and then translocated across the ER membrane to the luminal face through the action of a flippase enzyme RFT1 [16]. Further processing by ER-resident glycosyltransferases generates the final precursor glycan, Dol-P-P-GlcNAc<sub>2</sub>Man<sub>9</sub>Glc<sub>3</sub>, which is then transferred to receptive asparagine residues on nascent proteins as they are translocated into the ER lumen by the oligosaccharyltransferase (OST) enzyme complex [16]. Transfer of the complete glycan precursor leaves behind Dol-P-P, which can be reused for precursor synthesis by conversion to Dol-P via a dolichol phosphatase (DOLPP) [17].

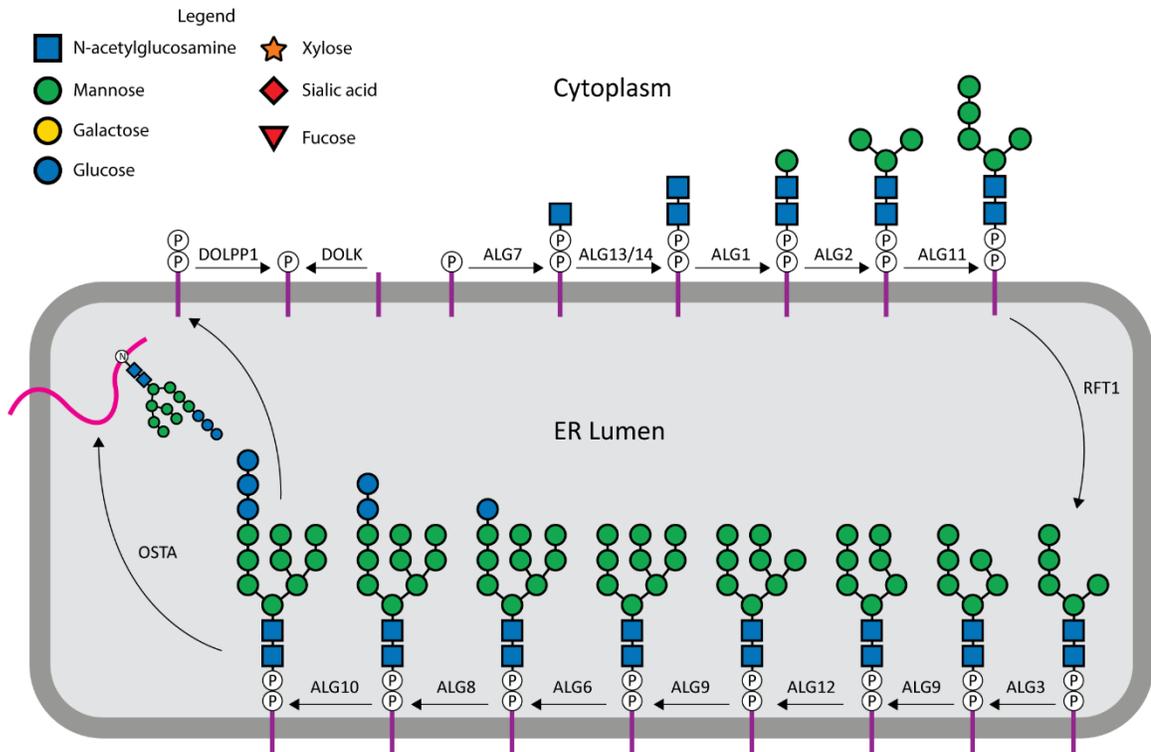


**Figure 2. Synthesis of the dolichol-phosphate precursor.**

The initial synthesis of the N-glycan precursor begins on the cytoplasmic face of the ER with the phosphorylation of dolichol by DOLK and attachment of 2 GlcNAc and 5 mannose residues by the N-acetylglucosaminyltransferases ALG7/13/14 and the mannosyltransferases ALG1/2/11. The Dol-P-P-GlcNAc<sub>2</sub>Man<sub>5</sub> structure is flipped to the ER lumen by RFT1 and expanded by subsequent mannosyltransferases ALG3/9/12 and glucosyltransferases ALG6/8/10 to form the full-length precursor Dol-P-P-GlcNAc<sub>2</sub>Man<sub>9</sub>Glc<sub>3</sub>. Transfer of the precursor glycan onto asparagine residues of nascent peptides is performed by OSTA, while the leftover Dol-P-P is recycled to the cytoplasmic face of the ER and processed by DOLPP to regenerate dolichol phosphate.

### 1.2.2: Initial glycan processing and quality control of protein folding

The second phase of N-glycan biosynthesis takes place exclusively in the ER and in the Golgi apparatus and involves a number of glycosidases and glycosyltransferases that trim the precursor glycan down to the GlcNAc<sub>2</sub>Man<sub>3</sub> core and rebuild it into the various complex type glycans typically seen on mature glycoproteins (Figure 4). It is during this phase that the quality control systems for protein folding primarily operate (Figure 3). The initial trimming of two of the Glc residues by glucosidase I and II (GI and GII, or MOBS and GANAB) generates a monoglucosylated structure that is recognized by either calnexin (CNX) or calreticulin (CRT), which form part of a loose complex of protein chaperones that includes BiP/Grp78, ERp57, and Grp94 among others [18]. Both CNX and CRT contain ER retention signals, and their binding to N-glycosylated proteins bearing a single glucose prevents premature export to the Golgi apparatus, giving the immature proteins time to properly fold and form oligomeric structures, if necessary, as well as form disulfide bonds (which are catalyzed by the ERp57 oxidoreductase) [19]. Proteins that fail these steps and remain unfolded are acted upon by the ER degradation-enhancing  $\alpha$ -mannosidase-like proteins (EDEMs), which generate an isomer of Man<sub>7</sub>GlcNAc<sub>2</sub> that contains an exposed  $\alpha$ 1,6-mannose residue which is specifically targeted by the lectin OS9 [20, 21]. Binding by OS9 leads to retrotranslocation of the protein to the cytosol, ubiquitinylation, and degradation of the misfolded protein by the proteasome. A second reaction by GII results in the removal of the final Glc residue, preventing CNX/CRT binding and allowing for export of the glycosylated proteins to the *cis*-Golgi [22]. This can be reversed by an enzyme called UGGT, which causes the misfolded protein to re-bind to CNX/CRT and continue folding.

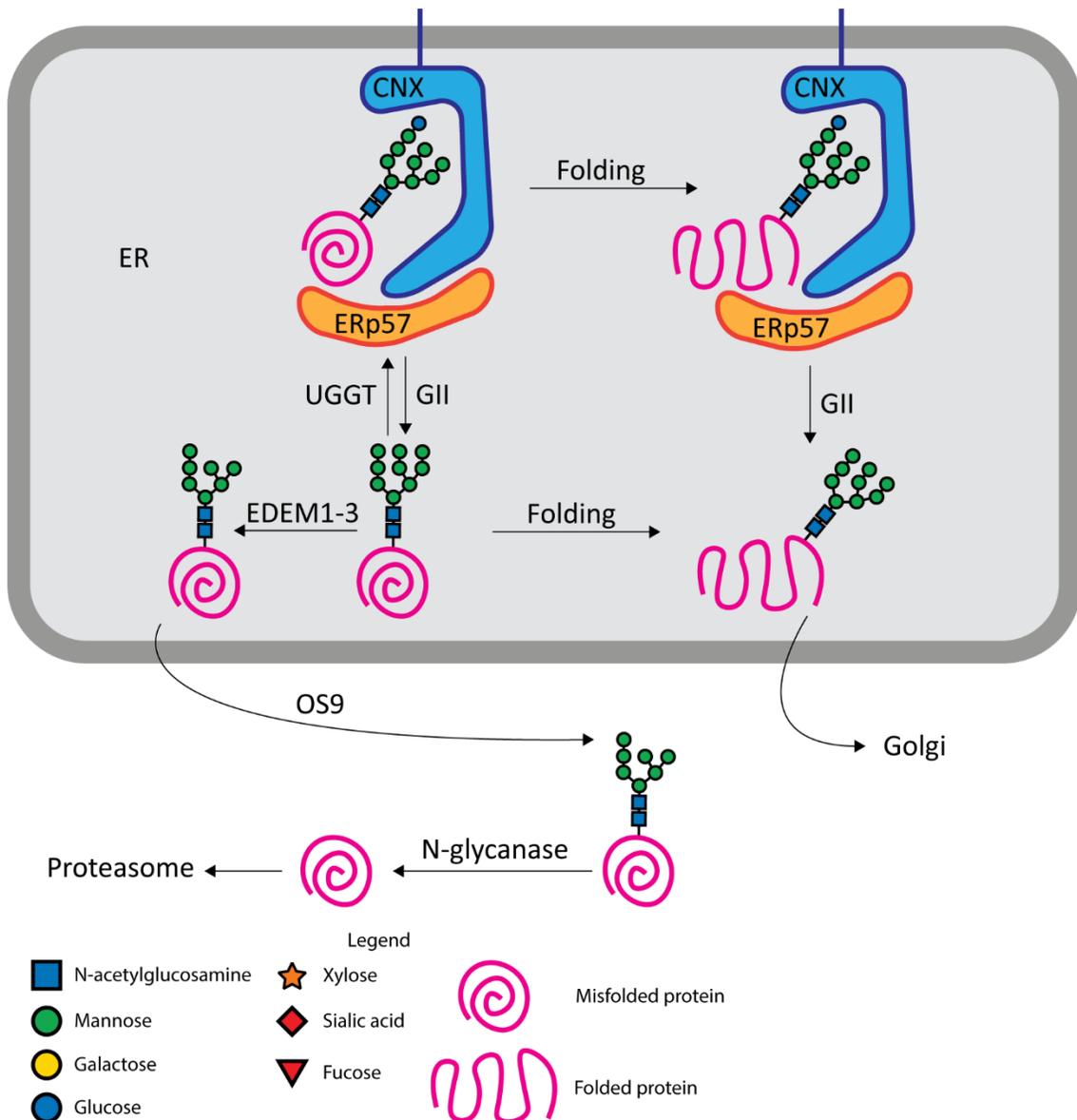


**Figure 3. Simplified diagram of protein quality control in the ER.**

CNX/CRT binds to glucosylated N-glycans and increases protein residence time in the ER. Proteins that remain misfolded after the GII enzyme removes the glucose are trimmed by EDEMs and retrotranslocated by the lectin OS9 to the cytosol, where an N-glycanase removes the glycan and the protein is degraded. The enzyme UGGT can re-catalyze the addition of this glucose, allowing for more folding time. Properly folded proteins will be translocated to the Golgi apparatus as normal.

Typically, proteins exported to the *cis*-Golgi contain 8-9 Man residues, depending on whether or not they were acted on by ER  $\alpha$ -mannosidase I (MAN1B1), which removes the terminal Man from the central arm of the glycan [23]. In the *cis*- and *medial*-Golgi, further trimming of high-mannose glycans (which contain anywhere between 5 and 9 terminal Man residues) is performed by  $\alpha$ -mannosidases 1A and 1B (MAN1A1 and MAN1A2), which ultimately leads to Man<sub>5</sub>GlcNAc<sub>2</sub>, a structure which can undergo further processing to generate complex- or hybrid-type glycans or can remain on the final exported protein [24]. Some proteins retain their high-mannose glycans, in particular proteins that are destined to remain within the organelle compartments of the cell, as these glycans are known to play a role in intracellular trafficking of proteins to the lysosome through the binding of the mannose-6-phosphate receptor [1]. In most circumstances, high-mannose glycans are processed to either of these advanced forms prior to secretion or insertion of the mature protein into the plasma membrane. However, in some cases cellular stress due to cancer, infection, or other disease can result in inefficient processing leading to an increase in the proportion of these glycans on the cell surface, the consequences of which are discussed in a subsequent section.

### 1.2.3: Processing of hybrid and complex glycans

Further processing of glycans (Figure 4) is initiated in the *cis/medial*-Golgi by the N-acetylglucosaminyltransferase MGAT1, which adds a  $\beta$ 1,2-GlcNAc residue to the  $\alpha$ 3 arm of the trimannose core forming the hybrid glycan GlcNAcMan<sub>5</sub>GlcNAc<sub>2</sub> [25]. The remaining Man residues (apart from the trimannose core) are trimmed away by the enzymes MAN2A1 and MAN2A2, which can only act on glycan substrates that have

been acted on by MGAT1 [24]. In plants and some invertebrates, the action of MGAT1 can be reversed by a hexoseaminidase in the Golgi forming what are referred to as paucimannose structures ( $\text{Man}_{3-4}\text{GlcNAc}_2$ ) [26]. While some hybrid glycans appear on exported proteins, most have both the  $\alpha 3$  and  $\alpha 6$  arm of the trimannose core extended by GlcNAc, the second of which is added by the enzyme MGAT2. This structure,  $\text{GlcNAc}_2\text{Man}_3\text{GlcNAc}_2$  (or GnGn for short), can have additional GlcNAc residues added by other enzymes in the MGAT family (MGAT3, MGAT4A/B, MGAT5/5A/5B, and MGAT6), which generate large multi-antennary and bisecting structures (Figure 6) [1]. These terminal GlcNAc residues form the starting points for N-glycan maturation, which consists of the further addition of sugar residues to the core, elongation of the GlcNAc residues, and capping of these elongated branches. Most mammalian complex glycans contain an  $\alpha 1,6$ -linked Fuc residue on the innermost core GlcNAc that is added by the enzyme Fuc-TVIII (encoded by the *FUT8* gene) [27]. In plants, this core fucose is attached with an alternative  $\alpha 1,3$  linkage by an  $\alpha 1,3$ -fucosyltransferase. Plant glycans also commonly contain a  $\beta 1,2$ -xylose residue attached to the central mannose residue of the trimannose core [26]. The presence of plant-derived core xylose and fucose is controversially implicated in hypersensitivity reactions to plant allergens and is hypothetically a safety concern for recombinant therapeutic proteins manufactured in plant-based platforms, though the safety (or lack thereof) of plant glycans is much debated [28, 29].

The number of possible mature N-glycoforms is extensive. The majority of complex and hybrid glycans begin with the addition of Gal to the terminal GlcNAc residues forming  $\text{Gal}\beta 1-4\text{GlcNAc}$ , or type 2 N-acetyllactosamine (LacNAc). Under

certain circumstances, LacNAc sequences are repeated to create poly-LacNAc glycans, which have many different structures and separate biosynthesis pathways that are beyond the scope of this work [30]. The most important sugars in mammals for capping are Fuc, Gal, GlcNAc, and the sialic acids (Sia). These sugars are almost always  $\alpha$ -linked, which causes them to point away from the main glycan structure and allows them to interact with lectins and antibodies more easily [31]. The Sia family of sugars are particularly abundant on mature glycoproteins and have diverse structures [32]. The most common sialic acid in humans is 5-N-acetylneuraminic acid (Neu5Ac), and unlike other monosaccharides these can be repeatedly extended with additional sialic acid residues to create polysialic acid chains [33]. Sialic acids impart a number of biological functions to glycans, and polysialic acids in particular are abundant on cellular adhesion molecules like NCAM where they mediate intercellular interactions and regulate neuronal development [34]. Among other functions, sialic acids protect the underlying glycan or glycoprotein from degradation or recognition by host-cell receptors or proteases and pathogen-associated receptors or toxins [31]. The abundance of sialic acids on mammalian glycoproteins, however, has led to many animal pathogens evolving to recognize these residues. A notable example of this is influenza virus hemagglutinin (HA), which agglutinates erythrocytes by binding to sialylated receptors on their surface [35].

In summary, N-glycosylation is a complex yet integral part of cell physiology that is necessary for protein maturation, structure, and function. N-glycans are incredibly diverse, and the impact of individual glycan structures on the function of the underlying protein is in most cases still being elucidated. However, one thing that is becoming

increasingly clear is that changes to the typical glycoforms produced by the cell can be induced by cellular stress such as that from viral infection, inflammation, and cancer. Changes to the normal glycan structures therefore represent potential glycobiomarkers of disease that could be targeted for diagnostic or therapeutic purposes, to be discussed further.

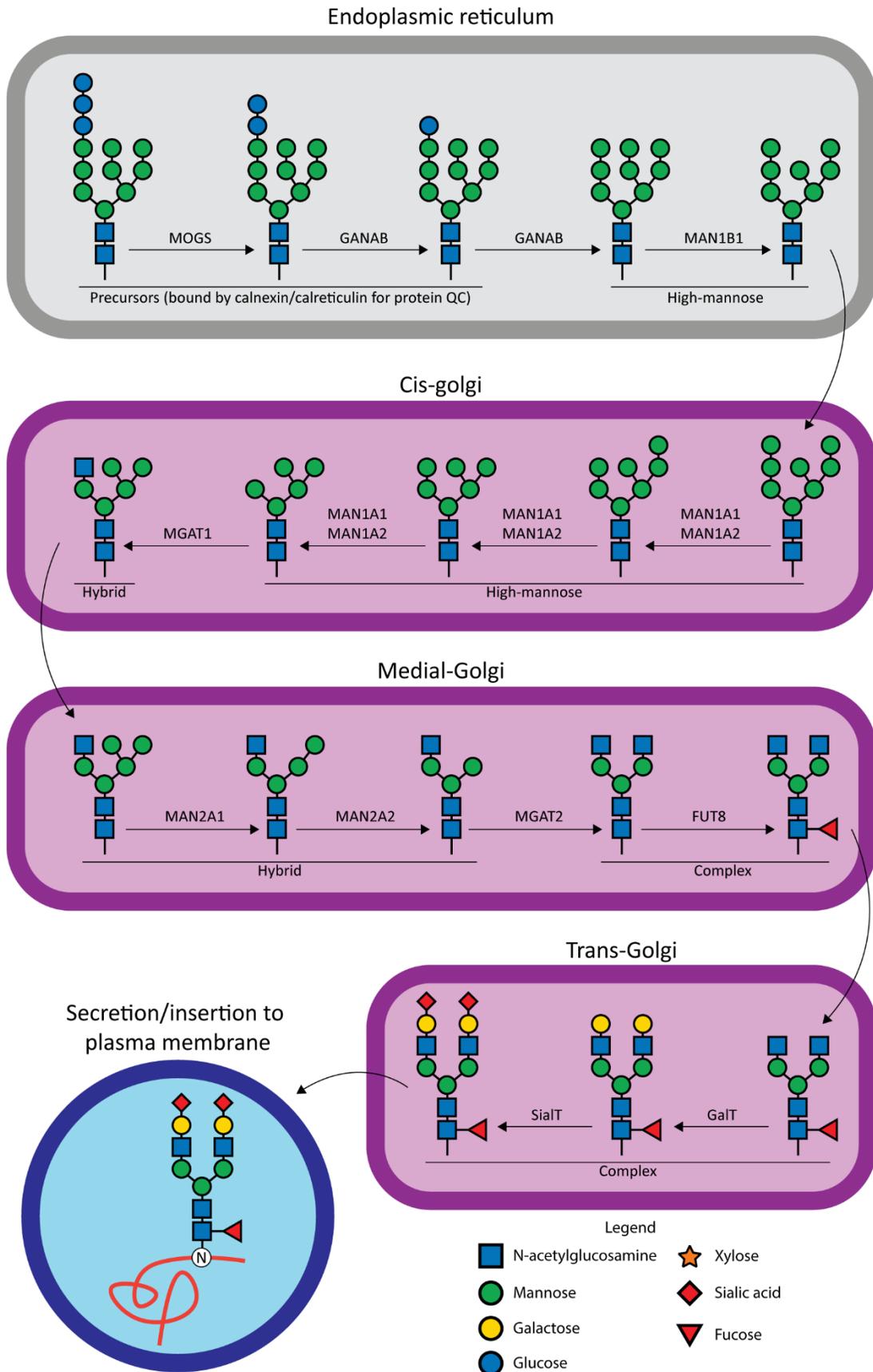


**Figure 4. General outline of N-glycosylation in mammals.**

The precursor glycans assembled in the ER and transferred onto NXS/T-containing proteins by OSTA are trimmed by a series of glucosidases and mannosidases in the ER and *cis*-Golgi, ultimately forming GlcNAc<sub>2</sub>Man<sub>5</sub>. The enzyme MGAT1 catalyzes the addition of the first GlcNAc to the  $\alpha$ 3 arm of the trimannose core, forming a hybrid glycan structure. Further trimming by mannosidases is followed by the addition of a second GlcNAc to the  $\alpha$ 6 arm of the trimannose core, which begins the synthesis of the complex glycans in the *medial*- and *trans*-Golgi. A series of sugar “capping” and core modifications is then performed to generate the final diversity of N-glycan structures, in particular through the addition of galactose, sialic acids, and core  $\alpha$ 1,6-fucose. The number of different complex N-glycans that can be synthesized is very large, and the relative proportions of each structure can change under certain cellular conditions.

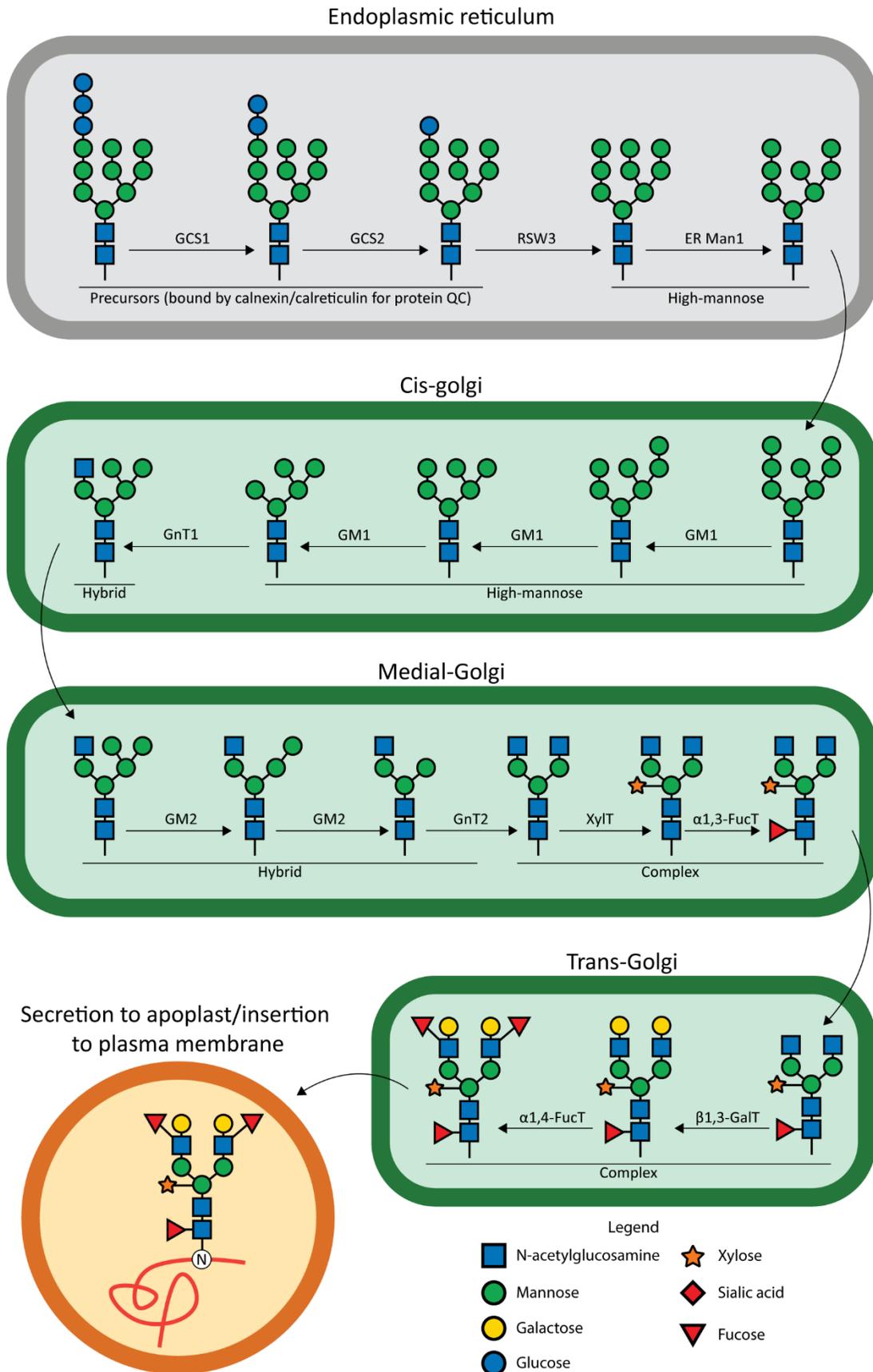


**Figure 5. General outline of N-glycosylation in plants.**

N-glycosylation in plants proceeds along much the same path as it does in mammals, albeit with different enzymes and different final glycan structures. The major differences occur after the addition of the second GlcNAc residue to the  $\alpha$ 6 arm of the trimannose core in the *medial*-Golgi, forming the so-called “GnGn” glycoform. In mammals, this is typically followed by the addition of a core  $\alpha$ 1,6-fucose residue and extension of the GlcNAc residues by galactose and other sugars. In plants, however, the generation of the GnGn glycan is followed by the addition of a core  $\beta$ 1,2-linked xylose residue to the first core mannose and a  $\alpha$ 1,3-linked fucose residue to the innermost core GlcNAc. These sugars, in this particular arrangement, are generally considered to be plant-specific. As with mammals, the number of complex N-glycans from plants is large and can change depending on the cellular conditions.

### 1.3: N-glycosylation and disease

Changes to the normal patterns of N-glycans produced by cells or the introduction of rare and cryptic glycans have been identified as hallmarks of diseases such as cancer and viral infection [13, 36]. Indeed, aberrant glycoforms have been explored and identified for their potential use as biomarkers and druggable targets, and some of the relevant findings will be discussed here with a particular focus on high-mannose glycans.

#### 1.3.1: N-glycosylation of viral glycoproteins

Changes to the normal pattern of N-glycosylation described above can often be the consequence of viral infection. The surface glycoproteins of enveloped viruses are often used for cellular attachment and membrane fusion leading to infection of the target cells, and as such the proper folding and function of these proteins is integral to virus replication and survival. As N-glycosylation is a critical determinant for the final structure and function of any glycoprotein, so it is also for viruses. Many glycoproteins belonging to enveloped viruses are heavily decorated with N-glycans, which have evolved over time to modulate the affinity of viral entry proteins to their cognate receptors on the host cell as well as mask the underlying protein epitopes from the immune system [36, 37]. This high glycan density places significant stress on the cellular glycosylation machinery resulting in aberrant glycosylation not only on host proteins but on the viral glycoproteins themselves [37]. It is this property that allows for potential discrimination of virally-infected tissues from non-infected, making these glycan changes potentially druggable or diagnostic targets.

One of the most commonly observed glycan changes observed on the surface of highly glycosylated viral glycoproteins is an overabundance of high-mannose glycans. This phenotype has been identified on a wide range of viruses including influenza virus [38], human immunodeficiency virus (HIV) [39], hepatitis C virus (HCV) [40], the human coronaviruses (MERS, SARS, SARS-2, HKU1, and 229E) [41-43], West Nile Virus [44], Lassa virus [45], the Ebola viruses [46], herpes simplex virus 1 and 2 [47], and many others. While it is not known for certain why these glycans are overrepresented on these viruses, there are at least two hypotheses. The first is that the infection itself and resulting inflammatory signaling may cause changes in cellular metabolism that promotes the production of high-mannose glycans, and that they may constitute a type of danger signal that allows for the mounting of an appropriate immune response by cells bearing mannose-recognizing C-type lectins (mrCLRs) [14, 48]. A recent study also suggested that IFN $\alpha$ , an important mediator of the antiviral response, may alter host glycosylation patterns including the upregulation of high-mannose glycans [49]. Similarly, infection of cells by influenza virus was found to activate the ER unfolded protein response, which results in improper glycan processing and upregulation of high-mannose glycans on the cell surface which can then be recognized by the mannose-binding lectin leading to inflammation [50]. The second hypothesis is that the overexpression of viral glycoproteins produces steric hindrance and saturation of the N-glycosylation pathway, preventing the trimming of certain occluded glycans and forcing the rapid movement of proteins through the secretory pathway [37]. This could certainly be the case for viruses like HIV, whose spike glycoprotein gp120 exists as a trimer on the surface of the virus and can contain as many as 30 N-glycans per monomer, the majority of which are high-

mannose glycans [39]. This huge density of glycans and their rapid production during viral replication places tremendous stress on the glycosylation machinery and combined with the lack of access by mannosidases to their substrates, may help explain the abundance of high-mannose glycans [51]. Other enveloped viruses such as West Nile virus are not abundantly glycosylated (with only 1 or 2 glycans per envelope protein) yet also display high-mannose glycans, allowing them to infect cells through the mannose-binding lectins DC-SIGN and DC-SIGNR, though the mechanism for this is less clear [52]. What is clear is that high-mannose glycans are a common viral glyco-biomarker, one which can potentially be taken advantage of as a druggable target. Indeed, a number of antibody-based and lectin-based therapeutics have been developed for this purpose [53, 54].

### 1.3.2: Aberrant N-glycosylation in cancer

While much work remains to elucidate the exact role that N-glycans play in oncogenesis and metastasis, aberrant changes associated with cancer have been described for decades and have provided targets for diagnostic and therapeutic strategies [13]. As mentioned previously, N-glycans are incredibly diverse structures whose compositions are largely determined by intrinsic factors such as substrate availability, glycosyltransferase and glycosidase expression levels, and compartmentalization of these enzymes within the cell. Two broad processes have been identified which define the tumor-associated changes to glycan structures and can be used to generally classify the aberrant changes: the incomplete synthesis and neo-synthesis processes [55]. Incomplete synthesis of glycans refers to the impairment of normal glycan synthesis and the

upregulation of truncated or immature structures. Alternatively, glycan neo-synthesis involves the expression of glycosyltransferases and other genes that result in the generation of novel carbohydrates. These processes however are simply descriptive terms that describe the outcome of glycosylation changes, and don't necessarily provide a framework for how they occur. Realistically, shifts away from normal glycosylation patterns during oncogenic transformation are the result of a number of intrinsic and extrinsic factors. The first of these is the altered expression (over or under) of the various glycosyltransferases and glycosidases, which may occur due to transcriptional or translational disruption [56, 57]. Altered glycan expression can also be the result of changes to the availability of the various sugar nucleotide donors and enzymatic cofactors as a result of metabolic disturbance [58]. Lastly, normal glycan structures can be disrupted by changes to the localization of glycosyltransferases and glycosidases, especially those that are present in the Golgi apparatus where the complex N-glycans are mostly formed [59].

For N-glycans, the most consistently observed alterations in cancer are increased core fucosylation and the upregulation of branching and poly-LacNAc structures (Figure 6) [13, 60]. As described previously, many complex mammalian glycans are decorated with the addition of an  $\alpha$ 1,6-linked fucose residue to the innermost GlcNAc of the N-glycan core. The increase in core fucosylation is due to overexpression of the *FUT8* gene, which encodes the Fuc-TVIII enzyme that catalyzes the addition of the sugar. Abundant core fucosylation is a well-established phenomenon in lung, liver, and breast cancers, and can even be used to diagnostically differentiate between hepatocellular carcinoma and other chronic liver disorders [61-64].

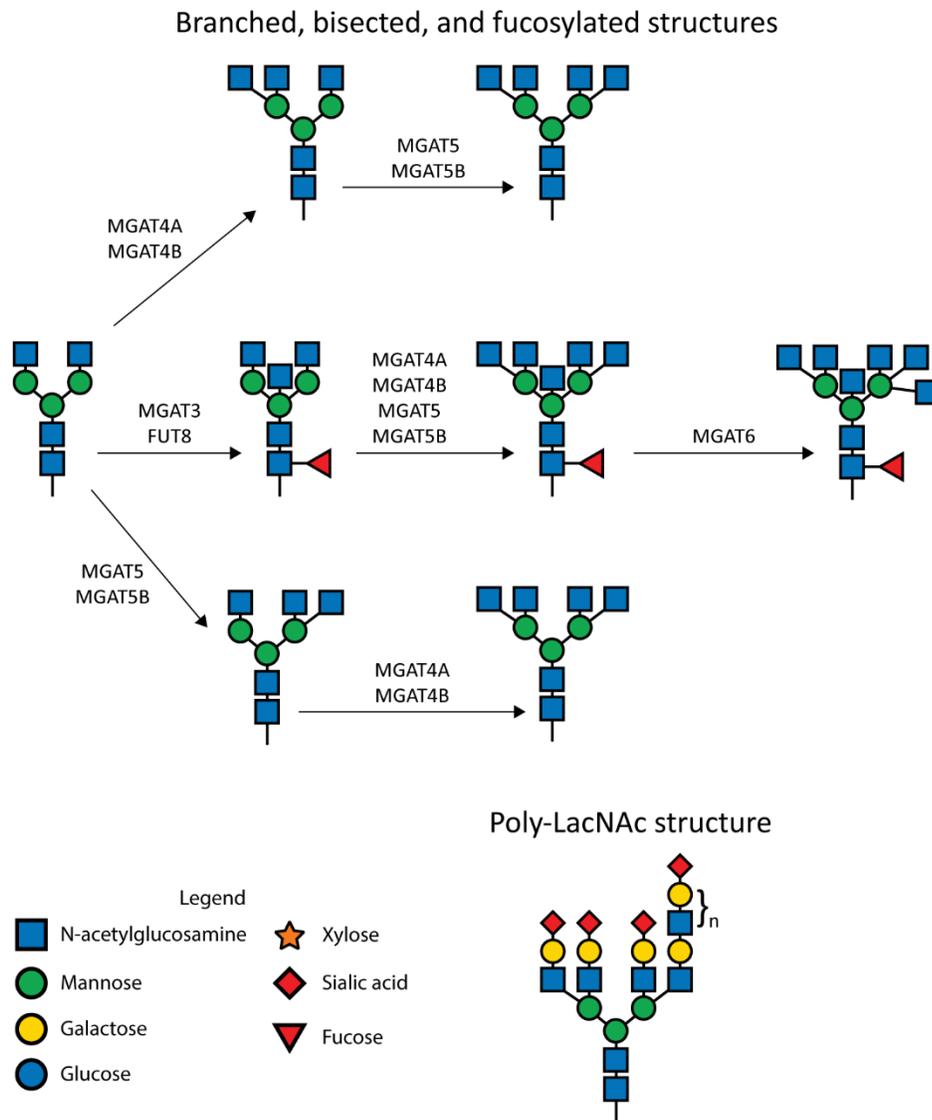


**Figure 6. Structure of poly-LacNAc and generation of branched, bisected, and fucosylated N-glycans.**

Branched and bisected structures are generated through the action of the N-acetylglucosaminyltransferases MGAT4A, MGAT4B, MGAT5, MGAT5B, and MGAT6. Each GlcNAc residue, except for the bisecting GlcNAc, can be modified with additional galactose, GalNAc, and sialic acid residues creating large and complicated structures. Increases in the proportions of branched N-glycans and Poly-LacNAc is commonly observed in cancer.

The increase in expression of complex branching structures is primarily due to the upregulation of the *MGAT5* gene, which encodes the N-acetylglucosaminyltransferase GnT-V. GnT-V catalyzes the addition of  $\beta$ 1,6-linked GlcNAc to the trimannose core which leads to the generation of tri- and tetra-antennary structures that are further decorated with LacNAc residues. Interestingly, *MGAT5* expression appears to be regulated by the RAS/RAF/MAPK signaling pathway, which itself is activated in many cancers [60]. The principal consequence of this is the increased generation of poly-LacNAc chains that are the primary ligands for the S-type galectins, which bind to these glycoproteins and form large lattice complexes in the extracellular matrix. Galectins contribute to the transformation to cancer possibly by helping to regulate the process of angiogenesis, which is critical for tumor survival and ultimately metastasis [65]. In addition, branching N-glycans seem to play a significant role in regulating the function of some receptors and adhesion molecules including E-cadherin, integrins, and EGFR. In several *in vivo* studies, upregulation of *MGAT5* resulted in the loss of contact inhibition of cancer cells and increased tumor formation [66, 67], while downregulation suppressed tumor growth and metastasis [66]. A seminal publication by Granovsky et al. in 2000 effectively demonstrated this effect through the generation of *Mgat5*<sup>-/-</sup> mice, which significantly suppressed viral oncogene-induced breast cancer production and metastasis [68]. Overexpression of *MGAT5* also negatively impacts E-cadherin structure and function, resulting in significant loss of functional protein and loss of effective cell adhesion [69]. Conversely, the addition of bisecting GlcNAc, catalyzed by GnT-III (*MGAT3*), precludes the generation of branching structures by enzymatic competition and acts as a tumor suppressor, significantly limiting the lung metastasis of B16 cells and

delaying the recycling of E-cadherin at the cell surface (which may help to suppress the epithelial-to-mesenchymal transition, or EMT) [69-71].

One change to the normal N-glycosylation pattern of cancer cells that has been more recently elucidated is an increase in the proportion of high-mannose glycans. As described previously, high-mannose glycans are immature glycoforms that are generally processed by mannosidases and modified into complex forms prior to the secretion of the glycoprotein from the cell or its insertion into the plasma membrane. Their presence on the cell surface, therefore, is indicative of a disruption to glycan processing that prevents complete glycan maturation. Increases in the expression of high-mannose glycans have been found in breast cancer [72], colorectal cancer [73-75], hepatocellular carcinoma [76, 77], cholangiocarcinoma [78], lung adenocarcinoma [79], pancreatic cancer [80], ovarian cancer [81, 82], prostate cancer [83], and some skin cancers [84]. Interestingly, high-mannose glycans are also overrepresented on the surface of human embryonic stem cells, an observation that may be linked to their appearance in cancer as cancer cells often take on a more stem-cell-like phenotype during EMT [85]. The mechanism by which cancer cells produce greater numbers of high-mannose glycans are not clearly established, and different mechanisms likely exist in cancers from different cell and tissue types. The mannosidase MAN1A1, which is a key enzyme responsible for trimming Man8 to Man5, has been implicated as the culprit in a number of cancer cells. For instance, MAN1A1 was found to be downregulated in metastatic cholangiocarcinoma cells and differentially localized to Golgi compartments in aggressive prostate cancer cells [78, 86-88]. Downregulation of mannosidases was also speculated as the reason for increased abundance of high-mannose glycans on colorectal cancer cells [89]. Interestingly,

expression of high-mannose glycans could be modulated through expression of certain O-glycans, in particular O-GlcNAc, suggesting that regulation of the two processes may be linked [88].

The biological consequences of the overexpression of high-mannose glycans on the cell surface are not well understood. In 2011, de Leoz et al. demonstrated that high-mannose glycans expression levels correlated with the progression of breast cancer, suggesting that they may play a broad role in tumor migration, invasion, and metastasis [72]. Subsequently, more mechanistic studies showed that the increase in high mannose glycans resulted in the increased migration and invasion of cholangiocarcinoma cells, the effect of which could be masked through the use of high-mannose glycan-binding lectins such as *Pisum sativum* Agglutinin [88]. Inhibition of MAN1A1 in metastatic cholangiocarcinoma cells through the use of the chemical inhibitor kifunensine resulted in significant increases in migration and invasion, activity which may have been mediated by the mannosylation of specific membrane receptors including the transferrin receptor (TFR1), integrin  $\alpha$ -V (ITGAV), and nicastrin (NCSTN) [78]. An increase in Man9 on the TFR1, for instance, resulted in a significant increase in homodimer stability and transferrin affinity, suggesting that high-mannose glycans affect cell-surface protein dynamics in a way that may promote cancer growth [78]. Another well-established example of this is the presence of high-mannose glycans on EGFR, which has long been known to be prognostic in lung cancer patients [90, 91]. A recent study by Alonso-Garcia et al. has shed some light on a possible biophysical mechanism to explain the enhanced invasiveness of high-mannose glycan-bearing cells [92]. In this study, knockdown of MAN1A1 in mesenchymal stromal cells (MSCs) using shRNA constructs resulted in

increased cell migration. Similarly, the use of kifunensine resulted in both enhanced migration and structural changes to the cells that may lead to enhanced motility and tissue invasion, including a decrease in cell contact area and a reduction of cell stiffness [92]. In summary, while it is increasingly clear that the increase in cell-surface high-mannose glycans is a potentially useful and broad glyco-biomarker of cancer that may not only constitute a diagnostic marker but a druggable target, the functional consequences of that increase are still not clear.

#### 1.4: Avaren-Fc, a novel high-mannose-binding agent

The search for therapeutic carbohydrate-binding agents targeting disease-associated glyco-biomarkers has remained somewhat elusive. The vast majority of mAb therapeutics are IgGs, as they are capable of high-affinity binding and inducing immune-mediated effector functions while maintaining a long serum half-life. IgGs targeting glycans are notoriously hard to generate, however, as glycans alone make poor epitopes and do not typically present on MHC-class molecules, which precludes isotype switching and affinity maturation [93]. To date, the GD2 ganglioside-binding mAb dinutuximab remains the only FDA-approved cancer therapeutic targeting a carbohydrate epitope [94]. Furthermore, antibodies specifically targeting cancer-associated high-mannose glycans are practically nonexistent. One such antibody, TM10, was found to bind selectively to cancer cells but was completely devoid of activity *in vivo*. The most likely due to the fact that TM10 is an IgM-class antibody, which are large, low-affinity antibodies that lack effector functions [95].

Lectins, which are proteins that specifically bind to carbohydrates, are an incredibly diverse set of proteins found across the tree of life and offer a powerful alternative to mAbs for therapeutic carbohydrate binding. They not only play important roles in biological processes – from cell signaling to immune cell trafficking and pathogen defense – they have found use in biotechnological applications including in microarrays, chromatography, and medical diagnostics and imaging [96]. Furthermore, some lectins have been found to have antimicrobial and anticancer activity, suggesting that they may have therapeutic utility by targeting disease-associated glycobiomarkers [53, 97]. Unfortunately, lectin therapeutic development has been somewhat limited due to toxicity, off-target effects, and lack of producibility. Thus, there is considerable room in the field for novel lectin agents that overcome these downsides.

To that end, our lab has pioneered the development of a novel lectin-Fc fusion protein, or lectibody, called Avaren-Fc (AvFc). AvFc is a first-in-class antibody-like carbohydrate-binding agent that has high affinity for clusters of high-mannose glycans, a type of immature N-glycan that is enriched on the surface of some highly-glycosylated viral glycoproteins as well as on the surface of many types of cancer (as described in section 1.3.1 and 1.3.2). In addition to exhibiting high-affinity binding to these glycans, the inclusion of the Fc region allows for the induction of immune-cell-mediated effector functions including antibody-dependent cell-mediated cytotoxicity (ADCC), antibody-dependent phagocytosis (ADP), and complement-dependent cytotoxicity (CDC). Interestingly, unlike other mannose-binding lectins such as concanavalin A (ConA), AvFc demonstrates a high degree of selectivity for high-mannose glycans, is not cytotoxic or mitogenic to normal cells *in vitro*, and has not shown any signs of toxicity *in*

*vivo* [98, 99]. This combination of sugar binding and antibody-like functions in the immune system make AvFc a unique and powerful molecule. This section will detail its structure and activity.

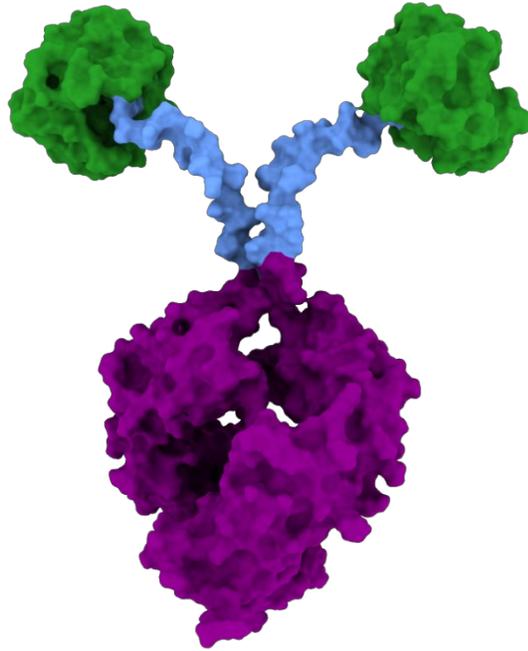


**Figure 7. The predicted 3D structure of Avaren-Fc.**

The 3-dimensional structure of AvFc was predicted using AlphaFold. The lectin Avaren (green) is linked by a GGGS linker to the hinge region (blue) of the Fc region from a human IgG1 molecule (purple).

#### 1.4.1: Design and antiviral activity

The design and anti-HIV activity was summarized by Hamorsky, Kouokam, and Dent et al. in 2019. Key points from this manuscript are reiterated herein. The lectin Avaren is a mutant derived from the actinomycete lectin actinohivin (AH), which was discovered by screening microorganisms for novel anti-HIV compounds using a standardized syncytium-formation assay [100]. AH was capable of neutralizing multiple strains of HIV without inducing toxicity or mitogenicity to human blood cells by binding to terminal  $\alpha$ 1,2-linked mannose residues, which are found on high-mannose glycans [101-104]. However, a major drawback with AH is its lack of manufacturability in recombinant systems, owing to its high hydrophobicity and propensity for aggregation [102]. In order to improve the biochemical properties of AH, a number of variants were generated and tested in the *Nicotiana benthamiana*-based transient overexpression platform. Structurally, AH consists of 3 near-homologous repeated domains of approximately 38 amino acids, each of which is capable of binding a single high-mannose glycan [101, 103]. 11 variants of AH were generated by structure-guided mutation of one or two domains to corresponding residues in the others with the intention of neutralizing its surface charge variation. One of these variants retained much of the parent molecule's gp120-binding ability while significantly improving its solubility and producibility. This variant was termed "Avaren" (actinohivin variant expressed in *Nicotiana*) and was subsequently fused to the fragment crystallizable (Fc) region of human IgG1, which had the dual purpose of dimerizing the lectin and introducing the ability to induce immune-mediated effector functions (Figure 7). The resulting molecule

retained its sugar-binding specificity while greatly improving its affinity to high-mannose glycans and binding to Fc-receptors.

Dimerization of the lectin Avaren in AvFc improved upon the anti-HIV activity of the parent lectin. Cross-clade neutralization of HIV strains (from groups M and O as well as HIV-2) was observed with a mean IC<sub>50</sub> value of 20 ng/mL (259 pM) in pseudovirus neutralization assays. AvFc was also capable of neutralizing simian immunodeficiency virus (SIV) and could recognize infected mesenteric lymph node cells isolated from rhesus macaques. Significant anti-HIV activity was also observed using the antibody-dependent cell-mediated virus inhibition assay with primary human PBMCs, indicating that AvFc could neutralize virus by both binding and through Fc-mediated functions. Furthermore, co-incubation with PBMCs did not induce activation of immune cells nor did it result in cytokine release, and its administration was well tolerated in rats and macaques, indicating a lack of major toxicity. These data together suggest that AvFc has potent antiviral activity while lacking the toxicity typically associated with other lectins, which warranted additional exploration of its therapeutic use against HIV and other highly-glycosylated viruses. The activity of AvFc against hepatitis C virus (HCV) is described in Chapter 4.

#### 1.4.2: Anti-cancer activity and possible mechanism of action

As mentioned previously, high-mannose glycans are often enriched on the surface of cancer cells and have been identified as aberrantly overrepresented in a number of human cancer types (see section 1.3.2). This fact led us to hypothesize that in addition to its antiviral activity, AvFc may selectively recognize cancer cells and exhibit anticancer

activity, and some of the preliminary work on this indication has been described by Oh et al. in 2021, which is currently undergoing secondary review [105]. Indeed, AvFc was found to bind at low nanomolar concentrations to many established human cancer cell lines from a number of tissues and could selectively discriminate between human lung tumor tissues and adjacent tissues. This binding was dependent on the presence of high-mannose glycans as digestion of the cell surface with the enzyme endoglycosidase H (EndoH), which cleaves high-mannose glycans from proteins, nearly eliminated the ability of AvFc to bind to A549 lung cancer cells. Further analysis of AvFc's activity against A549 and H460 non-small-cell lung cancer (NSCLC) revealed that by binding to the cell surface AvFc could both induce ADCC as well as bind to and inhibit cell-surface glycoproteins, in particular the receptors EGFR and IGF1R. This combined activity led to AvFc exhibiting potent anticancer activity *in vivo* in A549 and H460 flank tumor xenograft models, as treatment with 25 mg/kg of AvFc slowed tumor growth substantially over time. Conversely, the FDA-approved cancer immunotherapeutic cetuximab, which targets EGFR, only had activity against A549 tumors, illustrating the broader range of activity of AvFc caused by binding to a glycan as opposed to an individual receptor. Questions remain, however, as to what the predominant mechanism of action of AvFc is, and what the relative contributions of receptor binding and ADCC may be to this. The anticancer activity of AvFc is expanded upon in Chapters 5 and 6.

### 1.5: Antibody-mediated immune effector functions in cancer

Therapeutic mAbs with anticancer activity express this activity through a number of direct and indirect mechanisms. Direct inhibition mechanisms are mediated by the

interaction of the antigen-binding fragment (Fab) with the target antigen on the cell surface. A well-known example of this is the FDA-approved therapeutic cetuximab, which targets the epithelial growth factor receptor (EGFR) found to be overexpressed in several carcinomas. Other anticancer antibodies such as bevacizumab act by inhibiting host processes such as angiogenesis by binding to and inhibiting the vascular endothelial growth factor (VEGF). Antibodies also exhibit anticancer activity through their Fc regions by interacting with complement and Fc receptor-bearing cells of the immune system, leading to cellular activation, degranulation and phagocytosis, and target cell death. Immune-mediated mechanisms are increasingly being recognized as major mechanisms of action for mAb therapeutics and contribute heavily to their clinical success. This section will discuss the three major Fc-mediated effector functions that are generally considered integral to therapeutic antibody function *in vivo*.

#### 1.5.1: The classical complement pathway

The complement system is an ancient protein-based antimicrobial system that evolved as a part of the innate immune system and is localized to the bloodstream. It has three major functions: induction of inflammation, the opsonization of pathogens to facilitate uptake by phagocytic cells, and the synthesis of the membrane attack complex to kill infected or malignant cells. The system is a complicated cascade composed of a number of inactivated proteases called zymogens, all bearing the letter C and a number, that are sequentially activated by proteolytic cleavage from other enzymes in the pathway. The initial activation of the cascade is triggered following recognition of pathogens or malignancies by pattern recognition receptors or by specific antibodies. As

such, three pathways to complement activation have been described: the classical or antibody-dependent pathway, the alternative pathway, and the lectin pathway. No matter the mechanism of activation, all complement pathways lead to the generation of a C3 convertase complex on the surface of targeted cells and pathogens.

The classical pathway, so named for it being the first discovered and not because it is the most evolutionarily ancient, is activated by the C1 protein complex (Figure 8A). The C1 protein complex is composed of the hexameric C1q subunit, which specifically recognizes the Fc region of antibodies (mostly IgG3), and the proteases C1r and C1s. Upon activation these proteases cleave C2 and C4 into the C2a/b and C4a/b fragments. The binding of C2a and C4b generates the C3 convertase complex, which rests on the surface of the targeted cells and pathogens. As the name implies, the C3 convertase complex cleaves C3 into C3a and C3b fragments, which the latter of which forms a complex with C2aC4b to form the C5 convertase complex on the membrane surface. This complex then cleaves C5 to C5a and C5b. C5b remains on the membrane surface and recruits C6, C7, C8, and C9, which insert themselves into the membrane to form a pore called the membrane attack complex (MAC) that causes rapid loss of membrane potential and cell lysis. The soluble fragments C4a, C3a, and C5a are referred to as the anaphylatoxins, named due to their ability to create an anaphylactic-like shock reaction if overactivated. These proteins are extremely potent mediators of inflammation and do so by enhancing phagocytic uptake of antigens and pathogens for lysis and presentation to lymphocytes and by recruiting immune cells (in particular neutrophils) to sites of infection or cancer.

The complement system is an important system in the inflammatory response, which is heavily involved in the various stages of tumor progression and oncogenesis. The evidence however suggests that complement activation is mostly pro-tumor, which is a counterintuitive notion given its anti-pathogenic properties [106]. For instance, C3-deficient mice were shown to be protected against chemically-induced carcinogenesis while mice lacking PTX3, an important negative regulator of complement activation, causes susceptibility to carcinogenesis through increased inflammation [107]. One potential explanation for this is that tumor cells evade immune surveillance by the complement system by expressing complement receptor proteins that limits complement activation in the tumor microenvironment [108]. Tumor cells also appear to express anaphylatoxin receptors like C5aR and C3aR, which promote cell survival and the EMT transition [109, 110]. There is also evidence to suggest that complement activation does not play as much of a role in the antitumor effects of monoclonal antibody therapeutics such as rituximab as previously thought. Deposition of complement protein C3b on B cells was shown to completely inhibit the activity of rituximab, while its antitumor activity was enhanced in complement-deficient mice [111, 112]. Overall, these results seem to suggest that complement-mediated lysis is not a major mechanism of action for therapeutic mAbs, and indeed complement activation may have significant protumor effects.

#### 1.5.2: Antibody-dependent phagocytosis

Antibody-dependent phagocytosis (ADP) of tumor cells primarily occurs following the activation of Fc $\gamma$ RI on immune cells by antibodies, but can also be induced

by the other activating FcγRs II and IIIa in humans and IV in mice (Figure 8C) [113]. While macrophages and monocytes are the primary mediators of this phenomenon, some evidence suggests that neutrophils also play a role in tumor phagocytosis [114]. Antibody decoration of tumor cells results in their uptake by phagocytosing cells, which deposit them into a specialized vacuole called a phagosome that matures and fuses with lysosomes, which then become highly oxidative and acidic resulting in destruction of the contents of the vacuole [115]. ADP has been demonstrated to be an important mechanism of action for some therapeutic mAbs including the anti-CD38 mAb daratumumab, and many tumor-associated antigens are known to induce high levels of ADP [116, 117]. Macrophage phagocytosis of tumor cells also leads to greater tumor antigen presentation, enhancing the antitumor immune response by inducing cytotoxic T lymphocytes [118]. A number of strategies have been developed to improve ADP functions of mAb therapies, including CD47 blockade (inhibiting the so-called “don’t eat me” signal), FcγRIIb blockade, and improvement of the affinity of the Fc region for FcγRI and reduction of its affinity for the inhibitory receptor FcγRIIb [119]. Removal of the lone C<sub>H2</sub> glycan and Fc modification of trastuzumab, for instance, was shown to greatly enhance ADP by increasing affinity for FcγRIIIa over the inhibitory receptor [120]. Overall, the evidence suggests an important role for macrophages in cancer therapy in the removal of circulating tumor cells and the induction of cytotoxic responses, and antibodies that make use of this function can potentially have greater therapeutic impact.

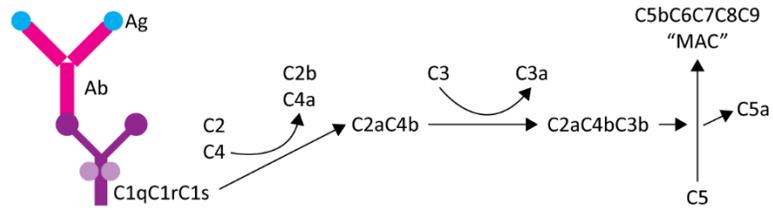
### 1.5.3: Antibody-dependent cell-mediated cytotoxicity

Antibody-dependent cell-mediated cytotoxicity (ADCC) is a well-known mechanism of action inducing cell death by mAbs and plays a key role in the anticancer activity of antibodies like rituximab and trastuzumab [121, 122]. Anticancer mAbs that target tumor-associated antigens activate ADCC by forming immune complexes that interact with and cross-link Fc $\gamma$ RIIIa on the surface of natural killer (NK) cells, which results in the phosphorylation of immunoreceptor tyrosine-based activation motifs by src kinases (Figure 8B) [123]. Activation of NK cells in this manner results in the phosphorylation of the transcription factor NFAT, which upregulates pro-inflammatory cytokine expression (in particular IFN $\gamma$ ) and induces degranulation, releasing granzymes and perforins that permeabilize the target cell membrane and induce apoptosis by cleaving caspase pro-enzymes [123]. The level of induction of ADCC is dependent on both the density of the target antigen on the cell and the affinity of the Fc region for the Fc receptor. While the density of the target antigen is largely dependent on the nature of the antigen and of the cancer, much research by both industry and academia has been dedicated to improving the affinity of the Fc region for Fc $\gamma$ RIIIa as these modifications allow for significant improvements in clinical efficacy of mAb therapeutics.

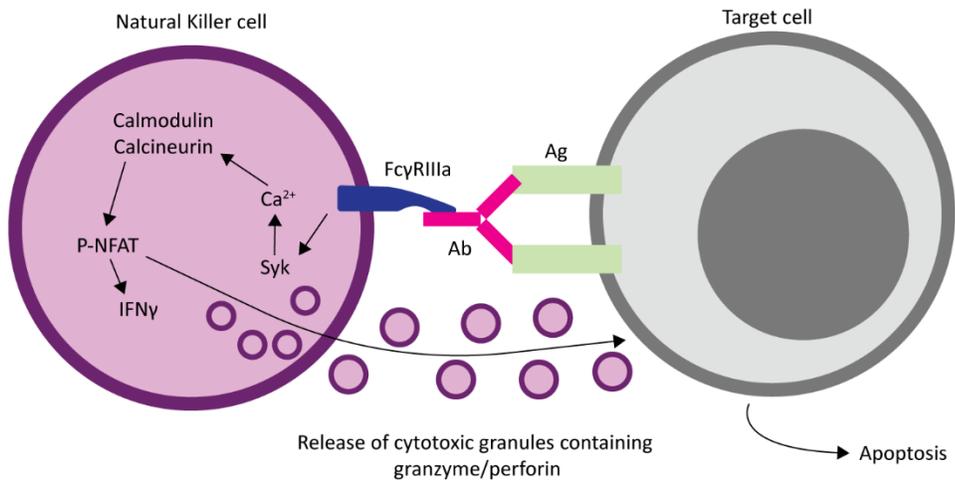
There are two major approaches to improving Fc affinity to Fc $\gamma$ RIIIa: engineering of the Fc region through amino acid substitutions and glycoengineering of the Fc N-glycan [124, 125]. The Fc $\gamma$ RIIIa binds to the Fc region of IgGs (primarily IgG1) by interacting with the hinge region between C<sub>H1</sub> and C<sub>H2</sub> and with the C<sub>H2</sub> N-glycan, and removal of this glycan obviates Fc receptor binding [126, 127]. One well-established Fc modification that affects this interaction is the GASDALIE

(G236A/S239D/A330L/I332E) mutation, which exhibits higher affinity for the receptor by increasing electrostatic interactions between it and the Fc and has increased effector functions *in vivo* [128, 129]. However, removal of the core  $\alpha$ 1,6 fucose from the C<sub>H2</sub> N-glycan by host glycoengineering is the most widely recognized modification and is the most effective approach to enhance ADCC activity [125]. Mechanistically, this may be due to the generation of several hydrogen bonds between the normally occluded core GlcNAc residues and the Fc receptor [126]. This concept is illustrated beautifully in the HIV field, as naturally generated antibodies with reduced fucosylation are observed in many HIV-specific antibodies and are generally associated with improved antiviral activity and control of HIV replication [130]. Defucosylation can be achieved in mammalian recombinant manufacturing platforms by knockdown or knockout of the *FUT8* gene, which as discussed previously catalyzes the addition of the core  $\alpha$ 1,6 fucose to the inner GlcNAc residue [131]. Similar results can be achieved in plants using RNAi to knockdown or CRISPR/Cas9 to knockout the related core-modifying glycosyltransferases  $\alpha$ 1,3-fucosyltransferase and  $\beta$ 1,2-xylosyltransferase (Figure 5) [132, 133]. With these modifications, therapeutic mAbs can be manufactured and defucosylated to a high homogeneity, significantly impacting their effectiveness *in vivo* and beyond.

A: The classical complement pathway



B: Antibody-dependent cell-mediated cytotoxicity (ADCC)



C: Antibody-dependent phagocytosis

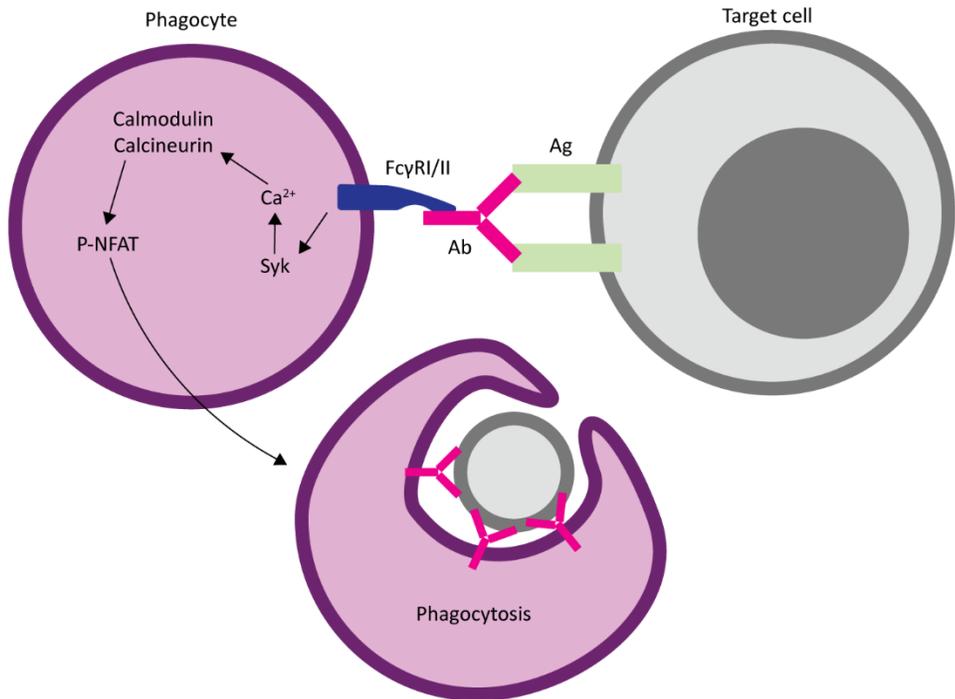


**Figure 8. Simplified diagram of various Fc-mediated effector functions.**

A) The classical complement pathway is initiated by the binding of C1q to antibody:antigen complexes. Associated C1r and C1s proteases cleave C4 and C2 to form the C3 convertase C2aC4b, which then cleaves C3 to form C2aC4bC3b. This complex, also called the C5 convertase, then cleaves C5 to form C5a and C5b, the latter of which embeds itself into the target cell membrane and recruits C6-9, forming the membrane attack complex (MAC). B) ADCC occurs when NK cells (and other FcγRIIIa-expressing cells, rarely) encounter antibody-opsonized target cells or pathogens, which can be infected cells or tumors. Cross-linking of FcγRIIIa with these antibody:antigen complexes leads to the release of cytotoxic granules containing perforin and granzymes, which permeabilize and cause induce apoptosis in the target cell. Activation of FcγRIIIa also activates the NFAT transcription factor, leading to pro-inflammatory cytokine production. C) ADP occurs when phagocytes encounter antibody-opsonized target cells or pathogens, which similarly can be infected cells or tumors. Cross-linking of FcγRI or FcγRIIIa with antibody:antigen complexes leads to envelopment and phagocytosis of the target.

## CHAPTER 2: CANCER BIOLOGICS MADE IN PLANTS

### 2.1: Introduction<sup>1</sup>

The 1997 approval of rituximab, which was the first anti-cancer monoclonal antibody (mAb) approved for use in the U.S., began a biologic explosion that has transformed the landscape of cancer therapy and dramatically altered and improved patient survival and quality of life. According to the U.S. National Cancer Institute, this broad category of pharmaceuticals includes immune checkpoint inhibitors, immune cell therapy, therapeutic mAbs and other immune system molecules, therapeutic vaccines and immune system modulators, which now combined make up the majority of total pharmaceutical sales globally (with a market value of approximately 1 trillion dollars in 2016) [135]. Since 1997 hundreds of biologic drugs have been approved or clinically evaluated, and the development of mAbs targeting immune checkpoints like PD-1 and CTLA-4 was even the subject of the 2018 Nobel Prize in Medicine or Physiology, a testament to the impact that biologics have had on medicine. Despite their promise, biologic drugs remain expensive due to manufacturing costs and the lack of significant generic competition from biosimilars (the first was only approved in 2015) [136]. Cell-

---

<sup>1</sup> The following chapter was reproduced for this dissertation from “Cancer Biologics Made in Plants”, by Dent et al., with modifications made for presentability and formatting of text. The original manuscript was published in *Current Opinion in Biotechnology* in 2020 [134]. The right to reproduce for a thesis/dissertation is retained by the author, as per publisher guidelines.

culture based manufacturing systems are also slow to implement for initial screening and proof-of-concept (POC) studies, prolonging preclinical development of novel drugs, though alternative methods have some important advantages.

Cancer biologic production in plants has a long history, beginning with the early production of mAbs against tumor-associated antigens (TAAs) like CO17-A [137]. In contrast to transgenic plants, the recent advent of transient overexpression vectors allow relatively short time for novel biologic drugs to be produced at scale and tested, making plants an ideal platform for preclinical biologic development [138]. A large number of recent advances in the field have come from the area of plant virus nanoparticles (PVNs), particularly those derived from cowpea mosaic virus (CPMV), tobacco mosaic virus (TMV), and potato virus X (PVX), which have shown efficacy as both immunostimulatory agents/therapeutic vaccines and as drug delivery modalities capable of delivering chemotherapy payloads to tumor sites *in vivo*. While much of the literature is dominated by these advancements, steps have also been made towards the development of recombinant cancer vaccines based on tumor antigens and anti-cancer lectins. This review sets out to catalog recent advancements in plant-made cancer biologics and their future.

## 2.2: Cancer vaccines and immunotherapy

The goal of cancer vaccination is to induce tumor-specific immunity and activate immune cells in the tumor microenvironment to elicit anti-cancer activity. Cancer vaccines are immunostimulatory agents that often make use of TAAs, which are antigens capable of distinguishing cancer and non-cancer tissue or antigens that are overexpressed

in cancer tissues compared to normal tissue, such as epidermal growth factor receptor (EGFR) and its family in some cancers. One such example is human prostatic acid phosphatase, or PAP, which is a secreted glycoprotein used historically as a marker for prostate cancer. A recombinant PAP fused to granulocyte-macrophage colony-stimulation factor (GM-CSF) is used as a part of spuleucel-T (Provenge®) vaccine, an FDA-approved autologous cellular immunotherapy for prostate cancer [139]. To enhance immunogenicity and expression, Kang et al. has successfully expressed PAP-fused to the Fc region of human IgM in transgenic tobacco (*Nicotiana tabacum*) [140]. Other tumor antigens that have been expressed in plants include the colorectal cancer antigen GA733-2-Fc fusion with an additional KDEL receptor, which was reported to have increased immunotherapeutic effects [141], and idiotypic antibody-keyhole limpet hemocyanin (Id-KLH) conjugate vaccines for Non-Hodgkin's Lymphoma [142-144]. More recently, a phase I safety and immunogenicity trial of Id-KLH conjugate vaccines in 11 patients showed that immunization resulted in a vaccine-induced, idio-type-specific cellular and humoral immune response without any serious adverse events reported [142].

Some chronic infections are known to be risk factors for cancer. A recent report estimated that approximately 15% (2.2 million) of 14 million worldwide new cancer cases in 2012 were attributable to infectious agents, including *Helicobacter pylori*, human papillomavirus (HPV), hepatitis B virus, hepatitis C virus and Epstein-Barr virus [145]. Thus, vaccines against these infections have significant implications for cancer prevention, and a number of efforts have been made for the development of plant-made vaccines against cancer-causing pathogens. However, these vaccines are beyond the scope of this review as they are not strictly categorized as “cancer biologics” with the

exception of therapeutic vaccines against HPV E6 and E7 oncoproteins. HPV infection is the cause of approximately 5% of all human cancers, in particular, malignancies of the genitalia (penile, vulval, anal, and cervical cancers) and oral cavity [145]. The E6 and E7 proteins are ideal targets because they are constitutively expressed in HPV-associated malignant cells and thus may be more effective at generating an immune response to infected cells than L1-based vaccines [146]. One interesting vaccine candidate that has been produced by transient expression in *N. benthamiana* is LALF<sub>32-51</sub>-E7, which is a fusion of the HPV E7 protein to the bacterial cell-penetrating peptide LALF [147]. LALF, or *Limulus polyphemus* anti-lipopolysaccharide factor, can penetrate mammalian cell membranes and has immunomodulatory properties. While plant-made LALF<sub>32-51</sub>-E7 has not been evaluated in animals, it does form the appropriate protein body-like structures in leaf tissue and can be purified to a high degree and may be a cost-effective therapeutic vaccine candidate [148].

Extensive work in the plant-made pharmaceutical (PMP) research field has been dedicated to the use of PVNs as *in situ* vaccination/immunostimulatory agents with or without the delivery of tumor antigen epitopes, beginning with the first POC study in 2006 with TMV-peptide fusion vaccines [149]. This strategy ultimately aims at the reactivation of tumor-suppressed immune cells in the tumor microenvironment and the induction of systemic anti-cancer immunity. The most well-studied of these PVNs are derived from CPMV, which have demonstrated efficacy in murine 4T1 breast, CT-26, colon, B16F10 melanoma, GL261 glioma, and ID8 ovarian cancer models [150-155]. The icosahedral structure of CPMV appears to be more efficiently taken up by antigen presenting cells (APCs), resulting in higher APC activation and better transport of PVNs

to and retention in lymph nodes than high-aspect-ratio viruses like PVX [151, 156]. Additionally, as has been recently demonstrated, *in situ* vaccination can result in the conversion of immunosuppressive cells like M2 macrophages and N2 neutrophils to their M1 and N1 counterparts, helping to break tumor immunotolerance [153]. What remains to be seen is the potential efficacy of these particles in humans, as mouse models in these studies used immunodeficient mice for human cancer xenograft, which may have a limited predictive value for immunotherapeutic effects in humans. Nevertheless, the results obtained in recent years hold much promise for their development.

Plants have long been used as production platforms for cancer-targeting immunotherapeutics, including mAbs and cytokines. One such example is the production of CCL21 in tomato, which may potentially be used as an anti-metastatic agent for many cancer types [157]. Recently, several groups have published the production of anti-cancer mAbs including the anti-HER2 mAb trastuzumab [158], the anti-GA733 mAb C017-1A [159], and the anti-CD20 mAbs ofatumumab and rituximab [160, 161], as well as an anti-HER2 single chain variable fragment-Fc (scFv-Fc) fusion [162]. Importantly, trastuzumab and rituximab were produced in glycoengineered plants and showed greater anti-cancer activity owing to the lack of core fucose on the single *N*-glycan in the Fc region, which increases the affinity for Fc $\gamma$ RIIIa and potently elicits antibody-dependent cell-mediated cytotoxicity [163]. Similar increases in Fc effector functions were also seen for a plant-produced anti-CD20-hIL-2 immunocytokine, made by the fusion of an anti-CD20 mAb and human IL-2 [164]. The resulting immunocytokine was also highly efficient at activating T cells, potentially resulting in greater cytotoxic T cell responses against malignant cells. The relative ease of plant glycoengineering compared to

mammalian or insect cell culture systems make them a useful alternative for mAb production [133].

### 2.3: Drug delivery and imaging

Considerable research has been conducted into novel drug delivery systems, with the goal of improving the pharmacokinetics and pharmacodynamics of small molecule and biologic drugs by affecting their absorption and distribution in the body. PVNs have been particularly attractive owing their ability to deliver larger payloads than antibody-drug conjugates, the relative ease at which they can be decorated with targeting ligands for tissue-specific delivery of drugs, the wide array of possible chemistries, and the ease of manufacturing them *in planta*. So-called high-aspect-ratio viruses, like TMV and PVX, are particularly useful as they are not taken up as easily by phagocytosis and may have a prolonged serum half-life compared to icosahedral viruses. Several recent reports have described PVNs for chemotherapeutic and imaging reagent delivery, including those derived from TMV [165-170], PVX [171-173], red clover necrotic mosaic virus (RCNMV) [174], Pepino mosaic virus (PeMV) [173], and Johnsongrass chlorotic stripe mosaic virus (JgCSMV) [175, 176].

Much of the recent work regarding PVNs as drug delivery modalities has focused on the use of high-aspect ratio, or filamentous, viruses. Among these, TMV PVNs have been extensively researched and used in medical imaging and animal models of cancer. Notably, Franke et al. demonstrated that the conjugation of cisplatin to tobacco mosaic virus PVNs restored the efficacy of the chemotherapeutic to OVCAR3 cells, which are typically cisplatin resistant [169]. Because resistance to cisplatin is common among

patients with recurrent ovarian cancer [177], the results justify further preclinical validation. Similarly, PVX particles loaded with doxorubicin or presenting tumor necrosis factor-related apoptosis-inducing ligand (TRAIL) have also shown to be efficacious in mice xenografted with the human breast cancer cell line MDA-MB-231 [171, 172]. PVX however may have less desirable pharmacokinetic and tumor homing properties compared to another filamentous virus, PeMV [173]. Overall, much work remains to demonstrate how these particles end up at the tumor site and how that can be improved, in addition to further demonstration of efficacy in animal models.

A number of icosahedral viruses have also been used as drug delivery systems, including RCNMV and JgCSMV. While icosahedral virus particles have short serum half-life as efficiently taken up by the immune system, these PVNs appear to have excellent tumor penetration and drug carrying capacity. For example, RCNMV particles loaded with doxorubicin showed more efficacy at a lower dose in an SKOV3 human ovarian cancer xenograft model than the pegylated liposomal form of the drug, indicating a greater degree of tumor targeting by the PVNs [174]. Alemzadeh et al. also recently demonstrated the loading of JgCSMV particles with doxorubicin and their efficacy in the MCF-7 human xenograft breast cancer model in mice [175, 176]. Interestingly, encapsulation of drug in JgCSMV particles led to increased uptake of doxorubicin in the breast cancer tissue and actually led to decreased cardiotoxicity [175].

Many recent advances have come in the area of medical imaging. TMV PVNs have, for example, been successfully conjugated to the contrast agent dysprosium and used to image prostate cancer cells in mice using both ultra-high-field magnetic resonance and near-infrared fluorescence imaging [167]. Serum-albumin-coated particles,

which may reduce the potential immune response to the TMV, have also been characterized and used to deliver doxorubicin and the contrast agent gadolinium in mouse models of human breast cancer. Dubbed a “theranostic”, this approach successfully combined treatment and MRI imaging, demonstrating the dual capacity of PVNs and their superiority over conventional drug-delivery modalities.

#### 2.4: Anti-cancer lectins

Lectins are a diverse group of carbohydrate-binding proteins that have garnered much interest for their potential immunomodulating and cancer-targeting abilities. In recent years, a great number of fungal and plant lectins with anti-cancer activity have been isolated, characterized, and described in the literature [178, 179]. Plant lectins in particular have been historically important as alternative or adjuvant therapies for cancer especially in Europe, where arguably the most well-known is a lectin-containing extract from European mistletoe (*Viscum album*). One of the active ingredients in the extract, viscummin (also called mistletoe lectin or ML), is a holotoxin consisting of a single ribosome-inactivating A chain and a single sialic acid-specific lectin B chain covalently linked with a disulfide bond [180, 181]. Though a comprehensive systematic review of the use of mistletoe extract in addition to chemotherapy concluded that it offered no additional benefit in terms of survival or quality of life, isolated viscummin may still have useful anti-cancer activity *in vivo* [182-184]. To this end, Gengenbach et al. recently published the expression and purification of recombinant viscummin in *N. benthamiana*, with a yield of  $\approx 7$  mg/kg fresh weight. The plant-derived lectin exhibited greater cytotoxicity to THP-1 cells than *E. coli*-made viscummin and was significantly more cost

effective to produce [185]. While promising, further *in vitro* and *in vivo* studies are warranted to demonstrate efficacy in multiple models and to demonstrate the selectivity of viscumin for cancer over healthy tissue. Additionally, improvements in yield are necessary to facilitate preclinical development.

Cholera toxin B subunit (CTB) is a non-toxic lectin component of the holotoxin that recognizes the Gal $\beta$ 1–3GalNAc moiety of GM1 ganglioside found on the surface of intestinal epithelial cells (where the toxin normally exerts its activity). We have recently demonstrated that oral administration of a CTB variant (containing a KDEL endoplasmic reticulum retention motif) produced in *N. benthamiana* can facilitate mucosal healing and reduce tumorigenesis in a colitis-associated colorectal cancer mouse model [186].

Epidemiological evidence has pointed to an increase in colorectal cancer incidence in inflammatory bowel disease patients [187, 188]. Thus, the plant-made CTB variant as a treatment for chronic intestinal inflammation may also have anti-cancer properties that should be investigated further.

Lastly, aberrant glycosylation has been recognized a hallmark of cancer, and in particular high-mannose glycans have been demonstrated to be over-represented in the glycocalyx of many human cancers [189, 190], making them a potentially useful biomarker or druggable target [191]. Our lab has recently developed Avaren-Fc, a plant-produced “lectibody” targeting a cluster of high-mannose glycans that are widely found on the surface of enveloped viruses and malignant cells [98, 192]. While originally developed as an anti-HIV agent, we observe that Avaren-Fc also has strong anti-cancer activity *in vitro* and in human cancer cell xenograft and syngeneic mouse models (Dent

and Matoba, unpublished), highlighting the druggability of HIV- and tumor-associated high-mannose glycans.

## 2.5: Conclusions

Transient expression of proteins in plants is a powerful method for the rapid, robust production of recombinant proteins, which will significantly facilitate the preclinical development of biosimilar, biobetter and innovator anti-cancer proteins as well as vaccines. PVNs show promise as immunostimulatory agents, drug delivery platforms and imaging probes. Since aberrant protein glycosylation is a hallmark of cancer [2, 193], plant-derived lectins and their derivatives such as “lectibodies” may have unique potential as cancer biologics.

As regulatory frameworks for plant-based biomanufacturing system are becoming well established [142, 194-197], the technology has finally come of age. In addition to transient expression, other technologies based on transgenic plants and plant-cell culture offer some potential advantages that may facilitate the commercialization of plant-made biologics. Transgenic plants, for instance, offer greater scalability and simpler upstream processing, while plant-cell culture is similar to existing platforms that are well-established in the pharmaceutical industry, allowing for the adaptation of conventional chemical engineering and regulatory approaches. Though there are still challenges to be addressed in regard to plant growth conditions, transgene expression regulation, post-translational modifications, and product isolation and recovery, we will soon witness some plant-made cancer biologic products being tested for their clinical efficacy – the

most important step that will further cement plants as a viable alternative to other more established production methods.

## CHAPTER 3: METHODS AND MATERIALS

### **Animal studies**

The use of animals throughout this dissertation was approved by the University of Louisville's Institutional Animal Care and Use Committee (protocols 20714, 21910, 18910, and 15009). Studies conducted by PhoenixBio Co., Ltd., in their facilities were approved by its internal Animal Ethics Committee (resolution 2281). Regardless of study location, all animals were given a standard diet and water *ad libitum* and were housed in a temperature- and humidity-controlled facility with a 12-hour day/night cycle. Prior to the beginning of each study, animals were acclimated to their environment for one week.

### **Cell culture**

B16F10, Huh-7, HEK-293T, CAO3, SKOV3, A2780, and SW626 cells were acquired from the American Type Culture Collection (Manassas, VA) and cultured in high-glucose Dulbecco's Modified Eagle Medium (DMEM) containing L-glutamine and sodium pyruvate supplemented with 10% fetal bovine serum and 1X penicillin/streptomycin. The engineered Jurkat cells used in the ADCC reporter assay, which constitutively express human FcγRIIIa as well as firefly luciferase downstream of an NFAT response element, were obtained from Promega (Madison, WI) and cultured according to the manufacturer's protocol. The murine ovarian cancer cell lines ID8 and ID8-luciferase were a generous gift from the labs of Dr. Zong Seng at the University of

Pittsburgh School of Medicine and Dr. Steven Fiering at the Geisel School of Medicine at Dartmouth University. ID8 cells were cultured in DMEM containing L-glutamine and sodium pyruvate supplemented with 4% FBS, 1X insulin-transferrin-selenium solution, and 1X penicillin and streptomycin. ID8-luciferase cells were additionally maintained with 1 µg/mL blasticidin. Each cell line was tested for mycoplasma using ATCC's Universal Mycoplasma Detection Kit, and to prevent contamination between tests the antibiotic Normocin™ (Invivogen, San Diego, CA) was routinely added to the culture medium according to the manufacturer's specifications. All cell lines were maintained at 37°C with a 5% CO<sub>2</sub> atmosphere.

### **Plant growth**

*Nicotiana benthamiana* was grown in a temperature-controlled room kept at a low humidity, with fluorescent lighting timed to a 16/8-hour day/night cycle. Plants were seeded into new 4-inch pots containing damp Jiffy Coco Mix, with 3-5 seeds per pot. Following seeding, plants were fertilized with diluted Peters Peat-Life Special 17-3-17 (nitrogen-phosphate-potash) fertilizer, covered with plastic wrap and allowed to germinate for 12 days, after which they were thinned and separated to a lower growth density. Fertilization and watering continued every other day until 4 weeks of age, at which point plants were ready for agroinfiltration.

### **Expression in and purification of Avaren-Fc and variants from *N. benthamiana***

Table 1 summarizes the variants of AvFc used throughout this dissertation. Each variant was expressed in and purified from wild type *N. benthamiana* plants with the

exception of AvFc<sup>ΔXF</sup>, which was expressed in a glycoengineered line of plants containing RNAi knockdowns of β1,2-xylosyltransferase and α1,3-fucosyltransferase, which are hereafter referred to as ΔXF plants. Recombinant expression in plants was performed by agroinfiltration using the deconstructed tobacco-mosaic-virus-derived three-component vector system magnICON<sup>®</sup> and purified with Protein A and ceramic hydroxyapatite (CHT) resins on an ÄKTA Pure fast protein liquid chromatography (FPLC) system (Cytiva Life Sciences, Marlborough, MA). The three-component vector system consists of 3 modules: a 5' plasmid that contains promoter elements, a 3' plasmid that contains the gene of interest (in this case AvFc) as well as terminator elements, and an integrase plasmid which combines the two *in planta* to create an RNA replicon which drives the high-level expression of the target gene. Each of these plasmids is maintained in separately transformed *Agrobacterium tumefaciens* GV3101 lines, which are combined prior to agroinfiltration of leaf tissue. In addition to this, each variant of AvFc has an N-terminal signal peptide derived from rice α-amylase to direct nascent peptides to the ER for processing in the endomembrane system.

For agroinfiltration, 3 transformed *A. tumefaciens* GV3101 1 mL frozen stocks, each containing one of the aforementioned plasmids, were individually cultured overnight at 30°C in 150 mL of LB medium containing rifampicin (50 µg/mL) and carbenicillin (100 µg/mL). The following morning, bacteria were collected by centrifugation at 6000 xg for 10 minutes, and the culture medium was decanted and replaced with 15 mL of MES agroinfiltration buffer (10 mM MES hydrate, 10 mM MgSO<sub>4</sub> heptahydrate, pH 5.5). The concentration of bacteria in this buffer was determined by measuring the optical density at 600 nm (OD<sub>600</sub>) on a Nanodrop One C

(Thermo Fisher Scientific, Waltham, MA). Each of the three bacterial solutions was then diluted in 5 L to a final OD<sub>600</sub> value of 0.03, making the total OD<sub>600</sub> of the final agroinfiltration solution  $\approx$  0.1. This mixture was then introduced to *N. benthamiana* leaf tissues using the vacuum method [198]. Briefly, plants were submerged in the agroinfiltration buffer inside a vacuum tank under a vacuum for 3-5 minutes to draw air out of the leaf tissues, at which point the chamber was slowly repressurized to force the buffer into the interstitial spaces. Infiltrated plants were placed back into the growth chamber and maintained as described above for 7 days.

After incubation in the growth chamber, leaf tissues were harvested, weighed, and homogenized in an extraction buffer (20 mM NaPi, 40 mM ascorbic acid, pH 7) at a ratio of 2 mL of buffer per gram of tissue weight using a stainless-steel blender. Crude extract was first filtered using a layer of cheesecloth and miracloth, then the pH of the filtrate was lowered to  $\approx$  5.2 using HCl and clarified by centrifugation at 15,000 xg for 10 minutes at 4°C. The clarified supernatant was decanted and neutralized with NaOH, then clarified again in the same manner before being filtered through a 0.2  $\mu$ m vacuum filter. This material was then applied to a protein A column at a flow rate calculated to allow for a 2-minute residence time with the resin. Unbound material was washed away using 10 column volumes (CVs) of 5 mM NaPi at pH 7 and elution was performed using 10 CVs of 2 M arginine at pH 3, which was applied to the column in a single step and collected into 5 mL fractions and neutralized with 1 M tris base.

Elution fractions containing protein, as determined by the FPLC system's spectrophotometer, were combined and diluted 20x with deionized water before being applied to a CHT column at a flow rate calculated to provide a 2-minute residence time

with the resin. The columns were washed with 10 CVs of 5 mM NaPi at pH 7 and eluted with a gradient from 5 mM NaPi and no salt to 5 mM NaPi with 1 M NaCl over 10 CVs, collected into 5 mL fractions. Columns were stripped with 5 CV of 5 mM NaPi and 2 M NaCl before being cleaned with and stored in 0.1 M NaOH. Fractions containing protein were then combined and concentrated on a 30 KDa MWCO centrifuge filter (Millipore Sigma, Burlington, MA) before endotoxin removal by phase separation (see below). Endotoxin-free protein was then formulated into a histidine buffer (30 mM histidine, 100 mM sucrose, 100 mM NaCl, see below for details) on a 30 KDa MWCO centrifuge filter before being filter sterilized and stored at -80°C. The purity of the protein was confirmed by SDS-PAGE and densitometry analysis (see below).

<b>Variant</b>	<b>Description of variant</b>	<b>Function</b>
AvFc <sup>WT</sup>	Normal AvFc expressed in wild type <i>N. benthamiana</i> plants. Displays plant-specific glycans containing $\beta$ 1,2-xylose and $\alpha$ 1,3-fucose at the C <sub>H2</sub> N-glycan site (N200).	“Normal” function
AvFc <sup><math>\Delta</math>XF</sup>	Expressed in a stable $\Delta$ XylT/ $\Delta$ FucT RNAi knockdown line of <i>N. benthamiana</i> plants ( $\Delta$ XF) [133]. Contains primarily terminal GlcNAc residues (GnGn) and lacks plant-specific glycans.	Increased ADCC activity
AvFc <sup>CHO</sup>	Expressed and purified from Chinese hamster ovary (CHO) cell culture. Contains mammalian glycans (importantly, core $\alpha$ 1,6-fucose).	“Normal” function
AvFc <sup><math>\Delta</math>gly</sup>	A single asparagine to glutamine substitution (N200Q) which renders the C <sub>H2</sub> domain of AvFc aglycosylated.	Disables Fc-mediated effector functions
AvFc <sup><math>\Delta</math>lec</sup>	A series of three point mutations in the lectin Avaren (Y32A, Y70A, Y108A). May also be referred to as AvFc <sup>lec-</sup> .	Removes high-mannose binding activity

**Table 1. Definition and description of AvFc variants used in these studies.**

### **Endotoxin separation by phase separation**

Endotoxin was removed from proteins using triton X-114 phase separation. The detergent was first added to the protein solution to a final concentration of 2%, mixed vigorously, and then incubated on ice for 30 minutes. Samples were then incubated at 37°C for 10 minutes and centrifuged at the same temperature at max speed for 20-30 minutes. The aqueous endotoxin-poor layer was removed by careful pipetting. To remove residual detergent, 5 g of Bio-Beads (Bio-Rad Laboratories, Hercules, CA) per 25 mL of solution was then added and incubated at room temperature for 2 hours. The protein sample was then removed by pipetting and endotoxin levels were measured using the Limulus Amebocyte Lysate test on an Endosafe PTS system (Charles River, Wilmington, MA).

### **Glycan analysis**

The N-linked glycans were released from 1 mg of purified recombinant AvFc by hydrazinolysis (Fujiyama et al., 2006). After N-acetylation with saturated sodium bicarbonate and acetic anhydride, the hydrazinolysate was desalted using Dowex 50 × 2 (Muromachi Kagaku Kogyo Kaisya, chuo-ku, Tokyo, Japan), and lyophilized. The oligosaccharides obtained were pyridylaminated (PA) as described previously (Kondo et al., 1990; Fujiyama et al., 2006). PA-sugar chains were purified by HPLC and monitored on the basis of the fluorescence intensity ( $\lambda_{exc} = 310 \text{ nm}$ ,  $\lambda_{em} = 380$ ). For RP-HPLC, PA-sugar chains were eluted from a Cosmosil 5C18-AR-II column (Nacalai Tesque, Nakagyo-ku, Kyoto, Japan) by linearly increasing the acetonitrile concentration in 0.02% trifluoroacetic acid (TFA) from 0% to 4% for 35 min at a flow rate of 1.2 mL/min. For

SF-HPLC, using an Asahipak NH2P-50 4E column (Showa Denko), the PA-sugar chains were eluted by linearly increasing the water content of the water–acetonitrile mixture from 26% to 50% for 20 min at a flow rate of 0.7 mL/min.

### **SDS-PAGE analysis of AvFc**

Purity of AvFc was determined by SDS-PAGE using 4-20% Bio-Rad Mini-PROTEAN™ gels and Coomassie Brilliant Blue (CBB) staining. 10-15 µg of protein was mixed with Laemmli sample buffer and run in a tris-glycine-SDS running buffer (25 mM tris, 192 mM glycine, 0.1% SDS, pH ≈ 8.5) at 200 V for 35 minutes under denatured and reducing or non-reducing conditions (with or without 1% 2-mercaptoethanol). After gels were removed from their cassettes they were washed with water and stained for 20 minutes with Coomassie stain (0.3% Coomassie Brilliant Blue, 45% methanol, 10% acetic acid). Stained gels were washed and placed in a destaining buffer (12% ethanol, 10% acetic acid), heated for 1 minute in a microwave, and left to destain with gentle agitation until the background was clear. Gels were imaged on an Amersham Imager 600 (Cytiva Life Sciences). Densitometry analysis to estimate purity was performed using Gel Analyzer software ([www.gelanalyzer.com](http://www.gelanalyzer.com), by Istvan Lazar, Jr., and Istvan Lazar, Sr.).

### **Hepatitis C neutralization assay**

To produce cell-culture-derived hepatitis C virus (HCVcc), we used a modified version of the plasmid encoding a genotype 2a virus JFH1 genome backbone provided by Dr. Takaji Wakita from the National Institute of Infectious Diseases in Tokyo, Japan [199]. The H77/JFH1 genotype 1a/2a chimeric virus was generated as described by

Maurin et al. [200]. Chimeras from genotype 4a (ED43/JFH1), genotype 5a (SA13/JFH1), and genotype 6a (HK6a/JFH153) were provided by Dr. Jens Bukh from the University of Copenhagen in Copenhagen, Denmark [201-203]. Viral pseudoparticles (HCVcc) using an HIV-derived lentivirus backbone and bearing the envelope glycoproteins from genotype 2a JFH1 strain, as well as expressing the Firefly luciferase reporter gene, were produced in HEK-293T as previously described [204]. The inhibitory effects of AvFc were determined by quantifying its impact on infectivity with indirect immunofluorescence of infected Huh-7 cells, using the anti-E1 monoclonal antibody A455 or an anti-NS5A polyclonal antibody kindly provided by Dr. Mark Harris from the University of Leeds in Leeds, UK to identify and count infected foci. IC<sub>50</sub> values were calculated by 4 parameter non-linear regression.

### **Optimization of AvFc formulation buffer**

In order to determine a more suitable buffer for drug stability and *in vivo* studies, we performed an initial buffer screening of AvFc in 30 mM glutamate, acetate, citrate, succinate, histidine, tris, and phosphate buffers with pH values ranging from pH 4.5-7.5. These buffers are summarized in Table 3. All buffer agents were acquired from Millipore-Sigma (Burlington, MA). For each buffer, AvFc was diafiltrated using a 30 KDa MWCO centrifuge filter and adjusted to a final concentration of 1 mg/mL ( $\approx$  13  $\mu$ M). Stability in these initial conditions was determined by SDS-PAGE after incubation for 2 weeks at 37°C. Melting temperatures of AvFc were determined by differential scanning fluorimetry (DSF) which was performed on an Applied Biosystems StepOnePlus qPCR system. Using a 96-well template, AvFc in various buffers was made

to a concentration of 50  $\mu\text{M}$  and mixed with 50x SYPRO Orange dye (Thermo Fisher Scientific) before slowly heating to 98°C, which exposes hydrophobic regions in the protein and allows the fluorescent dye to bind. The melting temperature was defined as the vertex of the first derivative of the relative fluorescence values in the resulting melt curves. To compare the stability of AvFc in the optimized histidine buffer and in PBS, the drug was formulated in each buffer to a concentration of 10 mg/mL ( $\approx 130 \mu\text{m}$ ) and incubated at 4°C or room temperature. Measurements of the absorbance at 280 nm and 600 nm were made prior to incubation, at 16 hours, and again after 72 hours.  $A_{280}$  measurements were made after centrifuging any precipitates. Accelerated degradation was assessed by overnight incubation of AvFc in either buffer at 56°C and SDS-PAGE.

### **Pharmacokinetic analyses**

A pharmacokinetic profile for AvFc <sup>$\Delta\text{XF}$</sup>  was generated following a single 25 mg/kg intraperitoneal injection in male and female C57bl/6 mice (The Jackson Laboratory, Bar Harbor, ME). Equal numbers of males and females were used, with n=4 animals per time point. Blood was sampled at 0.5, 1, 2, 4, 8, 12, 24, and 48 hours after injection by either submandibular vein or cardiac puncture. The pharmacokinetics of AvFc<sup>WT</sup> were separately assessed in both male and female C57bl/6 mice using a modified version of the protocol described by Joyce et al. [205]. AvFc was administered intravenously at a dose level of 10 mg/kg followed by blood sampling via tail vein at regular intervals (0.5, 1, 3, 9, 24, and 72 hours). For serial tail blood sampling, animals were warmed under a heat lamp and a 25 G needle was used to prick the vein beginning at the most distal end of the tail and moving more proximally for each subsequent

sample. Using a glass microcapillary tube (Drummond Scientific Company), 10  $\mu$ L was collected and mixed into 90  $\mu$ L of an anticoagulant solution containing DPBS and 1.5 mg/ml Na<sub>2</sub>EDTA. Diluted blood was then spun down at 1500 g for 10 minutes. The concentration of AvFc in the serum for both variants was then determined by gp120 ELISA (described below) using purified AvFc as a standard. Pharmacokinetic parameters for both were calculated from these measurements using PK Solver [206].

### **Hepatitis C challenge and toxicological analysis of AvFc in PXB-mice<sup>®</sup>**

The mouse model of toxicological analysis and HCV infection and toxicological analysis was performed in PXB-mice<sup>®</sup> (cDNA-uPA<sup>wild/+</sup>/SCID, cDNA-uPA<sup>wild/+</sup>; B6;129SvEv-Plau, SCID: C.B-17/Icr-*scid/scid* Jcl; reviewed in: [207]) by PhoenixBio Co. These mice contain transplanted human hepatocytes with a replacement index of greater than 70% as determined by blood human albumin (h-Alb) measurements prior to virus inoculation [208]. Blood h-Alb levels indicate the level and integrity of human hepatocyte engraftment in the mouse liver. Mice were separated into 3 treatment groups: AvFc<sup>lec-</sup> (25 mg/kg, n=5) for 11 doses, or AvFc (25 mg/kg, n=5 each) for 8 or 11 doses. The initial treatment was co-administered i.p. with virus inoculation ( $5 \times 10^5$  copies/kg) on day 0 with a genotype 1a strain (PBC002), and treatment continued every other day thereafter. The general conditions and body weights of the animals were monitored every other day, while serum HCV RNA and blood h-Alb were measured every 7 days by RT-PCR and latex agglutination immunonephelometry (LZ Test “Eiken” U-ALB, Eiken Chemical Co., Ltd.) respectively. The HCV RNA RT-PCR assay was developed based on a method described by Takeuchi et al. [209] with modifications and validated by PhoenixBio for

use in this animal model. The lower limit of quantification was determined to be  $4.0 \times 10^4$  copies/mL. Serum alanine aminotransferase 1 (ALT) levels were determined either using a Fujifilm DRI-CHEM NX500sV clinical chemistry instrument or by ELISA (Institute of Immunology Co., Ltd., Tokyo, Japan). At the study termination on day 35, animals were euthanized and subject to gross necropsy and general health. Blood was also drawn via cardiac puncture and used for ALT, HCV RNA, and h-Alb analyses.

### **Histopathologic analysis of liver tissues**

Hematoxylin and eosin-stained liver sections from 3-4 mice per group were generated by Nara Pathology Research Institute Co., Ltd. (Nara, Japan) and evaluated by pathologists at SkyPatho, LLC. All slides were examined by a blinded, board-certified veterinary pathologist under a light microscope (BX43, Olympus Corporation, Tokyo, Japan). The tissues were assigned a severity score for a number of characteristics based on the 5-point scoring system of the CDISC SEND Controlled Terminology where 0: unremarkable, 1: minimal, 2: mild, 3: moderate, 4: marked; 5: severe; and P: present.

### **Detection of AvFc using a gp120-coated capture ELISA**

Recombinant envelope glycoprotein gp120 from HIV-1 (strain CM235, NIH Aids Reagent Program) was coated overnight at 4°C at 0.3 µg/mL in carbonate buffer, pH 9.5. After coating, wells were blocked with PBST containing 5% dry milk for 1 hour at 37°C. AvFc variants were then incubated on the plate beginning at 13 nM with 1:5 serial dilutions for 1 hour at 37°C, followed by detection with a goat anti-human IgG-HRP (Southern Biotech 2040-05, Birmingham, AL). Plates were developed for 5 minutes with

TMB substrate (VWR 95059-286), with development stopped with an equal volume of 2 N sulfuric acid and plates read at 450 nm. To measure the concentration of AvFc in serum, purified AvFc at 13 nM with 1:5 serial dilutions was used as a standard curve and compared to serial 1:10 dilutions of serum. Dose-response curves were fit with 4-parameter non-linear regression in GraphPad Prism which were used to calculate EC<sub>50</sub> values or to interpolate unknown values.

### **Flow cytometry to assess cancer cell binding**

B16F10 and other cancer cells were harvested and stained with AvFc variants at 150, 15, and 1.5 nM followed by detection with a goat anti-human Fc FITC secondary antibody (Abcam, Cambridge, UK) at 1:200 and fixation in 4% formalin. Unstained cells incubated with the secondary antibody only and AvFc<sup>Δlec</sup> (150 nM) were used as controls to determine background. To detect anti-tumor antibodies, B16F10 cells were stained with a 1:10 dilution of animal serum followed by detection with a 1:1000 dilution of a goat anti-mouse Fc FITC secondary (Abcam) and fixation with 4% formalin. Flow cytometry was performed on a BD FACSCalibur and all data were analyzed in FlowJo. Statistical comparisons were made with One-way ANOVA followed by multiple comparisons with Tukey's multiple comparison test.

### **ADCC reporter assay**

B16F10 and other cancer cells were plated at 10,000 cells/well on a solid white 96-well plate and incubated overnight at 37°C to allow attachment. The following day AvFc or its variants were serially diluted (from 650 nM to 8.32 pM in 1:5 steps) in

ADCC assay buffer, which consisted of RPMI-1640 medium supplemented with 1% Ultra Low IgG Fetal Bovine Serum (VWR) and added to the wells. To determine the effect of ADA-containing serum on ADCC activity, serum was added to the assay buffer to a concentration of 5%. To determine ADCC activity of ATAs in serum, 1:5 serial dilutions of serum were made beginning from 5%. Jurkat effector cells, which were also suspended in ADCC assay buffer, were then added to each well to give a total effector:target cell ratio of 15:1 (150,000 cells) and incubated overnight. After incubating, culture medium was carefully removed, and luminescence was measured on a BioTek plate reader using the Britelite Plus Reporter Gene Assay System (Perkin Elmer, Waltham, MA). Each assay included a no drug control and a cell only control, with and without 5% serum as necessary. Fold luminescence induction was plotted against the log drug concentration and was calculated as the ratio between the relative luminescence units (RLUs) of the wells containing drug and the average RLU values for the no drug control. The resulting dose-response curves were fit with a 4-parameter non-linear regression model in GraphPad Prism to calculate the  $EC_{50}$ .

### **MTS cell viability assay**

B16F10 cells were plated at 5,000 cells per well and incubated with AvFc (beginning at 650 nM with 1:5 serial dilutions) for 48 hours. The toxic mannose-binding lectin Concanavalin A was used in equimolar concentrations as a positive control. After incubation, 20  $\mu$ L of MTS reagent (Abcam) was added to each well and incubated for 4 hours, at which point the reaction was stopped by adding 10  $\mu$ L of 10% SDS. Plates were then read in a BioTek plate reader at 490 nm. Percent viability was calculated relative to

untreated controls and plotted against concentration. Dose-response curves were fit using non-linear regression in GraphPad Prism to calculate IC<sub>50</sub> values.

### **Annexin V/propidium iodide staining of apoptotic cells**

B16F10 cells ( $1.5 \times 10^5$  cells/well) were seeded into 6 well plates with AvFc variants or concanavalin A at 650 nM and incubated for 48 hours at 37°C. Following incubation cells were harvested and stained with an annexin V-488A (ANXV) conjugate and propidium iodide (PI) according to Rieger et al. [210]. Briefly, cells were stained with 2.5 µg/mL annexin V conjugate and 2 µg/mL PI for 15 minutes each at room temperature in the dark. Following fixation with a 1% formalin solution, cells were incubated with 50 µg/mL RNase A and measured on a BD FACSCalibur flow cytometer. Apoptotic cells, in the early and late stages, were defined as ANXV+/PI- and ANXV+/PI+, respectively, with unstained cells used to define the quadrant gates. Data were processed and analyzed using FlowJo, and statistical comparisons between groups were made with 2-way ANOVA with  $p=0.05$  as the threshold of significance.

### **Surface plasmon resonance for FcγR binding**

Surface plasmon resonance experiments were performed on a Biacore T200 (Cytiva Life Sciences). Binding affinity of AvFc for human FcγRIIIa (hFcγRIIIa) and mouse FcγRIV (mFcγRIV) was assessed using a 6xHis-capture approach. To achieve this, an anti-6xHis-tag monoclonal antibody (Thermo Fisher Scientific) at 50 µg/mL was conjugated via amine linkage to two parallel flow cells on the surface of a CM5 chip at  $\approx$  10,000 response units (RUs). Recombinant Fc receptors obtained from R&D Systems

were captured by flowing them over the chip surface at 5  $\mu\text{g}/\text{mL}$  for 60 seconds with a flow rate of 10  $\mu\text{L}/\text{min}$ . A second flow cell was used for reference subtraction and was not used to capture the receptors. AvFc variants ( $\Delta\text{XF}$ , WT,  $\Delta\text{gly}$ ) were flowed over both cells at multiple concentrations with a flow rate of 30  $\mu\text{L}/\text{min}$ , using an association time of 240 seconds and a dissociation time of 600 seconds. For both hFc $\gamma$ RIIIa and mFc $\gamma$ RIV, 5 concentrations of AvFc were used to measure affinity starting at 2  $\mu\text{M}$  with 1:2 serial dilutions, repeating the middle concentration and including a blank cycle. Regeneration was performed by washing the chip surface for 60 seconds at a flow rate of 30  $\mu\text{L}/\text{min}$  with glycine at pH 1.5. Sensorgrams were fit with a 1:1 binding model with  $R_{\text{max}}$  set to fit local using the Biacore Evaluation software.

For hFc $\gamma$ RI, recombinant receptor was captured on the surface of an NTA-conjugated chip following a 60 second injection of  $\text{Ni}^{2+}$  at 0.5 mM. The receptor was captured by flowing at 10  $\mu\text{L}/\text{min}$  at a concentration of 1  $\mu\text{g}/\text{mL}$  for 100 seconds to achieve a capture level of  $\approx 200$  RUs. A second flow cell was left blank for reference subtraction. 5 concentrations of AvFc were used to measure affinity starting at 324 nM with 1:3 serial dilutions, repeating the middle concentration and including a blank cycle. Regeneration was performed by washing the chip surface for 60 seconds at a flow rate of 30  $\mu\text{L}/\text{min}$  with 350 mM EDTA. Sensorgrams were fit with a 1:1 binding model with  $R_{\text{max}}$  set to fit local using the Biacore Evaluation software.

### **PET/CT imaging**

The *in vivo* tumor-targeting property of AvFc was determined with radiolabeled AvFc ( $^{64}\text{Cu}$ -NOTA-AvFc) in B16F10 melanoma-bearing C57bl/6 mice using small

animal PET/CT. The mice (n = 2) were each subcutaneously inoculated with  $1 \times 10^6$  B16F10 cells on the right flank to generate tumors. The animals were submitted to imaging when tumor weights reached approximately 0.2 g at 10 days post-cell inoculation. Approximately 3.7 MBq of purified  $^{64}\text{Cu}$ -AvFc was injected into each mouse via the tail vein. The mice were scanned with small animal PET and CT at 24 h post-injection. A ten-minute CT scan (MicroCAT II) was immediately followed by 30 min PET imaging on MicroPET (Siemens R4) using the same animal bed. The PET and CT data obtained were reconstructed and merged by the Siemens IRW software.

### **B16F10 flank tumor challenge model**

On day 0, 100,000 B16F10 cells in 100  $\mu\text{L}$  of DPBS was injected subcutaneously into the hind left flank of each C57BL/6 mouse. Intraperitoneal administration of 200  $\mu\text{L}$  of AvFc, AvFc<sup>N200Q</sup>, or vehicle (AvFc formulation buffer, see above) at the indicated dose level began on day 5 and continued Q2D until day 16. Tumor measurements were taken every other day from day 1 using digital calipers, and tumor volume was estimated as: *tumor width x tumor height*<sup>2</sup>.

To determine the impact of anti-drug antibodies on the efficacy of AvFc in this model, groups of animals were pre-pretreated with 6 doses of AvFc at 25 mg/kg Q2D followed by tumor implantation 11 days after the final dose (day 21). Treatment with AvFc was then performed as before, beginning on day 5 and continuing Q2D for a maximum of 6 doses. The primary endpoint was survival, defined as the time until animals reached a tumor volume of 1500 mm<sup>3</sup>, at which point the animal was euthanized. Blood was collected to determine anti-drug antibody titers on day -1 and day 20 via

submandibular vein before pretreatment and before B16F10 implantation, and again via cardiac puncture at the time of euthanasia. Survival curves were compared using the Mantel-Cox test in GraphPad Prism. Multiple comparisons of individual survival curves were made using the Mantel-Cox test, which was corrected using the Bonferroni method (corrected p value threshold was 0.0083).

### **Immunophenotyping of B16F10 tumor-infiltrating immune cells**

Immunophenotyping was performed with the assistance of Dr. Noel Verjan Garcia, who also performed the gating. B16F10 melanoma cells ( $1 \times 10^5$ ) were injected subcutaneously into the hind left flank of C57BL/6 ( $n=6/\text{group}$ ) mice pre-treated with AvFc $\Delta^{\text{XF}}$  at 25 mg/kg or vehicle (AvFc formulation buffer). Tumor measurements were taken every day by using digital calipers until the tumor volume reached  $500 \text{ mm}^3$ , at this time the animals were euthanized, and the tumors dissected, weighed, and minced for cell isolation. The minced cell suspension was digested in complete RPMI medium containing 2.5 mg/mL of Collagenase type IV (ThermoFisher Scientific) and 40  $\mu\text{g/mL}$  of DNase I (MilliporeSigma, Saint Louis, MO) at 37 °C for 20 min under shaking conditions (200 rpm). Subsequently, the cells suspension was passed through a 40  $\mu\text{m}$  cell strainer and the cell pellet resuspended and washed twice with FACS buffer, the cells were counted and incubated with 20  $\mu\text{g/mL}$  of mouse gamma globulins to block FC-gamma receptors. A total of  $1 \times 10^6$  Cells were stained for 30 min with 2  $\mu\text{g/mL}$  of different combination of the following fluorochrome-labeled antibodies: anti-CD45eFluor450 or anti-CD45-FITC (30-F11), anti-CD3-FITC (17A2), anti-CD3-APC (17A2), anti-CD161 (NK1.1)-BV605 (PK136), anti-CD49b-PE (DX5), anti-CD107-

AlexaFluor700 (1D4B), anti-CD335 (NKp46)-BV650 (29A1.4), anti-CD16.2-PE-Dazzle 594 (9E9), anti-CD11b-APC-Cy7 (M1/70), anti-CD11c-PE (N418), anti-IA-IE-BV421 (M5/114.15.5), anti-F4/80-PE-Cy7 (BM8), anti-Ly6G-APC (1A8), antiLy6C-AlexaFluor700 (HK1.4), anti-CX3CR1-BV605 (SA011F11), anti-CD206-BV650 (C068C2), anti-CD103-PE-Dazzle 594 (QA17A24), anti-CD80-BV605 (16-10A1), anti-CD69-BV650 (H1.2F3), anti-CD68-AlexaFluor700 (FA-11), anti-CDC86-PE-Dazzle 594 (GL-1), anti-CD4-BV605 (RM4-5), anti-CD8-BV650 (53-6.7), anti-IFN $\gamma$ R $\beta$ -APC (MOB-47), anti-CD69-FITC (H1.2F3), anti-IL-33R-PE-Dazzle 594 (DIH4), anti-CD62L-APC-Cy7 (MEL-14), anti-TCR $\beta$ -PE-Cy7 (H57-597), anti-IL23R-BV421 (12B2B64) and anti-TCR $\gamma/\delta$ -PE (UC7-13D5). After two washing steps the cells were incubated with 7-aminoactinomycin D for 15 minutes and analyzed with a BD LSRFortessa<sup>TM</sup> flow cytometer. Data were processed with FlowJo software.

### **Calculation of anti-drug antibody titers**

Anti-drug antibody titers were measured by ELISA. AvFc was coated on a 96-well plate at 1  $\mu$ g/mL overnight at 4°C, followed by blocking for 1 hour with 3% BSA-PBST at room temperature. Mouse serum was plated at a minimum dilution of 1:50 and serially diluted further with 1:10 dilutions, followed by a 2-hour incubation at room temperature. Bound serum antibodies were then detected with a goat anti-mouse IgG-HRP secondary antibody (Southern Biotech, Birmingham, AL) at 1:10,000 for 1 hour at room temperature. Lastly, plates were developed with TMB substrate for 5 minutes and stopped with 2 N sulfuric acid prior to measuring the absorbance at 450 nm on a BioTek plate reader. Titers were interpolated using non-linear regression in GraphPad Prism,

with the cutoff value set at the limit of quantification for the assay (average absorbance of the blanks + 10 standard deviations). Statistical comparisons between groups were made using a Two-way ANOVA, while multiple corrections were made with the Tukey multiple comparisons test.

### **B16F10 metastasis challenge model**

On day 0, 250,000 B16F10 cells suspended in 100  $\mu$ L of DPBS was administered into each C57BL/6 mouse intravenously via the tail vein using a heat lamp to facilitate the injections. Intraperitoneal administration of 200  $\mu$ L of AvFc, AvFc <sup>$\Delta$ lec</sup>, or vehicle (AvFc formulation buffer, see above) at the indicated dose level began concurrently with tumor implantation and continued Q2D for a total of 6 doses (ending on day 10). Animals were monitored until day 21, at which point they were euthanized and their lungs removed for analysis. The tumor burden was calculated as the number of tumor nodules per lung per mouse. Statistical comparisons between treatment groups were made using the Kruskal-Wallis test, while multiple comparisons were made using Dunn's test.

### **Immunohistochemistry of human cancer tissues with AvFc**

IHC was performed on Ventana Discovery Ultra automated immunostainer (Ventana Medical Systems, Tucson, AZ) by US Biomax Inc. On-board antigen retrieval was performed with CC1, pH 8.0 for 56 minutes at 95C (Cat#950-124). Biocare Background Sniper was used for the blocking reagent (Cat #BS966, Biocare, Pacheco, CA) for 4 minutes and endogenous peroxidase was blocked by Discovery inhibitor (Cat#760-4840, Ventana) for 4 minutes. 5.0  $\mu$ g of the primary antibody was tagged with

digoxigenin using a Biocare Human-on-Human HRP-Polymer kit according to the manufacturer's instructions (Cat #BRR 4056K, Biocare). The tagged antibody was applied at a dilution of 1:100 and incubated for 36 minutes at 37°C.

Mouse anti-Digoxigenin from the Biocare kit was applied as the secondary antibody for 12 minutes at 37°C. This was followed by Anti-Mouse HQ (Cat#760-4814, Ventana) for 12 minutes at 37°C and Anti-HQ HRP (Cat#760-4820, Ventana) for 12 minutes at 37°C. Visualization was performed using ChromoMap DAB (Cat#760-159, Ventana). Nuclear counterstaining was applied with Ventana Hematoxylin II for 12 minutes followed by a Bluing reagent for 8 minutes. Slides were dehydrated, cleared, and mounted as in routine processing.

### **Identification of putative binding partners of AvFc on cancer cells**

Co-immunoprecipitation was used to isolate potential binding partners of AvFc on the surface of two human OVCA cell lines (SW626 and SKOV3) and one murine line (ID8). Co-immunoprecipitation was performed on AvFc- or AvFc<sup>Δlec</sup>-conjugated resins using the Pierce™ Co-Immunoprecipitation Kit (Thermo Fisher Scientific) according to the kit instructions. A single 75 cm<sup>2</sup> flask of cells were lysed using a buffer containing 1% NP-40 and 1X Halt™ protease and phosphatase inhibitor (Thermo Fisher Scientific) and centrifuged to separate debris from the lysate. The lysate was then pre-cleared with unconjugated agarose resin to remove any proteins that may bind non-specifically to the resin. It was then incubated with the conjugated resins for 2 hours at 4°C, after which the spin-tubes containing the mixture were placed in a spin column and washed 5 times with a neutral buffer provided by the manufacturer. Proteins bound to AvFc were eluted from

the column using a low pH buffer. Several elutions were performed, and each fraction was pooled together and neutralized with 1 M tris base prior to submission to the University of Louisville proteomics core for protein identification.

Protein samples were digested with trypsin (1:50 ratio) in a filter-aided sample preparation approach following reduction and alkylation with 100mM dithiothreitol and 50mM iodoacetamide. The tryptic digests (0.5 $\mu$ g) were separated using a Proxeon EASY n-LC (Thermo-Fisher Scientific) UHPLC system and Dionex (Sunnyvale, CA) 2cm Acclaim PepMap 100 trap and a 15cm Dionex Acclaim PepMap RSLC (C18, 2 $\mu$ m, 100 $\text{\AA}$ ) separating column. The eluate was introduced into an LTQ-Orbitrap ELITE (Thermo-Fisher Scientific) using a Nanospray Flex source and MS2 data collected in a data dependent fashion in a top-20 rapid CID method. All MS1 data were acquired using Fourier transform ion cyclotron resonance MS at 240,000 resolution and MS2 data using the linear ion trap. MSn data were searched using Proteome Discoverer 1.4 (Thermo Scientific) with Sequest HT (SageN) and Mascot, version 4.0 (Matrix Science) in a decoy database search strategy against UniProt Knowledgebase, Homo sapiens reference proteome. The searches were performed with a fragment ion mass tolerance of 1.0 Da and a parent ion tolerance of 50 ppm. The search data results file was imported into Scaffold, version 4.3.4 (Proteome Software Inc.) and filtered using a 2ppm mass error filter, removal of decoy hits, to control for <1.0% false discovery rates with PeptideProphet and ProteinProphet (Institute for Systems Biology). Peptide and protein identifications were accepted at >95.0% probability by the PeptideProphet or ProteinProphet algorithm. A comparison of protein abundance among the sample sets was conducted in Scaffold using the intensity based absolute quantification (iBAQ)

method or by normalizing the total spectra. Results were further refined using Gene Ontology (GO) terms to extract the most abundant membrane receptors, transporters, and adhesion molecules bound by AvFc and not AvFc<sup>lec-</sup>. The number of N-glycan sites for each protein were predicted using the NetNGly server from the Technical University of Denmark.

### **Orthotopic murine ID8-luciferase EOC challenge model**

The ID8-luciferase challenge model was performed using ID8-luciferase cells, which constitutively express the luciferase enzyme and are useful for bioluminescent monitoring of disease development. On day 0, 1 or 2x10<sup>6</sup> cells were injected in 200 µL of DPBS intraperitoneally to establish tumors. Intraperitoneal treatment of animals with either AvFc<sup>AXF</sup> at 25 mg/kg or a vehicle (AvFc formulation buffer, see above) began on day 7 and continued Q2D for 28 days. Disease progression was monitored through weekly measurements of abdomen circumference and body weight as well as by bioluminescent imaging, performed by the *In vivo* Molecular Imaging Core at the University of Louisville. Images were taken after injecting 150 mg/kg luciferin intraperitoneally and waiting 10 minutes for the substrate to disperse and generate signal. Animals were to be euthanized upon reaching 35 g or when moribund. The primary endpoint for these studies was survival. Survival curves were plotted and compared using the Gehan-Breslow-Wilcoxon test in GraphPad Prism. Multiple comparisons between curves were corrected for using the Bonferroni method, if necessary. Other statistical comparisons between body weights and abdomen circumferences were made with 2-way ANOVA.

CHAPTER 4: SAFETY AND EFFICACY OF AVAREN-FC LECTIBODY  
TARGETING HCV HIGH-MANNOSE GLYCANS IN A HUMAN LIVER CHIMERIC  
MOUSE MODEL

4.1: Introduction<sup>2</sup>

Hepatitis C virus (HCV) is an enveloped monopartite positive sense ssRNA virus in the family *Flaviviridae* and the causative agent of hepatitis C disease. Its genome encodes three structural (core, E1, E2) and seven non-structural proteins (p7, NS2, NS3, NS4A, NS4B, NS5A, NS5B) [212]. HCV is highly heterogenous and globally distributed, consisting of seven genotypes each further subdivided into multiple subtypes. Genotype 1 and 2 are the predominant genotypes worldwide and particularly concentrated in high-income and upper-middle income countries, whereas genotype 3 and 4 are more common in lower-middle and low-income countries [213]. In the United States, injection drug use represents the primary risk factor for contracting HCV infection [214, 215]. Around 15-25% of people acutely infected with HCV will clear the virus, while the remainder will develop chronic infection that can persist largely unnoticed for

---

<sup>2</sup> The following chapter was reproduced for this dissertation from “Safety and Efficacy of Avaren-Fc Lectibody Targeting HCV High-Mannose Glycans in a Human Liver Chimeric Mouse Model”, by Dent et al., with modifications made for presentability and formatting of text, figures, and tables. The original manuscript was published in *Cellular and Molecular Gastroenterology and Hepatology* in 2021 under a Creative Commons license [211]. The right to reproduce for a thesis/dissertation is retained by the author, as per publisher guidelines.

decades. Indeed, many HCV carriers discover their chronic infection after they have developed cirrhosis [216]. Chronic HCV infection is also associated with the development of hepatocellular carcinoma, and those with the disease are more likely to develop cryoglobulinemia and non-Hodgkin's lymphoma [217].

There is no vaccine currently available for HCV. Prior to 2011, the standard chronic HCV treatment was a non-specific antiviral medication using ribavirin combined with a pegylated interferon- $\alpha$ , which was associated with significant toxicity and limited treatment efficacy [218]. In 2011, the U.S. Food and Drug Administration approved the first generation of direct-acting antivirals (DAAs) for HCV: boceprevir and telaprevir, both of which inhibit the viral protease (NS3/4A) but required cotreatment with ribavirin and peginterferon [219, 220]. Further approval of more potent DAAs, such as NS3/4A, NS5B and NS5A inhibitors led to the development of oral ribavirin/peginterferon-free regimens [216]. Multi-DAA regimens achieve sustained virologic response (defined as a period of time with no viral RNA detection) rates as high as 100% and are less toxic and more tolerable than their predecessors [221-224]. While the cure rates are remarkable, there exist populations of patients who may not benefit from DAA therapy [225], especially patients with decompensated cirrhosis due to chronic HCV infection, for whom liver transplantation may be a last resort [226]. Moreover, recurrent infection occurs universally and rapidly post liver transplantation [227, 228], which increases the risk of accelerated cirrhosis, graft failure and death [229]. DAAs, by their nature, cannot prevent recurrent infection. Therefore, alternative or complementary therapies to DAAs that can block viral entry to target cells, such as antibodies or other molecules acting

alike, may need to be considered in these circumstances [229, 230]. However, there is currently no entry inhibitor approved for HCV treatment.

The HCV envelope proteins E1 and E2 are heavily glycosylated and, like glycoproteins of other enveloped viruses (HIV and the coronaviruses, for instance), have a high proportion of high-mannose-type *N*-glycans on their surface [40, 231, 232]. These glycans are typically processed to hybrid and complex forms on glycoproteins secreted by healthy cells [233]. Thus, the high-mannose glycans on the surface of HCV may be considered a druggable target. We have previously described the development of an high-mannose glycan-targeting lectin-Fc fusion protein, or “lectibody”, called Avaren-Fc (AvFc), which was shown to bind with high affinity to clusters of high-mannose glycans on the HIV envelope protein gp120 and effectively neutralize multiple HIV clades and groups including HIV-2 and simian immunodeficiency virus [98]. Further analysis indicated that AvFc can bind to HCV E2 protein [98]. Therefore, in this study, we aim to investigate the anti-HCV therapeutic potential of AvFc in *in vitro* neutralization assays and an *in vivo* HCV challenge study using PXB-mice®, a chimeric uPA/SCID mouse model transplanted with human hepatocytes (reviewed in: [207]).

## 4.2: Results

### 4.2.1: AvFc exhibits broad anti-HCV activity *in vitro*

Building on our previous observation that AvFc has affinity to a recombinant HCV E2 envelope protein [98], we first examined whether AvFc inhibits HCV infection *in vitro* using multiple genotypes of cell culture-produced virus (HCVcc) or pseudotyped virus (HCVpp). AvFc significantly blocked the infection of the human liver cell line

Huh-7 by HCVcc from genotypes 1a, 2a, 4a, 5a, and 6a, with 50% inhibitory concentration ( $IC_{50}$ ) values in the low nanomolar range (Table 2 and Figure 9A). Compared to Avaren monomer, AvFc overall showed approximately 2-log higher activity, while no inhibitory effect was observed for a plant-produced anti-HIV broadly neutralizing antibody VRC01 that shares the same human IgG1 Fc region with AvFc [234]. Additionally, Avaren and AvFc, but not VRC01, effectively neutralized HCVpp harboring a murine leukemia virus backbone, suggesting that the lectin and the lectibody act as an entry inhibitor (Figure 9B).

Virus	Genotype	Avaren IC <sub>50</sub> (nM)	AvFc IC <sub>50</sub> (nM)
JFH1/H77	1a	529.28 ± 158.78	1.69 ± 0.39
JFH1	2a	484.62 ± 109.16	1.69 ± 0.78
JFH1/ED43	4a	204.27 ± 1.65	2.85 ± 0.91
JFH1/SA13	5a	148.86 ± 2.48	2.33 ± 0.13
JFH1/HK6a	6a	114.95 ± 52.93	1.95 ± 0.78
<b>Average:</b>		<b>269.39 ± 65.00</b>	<b>2.10 ± 0.60</b>

**Table 2. IC<sub>50</sub> values for AvFc and Avaren against HCVcc.**

IC<sub>50</sub> = 50% inhibitory concentration derived from 4 parameter non-linear regression.

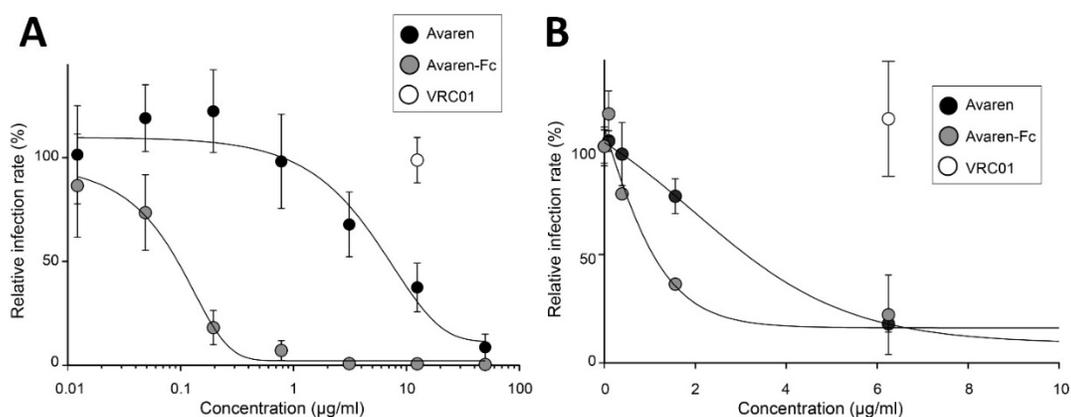


**Figure 9. *In vitro* HCV inhibition assays.**

(A) Avaren and Avaren-Fc (AvFc) inhibit cell culture derived HCV. JFH1 virus was preincubated with Avaren, AvFc or the control antibody VRC01 for 30 min at 37°C before incubation with Huh-7 cells. At 48 h post-infection, infected cells were quantified by indirect immunofluorescence with an HCV-specific antibody. Results are expressed as percentage of infection compared to a control infection in the absence of compound.

Error bars indicate standard errors of the mean (SEM) values from at least three independent experiments. (B) Avaren and AvFc inhibit HCV entry. Retroviral pseudotypes bearing HCV envelope glycoproteins of JFH1 virus (HCVpp) were

preincubated with Avaren, AvFc or the control antibody VRC01 for 30 min at 37°C

before incubation with Huh-7 cells. At 48 h post-infection, cells were lysed to quantify the luciferase activity. Results are expressed as percentage of infection compared to the control infection in the absence of compound. Error bars indicate SEM values from at least three independent experiments.

#### 4.2.2: Formulation of AvFc into a biocompatible buffer for *in vivo* studies

Previously, we found that AvFc has limited solubility in phosphate-buffered saline (PBS) at concentrations greater than 1 mg/mL (unpublished observation). To facilitate *in vivo* studies, we screened for an optimal liquid formulation for systemic administration that can impart improved stability and solubility to AvFc at higher concentrations. Initial buffer screening showed that AvFc is prone to degradation at and below a pH of 6.5, suggesting that AvFc is not stable in acidic pH conditions (Figure 10, Table 3). Further preformulation studies led us to identify an optimal buffer composed of 30 mmol/L histidine, pH 7.0, 100 mmol/L sucrose, and 100 mmol/L NaCl. Although AvFc showed comparable melting temperature in the histidine buffer and PBS in differential scanning fluorimetry ( $62.49^{\circ}\text{C} \pm 0.13^{\circ}\text{C}$  vs  $62.68^{\circ}\text{C} \pm 0.25^{\circ}\text{C}$ ) (Figure 11A), sodium dodecyl sulfate–polyacrylamide gel electrophoresis analysis showed that the lectin body holds superior stability in the histidine buffer upon accelerated stability testing via overnight incubation at  $55^{\circ}\text{C}$  (Figure 11B). When concentrated to approximately 10 mg/mL, AvFc remained stable in solution in the histidine buffer over 72 hours at  $4^{\circ}\text{C}$  and room temperature, while showed a significant concentration decrease concomitant with increasing turbidity in PBS (Figure 11C), further showing the histidine buffer's superiority for AvFc formulation.

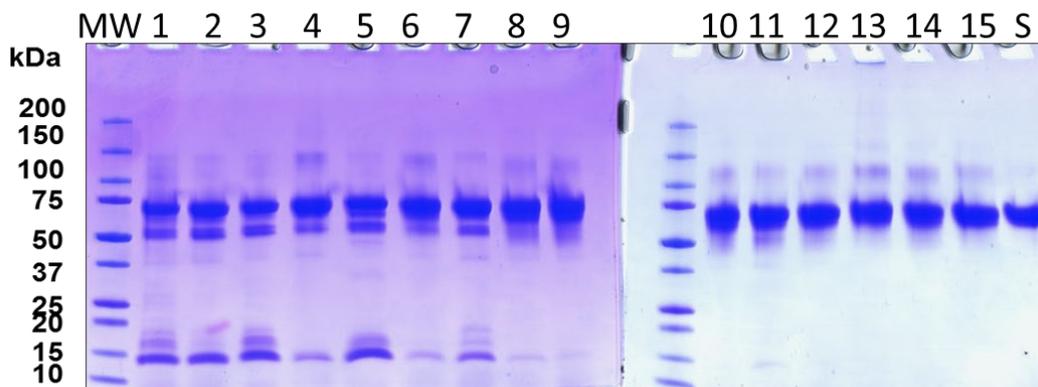


**Figure 10. Stability of AvFc in various buffers.**

The initial buffer screening was performed by incubating 1 mg/mL of AvFc at 37°C for 2 weeks in various buffers without any excipient (listed in Table 3), followed by sodium dodecyl sulfate–polyacrylamide gel electrophoresis analysis. The image shows a Coomassie Brilliant Blue–stained gel resolving 10 µg of AvFc from respective buffers, including glutamate at pH 4.5 (lane 1) and 5.0 (lane 2); acetate at pH 4.5 (lane 3) and 5.5 (lane 4); citrate at pH 5.0 (lane 5) and 6.0 (lane 6); succinate at pH 5.5 (lane 7) and 6.5 (lane 8); histidine at pH 6.0 (lane 9) and 7.0 (lane 10); phosphate at pH 6.5 (lane 11), 7.0 (lane 12), and 7.5 (lane 13); Tris at pH 7.5 (lane 14); and PBS (lane 15). At pH 6.0 and less (buffers 1–9), AvFc showed significant degradation after 2 weeks at 37°C. AvFc did not significantly degrade in buffers 10–15, and therefore these were chosen for further preformulation analysis. MW, molecular weight marker; S, standard AvFc control. SDS-PAGE was run by Dr. Krystal Hamorsky.

<b>Buffer</b>	<b>Formulation</b>	<b>pKa</b>	<b>pH</b>
30 mM glutamate	5.61 g/L sodium glutamate monohydrate	4.15	4.5*
30 mM glutamate	5.61 g/L sodium glutamate monohydrate	4.15	5.0*
30 mM acetate	2.46 g/L sodium acetate	4.76	4.5*
30 mM acetate	2.46 g/L sodium acetate	4.76	5.5*
30 mM citrate	350 mL 0.1 M citric acid monohydrate, 650 mL 0.1 M trisodium citrate dihydrate	4.76	5.0
30 mM citrate	115 mL 0.1 M citric acid monohydrate, 885 mL 0.1 M trisodium citrate dihydrate	4.76	6.0
30 mM succinate	4.86 g/L disodium succinate	5.60	5.5*
30 mM succinate	4.86 g/L disodium succinate	5.60	6.5*
30 mM histidine	4.65 g/L L-histidine	6.04	6.0*
30 mM histidine	4.65 g/L L-histidine	6.04	7.0*
30 mM phosphate	2.89 g/L sodium phosphate monohydrate, 2.42 g disodium phosphate heptahydrate	7.21	6.5
30 mM phosphate	1.75 g/L sodium phosphate monohydrate, 4.64 g disodium phosphate heptahydrate	7.21	7.0
30 mM phosphate	0.78 g/L sodium phosphate monohydrate, 6.53 g disodium phosphate heptahydrate	7.21	7.5
30 mM tris-HCl	3.63 g/L tris base	8.07	7.5*
PBS	0.144 g/L potassium phosphate, 9 g/L sodium chloride, 0.795 g/L disodium phosphate	7.21	7.2

\* pH adjusted with NaOH or HCl

**Table 3. Buffers used in the initial screening of AvFc preformulation analysis.**

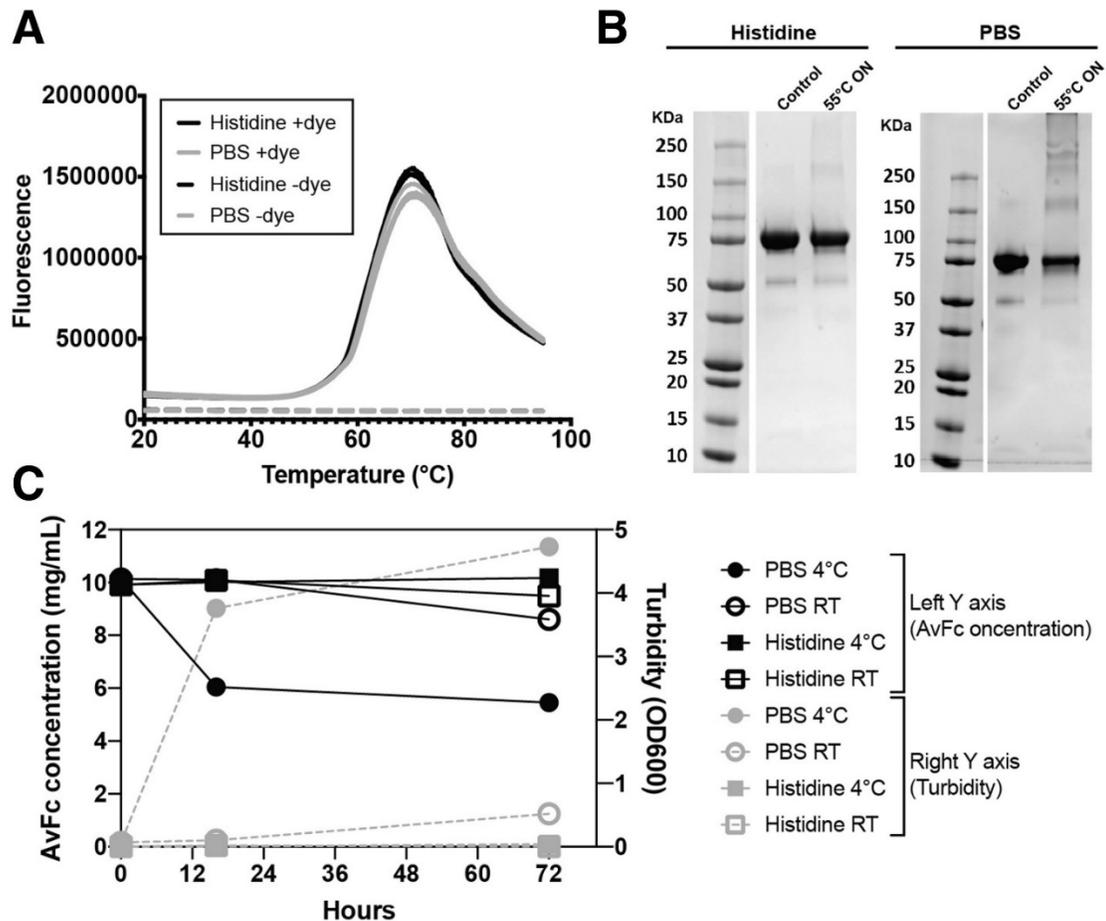


**Figure 11. Liquid formulation development for AvFc.**

(A) Differential scanning fluorimetry for melting temperature measurement. AvFc was prepared in 30 mmol/L histidine buffer, 100 mmol/L NaCl, 100 mmol/L sucrose (histidine, *black line*), or PBS (*grey line*) at a concentration of 1 mg/mL and analyzed in triplicate in the presence (*solid line*) or absence (*dashed line*) of the fluorescent dye SYPRO Orange (ThermoFisher Scientific, Waltham, MA). Melting temperature values were  $62.49^{\circ}\text{C} \pm 0.13^{\circ}\text{C}$  in the histidine buffer and  $62.68^{\circ}\text{C} \pm 0.25^{\circ}\text{C}$  in PBS, as determined by the vertex of the first derivative of the relative fluorescence unit values.

(B) Accelerated stability testing of AvFc in the histidine buffer and PBS. AvFc, prepared at 1 mg/mL in the histidine buffer or PBS were incubated overnight at 55°C, and 10  $\mu\text{g}$  of

the protein from each formulation was analyzed by sodium dodecyl sulfate–polyacrylamide gel electrophoresis under nonreducing conditions. A representative Coomassie-stained gel image is shown. The band at around 75 kilodaltons corresponds to AvFc. Note that after overnight incubation, PBS shows less band intensity for AvFc and more large-size aggregate bands than the histidine buffer. (C) Time course of concentration change and the turbidity of AvFc solution in the histidine buffer and PBS. AvFc was formulated at 10 mg/mL in respective buffers and incubated at 4°C or room temperature (RT). After 16 and 72 hours, the concentration was measured using a theoretical extinction coefficient at 280 nm of  $1.6493 \text{ (mg/mL)}^{-1} \text{ cm}^{-1}$ , whereas turbidity was assessed by absorbance at 600 nm. Representative data are shown for samples analyzed in triplicate.

#### 4.2.3: Pharmacological and toxicological analysis of AvFc in mice

To determine an optimal dosing regimen for an HCV challenge experiment, a pharmacokinetic analysis of AvFc was conducted in C57bl/6 mice. After a single i.p. injection of AvFc at a dose of 25 mg/kg, peak drug concentration was observed between 2 and 4 h, with a half-life of 24.5 h in male and 18.5 in female animals (Figure 12). After 48 h, in both male and female animals the plasma concentration of AvFc remained above a target trough concentration of 130 nM (10 µg/mL), at which AvFc showed >90% neutralization effects against HCV (see Figure 9). Consequently, these results suggested that administration of the drug every other day (Q2D) might be sufficient to keep the virus under control in a murine HCV challenge model.

We then assessed the safety of Q2D administration of AvFc in PXB-mice<sup>®</sup>. To effectively discern potential toxicity associated with AvFc's high-mannose glycan-binding activity, we included an AvFc variant lacking high-mannose glycan-binding activity as a control (AvFc<sup>lec-</sup>; Figure 13A, B). PXB mice received either the vehicle (the histidine buffer described above) Q2D for 11 total doses, AvFc at 25 mg/kg Q2D for a total of 8 or 11 doses, or AvFc<sup>lec-</sup> at 25 mg/kg Q2D for 11 total doses. As shown in Figure 14A-C, no significant differences in either body weights, blood h-Alb levels or serum ALT activity were observed. Additionally, no significant differences in relative liver weight were seen (Figure 14D). These results indicate that AvFc, formulated in the histidine buffer, is well tolerated in the immunocompromised mice engrafted with human hepatocytes.

Histopathology was performed to evaluate any potential toxicity to the human liver grafts due to AvFc administration (Table 1 and Figure 15). In the human hepatocyte

area, slight to moderate (score 2 to 3 in Table 4) macrovesicular fatty change, a characteristic change of human hepatocytes in the PXB-mouse, was observed in all mice including the vehicle-treated group (Figure 15A-C). Minimal inflammatory cell infiltration around vacuolated hepatocytes (Score 1) was seen in one mouse each from the 11 dose AvFc and AvFc<sup>lec-</sup> groups (Figure 15D, E); however, this was unlikely treatment-related as a similar change is occasionally seen in PXB-Mice (PhoenixBio, unpublished observation). No AvFc treatment-specific change was observed, except for an incidental build-up of pigmentation found in the Glisson's sheath in the liver of one mouse (Figure 15F). Collectively, it was concluded that there was no treatment-related adverse effect in the liver tissue.

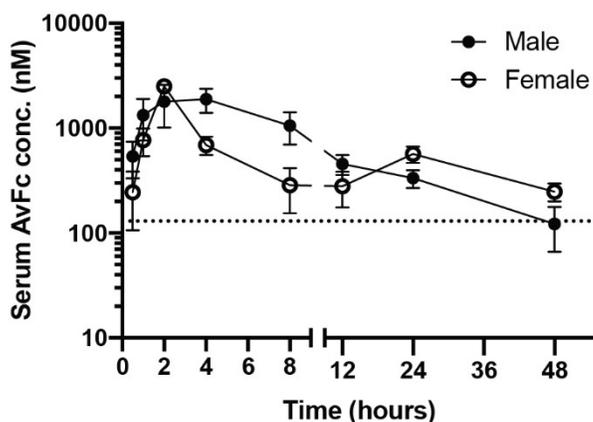


**Figure 12. Pharmacokinetics of AvFc in Mice.**

AvFc pharmacokinetics were evaluated in C57bl/6 mice following a single i.p. injection of 25 mg/kg with blood sampled at various time points. Data are expressed as mean  $\pm$  SEM from 4 mice per group. The average half-life was 24.5 h and 18.5h in male and female mice, respectively, as determined by the PKSolver Microsoft Excel Add-on. The peak concentration occurred between 2 and 4 h post administration. The target trough concentration of 130 nM (corresponding to 10  $\mu$ g/mL) is indicated by a dashed line.

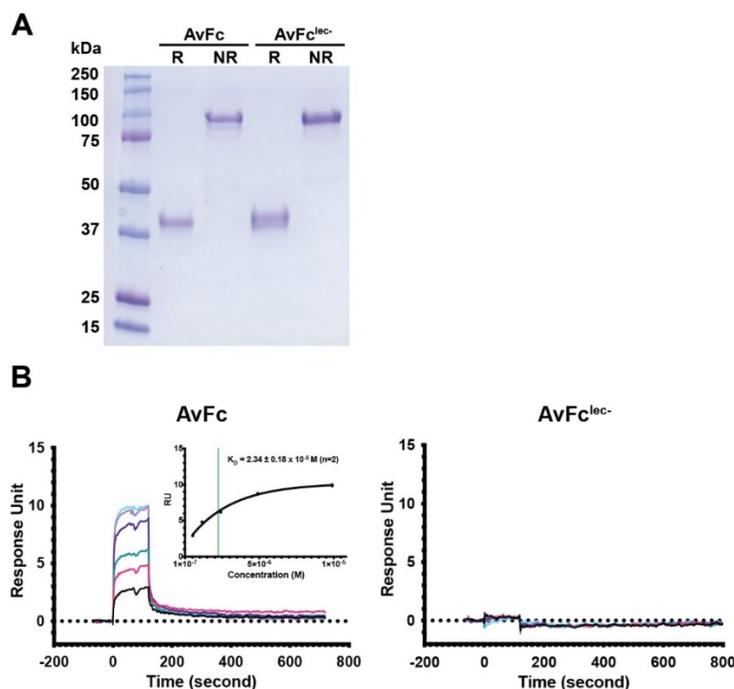


**Figure 13. Characterization of the non-sugar-binding mutant AvFc<sup>lec-</sup>.**

A variant of AvFc that does not bind to high-mannose glycans was generated by mutating a tyrosine residue in each of the three binding pockets of Avaren. (A) SDS-PAGE gel showing purified AvFc and AvFc<sup>lec-</sup> under reducing (R) and non-reducing (NR) conditions. Under R conditions, AvFc monomer is seen at 38.5 kDa and, whereas under NR conditions, AvFc dimer (via inter-polypeptide disulfide bonds in the Fc region) appears at 77 kDa. (B) Surface plasmon resonance analysis of HCV E2-binding affinity of AvFc and AvFc<sup>lec-</sup>. A recombinant E2 protein (Immune Technology Corp.) was immobilized to a CM5 chip using amine coupling to a surface density of  $\approx 200$  RU. AvFc or AvFc<sup>lec-</sup> was then injected over the chip surface at a rate of 30  $\mu\text{L}/\text{min}$  for 120 seconds followed by a 600 second dissociation period, with concentrations ranging from 10 to 0.625  $\mu\text{M}$ . Binding affinity was calculated using steady-state analysis and was determined to be  $2.34 \pm 0.18 \times 10^{-6}$  M ( $2.34 \pm 0.18$   $\mu\text{M}$ ) for AvFc. Binding affinity could not be determined for AvFc<sup>lec-</sup> due to lack of measurable binding.

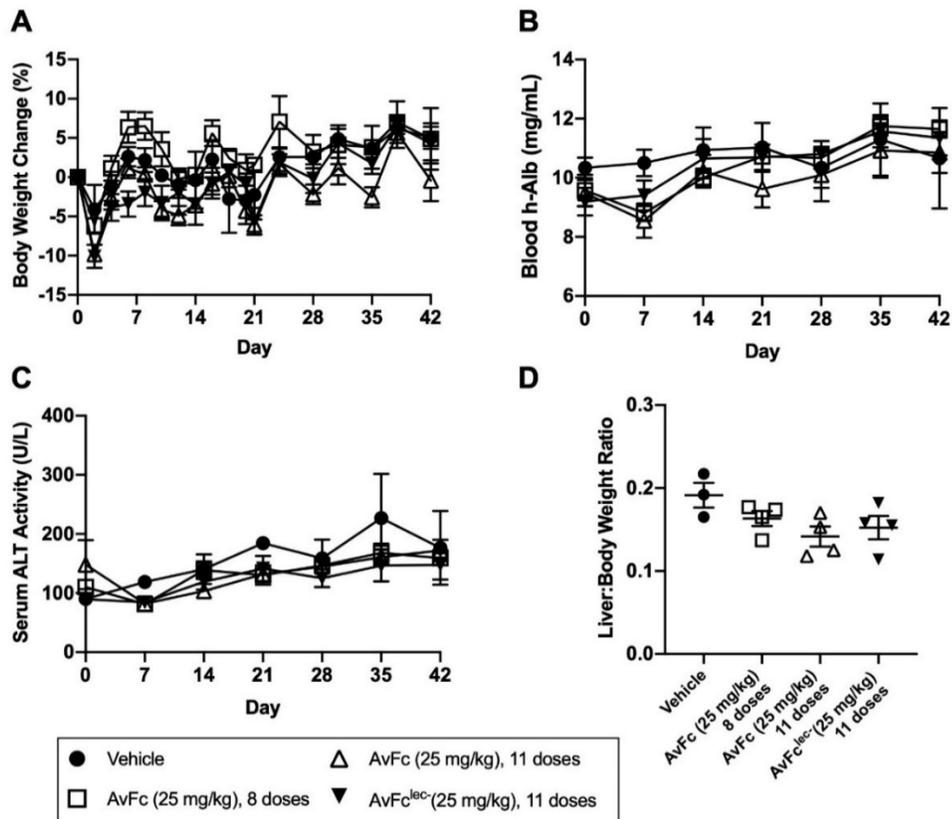


**Figure 14. Toxicological analysis of systemically administered AvFc in the PXB® human liver chimeric mouse model.**

PXB mice were administered i.p. with AvFc or AvFc<sup>lec-</sup> at 25 mg/kg (n=4 each), or the histidine buffer vehicle control (n=3) every 2 days (Q2D) and monitored for body weights, blood human albumin (h-Alb) levels and serum alanine aminotransferase (ALT) levels over 42 days. (A) Percent change of body weights from the initial day of dosing (Day 0). (B) Blood h-Alb levels. (C) Serum ALT levels. (D) Ratio of the liver weight to the body weight of individual mice at necropsy. Each data point represents mean ± SEM (A-C) and individual data with mean ± SEM (D) in each group. No significant changes in any of the safety endpoints were noted between the groups (A-C: two-way analysis of variance (ANOVA); D: one-way ANOVA). Experiment was conducted by PhoenixBio Co, Higashi-Hiroshima City, Japan.

	Vehicle			AvFc <sup>lec-</sup>				AvFc, 11 doses				AvFc, 8 doses			
	101	102	103	201	202	203	204	301	302	303	304	401	402	403	404
Mouse hepatocytes	0	0	0	0	0	0	0	0	0	0	0	0	0	0	0
Human hepatocytes															
Fatty change, macrovesicular	2	3	3	3	3	3	3	3	3	3	3	3	3	3	3
Infiltrate, inflammatory cell, around vacuolated hepatocyte	0	0	0	0	1	0	0	0	1	0	0	0	0	1	0
Portal canal and others															
Hepatocellular carcinoma, trabecular, with extramedullary hematopoiesis	P	0	0	0	0	0	0	0	0	0	0	0	0	0	0
Metaplasia, osseus	0	2	0	0	0	0	0	0	0	0	0	0	0	0	0
Pigmentation, brown, histiocyte, Glisson's sheath, focal	0	0	0	0	0	0	0	0	0	0	0	1	0	0	0

**Table 4. Histopathology of chimeric mouse liver tissue.**

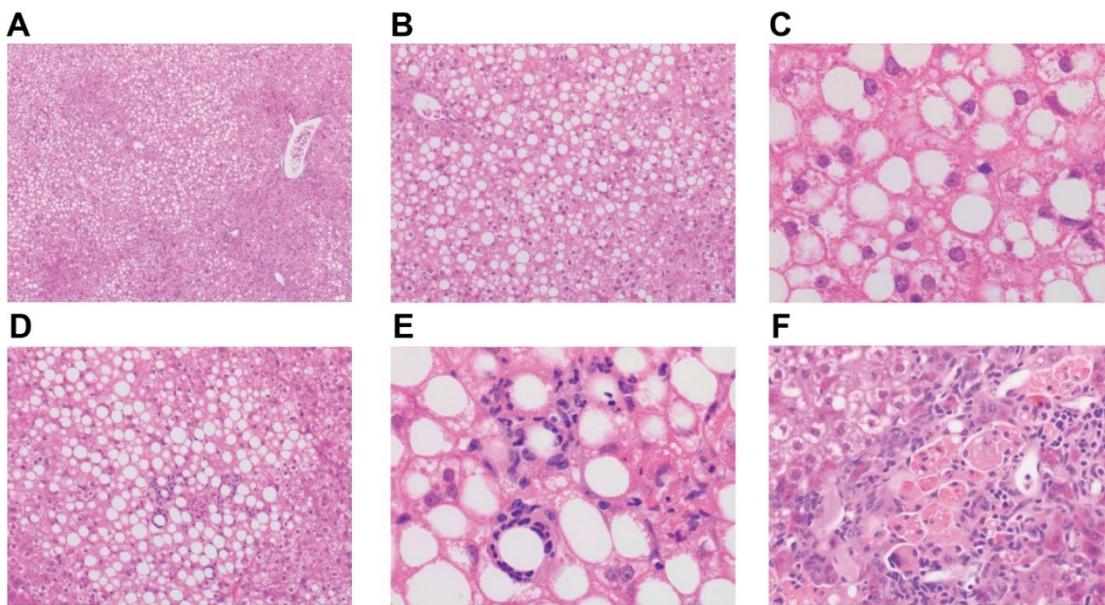


**Figure 15. Histopathological examination of PXB mouse liver tissues.**

Representative hematoxylin/eosin-stained liver tissue section images corresponding to histopathological findings in Table 4 are shown. Liver tissues are from the toxicological study in Figure 14. (A) A 4x image from an animal in the vehicle control group (mouse ID: 103 in Table 4) showing low magnification of vacuolated hepatocytes. (B) A 10x image from a portion of panel A, containing many human hepatocytes with a large, well-defined rounded vacuole. (C) Higher magnification (40x) of panel B. (D) A 10x image from an animal in the AvFlec- group (ID: 202 in Table 4), showing small foci of inflammatory cell infiltration in the human hepatocyte area. (E) Higher magnification (40x) of panel D. Inflammatory cells appear to surround vacuolated hepatocytes. (F) A 20x image from an animal in the AvFc group (8 total doses; ID: 401 in Table 4). Histiocytic brown pigmentation in the Glisson's sheath is noted only in this mouse. Histopathological analysis was conducted by Nara Pathology Research Institute Co., Ltd.

#### 4.2.4: AvFc protects against HCV infection *in vivo*

Lastly, we assessed AvFc's protective efficacy against HCV infection *in vivo* using the treatment regimen described above. PXB mice were inoculated i.p. with a genotype 1a virus along with initial treatment with 25 mg/kg of AvFc or AvFc<sup>lec-</sup> on day 0. As shown in Figure 16A, AvFc<sup>lec-</sup>-treated mice showed high serum HCV RNA levels from day 7 post challenge through the end of the study on day 35. In sharp contrast, animals treated with both 8 and 11 doses of AvFc did not show any quantifiable level ( $4.0 \times 10^4$  copies/mL) of HCV RNA in sera, indicating that the lectibody prevented the infection of human liver grafts by the virus. Similar to the results in Figure 14, overall no major toxicity signal was noted in body weights, h-Alb or h-ALT levels between the test groups although there was a temporal drop in body weight and h-Alb in one of the AvFc-treated group at an early timepoint, indicating that the liver grafts remained functional over the course of the study (Figure 16B-D).

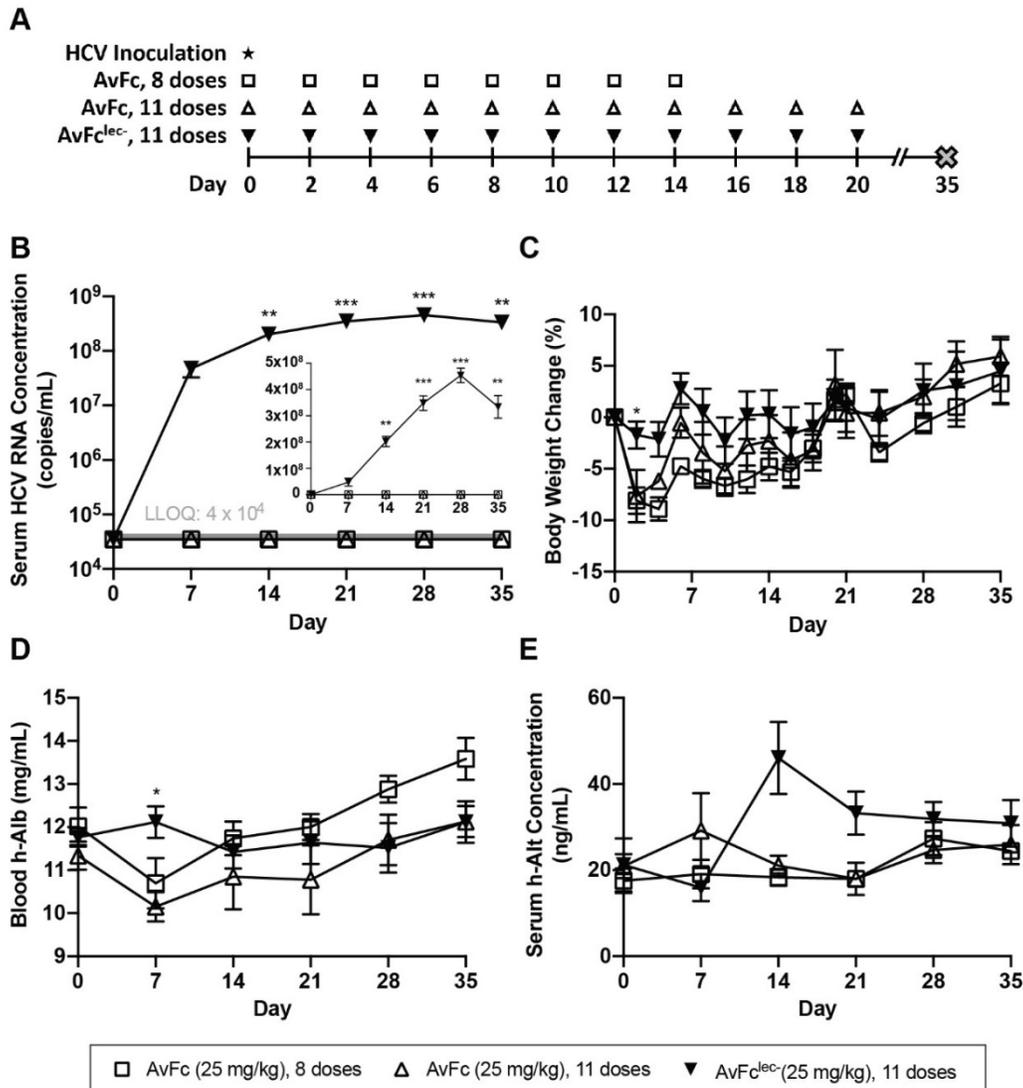


**Figure 16. The protective effect of AvFc against HCV challenge in PXB mice.**

(A) Study design. PXB mice were challenged i.p. with an HCV genotype 1a virus on Day 0 simultaneously with an initial treatment i.p. with either 25 mg/kg of AvFc or AvFc<sup>lec-</sup>. Treatment was continued Q2D for a total of 8 or 11 doses for AvFc and 11 doses for AvFc<sup>lec-</sup> (n=5 each). The general conditions and body weights of the animals were monitored every other day, while serum HCV RNA and blood h-Alb were measured every 7 days. (B) Serum HCV RNA levels. AvFc treatment (both 8 and 11 doses) showed no detectable HCV RNA at any time point. The gray line indicates the lower limit of

quantification (LLOQ), which was  $4 \times 10^4$  copies/mL in this assay. \*\*, \*\*\* $p < 0.01$ , 0.001 (AvFc<sup>lec-</sup> vs. both AvFc 8 and 11 doses); two-way ANOVA with Tukey's multiple comparison test. The graph in the inset shows the same data with y-axis on a linear scale. (C-E) Time course of body weight change from day 0 (C), blood h-Alb levels (D) and serum h-Alt concentrations (E). Each data point represents mean  $\pm$  SEM in each group. \* $p < 0.05$  (AvFc<sup>lec-</sup> vs. AvFc 8 doses in C and AvFc<sup>lec-</sup> vs. AvFc 11 doses in D]; two-way ANOVA with Tukey's multiple comparison test. No significant difference between groups at any timepoint was noted in E. Experiment was conducted by PhoenixBio Co, Higashi-Hiroshima City, Japan.

### 4.3: Discussion

In this study we demonstrated that the high-mannose glycan-binding lectibody AvFc exhibits broad genotype-independent anti-HCV activity. Additionally, systemic administration of AvFc effectively protected chimeric human-mouse liver mice from infection with a genotype 1a virus without apparent toxicity, providing the first *in vivo* proof-of-concept for the lectibody's antiviral potential.

The mechanism of HCV neutralization by AvFc is likely through binding to high-mannose glycans on the E1/E2 envelope protein dimer, which blocks their interaction with host cell receptors and viral entry. Unlike HIV envelope glycoproteins, whose glycan content can vary widely between strains, the number and position of glycosylation sites on E1/E2 are highly conserved, indicating their critical role in HCV's infectious processes [235]. The notion that AvFc functions as an entry inhibitor is supported by the facts that the lectibody has affinity to the E2 protein [98] and that other mannose-binding lectins, such as Griffithsin or Cyanovirin-N, inhibit entry in this manner [236, 237]. AvFc inhibited multiple genotypes of HCV with an average  $IC_{50}$  over 100-fold lower than that of the monomer Avaren lectin (Table 2), indicating that the multivalent recognition of high-mannose glycans on the surface of the virus, brought about by the dimerization of Avaren via Fc fusion, led to greater entry inhibition. Unlike other antiviral lectins, however, the inclusion of the human IgG1 Fc region implicates the possibility of Fc-mediated effector functions, such as antibody-dependent cell-mediated cytotoxicity, against infected cells. In fact, Fc-mediated effector functions greatly contributed to the antiviral potency of AvFc against HIV, as determined by a primary cell-based inhibition assay and an antibody-dependent cell-mediated viral inhibition assay [98]. Accordingly,

the remarkable efficacy seen in the present *in vivo* HCV challenge study may be partially Fc-mediated. Further investigations are necessary to address this possibility.

The present study also demonstrated that AvFc therapy is well tolerated in mice and human hepatocytes, as Q2D i.p. administration of 25 mg/kg of AvFc up to 11 doses did not show any obvious toxicity in PXB mice by gross necropsy or histopathology of engrafted human hepatocytes, nor did it result in significant changes in body weight, h-Alb, or ALT levels (Figure 14, Figure 15). This corroborates our previous observation that AvFc administration, both i.p. and intravenously, was well tolerated and produced no toxicity in mice, rats, and rhesus macaques [98]. We hypothesize that the lack of any significant toxicity is attributable to AvFc's unique high-mannose glycan-binding mechanism, whereby it requires multivalent interaction with several high-mannose glycans in proximity to exhibit high affinity binding to a glycoprotein target. In line with this hypothesis, Hoque et al. demonstrated that the three binding pockets of the parent lectin actinohivin can bind up to three independent high-mannose glycans, providing high affinity binding when the high-mannose glycans are in relatively close proximity [104]. This implies that AvFc may not effectively interact with healthy normal cells and tissues that do not usually exhibit clusters of high-mannose glycans on their surfaces. In contrast, glycoproteins of many enveloped viruses display a high proportion of these immature forms of *N*-glycans [40, 231, 232]. While HCV E2 has fewer *N*-glycosylation sites (around 11) than the HIV glycoprotein gp120 (which has between 20 and 30 depending on the strain), E2 is likely present on the surface of HCV at a higher density and thus provides higher local concentrations of high-mannose glycans [238]. Further studies are

necessary to reveal a threshold high-mannose glycan concentration which enables efficient interaction between AvFc and the surfaces of cells or viruses.

While alcoholic liver disease has now surpassed HCV infection as the number one indication for liver transplantation in the US, a large number of procedures will continue to be performed for the foreseeable future in patients with HCV-related decompensated cirrhosis [239]. A major outstanding issue is the lack of effective treatment protecting the allograft liver from recurrent infection by the virus that remained circulating in the periphery at the time of transplant. As a consequence, reinfection of donor livers universally occurs, as early as in the first 90 minutes upon reperfusion [228], and can result in accelerated fibrosis and increased risk of graft failure, cirrhosis, and hepatocellular carcinoma [240]. In fact, allograft failure due to reinfection is the leading cause of secondary transplants and death in HCV-infected patients who have received liver transplant [241]. Patients cured of HCV with DAAs after liver transplantation still have a higher than normal risk of hepatocellular carcinoma [242], and the high cost of the drugs represents a significant barrier to their widespread use. Furthermore, emergent drug resistance even in DAA combination therapies, though rare, represents a particular challenge for further treatment [243]. Unlike DAAs, entry inhibitors neutralize circulating viruses and physically block the viral infection of target cells. The use of entry inhibitors perioperatively upon liver transplantation, either alone or in combination with DAAs, may significantly improve treatment outcomes [241, 244]. Thus, while the effectiveness of DAAs is not in question, there are still unmet needs that may be addressed through the use of entry inhibitors.

As of yet, no entry inhibitor has been approved for the treatment or prevention of HCV. Two major drug candidates, Civacir® and MBL-HCV1, have shown some promise in clinical trials (NCT01804829, NCT01532908) [245, 246]. Though larger studies are needed, it appears that entry inhibitors in combination with DAAs may represent a new treatment paradigm for HCV patients receiving liver transplant. Despite that both MBL-HCV1 and Civacir® are capable of neutralizing a broad range of HCV genotypes, viral resistance can still develop through mutations in the envelope proteins E1/E2, in particular through shifting glycan positions [247, 248]. In this regard, AvFc in its own right could be less susceptible to amino acid mutations because it targets the glycan shield of the virus rather than a specific epitope. Deletions of glycans, even if occurring following prolonged exposure to a carbohydrate-binding agent like AvFc, may result in significant decrease in viral fitness by decreasing E1/E2 incorporation into HCV particles or increased susceptibility to humoral immunity due to breach in the glycan shield [235, 249]. Our results provide a foundation to test the above hypotheses and feasibility of the high-mannose glycan-targeting anti-HCV strategy. Of note, a unique advantage of AvFc over the two antibody-based entry inhibitor candidates described above is that the lectin body has the capacity to neutralize both HIV [98] and HCV (present study). Accordingly, AvFc may provide an effective means (e.g., pre-exposure prophylaxis) to protect high-risk populations against HIV/HCV co-infection, such as health care workers and injection drug users [250, 251].

In conclusion, the present study provided an important proof of concept for the therapeutic potential of AvFc against HCV infection via targeting envelope high-mannose glycans. In particular, the lectin body may provide a safe and efficacious means to

prevent recurrent infection upon liver transplantation in HCV-related end-stage liver disease patients. Other potential utilities of AvFc may be found in pre-exposure prophylaxis against HIV/HCV co-infection in high-risk populations, as well as in the context of transplantation of organs from HCV-infected donors to HCV-negative recipients, which may help alleviate the severe shortage of donor organs available for transplantation [252, 253]. Further studies are warranted to determine a dose-response relationship, therapeutic window, and feasibility of intravenous or subcutaneous dosing routes, as well as to assess the efficacy of AvFc against established infection.

## CHAPTER 5: THE ANTI-CANCER POTENTIAL OF AVAREN-FC AND ITS MECHANISM OF ACTION

### 5.1: Introduction

Cancer immunotherapy with monoclonal antibodies (mAbs) targeting tumor-associated antigens (TAAs) has forever altered treatment paradigms and has vastly improved patient survival and quality of life. MAbs exert their anti-cancer activities through a combination of immune-mediated and non-immune-mediated mechanisms such as direct receptor inhibition, antibody-dependent cell-mediated cytotoxicity (ADCC), antibody-mediated phagocytosis, and the complement system. The initiation of inflammatory responses by antibodies is largely dependent on the binding and activation of Fc $\gamma$  receptors (Fc $\gamma$ Rs), which are differentially expressed in several different immune cell types, in particular natural killer (NK) cells, neutrophils, macrophages, and monocytes [254]. Binding of the Fc region of an antibody to the activating Fc $\gamma$ Rs (Fc $\gamma$ RI, Fc $\gamma$ RIIa, Fc $\gamma$ RIIIa) results in the generation of signaling cascades through intracellular ITAM domains, leading to cellular activation, degranulation, or phagocytosis depending on the specific receptor and cell type expressing it [255]. Initiation of ADCC, for instance, is accomplished primarily by recognition of antibody-opsonized cells by Fc $\gamma$ RIIIa on NK cells, which subsequently release cytotoxic granules containing granzyme and perforin to initiate target cell death and begin to express IFN $\gamma$ . As these immune-mediated mechanisms play an important role in the effects of therapeutic mAb

drugs, even those whose primary mechanism is receptor antagonization [256], much research has been conducted into enhancing their ability to activate Fc functions by improving their affinity to the various Fc $\gamma$ Rs with the goal of improving clinical outcomes [257].

The strength of the Fc-mediated response reflects both the density of the target TAAs on the cell surface as well as the affinity of the mAb to the Fc $\gamma$ R [258]. The affinity of this interaction is determined by both the IgG isotype of the antibody as well as the composition of its N-glycans attached to the Asn297 within the Fc region [255, 259]. One method for improving the affinity of an Fc to the Fc $\gamma$ Rs is through point mutation of the Fc region. A well-known example of this is the GASDALIE mutation, which is a series of 4 amino acid substitutions in the C<sub>H</sub>2 and C<sub>H</sub>3 domains that significantly increases the affinity of the Fc for Fc $\gamma$ RIIIa [128, 260]. This mutation has been trialed on a number of mAb therapeutics and has consistently resulted in increased ADCC activity and *in vivo* efficacy in pre-clinical models of both viral diseases and cancer [129, 261]. Host glycoengineering is another method commonly used to modify Fc $\gamma$ R affinity. N-glycosylation of mAbs occurs at a single conserved site on the C<sub>H</sub>2 domain of the Fc region, the composition of which can be altered through manipulation of host glycosyltransferase enzyme expression [262]. This can be performed chemically through exposure to compounds such as kifunensine, which inhibits mannosidase I and results in an abundance of high-mannose-type glycans, or genetically through knockdowns or knockouts of glycosyltransferase genes by RNAi or CRISPR-Cas9 [132, 133, 263, 264]. In plants, recombinant expression of antibodies results in the majority of glycoforms containing  $\beta$ 1,2-xylose and  $\alpha$ 1,3-fucose residues [265]. Expression in

glycoengineered *N. benthamiana* plants containing RNAi knockdowns of  $\beta$ 1,2-xylosyltransferase and  $\alpha$ 1,3-fucosyltransferase genes ( $\Delta$ XylT/ $\Delta$ FucT, or  $\Delta$ XF), however, results in a near total loss of plant-typical glycans with the predominant glycoform consisting of the core trimannose and two N-acetylglucosamine residues [133]. Antibodies manufactured in these plants have significantly higher Fc $\gamma$ R affinity, which is similar to the effect achieved following removal of the core  $\alpha$ 1,6-fucose residue from antibodies expressed in mammalian cells [265, 266]. Thus, removal of plant-derived glycans is an attractive target to achieve for therapeutic antibody development, and indeed a number of stable transgenic *N. benthamiana* lines for recombinant protein expression have been generated with that goal in mind [132, 133, 267, 268].

Plants, in particular *Nicotiana benthamiana*, are quite amenable to glycoengineering owing to the relatively lower complexity of the *N*-glycosylation pathway compared to that of mammalian culture systems, which are currently the industry standard for mAb manufacturing. This makes them an attractive alternative platform that has already been used to manufacture dozens of antiviral and anticancer mAb and Fc-fusion protein therapeutics with glycan or amino acid modifications [164, 269-273]. Previously, we have described the development in plants of a novel lectin-Fc fusion protein, or lectibody, which targets cancer-associated high-mannose glycans called Avaren-Fc (AvFc) [98, 105]. The presence of aberrant glycosylation patterns on cell surface glycoproteins has been identified as a hallmark of cancer, and an overabundance of high-mannose glycans has been found in numerous human cancers including colorectal cancer [73-75], hepatocellular carcinoma [76, 77], cholangiocarcinoma [78], lung adenocarcinoma [79], pancreatic cancer [80], ovarian cancer [81, 82], prostate

cancer [83], and some skin cancers [84]. This suggests that display of these immature glycans may be common in cancer due to an inherent property of the transformation to malignancy, and this fact can potentially be exploited to create a new druggable target for therapy. We have previously reported that AvFc recognizes a large number of cancer cell lines through this mechanism, and that by binding to mannosylated forms of EGFR and IGF1R derived from lung cancer cell lines and tissues in addition to inducing ADCC, AvFc displays potent activity against A549 and H460 lung cancer both *in vitro* and *in vivo* [105]. To further explore and examine the contribution of ADCC to AvFc's antitumor mechanism of action, we have generated a variant of AvFc by expression in  $\Delta$ XF plants (AvFc $^{\Delta$ XF) that is devoid of plant-derived glycans and may hence exhibit greater ADCC activity due to the lack of core fucosylation. In this study, we set out to characterize this variant as well as investigate its activity by comparing it to an aglycosylated variant, AvFc $^{\Delta$ gly, and a variant lacking sugar-binding activity, AvFc $^{\Delta$ lec, using both *in vitro* assays as well as the syngeneic murine B16F10 melanoma model. Additionally, we explored the impact of the generation of anti-drug antibodies (ADAs) on the efficacy of AvFc in this model. The results demonstrate the importance of Fc modification on the therapeutic efficacy of AvFc, as well as the utility of the plant expression system for manufacturing glycoengineered AvFc variants.

## 5.2: Results

### 5.2.1: Analysis of C<sub>H2</sub> N-glycans of AvFc

In order to demonstrate the effects of expressing AvFc in glycoengineered plants, we first set out to characterize the composition of the lone N-glycan on the C<sub>H2</sub> domain

of the human Fc of AvFc produced in WT or  $\Delta$ XF plants (Table 5). HPLC analysis of Fc glycans revealed that AvFc expressed in WT plants contains a relatively large proportion of high mannose glycans (60.5%), with Man9 being the predominant form, followed by the expected plant glycans containing  $\beta$ 1,2-xylose and/or  $\alpha$ 1,3-fucose (33.0%), and a small amount of complex glycans (6.5%, primarily GnGn). Conversely, AvFc expressed in  $\Delta$ XF plants was entirely devoid of plant glycans and instead contained mostly complex glycans, particularly the expected GnGn glycoform (54.2%), and a similarly high proportion of high mannose glycans (40.0%). The use of RNAi to knockdown expression of the xylosyltransferase and fucosyltransferase was somewhat “leaky”, and the  $\Delta$ XF variant was found to contain small percentages of other complex glycans (a  $\beta$ 1,3-galactosylated glycoform) and some hybrid glycans (GNM3, GNM4, GNM5). As a point of comparison, when expressed in CHO cells, AvFc displays not only the typical mammalian glycoforms containing  $\alpha$ 1,6-fucose (primarily GN2M3F) but also a large proportion of high-mannose and galactosylated glycans.

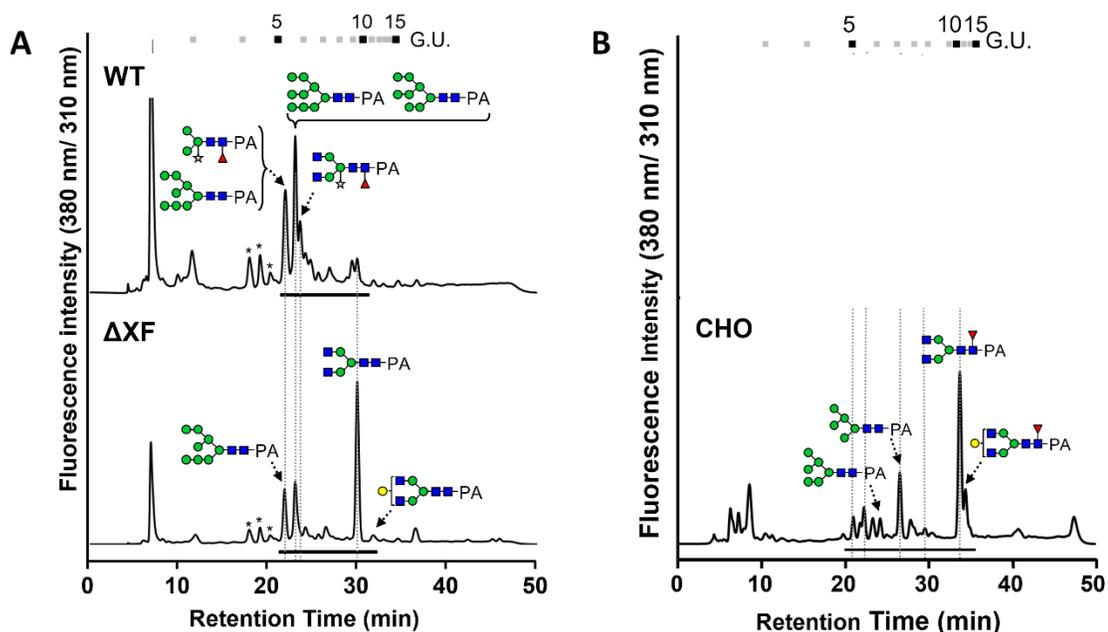


**Figure 17. Glycan analysis by HPLC.**

(A) Identification of Fc glycans by HPLC of WT and  $\Delta$ XF AvFc shows the large presence of high-mannose glycans between both variants. WT AvFc also contains significant amounts of plant glycans containing  $\alpha$ 1,3-fucose and  $\beta$ 1,2-xylose while  $\Delta$ XF is devoid of them. (B) Glycan analysis by HPLC shows that AvFc produce in CHO cells contains characteristic  $\alpha$ 1,6-fucose in addition to high-mannose glycans. Glycan analysis was performed by Drs. Kajiura and Fujiyama at Osaka University, Japan.

Glycan type	Structure	Ratio (%)		
		WT	$\Delta$ XF	CHO
Plant	M3X	1.1	-	-
	M3FX	11.9	-	-
	GNM3FX	3.5	-	-
	GN2M3X	2.5	-	-
	GN2M3FX	14.1	-	-
High-mannose	M5	-	-	24.5
	M6	-	-	5.5
	M7A	2.4	5.3	2.9
	M7B	5.0	3.3	
	M8A	18.0	14.8	3.1
	M9	35.2	16.6	3.1
Hybrid	GNM3	-	1.1	-
	GNM4	-	0.3	-
	GNM5	-	3.5	-
Complex	GN2M3 (GnGn)	6.5	54.2	-
	GN2M3F ( $\alpha$ 1,6)	-	-	50.6
	Gal( $\beta$ 1,4-)GN2M3F	-	-	10.3
	Gal( $\beta$ 1,3-)GN2M3	-	0.9	-
Totals	Plant	33.0	-	-
	High-mannose	60.5	40.0	39.1
	Hybrid	-	4.9	-
	Complex	6.5	55.1	60.9

**Table 5. CH2 glycan analysis of AvFc variants by LC-MS.**

Glycan composition was determined by HPLC. AvFc expressed in WT plants contained 33% plant glycans (which contain  $\beta$ 1,2-xylose,  $\alpha$ 1,3-fucose, or both), 60.5% high-mannose glycans (primarily Man8 and Man9), and 6.5% complex glycans. Expression in the glycoengineered *N. benthamiana* line  $\Delta$ XF resulted in GnGn becoming the predominant glycoform in addition to a large proportion of high-mannose glycans. Plant glycans were not detected in AvFc derived from either line, however AvFc from  $\Delta$ XF plants displayed a small percentage of hybrid glycans (4.9%) and a  $\beta$ 1,3-galactosylated glycoform. Plant glycans were also not found in AvFc expressed in CHO cells, which primarily displays the mammalian  $\alpha$ 1,6-fucosylated GnGn (GN2M3F) glycoform as well as a  $\beta$ 1,4-galactosylated form. Like the others, AvFc<sup>CHO</sup> contained a fairly large

proportion of high-mannose glycans. Symbols: M = mannose; X = xylose; F = fucose; GN = N-acetylglucosamine; Gal = galactose. Glycan analysis was performed by Drs. Kajiura and Fujiyama at Osaka University, Japan.

### 5.2.2: Expression, purity, and binding activity of AvFc variants

We have previously reported that AvFc<sup>WT</sup> is highly expressed in plants and has a purified yield of  $\approx 100$  mg/kg [98]. Yields of purified protein were not found to be significantly different between AvFc<sup>WT</sup>, AvFc <sup>$\Delta$ XF</sup>, or AvFc <sup>$\Delta$ lec</sup>, averaging between 100 and 150 mg/kg depending on plant conditions, as determined by A<sub>280</sub> measurements of purified proteins ( $\epsilon = 1.635$ ). Densitometry analysis of Coomassie-stained gels showed that proteins could be purified up to  $\approx 95\%$  homogeneity (Figure 18B). On the other hand, removal of the single N-glycan in the AvFc <sup>$\Delta$ gly</sup> variant resulted in a more than 50% decrease in yield, likely due to a decrease in stability *in planta*. All the variants were identical according to molecular weight ( $\approx 38.6$  kDa reduced,  $\approx 77.1$  kDa non-reduced, Figure 18A), though the amounts of a frequently observed 50 kDa band, likely corresponding to cleaved Fc dimer fragments, varied somewhat between the different forms of AvFc. Another minor impurity was detected at  $\approx 30$  kDa in reducing samples of each variant, and a faint  $\approx 150$  kDa band can be seen in the non-reduced  $\Delta$ gly variant, possibly suggesting an AvFc dimer. Overall, we concluded that change in the plant expression host did not significantly alter our manufacturing capability or the resulting protein purity and that, with the exception of the AvFc <sup>$\Delta$ gly</sup> variant, expression yields were consistently high.

Next, we set out to determine whether or not altering the glycosylation pattern of AvFc affected its ability to recognize cancer cells or induce Fc-mediated effector functions *in vitro*. Flow cytometry of AvFc variants binding to B16F10 cells showed that changes to the Fc glycans did not significantly impact cancer-cell binding kinetics (Figure 18D-E), with saturation of the cell surface occurring at  $\approx 15$  nM for AvFc <sup>$\Delta$ XF</sup>,

AvFc<sup>WT</sup>, and AvFc<sup>Δgly</sup>. Similarly, Fc modifications did not significantly impact binding to the highly-mannosylated HIV glycoprotein gp120 as determined by ELISA (Figure 18C), with EC<sub>50</sub> values of 0.048, 0.051, and 0.061 nM for the ΔXF, WT, and Δgly variants respectively. For the Δlec variant no binding to gp120 could be measured, though minimal binding to B16F10 cells was observed at the highest concentration. The results suggest that changes to the Fc glycan do not have an impact on sugar binding by the Avaren lectin.

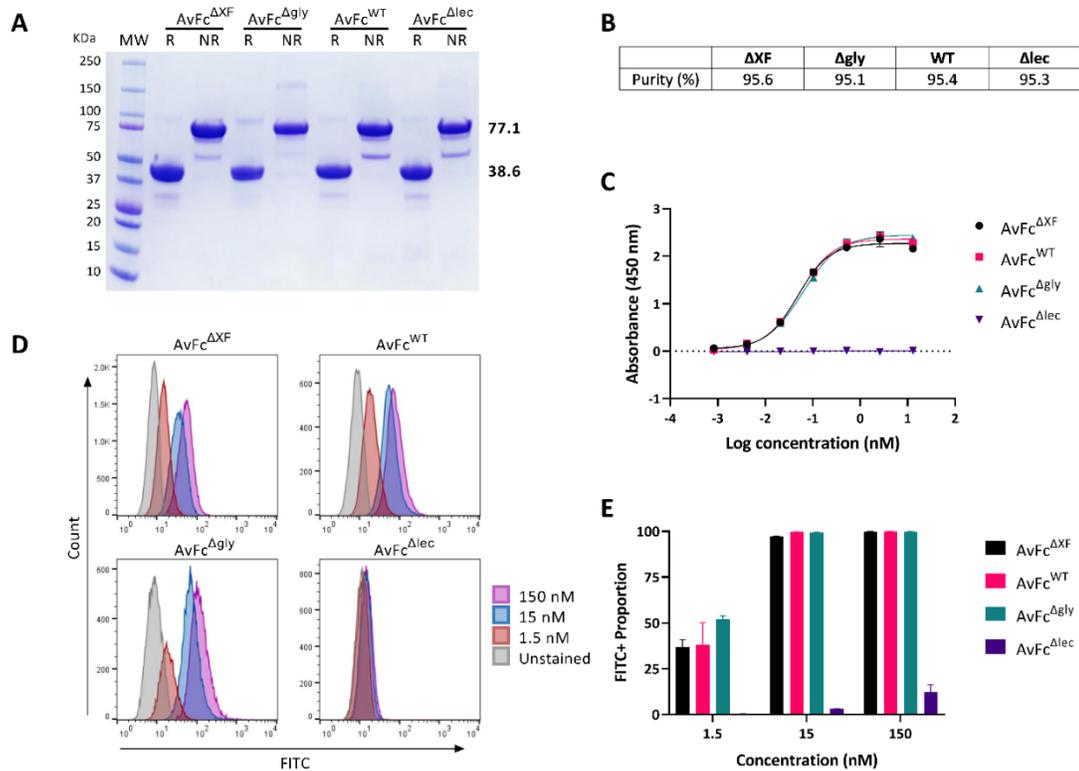


**Figure 18. Purity and binding activity of AvFc variants.**

(A) SDS-PAGE analysis of AvFc variants under denaturing and reducing/non-reducing conditions. Each lane contains 15  $\mu$ g of protein for purity determination. AvFc appears predominantly at 38.6 kDa under reducing conditions and 77.1 kDa under non-reducing conditions and is mostly pure. Some impurities are observed, in particular an  $\approx$  50 kDa fragment is seen with each variant in varying amounts, likely corresponding to dimerized Fc-fragments. Another fragment at  $\approx$  30 kDa is visible in each variant under reducing conditions, as well as a small amount of a possible dimer of AvFc at 150 kDa in the  $\Delta gly$  variant. (B) Purity of AvFc in panel A using densitometry. Densitometry was performed using GelAnalyzer and purity was calculated as the percentage of the total area of all visible bands made up by the main AvFc band. All variants were found to be around 95% purity (average of purity calculations under reducing and non-reducing conditions). (C)

Binding of AvFc variants to HIV-1 gp120 by ELISA. All variants of AvFc, excluding the non-sugar-binding mutant AvFc<sup>Δlec</sup>, bound to gp120 with nearly identical potency and efficacy. EC<sub>50</sub> values: AvFc<sup>ΔXF</sup> = 0.048 nM; AvFc<sup>WT</sup> = 0.051 nM; AvFc<sup>Δgly</sup> = 0.062 nM; AvFc<sup>Δlec</sup> = N/A. (D-E) Binding of AvFc variants to B16F10 cells by flow cytometry. Bound AvFc was detected with a goat anti-human IgG FITC secondary antibody. Panel D shows representative histograms for each, while E shows the quantification of binding determined by the proportion of cells with fluorescence intensity above the background. Binding was nearly equivalent for AvFc<sup>ΔXF</sup>, AvFc<sup>WT</sup>, and AvFc<sup>Δgly</sup>, with saturation occurring at ≈ 15 nM. The Δlec variant exhibited very weak binding at the highest concentration tested (150 nM) but was mostly devoid of activity. All data shown are mean ± SD.

### 5.2.3: AvFc<sup>ΔXF</sup> exhibits higher affinity to FcγRs from humans and mice

We then set out to determine the impact of glycoengineering on AvFc's affinity to FcγRs by performing a kinetic analysis of AvFc binding to FcγRs with surface plasmon resonance (SPR). For this we chose to assess affinity to human FcγRI (hFcγRI), hFcγRIIIa, and murine FcγRIV. The high-affinity receptor hFcγRI is most closely associated with the activation and phagocytosis of antibody-opsonized pathogens and cells by macrophages but is also expressed by eosinophils and neutrophils and has nanomolar affinity for IgG1. The low-affinity receptor hFcγRIIIa, on the other hand, is primarily associated with the induction of ADCC by NK cells and has micromolar affinity for IgG1. We also measured affinity to mFcγRIV, which is a low-affinity receptor roughly equivalent to FcγRIIIa in humans, as we wanted to determine whether or not glycoengineering would have an impact in mouse models.

Kinetic analysis of binding to FcγRs by SPR showed that the ΔXF variant had 1.9-fold increased affinity to human hFcγRI (though this was non-significant), 3.8-fold increased affinity to hFcγRIIIa, and 5.5-fold increased affinity to mouse FcγRIV (mFcγRIV) compared to AvFc<sup>WT</sup> (Figure 19). Representative sensorgrams are shown in Figure 19 along with a table summarizing the results. Table 6 shows representative measurements of dissociation and association rate constants ( $k_d$  and  $k_a$ ) as well as the overall dissociation constant  $K_D$  from an individual SPR experiment. For hFcγRI, the increase in affinity of ΔXF appears to be mostly due to a lengthening of the dissociation time, as indicated by a decrease in the  $k_d$  values, even though the WT variant showed slightly faster association (higher  $k_a$ , Table 6). For hFcγRIIIa, the increase in affinity by ΔXF seems to be both due to faster association (higher  $k_a$ ) and longer dissociation (lower

$k_d$ ), while interestingly the increase in affinity of  $\Delta XF$  for mFc $\gamma$ RIV was due almost entirely to an increase in association speed as the dissociation rate constants were nearly identical. In general, AvFc $\Delta XF$  also reached higher  $R_{max}$  values, however this is to be expected given its higher affinity for the receptors. No measurements could be made for the  $\Delta gly$  variant and signals seen in the sensorgrams are due almost entirely to bulk shift in the refractive index due to minor differences in running and sample buffer composition. Thus, we concluded that glycoengineering of AvFc resulted in the predictable increase in affinity for Fc $\gamma$ Rs, similar to what is observed for defucosylated mAbs, and should result in increased activity both *in vitro* and *in vivo*.

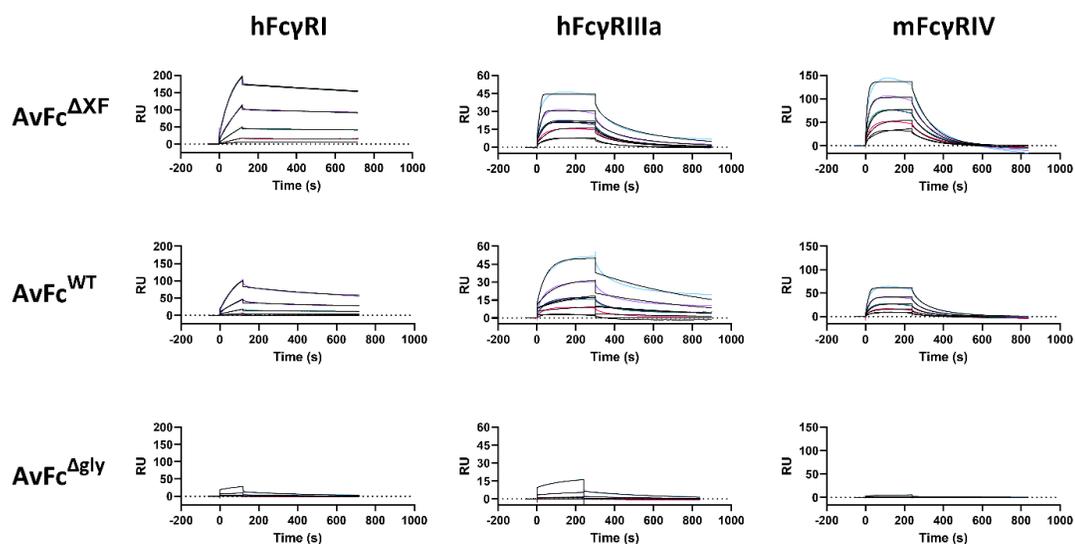


**Figure 19. Representative sensorgrams of AvFc variant binding to FcγRs.**

Shown are representative sensorgrams illustrating the association and dissociation kinetics of AvFc to the various FcγRs. Kinetics of binding to the high-affinity receptor hFcγRI are characterized by rapid association and slow dissociation, which results in low nanomolar  $K_D$  values. AvFc<sup>ΔXF</sup> had 1.9-fold increased affinity to this receptor compared to the WT variant. For hFcγRIIIa and mFcγRIV, binding kinetics were generally characterized by rapid association and dissociation resulting in high nanomolar  $K_D$  values. AvFc<sup>ΔXF</sup> had 3.8-fold higher affinity to hFcγRIIIa and 5.5-fold higher affinity to mFcγRIV than the WT variant. No affinity could be measured for the Δgly variant.

<b>hFcγRI</b>				
<b>VARIANT</b>	<b>k<sub>a</sub> (1/Ms)</b>	<b>k<sub>d</sub> (1/s)</b>	<b>K<sub>D</sub> (M)</b>	<b>R<sub>max</sub> (RU)</b>
WT	147145.162	0.001144	7.77559E-09	206.8
ΔXF	52669.55	0.000213	4.03824E-09	308.5
<b>hFcγRIIIa</b>				
<b>VARIANT</b>	<b>k<sub>a</sub> (1/Ms)</b>	<b>k<sub>d</sub> (1/s)</b>	<b>K<sub>D</sub> (M)</b>	<b>R<sub>max</sub> (RU)</b>
WT	19954.29	0.02487	1.24649E-06	21.6
ΔXF	45040.63	0.00609	1.35264E-07	30.4
<b>mFcγRIV</b>				
<b>VARIANT</b>	<b>k<sub>a</sub> (1/Ms)</b>	<b>k<sub>d</sub> (1/s)</b>	<b>K<sub>D</sub> (M)</b>	<b>R<sub>max</sub> (RU)</b>
WT	5188.43	0.01093	2.10717E-06	70.3
ΔXF	23801.737	0.01031	4.33267E-07	129.9

**Table 6. Representative example of SPR kinetic data.**

Shown in this table is a representative data set showing  $k_a$ ,  $k_d$ ,  $K_D$ , and  $R_{max}$  measurements from an individual SPR experiment for each receptor. For hFcγRI, AvFc<sup>WT</sup> showed faster association than ΔXF as indicated by the increase in  $k_a$  value. However, this was offset by a significant increase in  $k_d$ , which results in faster dissociation and ultimately lower affinity ( $K_D$ ). For hFcγRIIIa, AvFc<sup>ΔXF</sup> had both faster association and slower dissociation, resulting in significantly higher affinity. Interestingly, the increase in affinity for mFcγRIV was due almost entirely to an increase in association rate constant as the dissociation rate constants between the two variants were almost identical. No measurements could be made for the Δgly variant. Increased  $R_{max}$  values for ΔXF generally correspond to the increase in affinity.

#### 5.2.4: AvFc binding to B16F10 cells induces ADCC but not direct cytotoxicity

The impact of the increased affinity to hFcγRIIIa was demonstrated in an *in vitro* ADCC reporter assay, wherein activation of hFcγRIIIa on engineered Jurkat effector cells in the presence of an antibody and a target cell leads to the expression of luciferase, serving as a surrogate for Fc-mediated cell death. In this assay, using B16F10 as the target cell, neither the Δgly or Δlec variants of AvFc were capable of inducing luciferase expression due to the lack of significant affinity to FcγRIIIa or to B16F10 cells (Figure 20A). As hypothesized, incubation with AvFc<sup>ΔXF</sup> resulted in the highest level of luciferase induction (≈ 5.5-fold over background, EC50 = 2.75 nM) while AvFc<sup>WT</sup> showed only a moderate level of induction (≈ 2.9-fold over background, EC50 = 13.78 nM), indicating that increased hFcγRIIIa affinity has functional consequences that could potentially impact AvFc's activity *in vivo*. We further noted that AvFc, by binding to the cell surface alone, fails to induce cell death or inhibit cell proliferation after 48 hours of incubation with B16F10 cells as determined by an MTS viability assay (Figure 20B). Nor does co-incubation with AvFc and B16F10 cells lead to the induction of apoptosis as determined by annexin V/propidium iodide staining (Figure 20C-D). This is in direct contrast to concanavalin A, which is a known cytotoxic lectin that results in significant cell death when incubated with B16F10 cells (Figure 20B-D). Taken together, these results indicate that AvFc could have potent anti-cancer activity *in vivo* against B16F10 tumors due primarily to immune-mediated effector functions. To evaluate this, we opted to directly compare the ΔXF and Δgly variants in the flank tumor model as they represented the extreme ends of the spectrum of Fc-mediated activities, which would

allow us to demonstrate activity as well as infer the extent to which Fc-mediated functions are necessary for said activity.

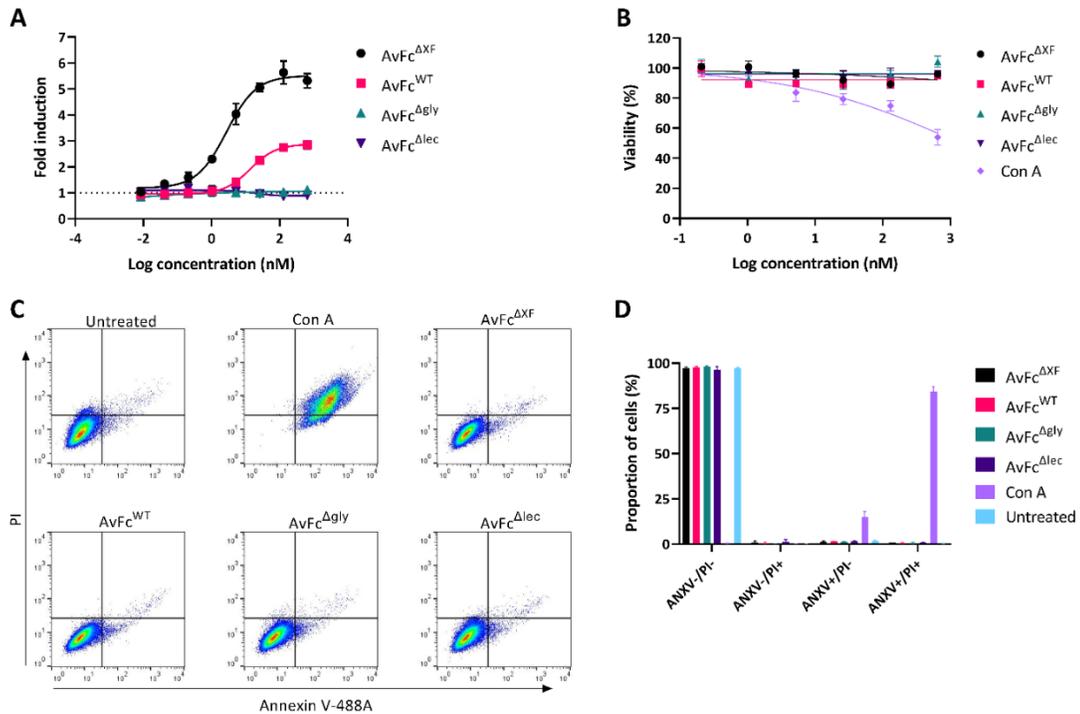


**Figure 20. Induction of ADCC but not cytotoxicity by AvFc.**

(A) Induction of ADCC by AvFc variants assessed using a reporter-cell based luciferase assay. AvFc<sup>ΔXF</sup> showed the highest levels of induction,  $\approx$  5.5-fold above background with an EC<sub>50</sub> of 2.75 nM. The WT variant, on the other hand, showed moderate induction,  $\approx$  2.9-fold over the background with an EC<sub>50</sub> of 13.8 nM. The  $\Delta$ gly and  $\Delta$ lec variants did not induce any luciferase expression, indicating lack of binding to the Fc receptor or to the B16F10 cells, respectively. (B) Impact of AvFc incubation on cell viability by MTS assay. B16F10 cells were co-incubated with AvFc variants or the cytotoxic lectin concanavalin A for 48 hours with concentrations beginning at 650 nM. No effect on cell viability was seen with the AvFc variants, while co-incubation with concanavalin A was found to significantly decrease cell viability at the highest concentrations tested. (C) Representative dot plots of annexin 5/PI staining following coincubation for 48 hours with AvFc variants or concanavalin A. (E) Quantification of results shown in panel C.

Nearly 100% of cells following treatment with any of the AvFc variants stained negative for both annexin v and PI, while nearly all of the cells treated with concanavalin A were in either early or late apoptosis (ANXV+/PI- and ANXV+/PI+, respectively), indicating that binding of AvFc to B16F10 cells likely does not induce apoptosis. All treatment groups were significantly different from concanavalin A in every quadrant except for ANXV-/PI+ (indicating necrosis or advanced cell death), where few cells from any treatment were found (2-way ANOVA). All data are shown as mean  $\pm$  SD.

### 5.2.5: Fc-mediated effector functions are required for AvFc's activity in the B16F10 flank tumor model

We first set out to demonstrate that AvFc recognizes B16F10 tumors *in vivo* using PET/CT imaging of mice with established B16F10 flank tumors. Animals were injected with  $1 \times 10^6$  cells subcutaneously in the hind right flank and imaged after 10 days, at which point 3.7 MBq of a radiolabeled  $^{64}\text{Cu}$ -NOTA-AvFc was administered intravenously. Analysis of the imaging data shows that AvFc strongly accumulates with the tumor (Figure 21D), though some additional signal was seen in the liver (Figure 21D, subpanel 3), spleen (Figure 21D, subpanel 4), and bladder (Figure 21D, subpanel 5). These organs are the primary sites of protein metabolism, and as such background signal in these organs is commonly observed in live animal PET imaging using antibody probes [274].

To assess treatment with AvFc in this model, 100,000 cells were injected subcutaneously into the hind left flank of the animal and tumor sizes were measured every other day beginning the day after implantation (Figure 21A). Intraperitoneal treatment with 25 mg/kg of AvFc $^{\Delta\text{XF}}$ , begun 5 days post-implantation, significantly slowed the growth of the tumors beginning from day 9, while showing no overt toxicity as indicated by the lack of significant deviations in body weight (Figure 21B-C). Aglycosylated AvFc, on the other hand, had no effect on tumor growth over time while maintaining a similar safety profile. These results corroborate our *in vitro* observations and show that not only does AvFc have activity *in vivo*, but that the activity of AvFc against B16F10 seems to be dependent on Fc-mediated effector functions and not through direct cytotoxicity.

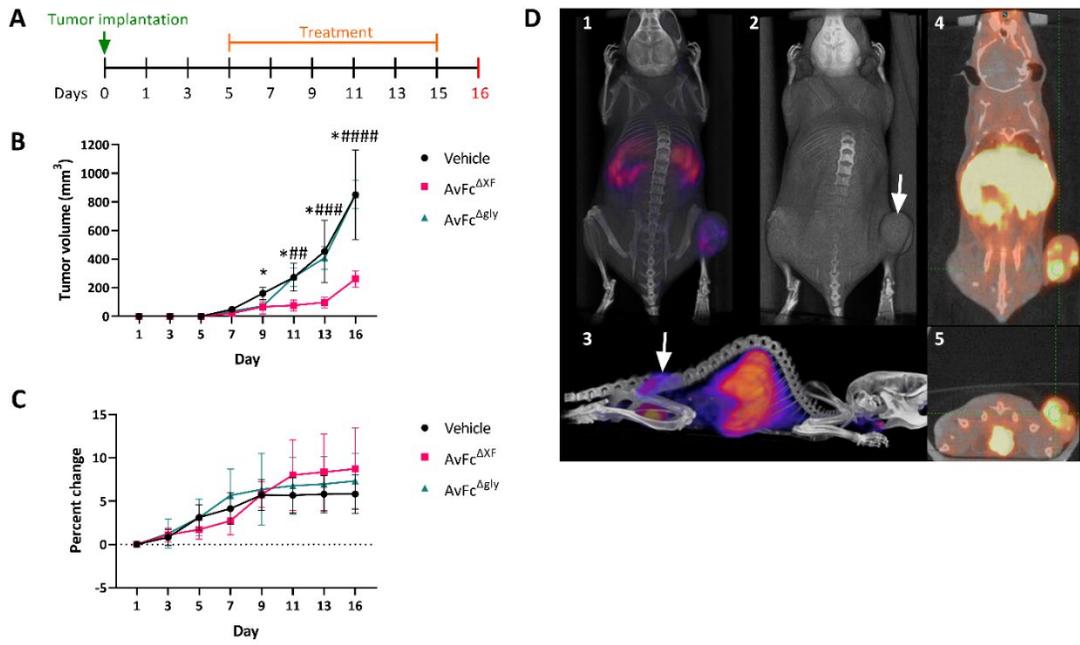


**Figure 21. Activity of AvFc in the B16F10 flank tumor model.**

(A) Study outline. Tumors were implanted into the hind left flank of C57bl/6 mice on day 0, with treatment beginning on day 5 and continuing Q2D until day 15. Treatment was with 25 mg/kg (500 μg) of AvFc<sup>ΔXF</sup> or AvFc<sup>Δgly</sup> administered intraperitoneally in 200 μL of vehicle (n=5/group). Tumor volumes and body weights were measured every other day from day 1 until day 16 when the study was terminated. (B) Change in tumor volumes over time. Beginning on day 9, AvFc<sup>ΔXF</sup> significantly delayed the growth of flank tumors compared to the vehicle-treated group (\*p<0.05 between ΔXF and vehicle). Conversely, the Δgly variant was unable to delay growth and was not significantly different from the vehicle (# p<0.05; ## p<0.01; ### p<0.001; #### p<0.0001; between AvFc<sup>ΔXF</sup> and AvFc<sup>Δgly</sup>). Data shown are mean ± SD. (C) Comparison of body weights between groups during the study, shown as percent change from day 0 weight. No significant differences were noted between groups. (D) Representative PET/CT image of C57bl/6 mice with colocalization of radiolabeled <sup>64</sup>Cu-NOTA-AvFc with B16F10 flank tumors. (D1) Whole

body PET/CT, dorsal view. Signal is clearly visible within the tumor and in the liver.

(D2) Whole body CT, dorsal view. Tumor is indicated by white arrowhead. (D3) Whole

body PET/CT, lateral view. (D4) Coronal slide view, PET/CT scan. Tumor is indicated

by the green crosshairs, which also correspond to the transverse slide view in subpanel 5.

(D5) Transverse slide view, PET/CT scan.

### 5.2.6: Protection against metastatic B16F10 challenge by AvFc requires high-mannose binding

We set out to further characterize AvFc's activity using a metastatic B16F10 melanoma challenge model, comparing AvFc<sup>ΔXF</sup> with the non-sugar-binding mutant AvFc<sup>Δlec</sup>. In this model, 250,000 cells were injected intravenously via the tail vein followed by co-treatment with 25 mg/kg of AvFc<sup>ΔXF</sup>, which began on day 0 and continued Q2D for a total of 6 doses (Figure 22A). This dose was found to significantly reduce the resulting lung tumor burden by more than 3-fold compared to the vehicle ( $p=0.0009$ ) while the non-sugar-binding mutant AvFc<sup>Δlec</sup> offered no protection at the same dose ( $p>0.9999$ , Figure 22B). There was also a significant difference in tumor counts between AvFc<sup>ΔXF</sup> and AvFc<sup>Δlec</sup> at both dose levels ( $p=0.0469$  and  $p=0.0366$ ). As described previously, repeated administration of AvFc was not associated with any overt toxicity or body weight effects (Figure 22C). These data suggest that AvFc has potent *in vivo* activity against B16F10 melanoma, and this mechanism appears to be both dependent on Fc-mediated effector functions and high-mannose binding but not by direct cytotoxicity.

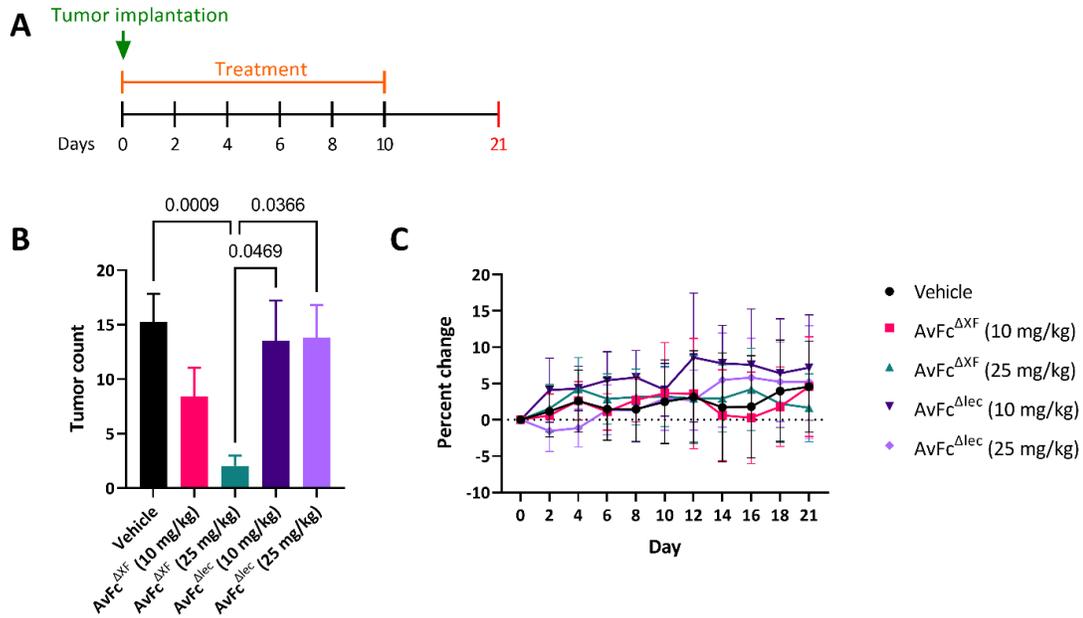


**Figure 22. Activity of AvFc<sup>ΔXF</sup> in the B16F10 melanoma metastasis model.**

(A) Study outline. On day 0,  $2.5 \times 10^5$  cells were injected intravenously into C57bl/6 mice followed by immediate treatment with vehicle, AvFc<sup>ΔXF</sup>, or AvFc<sup>Δlec</sup> at 10 or 25 mg/kg (vehicle n=39; ΔXF 10 mg/kg n=18; ΔXF 25 mg/kg n=28; Δlec 10 mg/kg n=10; Δlec 25 mg/kg n=10). Treatment continued Q2D for a total of 6 doses. Animals were euthanized on day 21, at which point lungs were removed and tumor nodules were counted. (B) Tumor counts. Treatment with AvFc<sup>ΔXF</sup> resulted in a dose dependent reduction in tumor number with significance at 25 mg/kg compared to the vehicle as well as both dose levels of AvFc<sup>Δlec</sup> as determined by the Kruskal-Wallis test. Neither dose level of AvFc<sup>Δlec</sup> showed any protective benefit. Data shown are mean  $\pm$  SEM. (C) Changes in body weight over time. No significant changes in body weight were observed as determined by 2-way ANOVA. Data shown are mean  $\pm$  SD.

### 5.2.7: Impact of pretreatment of mice with AvFc on its anticancer activity *in vivo*.

As a foreign protein, AvFc administration in mice results in the generation of anti-drug antibodies (ADAs), which in theory can compromise the safety and efficacy of the drug. In order to address the consequence of ADA generation on the activity of AvFc *in vivo*, we repeated the flank tumor model and divided it into 2 phases: a pretreatment phase, where groups of animals would receive either AvFc or a vehicle before tumor implantation to generate ADAs, and a treatment phase, where groups of animals would receive AvFc or vehicle following tumor implantation as described above (Figure 23A). The primary endpoint for this study however would be survival, which would be defined as the time from tumor implantation until they reached a volume of 1500 mm<sup>3</sup>, at which point animals were euthanized and blood and other organs taken for analysis. Pretreated animals received 6 doses of AvFc at 25 mg/kg Q2D followed by an 11-day waiting period before tumor implantation (Figure 23A). To confirm the presence of ADAs, serum titers were measured by AvFc-binding ELISA at three points: just prior to tumor implantation, at the beginning of the treatment phase of the study, and following euthanasia of the animals. The results of these assays are reported in Figure 23B. Before the pretreatment, all animals had titers at or near the lowest dilution tested (1:50), likely due to a small matrix effect caused by the mouse serum on the ELISA. By day 20, all of the pretreated animals had measurable ADA titers, with values between 10<sup>4</sup>-10<sup>5</sup> that continued to increase through the end of the study at varying rates. Animals that received AvFc only during the treatment-phase of the study also generated a robust ADA response by the time of euthanasia, between 10<sup>4</sup> and 10<sup>6</sup>. By far, the pretreated and AvFc-treated

group generated the largest ADA response, albeit a more variable one, with titers between  $10^4$  and  $10^8$  at euthanasia.

The effect of pretreatment on animal survival in this model are summarized in Figure 23C-D. Pretreatment with AvFc had no effect on the survival of vehicle-treated animals compared to non-pretreated animals ( $p=0.3049$ ). As was previously observed, treatment with AvFc of non-pretreated animals resulted in delayed tumor growth and increased survival compared to vehicle-treated animals ( $p=0.0067$  vs. non-pretreated animals,  $p=0.0083$  vs. pretreated animals). Interestingly, compared to the non-pretreated AvFc-treated group, pretreatment with AvFc extended the median survival time by nearly 5 days (25 vs. 29.5), though this effect failed to reach statistical significance ( $p=0.0323$ ). These data reveal that ADAs generated against AvFc do not appear to neutralize the drug and make it ineffective, nor did they present any obvious safety concerns over the course of the study with no major adverse events or body weight effects noted. On the contrary, it seems that the presence of ADAs may have increased the anti-tumor activity of AvFc, which challenges the conventional wisdom surrounding ADAs and cancer immunotherapy.

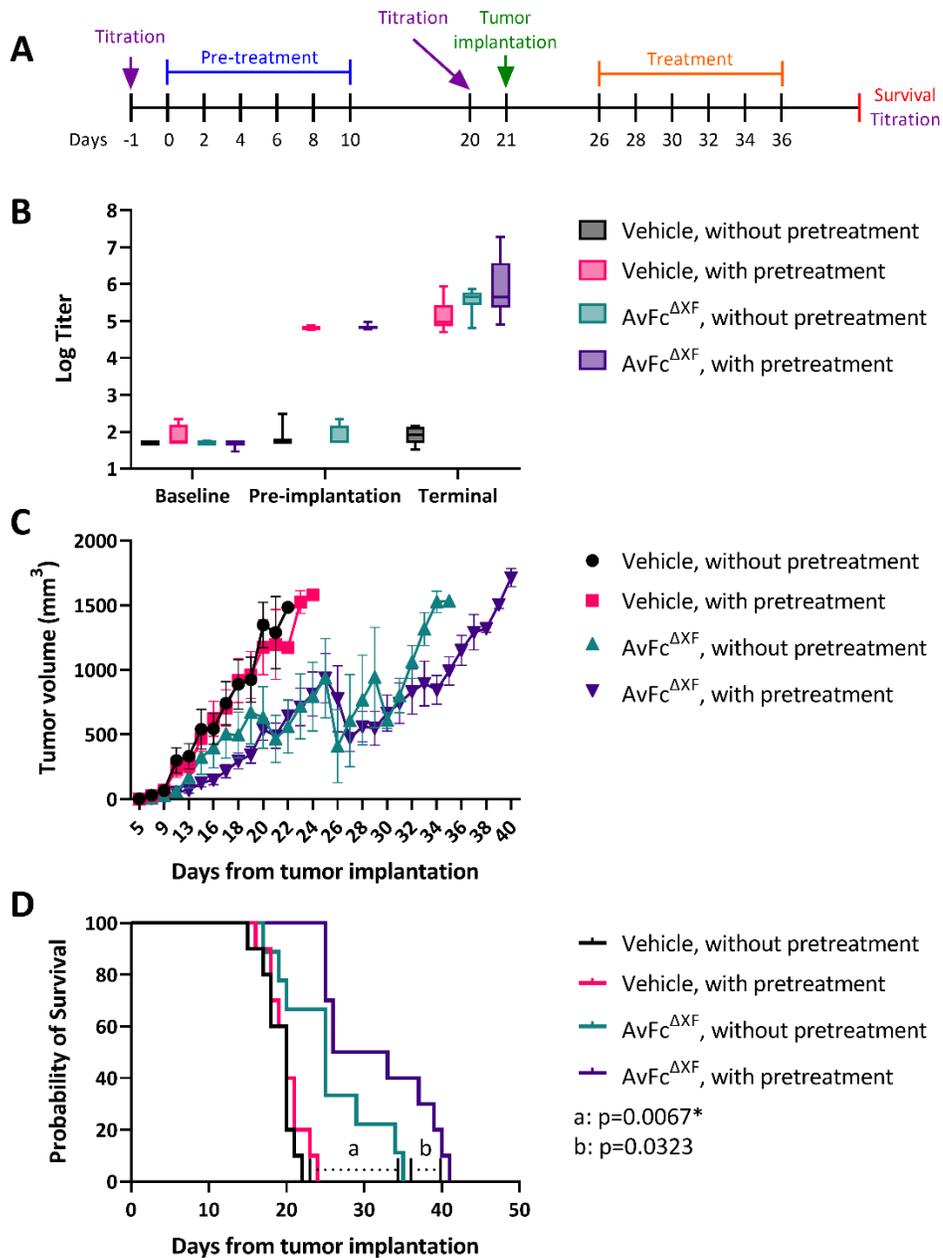


**Figure 23. Impact of pretreatment on the anticancer activity of AvFc *in vivo*.**

(A). Study outline. The study was divided into a pretreatment and a treatment phase that followed implantation of tumors. A set of 40 animals were divided into 4 groups, two of which would receive pretreatment and two that would not. Of the two that were either pretreated or not, one would receive vehicle as treatment during the second phase and the

other would receive AvFc<sup>ΔXF</sup>. Treatment was administered i.p. at 25 mg/kg, and blood was taken at different time points to monitor ADA generation. Animals were monitored by survival which was defined as the time necessary for tumors to reach  $\approx 1500 \text{ mm}^3$ . (B) ADA measurements. Animals were negative for ADAs at baseline (day -1). After pretreatment (day 20), pretreated animals had measurable ADAs in the  $10^4$  to  $10^5$  range. Following euthanasia (at survival endpoint), All animals that received AvFc<sup>ΔXF</sup> during either the pretreatment or treatment phase had measurable ADAs, the ranges of which varied between groups and was highest with the animals that received both pretreatment with AvFc<sup>ΔXF</sup> and were treated with it additionally. (C) Impact of AvFc on tumor volumes over time. Pretreatment with AvFc<sup>ΔXF</sup> had no effect on tumor growth rate in the vehicle treated groups, and tumors grew rapidly in both (black and red lines). Treatment with AvFc<sup>ΔXF</sup> was associated with slower tumor growth in the group that was not pretreated (green line). With both pretreatment and treatment, the delay of tumor growth was more significant (purple line). (D) Effect of pretreatment on survival. Pretreatment did not improve or worsen survival for the vehicle-treated groups, which both had median survival times of 20 days (black and red lines). Treatment of B16F10 tumors with AvFc<sup>ΔXF</sup> but without pretreatment resulted in a significant increase in median survival ( $p=0.0067$ , log-rank test) from 20 to 25 days. Pretreatment strengthened this effect, increasing median survival from 25 to 29.5 days though it was not statistically significant ( $p=0.0323$ , log-rank test).

### 5.2.8: Flow cytometry analysis of B16F10 tumor-infiltrating immune cells

One of the hallmarks of cancer is immune evasion and the conversion of the local immune microenvironment from a pro-inflammatory, anti-tumor response to an anti-inflammatory, pro-tumor response. Since AvFc is a foreign protein that provokes an immune response (see section 5.2.7), we hypothesized that administration of the drug to tumor-bearing mice may result in a shift towards a more inflammatory cell phenotype and increased cell infiltrates, which may play a role in its anti-cancer mechanism of action. To explore this hypothesis, we performed flow cytometry on immune cells isolated from B16F10 tumors after vehicle or AvFc treatment to assess changes in the composition due to drug treatment. In this experiment, tumors were implanted into the hind-left flank of C57bl/6 mice on day 0, with intraperitoneal treatment with 25 mg/kg AvFc or 200  $\mu$ L vehicle beginning on day 5. A total of 3 doses were given before the animals were euthanized on day 10 and tumors removed and digested for immune cell isolation. Cells were stained with 4 panels of antibodies for immunophenotyping: one for NK cells, one for myeloid cells, one for dendritic cells, and one for T lymphocytes. B cells were not analyzed in this experiment. The complete list of markers used is summarized in Table 7. Cell counts were normalized based on tumor weight. Consistent with results from the previous study (Section 5.2.5, 5.2.7), tumors from AvFc-treated animals were significantly smaller than those from the vehicle group (Figure 27A). In addition, all cell populations analyzed had a slight but non-significant trend towards increased cell numbers per gram tumor weight with the exception of non-classical Ly6C-monocytes, which were all significantly increased in AvFc-treated tumors (Figure 27,

Figure 30, Figure 34). These results suggest that part of AvFc's mechanism of action may be due to the increased recruitment of immune cells to the tumor site.

<b>Population</b>	<b>Markers</b>
NK Cells	CD45+, CD3-, NK1.1+
<b>Lymphocytes</b>	
CD8 T cells	CD8+, TCRβ+
CD4 T cells	CD4+, TCRβ+
Th1 CD4 T cells	As above, IFNγR+
Th2 CD4 T cells	As above, IL-33R+
Th17 CD4 T cells	As above, IL-23R+
<b>DCs</b>	
Classical DCs CD11b+	MHCII+, CD11c+, CD103-, CD11b+
	CX3CR1 <sup>hi</sup> /CD206+
	CX3CR1 <sup>lo</sup> /CD206-
Classical DCs CD11b-	MHCII+, CD11c+, CD103-, CD11b-
Activation/costimulatory markers	CD68, CD69, CD80, CD86
<b>Myeloid cells</b>	
Neutrophils	CD11b+, Ly6G+
Macrophages	MHCII+, Ly6C+, F4/80 <sup>hi</sup>
Classical Monocytes	MHCII+, Ly6C+, F4/80-
	CX3CR1 <sup>hi</sup>
	CX3CR1 <sup>lo</sup>
	CD206+
Non-classical monocytes	MHCII+, Ly6C-
	F4/80-, CX3CR1 <sup>lo</sup>
	F4/80-, CD206+
	CX3CR1 <sup>lo</sup> , CD206-
	CX3CR1 <sup>hi</sup>
	CX3CR1 <sup>hi</sup> , CD206-

**Table 7. Summary of cell-surface markers used in B16F10 tumor**

**immunophenotyping.**

The marker panel was designed with the assistance of Dr. Noel Verjan Garcia.

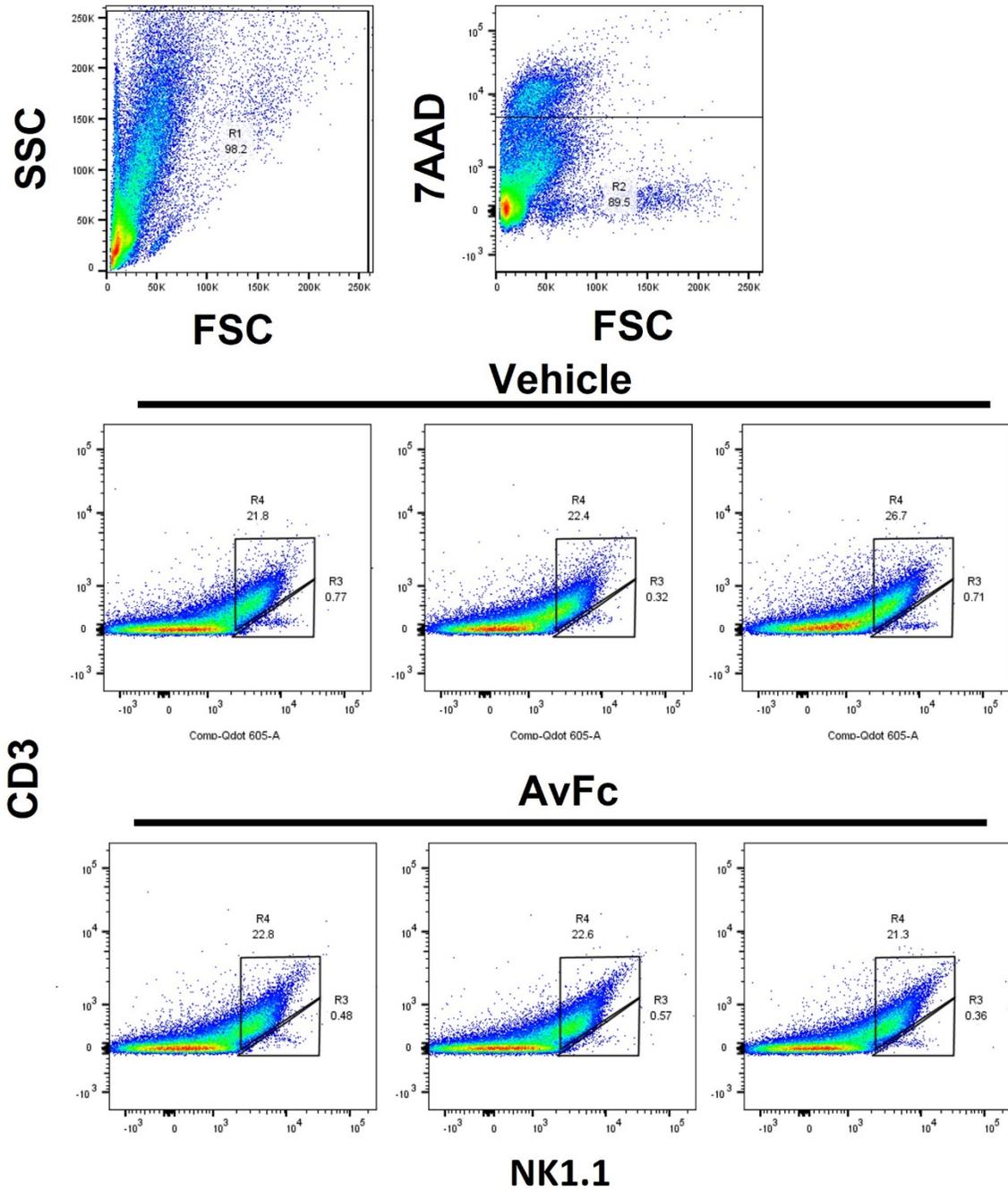


**Figure 24. NK cell gating strategy.**

Differentiation between lymphocytes and tumor cells was not possible through FSC/SSC gating, so all cells were chosen for further analysis. Live cells were defined as 7AAD-.

NK cells were defined as CD3-/NK1.1+. Gating was performed with the assistance of Dr.

Noel Verjan Garcia.

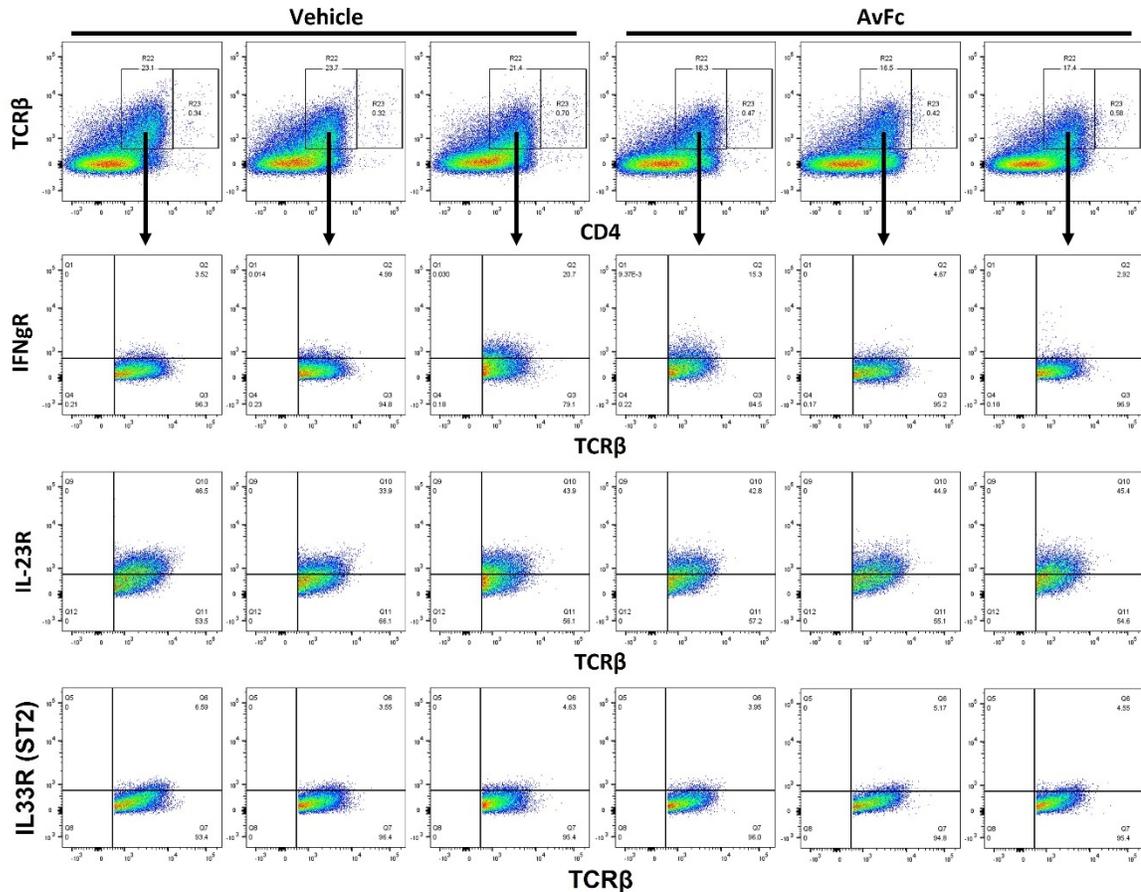


**Figure 25. CD4 T cell gating strategy.**

Differentiation between lymphocytes and tumor cells was not possible through FSC/SSC gating, so all cells were chosen for further analysis (not shown). Live cells were defined as 7AAD<sup>-</sup> (not shown). CD4 T cells were defined as TCRβ<sup>+</sup>/CD4<sup>+</sup>. A second population of increased CD4<sup>+</sup> expression was identified but not analyzed. Double positive cells were then separately analyzed for IFNγR (Th1), IL-23R (Th2), or IL-33R (Th17) expression on the Y axis using TCRβ as the X axis marker. Gating was performed with the assistance of Dr. Noel Verjan Garcia.

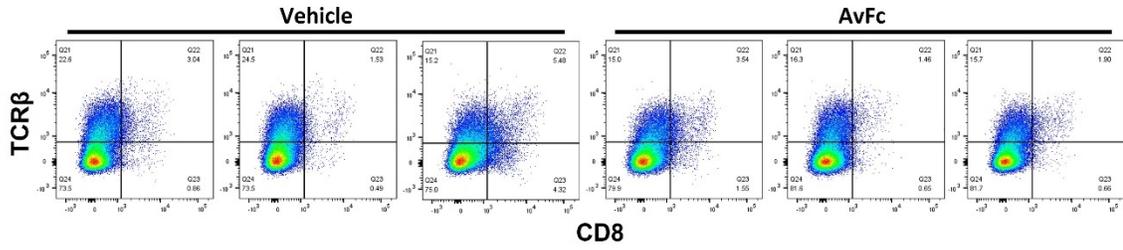


**Figure 26. CD8 T cell gating strategy.**

Differentiation between lymphocytes and tumor cells was not possible through FSC/SSC gating, so all cells were chosen for further analysis (not shown). Live cells were defined as 7AAD- (not shown). CD8 T cells were defined as TCRβ+/CD8+. Gating was performed with the assistance of Dr. Noel Verjan Garcia.

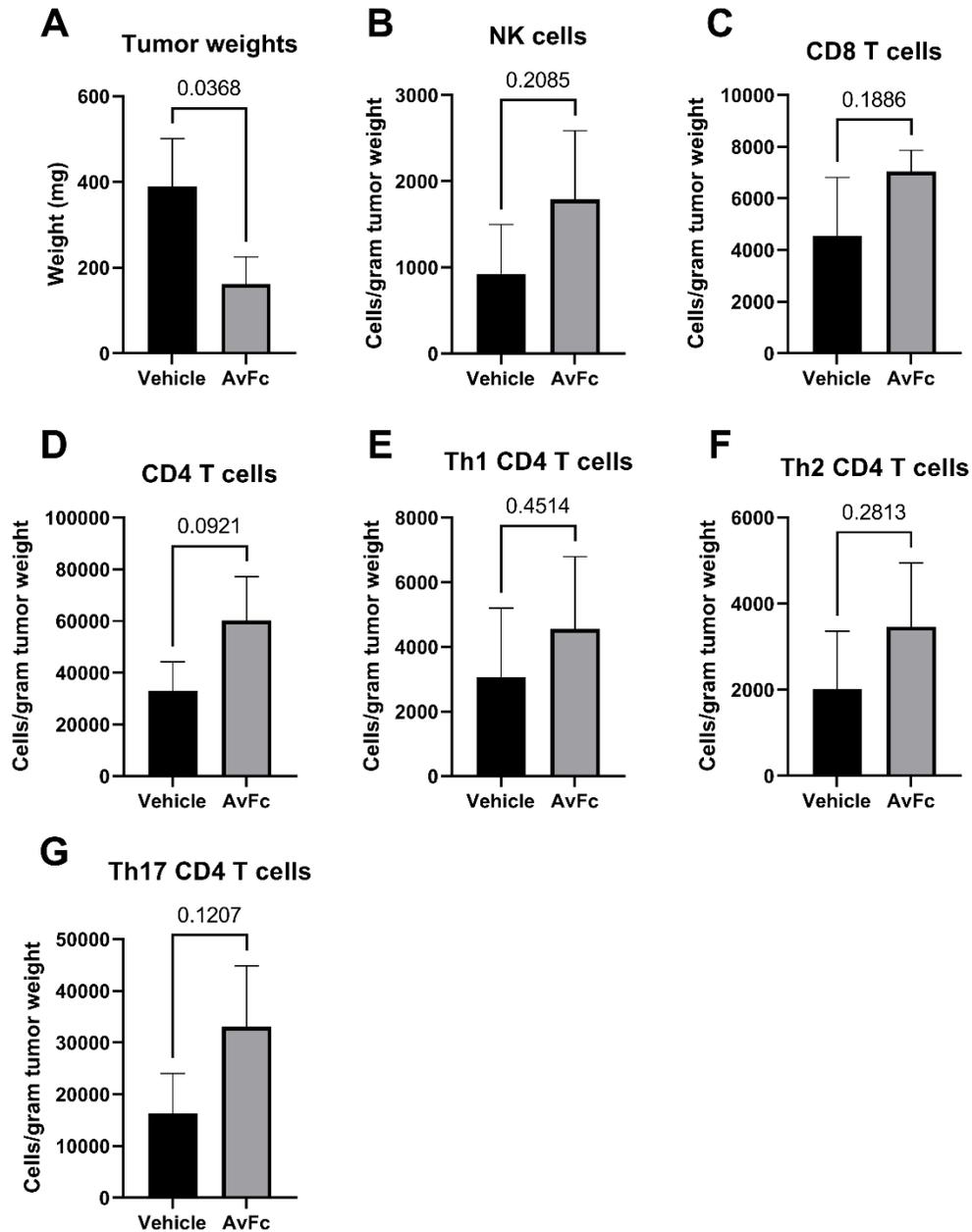


**Figure 27. Comparison of NK and T cell subsets within B16F10 tumors.**

All statistical comparisons were made with the Student's T test with Welch's correction.

(A) Comparison of tumor weights at the time of excision from the animals. Tumors removed from AvFc-treated animals were significantly smaller than those from vehicle-treated animals. While there was a trend towards increased cell numbers, no statistical significance was observed for each of the following populations: B, NK cells (CD3-

/NK1.1+); C, CD8+ T cells (TCR $\beta$ + /CD8+); D, CD4 T cells (TCR $\beta$ + /CD4+); E, Th1 cells (TCR $\beta$ + /CD4+ /IFN $\gamma$ R+); F, Th2 cells (TCR $\beta$ + /CD4+ /IL-23R+); G, Th17 cells (TCR $\beta$ + /CD4+ /IL-33R).

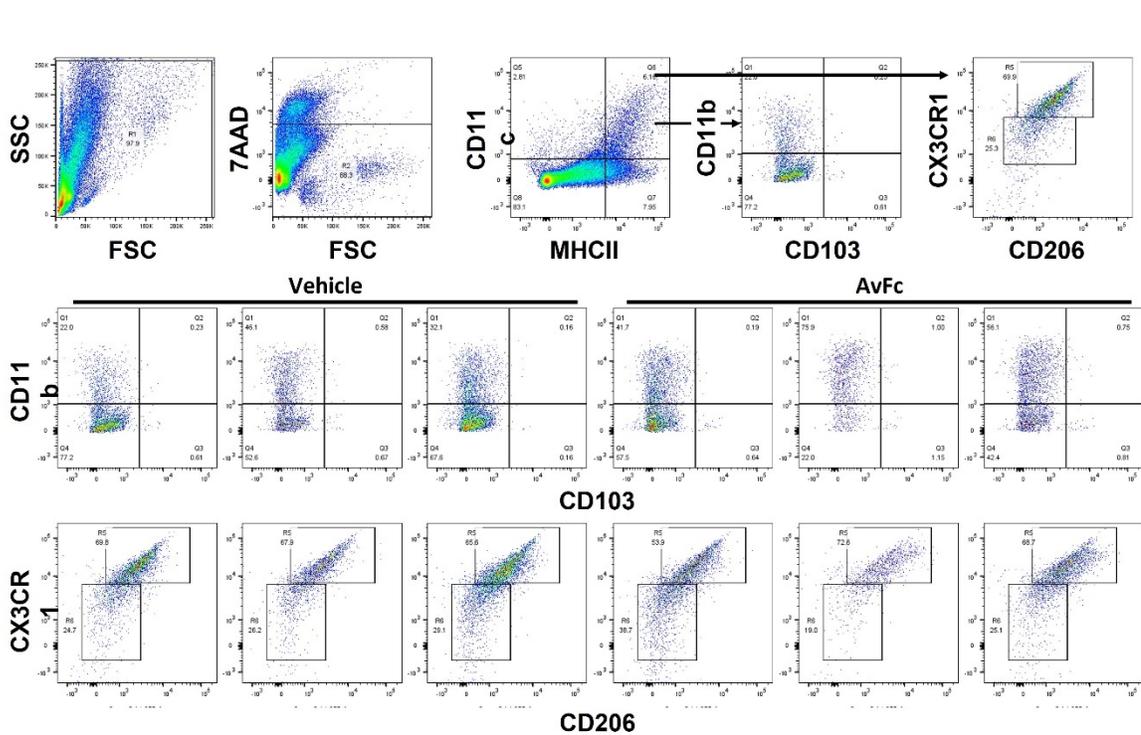


**Figure 28. Dendritic cell gating strategy.**

Differentiation between lymphocytes and tumor cells was not possible through FSC/SSC gating, so all cells were chosen for further analysis. Live cells were defined as 7AAD-. MHCII+/CD11c+ cells were subsequently analyzed for CD11b, CD103, CX3CR1, and CD206 expression. Gating was performed with the assistance of Dr. Noel Verjan Garcia.

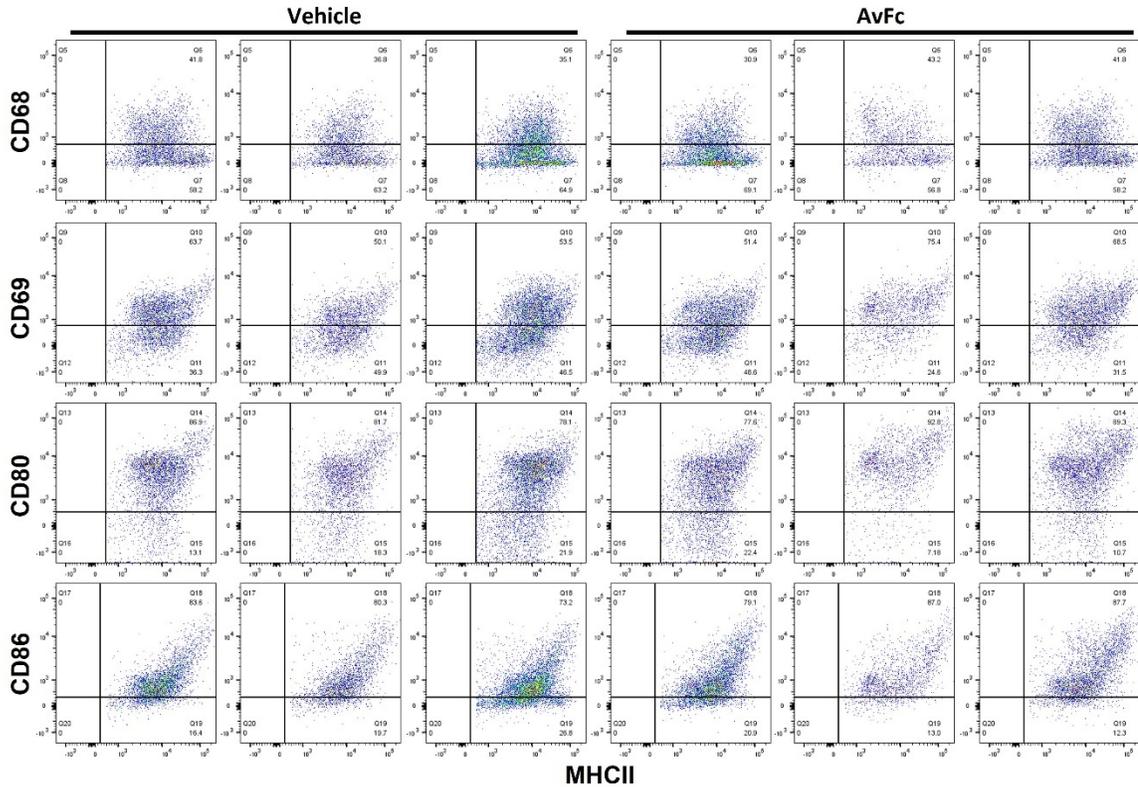


**Figure 29. Gating strategy for DC activation and costimulatory markers.**

Analysis of the activation status and costimulatory molecule expression of CD11b+/CD103- DCs from Figure 28 was performed by plotting CD68, CD69, CD80, and CD86 against MHCII. Gating was performed with the assistance of Dr. Noel Verjan Garcia.

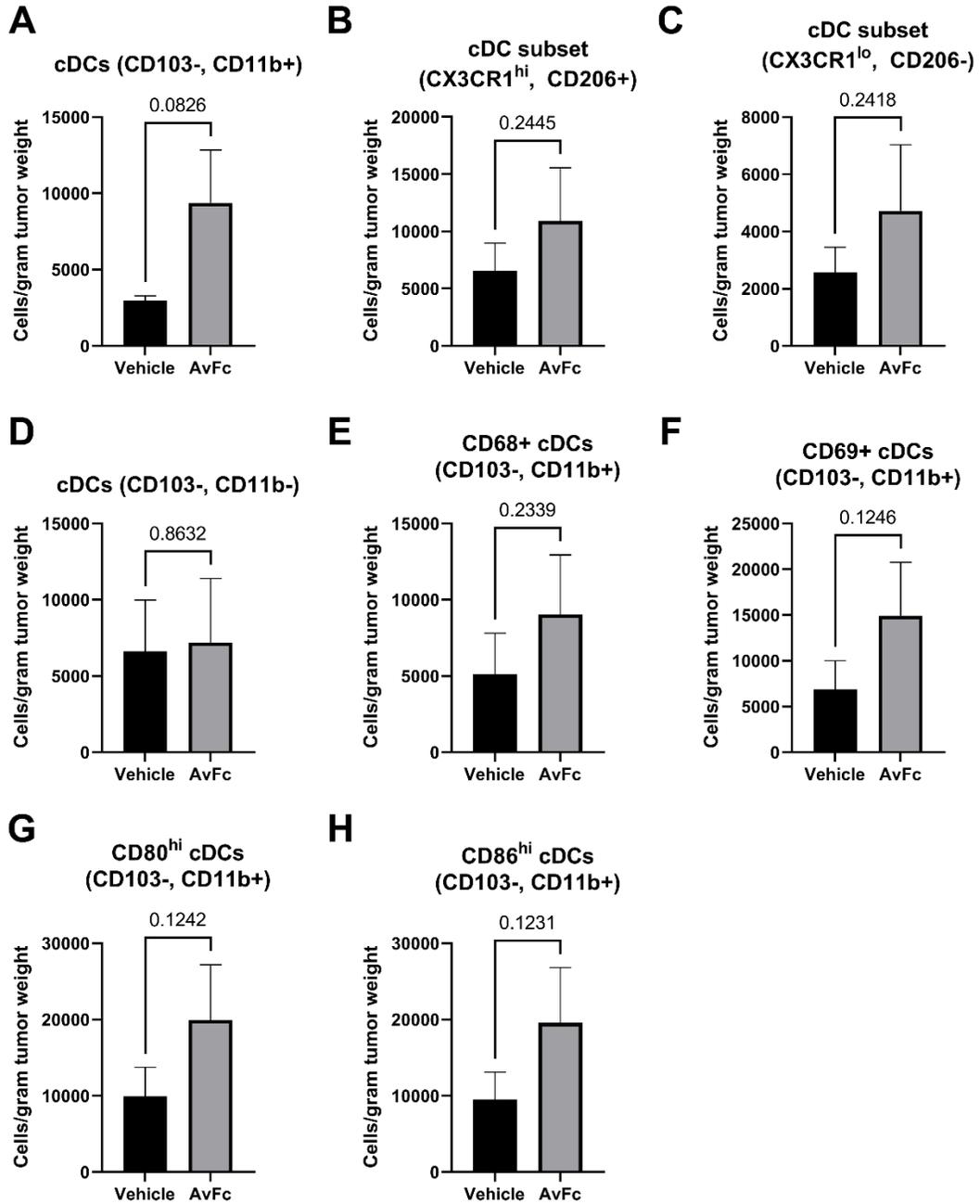


**Figure 30. Comparison of classical dendritic cell subsets within B16F10 tumors.**

All statistical comparisons were made with the Student's T test with Welch's correction.

No statistically significant increases were seen, however a trend towards increased intratumoral classical DCs (cDCs) and increased activation/costimulatory molecule expression was observed. A: cDCs (CD11c<sup>+</sup>/MHCII<sup>+</sup>/CD11b<sup>+</sup>/CD103<sup>-</sup>). B:

CX3CR1<sup>hi</sup>/CD206<sup>+</sup> subset of CD11b<sup>+</sup> cDCs in A. C: CX3CR1<sup>lo</sup>/CD206<sup>-</sup> subset of CD11b<sup>+</sup> cDCs in A. D: CD11b<sup>-</sup> cDCs (CD11c<sup>+</sup>/MHCII<sup>+</sup>/CD11b<sup>-</sup>/CD103<sup>-</sup>). E: CD68<sup>+</sup> cDCs (CD11b<sup>+</sup>/CD103<sup>-</sup>). F: CD69<sup>+</sup> cDCs (CD11b<sup>+</sup>/CD103<sup>-</sup>). G: CD80<sup>+</sup> cDCs (CD11b<sup>+</sup>/CD103<sup>-</sup>). H: CD86<sup>+</sup> cDCs (CD11b<sup>+</sup>/CD103<sup>-</sup>).

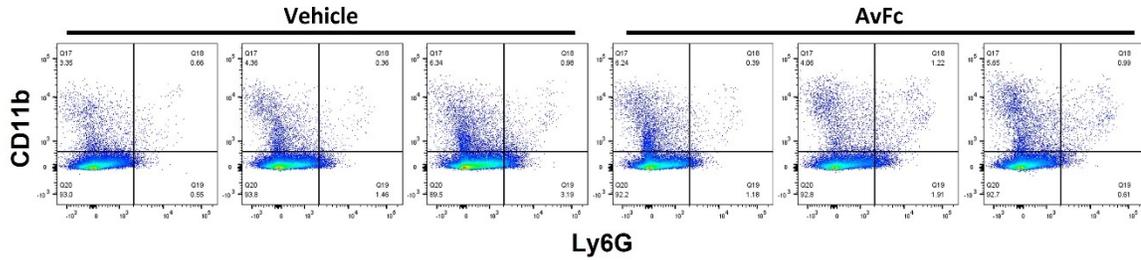


**Figure 31. Neutrophil gating strategy.**

Differentiation between lymphocytes and tumor cells was not possible through FSC/SSC gating, so all cells were chosen for further analysis (not shown). Live cells were defined as 7AAD- (not shown). Neutrophils were defined as CD11b+/Ly6G+. Gating was performed with the assistance of Dr. Noel Verjan Garcia.

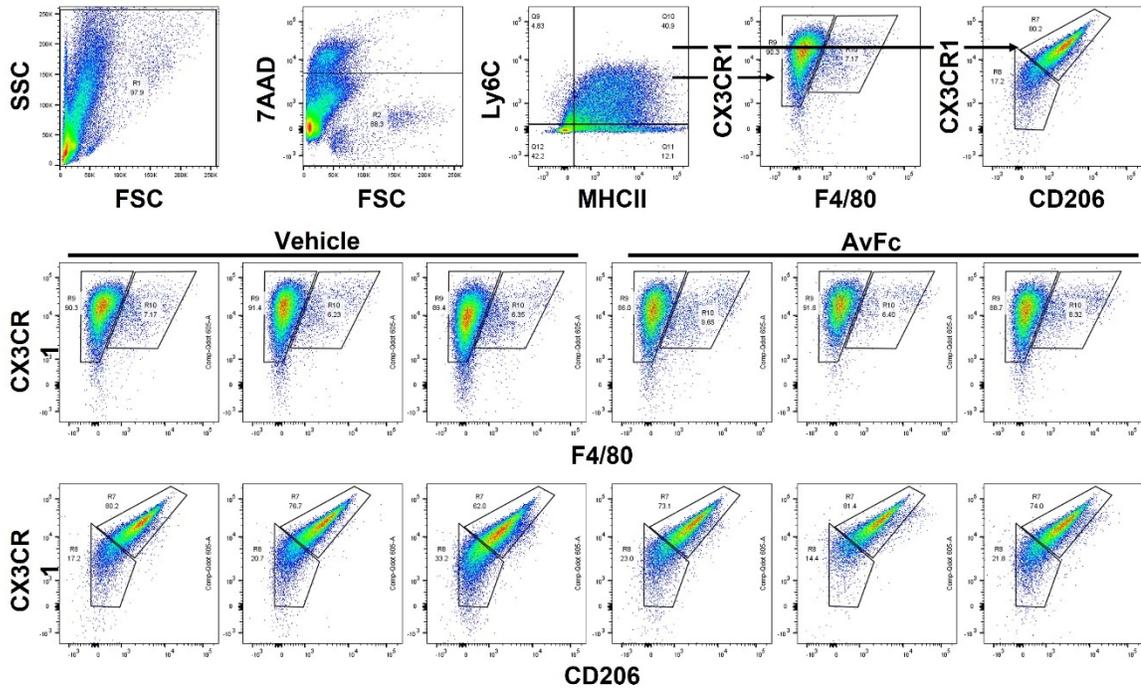


**Figure 32. Classical monocyte/macrophage gating strategy.**

Differentiation between lymphocytes and tumor cells was not possible through FSC/SSC gating, so all cells were chosen for further analysis. Live cells were defined as 7AAD-. Classical monocytes were defined as MHCII+/Ly6C+ cells. Macrophages are defined as MHCII+/Ly6C+/F480+. Double positive cells were then analyzed for CX3CR1, F4/80, and CD206 expression. Gating was performed with the assistance of Dr. Noel Verjan Garcia.

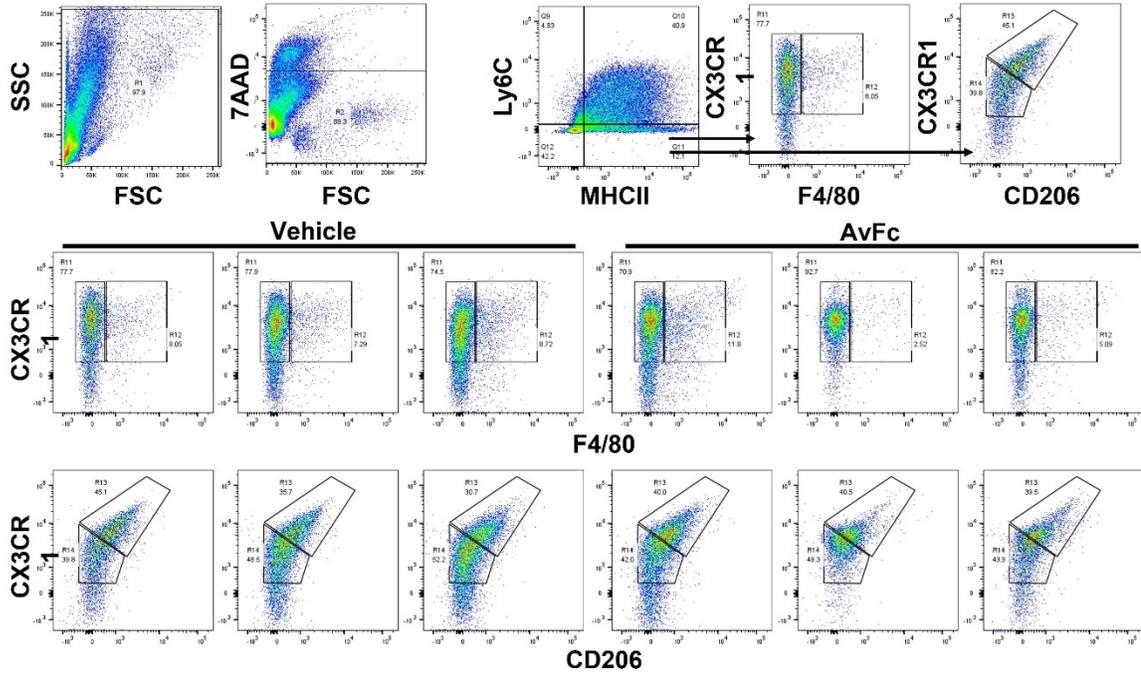


**Figure 33. Non-classical monocyte gating strategy.**

Differentiation between lymphocytes and tumor cells was not possible through FSC/SSC gating, so all cells were chosen for further analysis. Live cells were defined as 7AAD-. Non-classical monocytes were defined as MHCII+/Ly6C- cells. Double positive cells were then analyzed for CX3CR1, F4/80, and CD206 expression. Gating was performed with the assistance of Dr. Noel Verjan Garcia.

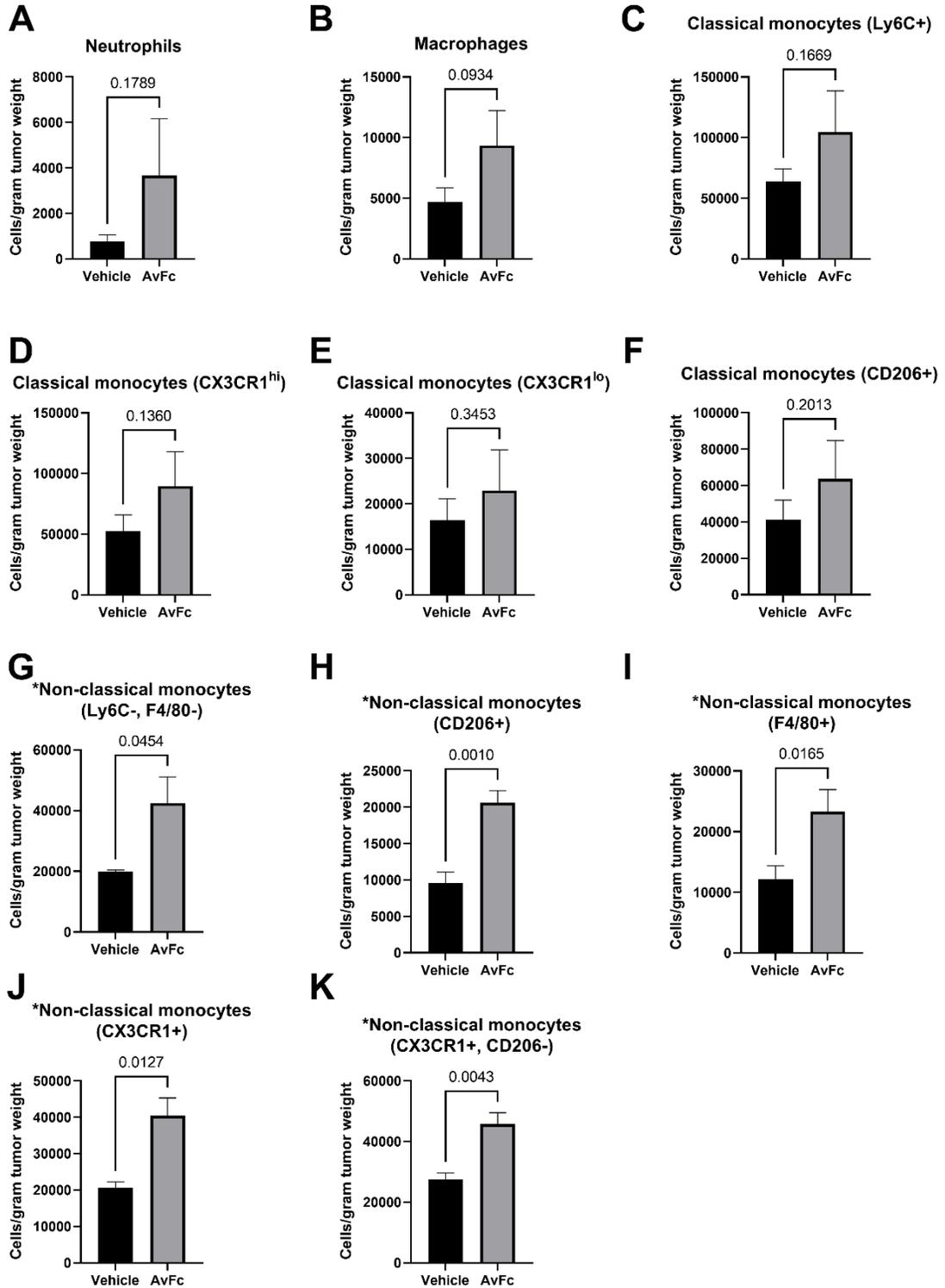


**Figure 34. Comparison of neutrophil, macrophage, and monocyte populations within B16F10 tumors.**

All statistical comparisons were made with the Student's T test with Welch's correction. No statistically significant changes were observed in neutrophils, macrophages, or classical monocytes (A-F), however as with other cell populations a trend towards an increase was seen. Statistically significant increases were observed in all subsets of non-classical monocytes (G-K). A: Neutrophils (CD11b+/Ly6G+). B: Macrophages (MHCII+, Ly6C+, F4/80<sup>hi</sup>). C: Classical monocytes (MHCII+/Ly6C+). D: CX3CR1<sup>hi</sup> subset of classical monocytes. E: CX3CR1<sup>lo</sup> subset of classical monocytes. F: CD206+ subset of classical monocytes. G: Non-classical monocytes (MHCII+/Ly6C-/F480-). H: CD206+ subset of non-classical monocytes in G. I: F4/80+ subset of non-classical monocytes. J: CX3CR1+ subset of non-classical monocytes in G. K: CX3CR1+/CD206- subset of non-classical monocytes in G.

### 5.3: Discussion

Plant-based recombinant expression systems have found some success as rapid, robust, and scalable alternative manufacturing platforms for pharmaceutical proteins [275, 276]. A useful characteristic of many of the plants used for pharmaceutical production, in particular *N. benthamiana*, is that they are generally readily amenable to engineering using modern techniques including RNA interference (RNAi), transcription activator-like effector nucleases (TALENs), zinc-finger nucleases, and CRISPR/Cas9 [277-280]. Therefore, *N. benthamiana* can be exploited to generate glycoengineered variants of biologics that have higher levels of activity *in vivo* and may obviate some safety concerns regarding the presence of plant N-glycans. Removal of either the human  $\alpha$ 1,6- or plant  $\alpha$ 1,3-linked core fucose residues through genetic engineering of the expression host has long been known to dramatically increase the affinity of monoclonal antibodies for Fc $\gamma$ Rs, especially hFc $\gamma$ RIIIa, and improve their activity both *in vitro* and *in vivo* [266, 281]. Thus, for therapeutic antibodies or other Fc-bearing molecules such as AvFc where ADCC is a major mechanism of action, such a modification would be highly valuable. In this study, we show that expression of our candidate anti-cancer immunotherapeutic AvFc in glycoengineered  $\Delta$ XF plants results in the total loss of plant-derived glycans, with the predominant glycoform being the truncated, “humanized”, GnGn form (Table 5, Figure 17). However, compared to mAbs expressed in WT or  $\Delta$ XF plants, AvFc displays some idiosyncrasies with regards to its glycan composition.

The first of these is that AvFc<sup>WT</sup> contains few plant-derived glycans, with glycoforms containing  $\beta$ 1,2-xylose and  $\alpha$ 1,3-fucose (XF) representing only 33% of the total glycan population compared to upwards of 90% for most plant-expressed mAbs

(Table 5) [265, 282-284]. The second is that both AvFc<sup>WT</sup> and AvFc<sup>ΔXF</sup> display large proportions of high-mannose glycans, which are typically only present on mAbs in very small amounts when expressed in plants [265, 282-284]. These two observations may indeed be somewhat linked, as an overabundance of high-mannose glycans on recombinant proteins can be the result of extended residency or accumulation in the endoplasmic reticulum, such as is seen when antibodies are tagged with the ER-retention signal KDEL [285]. Given that AvFc is a high-mannose-binding lectin, it is highly possible that it forms complexes with itself or with other ER-resident glycoproteins during expression, preventing export to the Golgi apparatus for further processing and resulting in an accumulation of high-mannose glycans. Similarly high levels of high-mannose glycans have been identified on mAbs with atypical structures such as mono- and multivalent single-chain variable fragments, which are hypothesized to be retained in the ER due to prolonged interaction with BiP in the absence of the light chain constant region [282, 286]. However, similar findings have not been reproduced for Fc fusion proteins produced in mammalian cells or in plants [287-293]. It should be noted that AvFc manufactured in CHO cells also has increased levels of high-mannose glycans compared to normal mAbs, though there are fewer, and the predominant form is Man5 (data not shown), indicating a greater degree of processing but also suggesting that the increase is due to a property of AvFc and not the production host. The increased presence of high-mannose glycans may also help to partially explain the relatively low half-life of AvFc<sup>ΔXF</sup> in mice and rhesus macaques ( $\approx 22$  and  $\approx 28$  hrs, respectively, as reported in [98, 211]) compared to normal mAbs, as antibodies and other Fc-bearing molecules containing high-mannose glycans are more rapidly cleared from the organism by the

immune system [294]. AvFc<sup>ΔXF</sup> also had a longer half-life in female mice than AvFc<sup>WT</sup> (≈ 14 hours for the WT variant, data not shown vs. ≈ 18.5 hrs for the ΔXF variant, Figure 35 and [211]), possibly due to the reduction in high-mannose glycan content compared to the WT (Table 5). Additionally, we have previously shown that AvFc has lower affinity to FcRn compared to normal human IgG1, which also impacts half-life [98].

Improvements to half-life could be made through the introduction of amino acid substitutions that improve FcRn affinity such as those described by Mackness et al. [295]. Work is being done to elucidate the cause of the increase in high-mannose, including by assessing the glycan profile of the non-sugar-binding mutant AvFc<sup>Δlec</sup>, which may not interact with itself or other proteins in the ER.

It is well known that removal of the core fucose residues increases the ADCC activity of mAbs [163]. Our results show that AvFc<sup>ΔXF</sup>, which lacks both core xylose and core fucose, does indeed have higher affinity to both hFcγRIIIa (and its murine equivalent mFcγRIV) and hFcγRI in addition as determined by SPR (Figure 19). Functionally, removal of plant glycans made the ΔXF variant of AvFc nearly twice as efficacious and 5 times more potent in the ADCC reporter assay against B16F10 cells, while neither the Δlec nor Δgly variants were capable of inducing ADCC (Figure 20A). AvFc<sup>ΔXF</sup> also had a longer half-life in mice than AvFc<sup>WT</sup> (≈ 14 hours for WT vs. ≈ 22 hrs, Figure 35 and [211]).

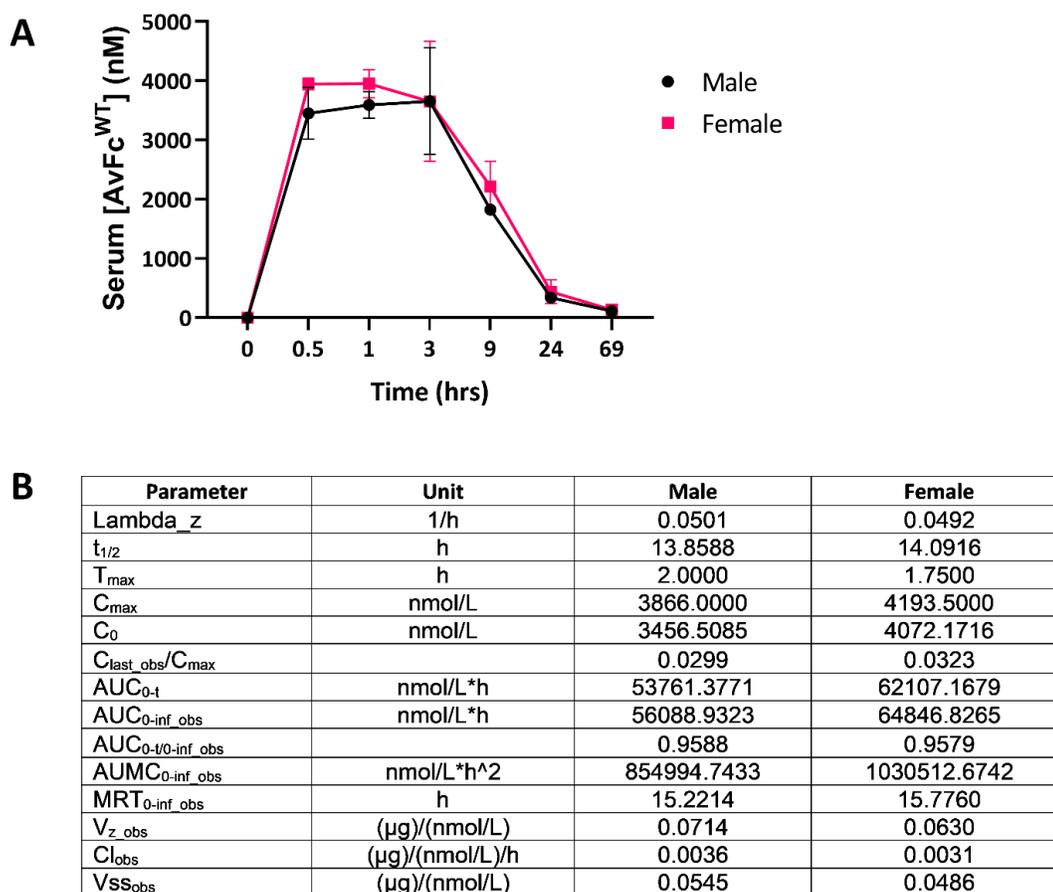


**Figure 35. Pharmacokinetic analysis of AvFc<sup>WT</sup>.**

Pharmacokinetic profiles for WT AvFc were measured in male and female C57bl/6 mice (n=3 per gender) following a single intravenous dose of 10 mg/kg. Serum concentrations of AvFc<sup>WT</sup> were determined by gp120-binding ELISA at various time points and PK parameters were calculated by PK Solver. These parameters were generally similar between the two sexes. The half-life of AvFc<sup>WT</sup> was determined to be approximately 14 hours in both male and female mice.

Results from the *in vitro* assays (Figure 20) and the B16F10 challenge model (Figure 21) suggest that the antitumor activity of AvFc is almost exclusively attributable to the induction of Fc-mediated effector functions, in particular ADCC. As shown in Figure 20, AvFc induced high levels of ADCC without directly causing cell death as determined by both an MTS assay and annexin V/propidium iodide staining, with the AvFc<sup>ΔXF</sup> variant producing a much higher ADCC response than AvFc<sup>WT</sup>. In addition, we did not find that AvFc inhibited B16F10 migration (data not shown), demonstrating that binding alone is likely not sufficient for AvFc to exert activity against B16F10 cells. However, we have also recently reported that AvFc can inhibit the migration of H460 and A549 human lung cancer cells in addition to inducing ADCC against these cell lines [105]. The discrepancy between the findings in the present study with B16F10 cells and the previous one with H460 and A549 may be partly explained by specific cell-surface glycoproteins targeted by AvFc; for example, in the previous study we showed that the lectin body's binding to EGFR and IGF1R led to the inhibition of receptor phosphorylation and downstream signaling [105]. Thus, we speculate that the collective antitumor mechanisms of AvFc may be dependent on the characteristics of cancer cells targeted although Fc-mediated activity is likely the lectin body's primary mode of action. We also reported in this study that administration of AvFc<sup>ΔXF</sup> but not AvFc<sup>Δgly</sup> delayed the growth of B16F10 flank tumors *in vivo* (Figure 21). AvFc<sup>ΔXF</sup> was also found to significantly reduce the number of tumor nodules in mouse lungs in the B16F10 metastasis model while the non-sugar-binding mutant AvFc<sup>Δlec</sup> did not (Figure 22). Combined, these results suggest that, at least in the B16F10 model, both sugar-binding activity and Fc-mediated

effector functions are necessary for AvFc's anti-cancer activity, and direct cell-killing likely does not occur.

A potential concern when administering foreign proteins as therapeutics is immunogenicity, which has the potential to limit drug efficacy after repeated dosing and can result in serious adverse events related to hypersensitivities, owing to the induction of ADAs and immunological memory to the drug [296]. One of the more striking findings in this study was that pretreatment with AvFc and generation of ADAs did not negate AvFc's activity (Figure 23). On the contrary, it appears that the presence of ADAs may have improved its activity, resulting in an increase in median survival time (defined as the time from tumor implantation to the time the tumor reached a volume of 1500 mm<sup>3</sup>) from 25 to 29.5 days compared to the AvFc<sup>ΔXF</sup>-treated group without preexisting ADAs. While this increase was not statistically significant after correcting for multiple comparisons (p=0.0323), the data show a clear trend that at the very least indicates that the ADA response to AvFc did not undermine the drug efficacy in this model. At most, it demonstrates that the presence of ADAs may actually have some benefit, though the reason for this is not known.

A concerning observation regarding animal safety came following the first administration of AvFc during the treatment phase (on day 26, see Figure 23A) in the group of animals that had previously received AvFc pretreatment. Approximately 2 hours after i.p. administration 6 of the 10 animals developed symptoms consistent with either anaphylaxis or a delayed-type hypersensitivity including labored breathing, closed eyes, hunching, lack of movement, and lack of response to touch [297, 298]. This development resulted in a medical case being opened by the veterinary staff, and the animals were

monitored for several hours until it appeared that they had recovered by the late afternoon. This reaction did not develop again after subsequent doses and was not seen in any other group except for those that had received pretreatment. While it cannot be conclusively determined whether or not the animals were having an anaphylactic reaction to the drug from this experiment alone, the possibility that the animals may develop a hypersensitive or anaphylactic response to AvFc certainly requires further investigation.

In recent years, it has become increasingly evident that tumors are highly adept at managing the local immune microenvironment, converting it from an immunogenic to an immunosuppressive environment [299-301]. This conversion makes tumors more aggressive and allows them to better invade the surrounding tissues and metastasize, leading to poorer clinical outcomes [302]. This fact has led to the institution of a novel paradigm of cancer immunotherapy whose objective is to target not the tumor but the host immune response, helping to convert immunologically “cold” tumors to immunologically “hot” ones that can be better treated [303]. The most prominent examples of this are the checkpoint inhibitors that target the inhibitory receptors PD-1 and CTLA-4 on T cells, preventing the tumor-initiated deactivation of cytotoxic T lymphocytes in the local microenvironment leading to a better anti-tumor immune response and better treatment outcomes [304]. Other approaches, such as vaccination with TAAs or administration of immunocytokines, work by increasing the anti-tumor antibody response as well as by stimulating the tumor immune microenvironment to become more inflammatory [305, 306].

We initially hypothesized that AvFc, as a foreign protein that selectively recognizes tumor cells, may work in a similar manner by stimulating the local immune

response to the tumor and increasing tumor antigen presentation and generation of anti-tumor antibodies (ATAs). A preliminary flow cytometry experiment using B16F10 cells stained with serum from pretreated and non-pretreated animals from this study and a goat anti-mouse IgG-FITC conjugate demonstrated a slight but non-significant increase in anti-tumor antibodies as inferred from the increased number of cells with a mean fluorescence greater than the background. (Figure 36). We also performed a modified ADCC assay by spiking AvFc<sup>ΔXF</sup> into solutions of pooled serum obtained from animals during the immunogenicity study shown in Figure 23 to assess whether or not ADAs or ATAs impact ADCC induction in the reporter cell assay (Figure 36A-C). With this method we found that while serum taken from any time point did not induce any luciferase expression alone (Figure 36A-B), the addition of AvFc<sup>ΔXF</sup> to the serum resulted in an increase in activity significantly greater than is induced by AvFc<sup>ΔXF</sup> alone (Figure 36C). Furthermore, the effect on induction is greatest with AvFc<sup>ΔXF</sup> spiked into serum from animals that received both pretreatment and treatment with AvFc<sup>ΔXF</sup> (Figure 36C). Taken together, these data suggest that perhaps the increased activity resulting from pretreatment is not necessarily due to an increase in anti-tumor antibodies but by both an additive or synergistic effect on ADCC between ADAs, ATAs, and AvFc in addition to changes in the cellular composition of the immune microenvironment following treatment. Such a phenomenon has been observed following the successful treatment of murine ID8 ovarian cancer by cowpea mosaic virus-like particles, which was similarly not affected by the generation of ADAs and resulted in substantial changes to the immune cell composition towards a more inflammatory phenotype [153, 307].

To explore this hypothesis, we have performed a preliminary flow cytometry analysis of infiltrating immune cells isolated from B16F10 tumors in which we observed a significant increase in the infiltration of non-classical monocytes (NCMs) (Figure 34G-K) and a non-significant increase in other cell types. NCMs are a functionally distinct subset of steady-state monocytes that express pro-inflammatory cytokines and FcγRs, in particular FcγRIIIa, allowing them to both recruit immune cells to sites of injury or cancer and undergo antibody-dependent phagocytosis (ADP) [308, 309]. While much of the biology of these cells remains unknown, recent studies have shown that they exhibit anti-cancer activity, especially in the control of metastasis, by scavenging and eliminating tumor cells in the vascular beds [310, 311]. The broad increase in myeloid cell infiltration as a result of AvFc administration, including by NCMs, macrophages, and neutrophils, as well as the relatively small number of intratumoral NK cells, suggests that the mechanism of action of AvFc against cancer may involve more than NK cell-mediated ADCC and that the impact of FcγR-expressing myeloid cells should be evaluated. While some myeloid cells can perform ADCC through FcγRIIIa, the primary goal of further studies with these cells and AvFc should be to assess the induction of ADP against tumor cells. Induction of ADP against B16F10 cells (or other cancer cells) can be assessed by coincubating cells with fluorescently-labeled AvFc and FcγRI-expressing macrophage cell lines (such as murine RAW 264.7 cells) or isolated intratumoral macrophages/monocytes and assessing uptake with flow cytometry [312]. The latter study would provide greater evidence for the role of ADP in AvFc's mechanism of action by showing uptake of cancer cells in absolute terms and allowing for comparison in ADP activity between different glycovariants of AvFc and between cells isolated from

treated/untreated animals. A combination of this assay and other *ex vivo* Fc $\gamma$ R-dependent assays, such as the CD107a NK cell ADCC assay, as well as further immunophenotyping should be done to assess the relative role of each of the different Fc-mediated mechanisms in greater detail. Even though these results are preliminary, they corroborate our assertion that Fc-mediated functions are crucial to the anti-cancer activity of AvFc and suggest that the recruitment of Fc $\gamma$ R-bearing cells into the tumor microenvironment may play a significant role in its mechanism of action.

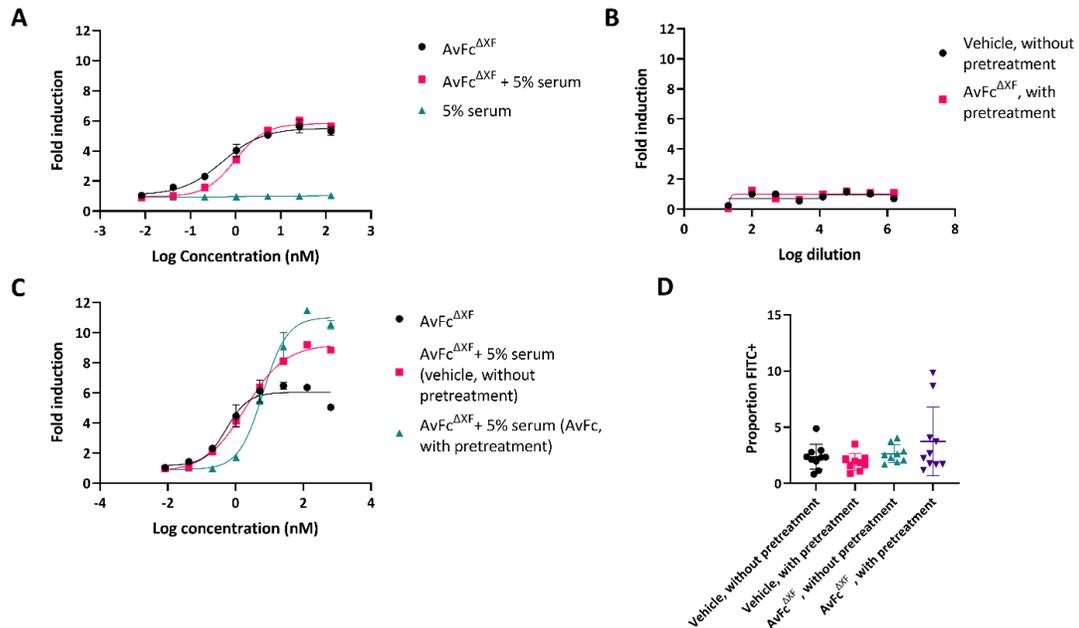


**Figure 36. Impact of ADAs and anti-tumor antibodies on ADCC activity.**

(A) ADCC assay in the presence of mouse serum from before pretreatment. Serum was collected and pooled from mice prior to pretreatment with AvFc<sup>ΔXF</sup> (see Figure 23A), and the ADCC assay was performed as described previously with AvFc<sup>ΔXF</sup> alone, AvFc<sup>ΔXF</sup> spiked into a solution of 5% serum, and 5% serum alone. No ADCC was induced by the 5% serum alone. Dose-response curves were nearly identical between AvFc<sup>ΔXF</sup> alone and AvFc<sup>ΔXF</sup> spiked into 5% serum, with some slight steepening of the curve. (B) ADCC assay in the presence of terminal mouse serum alone. Serum was pooled from blood taken at euthanasia of each animal in each treatment group. Neither serum from animals in the non-pretreated, vehicle-treated group nor serum from the animals in the pretreated, AvFc<sup>ΔXF</sup>-treated group was capable of inducing ADCC on its own beginning at a 1:20 dilution. (C) ADCC assay with AvFc<sup>ΔXF</sup> spiked into terminal mouse serum. The ADCC assay was performed as in panel B with purified AvFc<sup>ΔXF</sup> spiked into pooled serum from the non-pretreated, vehicle-treated group and the pretreated, AvFc<sup>ΔXF</sup>-treated group.

Compared to AvFc<sup>ΔXF</sup> alone, spiking into serum from the non-pretreated, vehicle-treated group resulted in an increase in the maximum fold induction from 6-fold to 9.2-fold and an increase in EC<sub>50</sub> from 0.53 nM to 1.94 nM. Spiking into serum from the pretreated, AvFc<sup>ΔXF</sup>-treated group resulted in an increase in the maximum fold induction from 6-fold to 11-fold and an increase in EC<sub>50</sub> from 0.53 nM to 6.44 nM. (D) Detection of anti-tumor antibodies with flow cytometry. Staining of B16F10 cells with a 1:10 dilution of pooled serum from each group followed by detection with a goat anti-mouse IgG FITC revealed no significant difference in the number of cells bound.

In conclusion, the present study has demonstrated the successful glycoengineering and activity of a novel immunotherapeutic drug, AvFc, which is a lectibody targeting cancer-associated high-mannose glycans. This glycoengineered AvFc, which lacks plant-derived glycans (in particular the core  $\alpha$ 1,3-fucose), induces more a potent ADCC response *in vitro* and delays the growth of murine B16F10 melanoma in both a flank tumor model as well as a model of metastasis *in vivo*. Additionally, pretreatment with AvFc and generation of ADAs did not negate AvFc's activity and indeed may have increased it through a yet undetermined mechanism. Lastly, treatment with AvFc <sup>$\Delta$ XF</sup> resulted in a significant increase in tumor-infiltrating non-classical monocytes, which suggests that ADP may play an equally important role in AvFc's mechanism of action. Further studies need to be conducted to determine the extent that AvFc and its variants can induce ADP by immune cells against cancer and to reproduce the findings in the immunophenotyping and pretreatment experiments using negative controls ( $\Delta$ gly and  $\Delta$ lec AvFc). Ultimately, these findings further substantiate the notion that high-mannose glycans may be a useful druggable biomarker in cancer therapy, and that glycoengineering is a powerful strategy to improve the antitumor activity of AvFc.

## CHAPTER 6: DEVELOPMENT OF AVAREN-FC AS AN IMMUNOTHERAPEUTIC AGAINST OVARIAN CANCER

### 6.1: Introduction

One goal of this project was to assess the feasibility of developing AvFc as a therapeutic for ovarian cancer (OVCA). OVCA, in particular epithelial ovarian cancer (EOC), is the deadliest gynecological cancer, ranking fifth in cancer death among women. EOC typically begins as small, borderline epithelial tumors on either the surface of the ovary, the fallopian tubes, or the mesothelium lining of the peritoneal cavity. These tumors grow and become well differentiated before metastasizing, primarily to the abdominal cavity but rarely to the lungs, liver, and brain [313]. According to the NCI Surveillance, Epidemiology, and End Results (SEER) Program, the overall 5-year-survival rate in the United States is 48.3% as of 2016, largely driven by the dismal survival rate (30.5%) of late-stage disease [314]. The age-adjusted mortality rate and rate of new cases of OVCA is 6.8 per 100,000 per year and 10.5 per 100,000 per year, respectively, slightly above that of the next deadliest gynecological cancer, uterine cancer, with a mortality rate of 5.0 per 100,000 per year [314]. This translates to an increase in 2016 of 22,530 new patients and 13,980 deaths. While the numbers of new cases and deaths are trending downwards slowly over the past 20 years, the prognosis of patients, especially those with late-stage disease, remains poor. This is largely due to ineffective population-based screening, innocuous presentation, and the lack of effective

second line therapies for chemo-resistant disease. Although patients generally respond very well to the primary treatment, the vast majority of women (75%) will experience disease recurrence that is incurable due to chemo-resistance [315].

Primary debulking surgery followed by chemotherapy has been the first-line standard of care for EOC for decades [315]. Surgery for advanced disease consists of total abdominal hysterectomy, bilateral salpingo-oophorectomy, and omentectomy, though patients with low grade disease can opt for a fertility conservation strategy. The vast majority of patients will also receive chemotherapy consisting of a platinum-based drug, most often carboplatin, and a taxane, such as paclitaxel. No residual disease following primary therapy is the most important prognostic indicator. While this is achievable for most patients regardless of disease stage, nearly all will inevitably experience fatal chemo-resistant disease. Treatment options at this stage are limited based on the platinum-free interval (the length of time between platinum drug treatments) of the patient and the amenability of the subsequent disease to secondary debulking surgery, though the likelihood of survival is poor regardless. For patients who have gone through the first-line standard of care, a greater benefit has been demonstrated with the use of long-term maintenance therapy, which consists of chemotherapeutics or biologics given after no residual disease is achieved to prolong survival. FDA approval of bevacizumab and poly ADP ribose polymerase (PARP) inhibitors has expanded the availability of maintenance therapy and improved progression-free survival; however, current clinical data have not demonstrated significant increases in overall survival and these drugs are associated with significant adverse events [316-320]. Furthermore, there is no FDA-approved targeted immunotherapy for EOC, and trials with checkpoint inhibitors have

not been conclusive [321, 322]. Thus, EOC therapy would benefit greatly from novel or complementary therapies that may cure the disease, prolong progression, and improve overall survival in patients, especially novel immunotherapeutics targeting a unique biomarker of EOC.

Aberrant glycosylation of cancer-cell surfaces is a well-described phenomenon and is considered to be a hallmark of the disease [323] Recent advances in tumor glycobiology have demonstrated that various tumor types display an increased level of high-mannose glycans on their surface, and that these glycans may play a role in malignancy and metastasis [323, 324]. High-mannose glycans occur early in the N-glycosylation pathway in the endoplasmic reticulum and are typically processed by mannosidases and glycosyltransferases prior to leaving the secretory pathway, and thus are not typically found on the surface of the cell under normal conditions[14]. However, quantitative N-glycan analysis by mass spectrometry with formalin-fixed, paraffin-embedded tissues show that high-mannose glycans are overexpressed on the surface of OVCA tumors [82]. Additionally, high-mannose glycans were shown to be significantly elevated in the membrane glycoproteins of EOC cell lines compared to non-cancerous ovarian epithelial cells and may increase metastatic activity in SKOV3 cells [325, 326]. It is becoming clear that high-mannose glycans may be a useful EOC biomarker and a potentially druggable target, therefore we hypothesize that AvFc may offer a powerful new option for EOC treatment by complementing or supplanting existing therapies for primary, secondary, or maintenance use. Such a therapy capable of improving overall survival in patients could potentially alter the paradigm of EOC management and introduce a new standard of care.

A number of studies were done to assess whether or not AvFc has activity against OVCA *in vitro* as well as establish murine challenge models that can be used to evaluate its efficacy *in vivo*. We first set out to confirm that AvFc indeed has selectivity for OVCA tissues and cell lines, and whether or not it could effectively induce ADCC against these lines. Next, we established the murine ID8 EOC challenge model in immunocompetent mice to perform pilot efficacy studies. This model is a standard orthotopic model in the field of ovarian cancer research and has been used for the assessment of therapeutic candidates, in particular immunotherapies which require a functional immune system, and results in the generation of ascites in the peritoneal cavity which is a common complication from OVCA [327, 328]. The results of these studies are summarized later in this chapter.

## 6.2: Results

### 6.2.1: AvFc recognizes human ovarian cancer tissues and cell lines and induces ADCC

We first determined whether or not AvFc could recognize OVCA tissues and cell lines by immunohistochemical staining and flow cytometry. Immunohistochemical analysis of 3 stage 1 high-grade serous ovarian carcinoma tissues from a 48-year-old, a 72-year-old, and a 55-year-old showed clear differentiation of malignant tissues by AvFc compared to both normal adjacent tissues as well as the non-sugar-binding mutant AvFc<sup>Alec</sup> as determined by the degree of DAB staining (Figure 37). This striking result led us to then evaluate AvFc's binding by flow cytometry to a number of established human and murine OVCA cell lines in order to build a better profile to guide future animal studies. In all, we tested binding to the following lines: A2780 (epithelial endometroid

carcinoma), CAOV3 (primary adenocarcinoma), SKOV3 (adenocarcinoma from ascites), SW626 (primary adenocarcinoma), ID8 (murine ovarian surface epithelial cells), and an engineered ID8 daughter cell line expressing murine VEGF and  $\beta$ -defensin 29 (ID8-VEGF-DEFB29). Of the 6 lines tested, all but SW626 and CAOV3 experienced near-saturation at a relatively low concentration of AvFc (15 nM, Figure 38A). AvFc bound strongest to A2780 cells, with almost 100% of cells bound at 1.5 nM while binding to CAOV3 was the weakest, with only  $\approx 56.5\%$  of cells bound at the highest concentration tested (150 nM). As expected, AvFc <sup>$\Delta$ lec</sup> exhibited negligible binding to each of the cell lines, indicating that binding is high-mannose-glycan-dependent.

We then assessed AvFc's ability to induce ADCC against OVCA cell lines, as we believe this is the primary anti-cancer mechanism of action for the drug. In general, the reporter-cell-based ADCC assay (Figure 38B-D) showed that AvFc <sup>$\Delta$ XF</sup> induced the highest levels of luciferase expression followed by AvFc<sup>WT</sup>, while the aglycosylated variant showed no activity, consistent with previous results (see Chapter 4). Fold induction by AvFc <sup>$\Delta$ XF</sup> (Figure 38B) ranged from  $\approx 3$  to 7-fold and between  $\approx 1.5$  to 4-fold by AvFc<sup>WT</sup> (Figure 38C) depending on the cell line. Based on these results, it appears that binding by flow cytometry was a poor predictor for ADCC-induction, as the highest level of induction was seen against CAOV3 cells, which were bound by AvFc the least, and the lowest levels of induction were seen against A2780, which showed the strongest degree of binding. Despite this observation, the levels of induction are consistent with other cancer cell lines and provide evidence that AvFc may have anti-OVCA activity *in vivo*, which we attempted to establish using the orthotopic murine ID8 EOC challenge model.

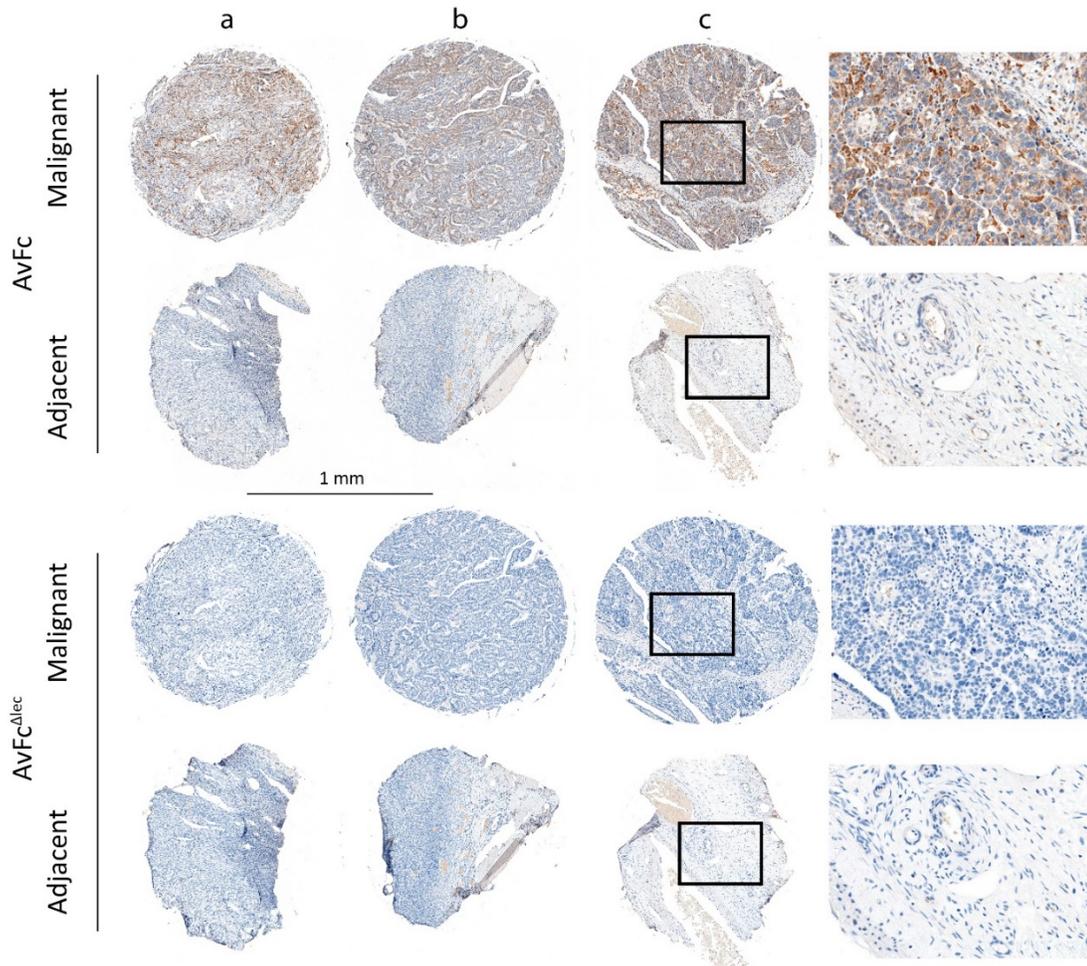


**Figure 37. Recognition of human OVCA tissues by AvFc with immunohistochemistry.**

Immunohistochemistry (IHC) was performed on a tissue array by US Biomax, Rockville, MD, which contained 3 Stage I HGSOV tissues from a 48-year-old (column a), 72-year-old (b), and a 55-year-old patient (c) and three adjacent normal ovary tissues (below). AvFc clearly delineates malignant from normal adjacent tissue as seen by the level of DAB staining, while AvFc<sup>Δlec</sup> recognizes neither tissue.

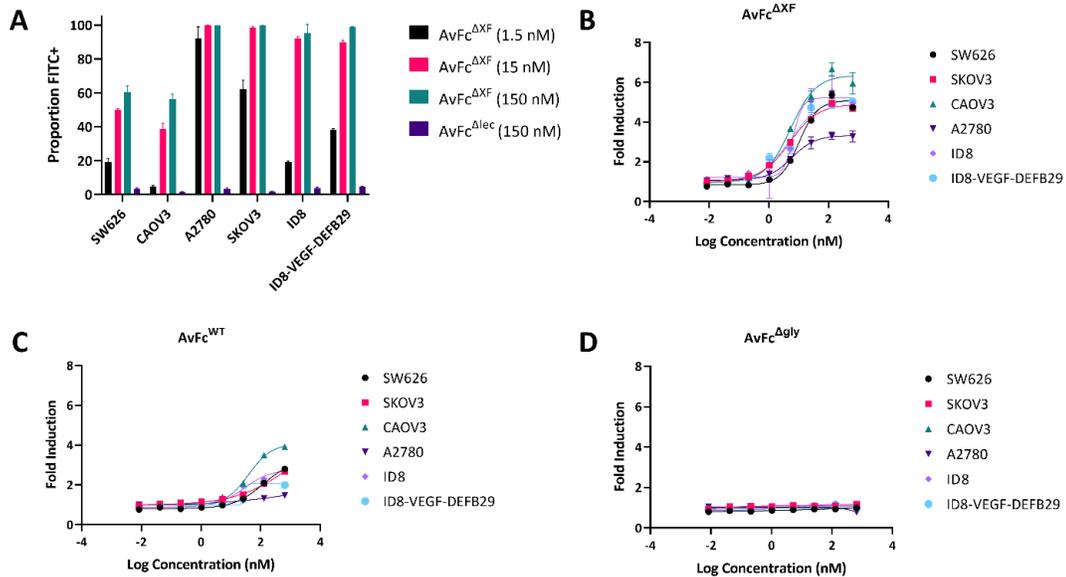


**Figure 38. AvFc binds to many OVCA cell lines and induces ADCC.**

(A) Single-color flow cytometry to assess AvFc binding to OVCA cell lines from humans and mice. The Y-axis shows percentage of FITC+ cells as determined by gating against background fluorescence. The experiment reveals high levels of binding to A2780, SKOV3, ID8, and ID8-VEGF-DEFB29 cells and intermediate binding to SW626 and CAOV3 cells. Binding was dose dependent with saturation occurring at  $\approx 15$  nM for most cell lines excluding SW626 and CAOV3. AvFc<sup>Δlec</sup> exhibited negligible binding to all cell lines tested at 150 nM. Panels B-D show dose-dependent induction of ADCC by AvFc variants against OVCA cell lines with a luciferase-based reporter cell assay. As expected, AvFc<sup>ΔXF</sup> induces the highest level of ADCC (average of  $5.0 \pm 0.9$ -fold, panel B) while AvFc<sup>WT</sup> only induces modest amounts (average of  $3.2 \pm 1.1$ -fold, panel C). AvFc<sup>Δgly</sup> induces no ADCC against any cell line tested (D). The highest level of induction was seen against CAOV3 cells, while the lowest observed was for A2780 cells. All data shown are mean  $\pm$  SD.

### 6.2.2: Establishment of the ID8-luciferase challenge model

The orthotopic murine ID8-luciferase EOC challenge model is a useful syngeneic model for assessing the activity of immunotherapeutic drugs against OVCA. However, it is a lengthy and multifactorial model with many possible endpoints and measures of activity. Thus, it was necessary to perform pilot experiments in order to gauge which parameters were necessary and sufficient to test AvFc's activity, in particular the number of cells used to establish disease. We initially compared the disease progression and treatment effect of AvFc following intraperitoneal administration of either 1 or  $2 \times 10^6$  cells per animal. For both studies, AvFc<sup>ΔXF</sup> at 25 mg/kg or a vehicle was administered intraperitoneally beginning on day 7 and continuing Q2D for 28 days (15 doses). When using  $2 \times 10^6$  cells per animal, disease became noticeable around the 6<sup>th</sup> week ( $\approx$  42 days) with the development of ascites and sudden increase in animal body weights and abdomen circumference compared to healthy mice (Figure 39B-C). Bioluminescent imaging performed on day 46 (Figure 39D) showed very low signal and no significant difference between the treatment groups. A second round of imaging a week later showed no signal at all (data not shown), precluding its usefulness as an endpoint measuring disease severity. Additionally, by the end of the study it became clear that body weights or abdomen circumference measurements were not reliable in determining the disease state of the animal, as animals rarely reached the 35 g humane endpoint for euthanasia before becoming extremely moribund. Using survival as the ultimate gauge of drug activity, we did find that AvFc<sup>ΔXF</sup> significantly prolonged the lives of the animals, increasing the median survival from 46 to 63 days (Figure 39A,  $p=0.0061$  by the Gehan-

Breslow-Wilcoxon test). This was despite the fact that 2 of the vehicle-treated animals never developed disease and were excluded from the analysis.

When using  $1 \times 10^6$  cells per animal, the development of the disease was noticeably slower with ascites not beginning to develop until after the 7<sup>th</sup> and 8<sup>th</sup> weeks. Similarly, we found that body weights and abdomen circumferences were poor predictors of the animals' health, with most of the subjects never reaching the humane endpoints (Figure 40B-C). Bioluminescent imaging was performed once at day 56, however no signal could be generated, and no meaningful comparisons could be made (data not shown), which most likely was due to an issue with the model or cell line. At this point, animals were only monitored every other day for their general health. Once disease was evident, indicated by the presence of ascites, animals decompensated and needed to be euthanized relatively quickly. While AvFc treatment was able to prolong the survival of the animals, the effect size was much smaller than in the previous study, as median survival only increased from 60 to 66 days ( $p=0.0076$ , Gehan-Breslow-Wilcoxon test). While the results show AvFc has some activity in this model, more work needs to be done in order to optimize the parameters for reliability and reproducibility.

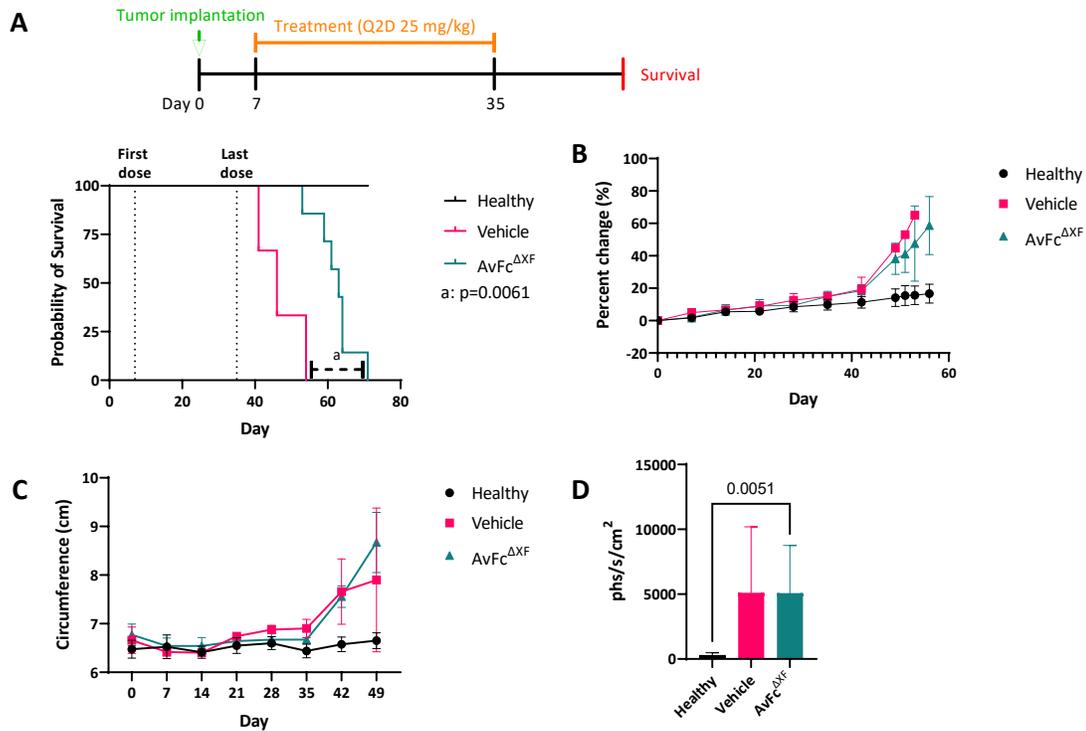


**Figure 39. ID8-luciferase challenge model with  $2 \times 10^6$  cells/animal.**

(A) For the first ID8-luciferase challenge model  $2 \times 10^6$  cells were administered intraperitoneally on day 0. Treatment began on day 7 and continued Q2D for 28 days (n=8 healthy, n=5 vehicle, n=7 AvFc<sup>ΔXF</sup> at 25 mg/kg). 2 animals in the vehicle group did not develop disease by day 71 and were excluded from the final analysis. (B) Kaplan-Meier curve comparing survival between the three groups. AvFc significantly increased survival (p=0.0061, Grehan-Breslow-Wilcoxon test) from a median of 46 to 63 days. Lines indicate the first and last dose of drug or vehicle. (C) Changes in body weight over time, calculated as percent change from day 0 weight. Animal weights in the vehicle and AvFc<sup>ΔXF</sup>-treated groups began to increase rapidly around day 42 with the development of ascites. (D) Comparison of abdomen circumferences over time. Corresponding to the development of ascites and increased body weights, circumferences in the vehicle and AvFc<sup>ΔXF</sup> groups began to increase around day 42. Healthy animals remained more or less

at a constant weight for the duration of the study. (E) *In vivo* bioluminescent imaging of animals at day 46 showed no significant differences in photons/second/cm<sup>2</sup> emitted between the vehicle and AvFc<sup>ΔXF</sup>-treated animals (Kruskal-Wallis test). All data shown are mean ± SD.

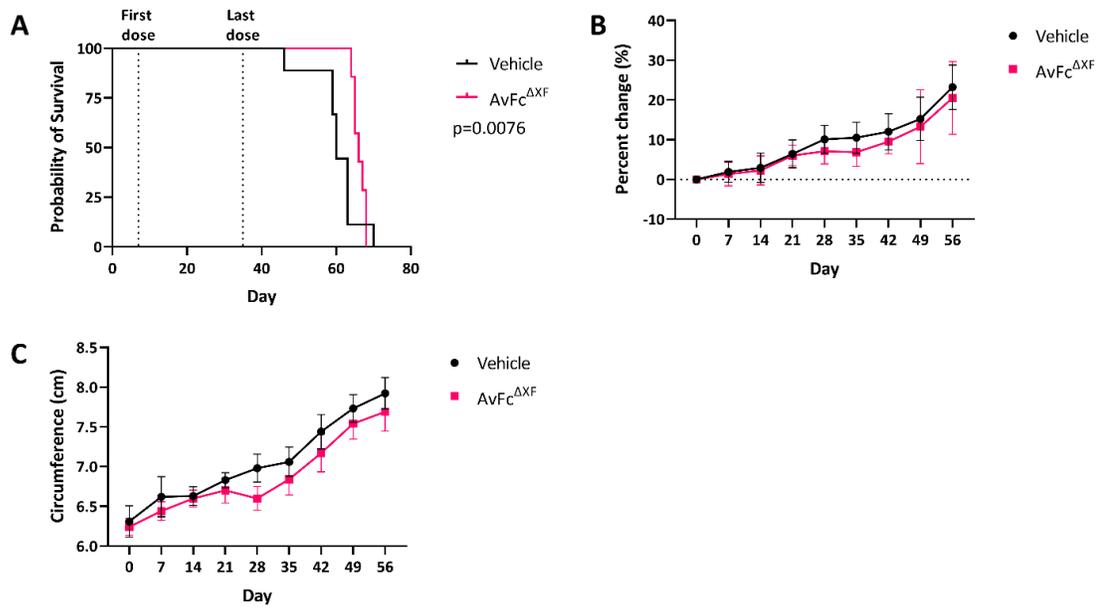


**Figure 40. ID8-luciferase challenge model with  $1 \times 10^6$  cells/animal.**

For the first ID8-luciferase challenge model  $1 \times 10^6$  cells were administered intraperitoneally on day 0. Treatment began on day 7 and continued Q2D for 28 days (n=10 vehicle, n=10 AvFc<sup>ΔXF</sup> at 25 mg/kg). (A) Kaplan-Meier curve comparing survival between the two groups. Similar to the previous study, AvFc significantly increased survival (p=0.0076, Grehan-Breslow-Wilcoxon test) albeit to a lesser degree, from a median survival time of 60 to 66 days. Lines indicate the first and last dose of drug or vehicle. (B) Changes in body weight over time, calculated as percent change from day 0 weight. Body weights increased slowly over the course of the study, to a lesser degree than seen following injection of  $2 \times 10^6$  cells/animal. Body weights were only monitored until day 56. (C) Similar to the body weights, changes in abdomen circumference were less severe than with the previous study (Figure 39). No significant changes were seen in either measurement. All data shown are mean  $\pm$  SD.

### 6.2.3: Proteomics analysis of AvFc binding partners on ovarian cancer cells

We have previously used proteomics techniques to identify potential binding partners on the surface of blood cancer and lung cancers, the latter of which were reported by Oh et al. [105] (manuscript in review at the time of writing). In order to build more evidence to suggest that AvFc may be useful as an anti-OVCA immunotherapeutic, as well as to identify possible additional mechanisms of action, we performed co-immunoprecipitation by incubating fixed AvFc and AvFc<sup>Δlec</sup> agarose resins with cell lysates from SW626, SKOV3, and ID8 cells in order to isolate bound glycoproteins containing high-mannose glycans. Bound proteins were then identified using electrospray UHPLC-MS and curated using GO terminology to separate integral membrane proteins from other cytoplasmic and organelle-resident proteins. The number of N-glycan sites was predicted using the NetNGlyc server. The results are summarized in Table 8. In general, AvFc was found to recognize a broad selection of glycosylated transporters (including SLC and ATP family transporters), receptors (such as EGFR, IGF1R, and IGF2R), and adhesion molecules (integrins, cadherins). A number of proteins were found on the surface of both SW626 and SKOV3 cells and may represent proteins that are commonly modified with high-mannose glycans in cancer and whose interactions with AvFc should be validated using other methods. Among those identified between them are the epithelial growth factor receptor (EGFR), insulin-like growth factor receptor 2 (IGF2R), transferrin receptor (TFR1), integrin  $\alpha$ -5 and  $\alpha$ -2 (ITGA5 and ITGA2), and sortilin-related receptor (SORL1). These proteins also generally contain large numbers of N-glycans, increasing the likelihood that many of those glycan sites are indeed occupied

by high-mannose glycans and can be recognized by AvFc. Further work is needed to validate these interactions.

**SW626 putative binding partners**

<b>Protein</b>	<b>Gene name</b>	<b>Accession number</b>	<b>Normalized iBAQ</b>	<b>Predicted N-glycans</b>
Integrin alpha-1	ITGA1	P56199	242170	21
CUB domain-containing protein 1	CDCP1	Q9H5V8	191430	11
Magnesium transporter protein 1	MAGT1	Q9H0U3	146460	2
Cleft lip and palate transmembrane protein 1	CLPTM1	O96005	90317	6
Neuroplastin	NPTN	Q9Y639	47158	6
Leucyl-cystinyl aminopeptidase	LNPEP	Q9UIQ6	42250	13
Stromal interaction molecule 1	STIM1	Q13586	31253	3
Integrin beta-4	ITGB4	P16144	29861	4
Integrin alpha-3	ITGA3	P26006	23124	11
Integrin beta-5	ITGB5	P18084	20369	7
Adhesion G protein-coupled receptor E5	ADGRE5	P48960	14898	8
Protocadherin Fat 1	FAT1	Q14517	5,021.60	23
Sodium channel protein type 5 subunit alpha	SCN5A	Q14524	4,842.00	15
Solute carrier family 12 member 2	SLC12A2	P55011	3,875.20	4
Contactin-1	CNTN1	Q12860	3,021.20	8
Disintegrin and metalloproteinase domain-containing protein 10	ADAM10	O14672	2,187.80	4
Agrin	AGRN	O00468	1,509.20	4

**SKOV3 putative binding partners**

<b>Protein</b>	<b>Gene name</b>	<b>Accession number</b>	<b>Normalized total spectra</b>	<b>Predicted N-glycans</b>
Integrin beta-1	ITGB1	P05556	18	12
Cadherin EGF LAG seven-pass G-type receptor 2	CELSR2	Q9HCU4	11	13
Cluster of Polycystin-2	PKD2	Q13563	11	7
Integrin beta-3	ITGB3	P05106	6	3
VPS10 domain-containing receptor SorCS2	SORCS2	Q96PQ0	5	7
Basigin	BSG	P35613	4	4
Adhesion G-protein coupled receptor G1	ADGRG1	Q9Y653	3	6

Neural cell adhesion molecule L1	L1CAM	P32004	3	16
Adhesion G protein-coupled receptor L2	ADGRL2	O95490	2	13
Attractin	ATRN	O75882	2	16
Cadherin EGF LAG seven-pass G-type receptor 1	CELSR1	Q9NYQ6	2	12
Leukocyte surface antigen CD47	CD47	Q08722	1	6
Dystroglycan	DAG1	Q14118	1	5
Inactive tyrosine-protein kinase 7	PTK7	Q13308	1	9
Poliovirus receptor	PVR	P15151	1	8
Lysosome membrane protein 2	SCARB2	Q14108	1	10
Neutral amino acid transporter B(0)	SLC1A5	Q15758	1	1
CD44 antigen	CD44	P16070	0	8

#### Shared binding partners (SW626 and SKOV3)

Protein	Gene name	Accession number	Predicted N-glycans
Tyrosine-protein kinase receptor UFO	AXL	P30530	7
Basal cell adhesion molecule	BCAM	P50895	4
Basigin	BSG	P35613	4
Epidermal growth factor receptor	EGFR	P00533	10
Cation-independent mannose-6-phosphate receptor	IGF2R	P11717	14
Integrin alpha-2	ITGA2	P17301	8
Integrin alpha-5	ITGA5	P08648	10
Cation-dependent mannose-6-phosphate receptor	M6PR	P20645	5
Plexin-B2	PLXNB2	O15031	10
Sortilin-related receptor	SORL1	Q92673	22
Transferrin receptor protein 1	TFR1	P02786	5

#### ID8 putative binding partners

Protein	Gene name	Accession number	Normalized iBAQ	Predicted N-glycans
Integrin beta-1	Itgb1	P09055	1370000.00	11

Integrin alpha-3	Itga3	Q62470	629000.00	11
Ataxin-10	Atxn10	P28658	626560.00	1
Leukocyte surface antigen CD47	Cd47	Q61735	575000.00	6
CD63 antigen	Cd63	P41731	545440.00	4
Neutral amino acid transporter B(0)	Slc1a5	P51912	154120.00	1
Integrin alpha-6	Itga6	Q61739	91600.00	6
Lysosome-associated membrane glycoprotein 1	Lamp1	P11438	82112.00	17
Transferrin receptor protein 1	TFR1	Q62351	59400.00	3
Dynamin-3	Dnm3	Q8BZ98	28688.00	4
Tight junction protein ZO-1	Tjp1	P39447	27796.00	8
Plexin-B2	Plxnb2	B2RXS4	15673.00	11
Exocyst complex component 1	Exoc1	Q8R3S6	7081.00	3
Epidermal growth factor receptor	Egfr	Q01279	4743.00	11

**Table 8. Identification of putative cell-surface binding partners of AvFc on human and murine OVCA cell lines.**

Co-immunoprecipitation was performed with lysates from SW626, SKOV3, and ID8 cells using AvFc- and AvFc<sup>Δlec</sup>-conjugated agarose resins. Bound proteins were then identified with LC-MS, and those that were identified in both the negative control samples were removed from the final analysis, as were any proteins identified not considered to be integral plasma membrane proteins (as determined by Gene Ontology keywords and literature searches). N-glycan sites were also predicted with the NetNGly server. AvFc was found to bind to a number of highly glycosylated transmembrane receptors, transporters, and adhesion molecules.

### 6.3: Discussion

The results described in this chapter demonstrate the potential utility of AvFc as an immunotherapeutic against OVCA. We found that AvFc can convincingly delineate malignant from normal-adjacent tissues from OVCA patients and that it binds strongly to a number of human and murine OVCA cell lines. Furthermore, AvFc shows signs of activity *in vivo* in our preliminary ID8-luciferase challenge experiments, significantly extending the survival of animals with intraperitoneal ID8 tumors. Lastly, we have identified a number of cell-surface receptors that may interact with AvFc and, in addition to ADCC, may contribute to its mechanism of action.

Consistent with the results from the flow cytometry and ADCC assays, AvFc displayed some activity in the orthotopic murine ID8-luciferase challenge model, significantly extending the median survival with an effect size dependent on the initial number of cells implanted. However, this is a lengthy and somewhat complicated model, and our results demonstrate that further optimization is necessary. One observation that was consistently made between the two experiments (with 1 or  $2 \times 10^6$  cells implanted) was that body weights and abdomen circumferences were poor predictors of the health of the animal, with many becoming moribund long before reaching the established humane endpoints (35 g and 10 cm). A potential explanation for this lies in the differential development of ascites between animals, which occurs when the tumor burden reaches a certain threshold and results in the filling of the peritoneal cavity with a bloody, serous fluid. Individual animals can accumulate as much as 15 mL of this fluid, which adds a tremendous amount of weight to the animal in some instances and seems to correspond to serious disease. In many cases however it was found that even a small amount of ascites

could greatly interfere with the health of the animal, causing them to become moribund long before accumulating enough weight to be euthanized. This generation of ascites may also help to explain why bioluminescent imaging of the animals failed to generate any usable data, as the injected luciferin was likely rapidly diluted to unusable levels in the ascitic fluid. Other studies have also suggested that regular removal of the ascites is necessary for bioluminescent imaging and prolongs the survival of animals in this model [329]. Lastly, generation of ascites may be incompatible with intraperitoneal treatment as dilution of the drug in the fluid may render it ineffective. Our results agree with this assessment, and it is clear that regular removal of the ascites is necessary in order to assess the tumor burden and the effect of treatment more accurately by body weight measurements and bioluminescent imaging. Recording to the time to ascites development as well as the volume of ascites removed may also be useful endpoints. Furthermore, since abdomen circumference is mostly affected by the generation of ascites, this is likely not a useful endpoint for the future if it is routinely removed.

Despite the fact that animals in the second study (Figure 40) received 50% fewer cells than in the first (Figure 39), the length of the studies was not tremendously different, with the last animal euthanized 71 days after implantation in the first study and 70 days after implantation in the second. Interestingly, the effect of AvFc treatment was much more pronounced in the first study with  $2 \times 10^6$  cells, increasing the median survival time from 46 to 63 days, than it was in the second, where the increase was only from 60 to 66 days. The exact reason for this is unclear from the data. One hypothesis is that in the ID8 model (and perhaps in the peritoneal cavity in general) AvFc acts more as a cancer-static drug, inducing cell death through ADCC and slowing growth without completely

eliminating the tumor, so that when drug administration ends the tumors resume growing at their normal rate. There are two observations that that corroborate this hypothesis. Firstly, the time between the last dose of drug and the first euthanasia in the first study was only 6 days, whereas in the second study with fewer cells that time was 11 days. The second observation is that the delay between dosing and euthanasia also seems to have affected the span of time between the first and last euthanasia within each group. For instance, in the first study ( $2 \times 10^6$  cells), the first vehicle animal was euthanized 41 days after tumor implantation and the last on day 54 (a span of 14 days). For the AvFc group, the first animal was euthanized on day 53 and the last on day 71 (a span of 19 days). In the second study ( $1 \times 10^6$  cells), the time from first to last euthanasia for the vehicle group was 17 days (with one outlier that was euthanized on day 70) but only 4 days for the AvFc group (64 to 68 days). Based on these observations it appears that with fewer cells implanted the disease progressed more slowly after drug administration ended, and when the animals began to develop severe enough disease to need to be euthanized the drug-effect was essentially nonexistent, as the time from the last dose was much greater, and all of the animals decompensated rapidly. Two modifications could be made to the model to determine if this is true and possibly improve the effectiveness of AvFc: inject more than  $2 \times 10^6$  cells and prolong the drug administration. These two changes would have the added effect of decreasing the median survival time for the vehicle group while also decreasing the amount of time between the end of drug administration and the beginning of the development of disease in the AvFc group, which in theory could be prolonged by extending the length of drug administration.

Using co-immunoprecipitation with conjugated AvFc and AvFc<sup>Δlec</sup> and LC-MS we identified a number of potential binding partners on the surface of SKOV3 and SW626 cells that may be decorated with high-mannose glycans, ranging from ion and amino acid transporters and growth factor receptors to intracellular adhesion molecules. Several of these were found to be commonly isolated between the two cell lines including the receptors EGFR, IGF2R, TFR1, and SORL1, adhesion proteins such as ITGA5 and ITGA2, and transporters like NPC1. These results are consistent with work that was previously conducted to determine binding partners on the surface of the lung and blood cancer cell lines A549, H460, HL-60, and K562. The results of the lung cancer experiments were reported by Oh et al. [105], and both the lung and blood cancer datasets are reproduced below in Table 9. Two of the proteins identified in lung cancer, EGFR and IGF1R, have had their interactions with AvFc validated using both co-immunoprecipitation with receptor specific-antibodies and *in vitro* receptor stimulation assays and western blotting with A549 and H460 cells. AvFc was found to both bind to and inhibit the function of these receptors leading to anti-cancer activity *in vivo* [105]. Interestingly, several other proteins have been identified as being recognized by AvFc in all 6 of the cancer cell lines tested: IGF2R, ITGA5, M6PR, PLXNB2, and TFR1. Each of these proteins individually are fairly heavily glycosylated, and all but PLXNB2 exist as dimers on the cell surface, which significantly increases the number of clustered glycans for AvFc to potentially recognize. While further work remains to validate these interactions, there is some evidence to suggest these proteins contribute to malignancy in a way that may be interfered with by binding to AvFc, contributing to its overall anti-cancer mechanism.

<b>Commonly identified in A549 and H460 lung cancer cells</b>			
<b>Protein</b>	<b>Gene name</b>	<b>Accession number</b>	<b>Predicted N-glycans</b>
Plexin-B2	PLXNB2	O15031	10
Epidermal growth factor receptor	EGFR	P00533	10
Transferrin receptor protein 1	TFR1	P02786	5
Insulin-like growth factor 1 receptor	IGF1R	P08069	14
Integrin alpha 5	ITGA5	P08648	10
Cation-independent mannose-6-phosphate receptor	IGF2R	P11717	14
Integrin alpha 2	ITGA2	P17301	8
Integrin beta 5	ITGB5	P18084	7
Cation-dependent mannose-6-phosphate receptor	M6PR	P20645	5
Contactin-associated protein 1	CNTP1	P78357	12
Neutral amino acid transporter B(0)	SLC1A5	Q15758	1
Sortilin-related receptor	SORL1	Q92673	22
Plexin-A1	PLXNA1	Q9UIW2	13
Endothelial protein C receptor	EPCR	Q9UNN8	4
<b>Commonly identified on K562 and HL-60 blood cancer cells</b>			
<b>Protein</b>	<b>Gene name</b>	<b>Accession number</b>	<b>Predicted N-glycans</b>
Plexin-B2	PLXNB2	O15031	10
Transferrin receptor protein 1	TFR1	P02786	5
Intercellular adhesion molecule 1	ICAM1	P05362	7
Integrin beta 1	ITGB1	P05556	12
Integrin alpha 5	ITGA5	P08648	10
Lysosome-associated membrane glycoprotein 1	LAMP1	P11279	17
Cation-independent mannose-6-phosphate receptor	IGF2R	P11717	14
Cation-dependent mannose-6-phosphate receptor	M6PR	P20645	5
Plexin-A1	PLXNA1	Q9UIW2	13
<b>Commonly identified in lung and ovarian cancer cell lines</b>			
<b>Protein</b>	<b>Gene name</b>	<b>Accession number</b>	<b>Predicted N-glycans</b>
Epidermal growth factor receptor	EGFR	P00533	10
Integrin alpha 2	ITGA2	P17301	8
Sortilin-related receptor 1	SORL1	Q92673	22
<b>Commonly identified in lung and blood cancer cell lines</b>			

<b>Protein</b>	<b>Gene name</b>	<b>Accession number</b>	<b>Predicted N-glycans</b>
Plexin-A1	PLXNA1	Q9UIW2	13
<b>Commonly identified in all cell lines</b>			
<b>Protein</b>	<b>Gene name</b>	<b>Accession number</b>	<b>Predicted N-glycans</b>
Cation-independent mannose-6-phosphate receptor	IGF2R	P11717	14
Integrin alpha 5	ITGA5	P08648	10
Cation-dependent mannose-6-phosphate receptor	M6PR	P20645	5
Plexin-B2	PLXNB2	O15031	10
Transferrin receptor protein 1	TFR1	P02786	5

**Table 9. Identification of putative cell-surface binding partners of AvFc on lung and blood cancer cell lines.**

In conclusion, the results described in this chapter demonstrate that AvFc has selectivity for OVCA tissues and cell lines by binding to high-mannose glycans, and that it is capable of potently inducing ADCC against them. Furthermore, AvFc administration was shown to prolong the survival of animals in the orthotopic murine ID8 EOC challenge model. Further optimization of the model is required to generate reliable and reproducible study conditions, and three major parameters have been identified which may be amenable to modification: routine removal of the ascites from diseased mice, increasing the number of cells implanted, and lengthening the time for drug administration. Lastly, activity against OVCA by AvFc may be due to a combination of ADCC and receptor binding, and several potential binding partners for AvFc have been identified on ID8, SKOV3, and SW626 cells. Overall, these data justify further development of AvFc as a drug against OVCA alone or in combination with other chemotherapeutics or immunotherapeutics.

## CHAPTER 7: SUMMARY AND FUTURE DIRECTIONS

### 7.1: Summary

The results presented herein summarize the work relating to the preclinical development of Avaren-Fc (AvFc), a lectibody targeting cancer and virus-associated high-mannose glycans, which consists of a fusion of the lectin Avaren and the Fc region of human IgG1. High-mannose glycans represent a relatively underutilized glycobiomarker that is aberrantly abundant on the surface of malignant cells and on the surface of some highly-glycosylated viral glycoproteins such as those from HIV and HCV.

Chapter 4 describes the *in vitro* activity of AvFc against HCV as well as the safety and efficacy of its administration in a chimeric human liver mouse model of HCV infection. We found that AvFc had high affinity for the E2 envelope glycoprotein, and that binding to those glycoproteins on the surface of the virus resulted in potent inhibition of viral entry in a genotype independent manner, determined using an *in vitro* neutralization assay with both pseudoviruses and replication-competent cell-culture-derived virus (Figure 9, Table 2). In order to facilitate the use of AvFc in mouse models as well as improve its stability following purification, we identified a more optimal buffer formulation composed of histidine, sucrose, and sodium chloride that allowed us to achieve concentrations as high as 10 mg/mL without precipitation and protected against degradation (Figure 10, Figure 11, Table 3). We then evaluated AvFc's activity *in vivo* using a chimeric human liver mouse model of HCV infection in PXB-mice<sup>®</sup> and found

that treatment Q2D with intraperitoneally administered AvFc at 25 mg/kg could completely prevent infection while a non-sugar-binding mutant AvFc<sup>Δlec</sup> failed to meaningfully inhibit virus, suggesting that AvFc inhibited HCV in a glycan-dependent manner (Figure 16). Up to 11 injections of drug were found not to result in any overt toxicity in the animals and did not result in damage to liver as determined by measurements of ALT, Alb, and by histopathology (Figure 14, Figure 15, Table 4).

The first report of the anticancer activity of AvFc was by Oh et al., which demonstrated the growth inhibition of A549 and H460 xenografts likely due to a combination of receptor inhibition (in particular EGFR and IGF1R) as well as ADCC, though the relative contributions of these functions *in vivo* are unclear [105]. Chapter 5 describes the further anticancer activity of AvFc against murine B16F10 melanoma while also demonstrating that Fc functions are likely the key mechanism of action against cancer. This was evaluated in mouse models using Fc variants of AvFc that had either high ADCC activity (AvFc<sup>ΔXF</sup>) or lacked it entirely (AvFc<sup>Δgly</sup>) to evaluate the relative contribution of Fc functions (Table 1). Modification of WT AvFc to create the ΔXF variant by defucosylation resulted in significantly increased affinity for the various FcγRs (Figure 19, Table 6). We showed that none of the variants exhibited changes in their cancer-binding ability, saturating B16F10 cells at nanomolar concentrations (Figure 18). Furthermore, while coincubation with AvFc was not found to directly induce cytotoxicity or inhibit cell proliferation, the high ADCC variant induced high levels of ADCC *in vitro* at nanomolar concentrations suggesting that it and not direct inhibition is the more important anticancer mechanism (Figure 20). This result was corroborated in the B16F10 flank tumor model, where we showed that removal of Fc effector functions with the

AvFc<sup>Δgly</sup> variant did not have any impact on the growth of tumors while the AvFc<sup>ΔXF</sup> variant significantly slowed tumor growth beginning 9 days after implantation (Figure 21). Interestingly, the presence of pre-existing immunity to AvFc in the form of ADAs did not eliminate its activity in the flank tumor model (Figure 23). Indeed, the presence of ADAs may have somewhat improved the activity of AvFc by extending the survival of tumor-bearing animals. The mechanism by which this occurred however will be the subject of future work. While some data seem to indicate that ADAs against AvFc increase ADCC activity against tumor cells (Figure 36), the contribution of changes to the tumor immune cell microenvironment have yet to be adequately measured, though preliminary studies have suggested that AvFc administration results in an increase in myeloid cell infiltration (Figure 27, Figure 30, Figure 34). Quantifying the impact of AvFc on the cellular makeup of this niche will be important for determining what impact AvFc has on tumor immunogenicity and whether or not it can act as an immunostimulating agent in addition to inducing ADCC.

Lastly, in Chapter 6, we presented data on the activity of AvFc against OVCA, the optimization of the murine ID8-luciferase model of OVCA, and the effects of AvFc treatment therein. We found that AvFc was highly selective for malignant human OVCA tissues over normal adjacent tissues, and that this was due to specific recognition of high-mannose glycans as the non-sugar-binding mutant displayed no binding to either tissue (Figure 37). Additionally, AvFc could potently bind and induce ADCC against a number of OVCA cell lines (both murine and human) and was found to recognize a number of important cell-surface receptors, the consequences of which are still being elucidated as these interactions are validated (Figure 38, Table 8). In the murine ID8-luciferase OVCA

challenge model, intraperitoneal administration of AvFc at 25 mg/kg Q2D resulted in a significant increase in survival time that was dependent on the number of cells originally administered (Figure 39, Figure 40). However, much work remains to optimize the model in terms of cells administered, dose amount, and dose duration in order to generate a reliable and reproducible model that can be used for future efficacy studies or to explore the efficacy of other molecules, such as lectikines (see below). Additionally, more relevant and translational data can be obtained *ex vivo* by conducting binding and immunophenotyping/immunoactivation studies on ascitic fluid from OVCA patients, since this fluid contains large numbers of both tumor cells and immune cells. In particular, aspects of immune function such as induction of ADCC and pro-inflammatory responses by drug administration can be measured using primary cell immunoassays like the CD107 assay as well as by measuring cytokine releases and by profiling the composition of immune cells using flow cytometry [330]. Overall, the data suggest that AvFc has activity against OVCA *in vivo*, and that further development is needed to fully demonstrate the utility of targeting high-mannose glycans in OVCA therapy.

## 7.2: Lectikines and other conjugates

Cytokines are small signaling molecules that act as key regulators of the immune system, both inducing and controlling inflammation. The forced induction of anti-inflammatory cytokines and localized deactivation of the immune system is considered a hallmark of cancer, and the conversion of tumors from an anti-inflammatory “cold” state into a pro-inflammatory “hot” state is seen as integral to modern immunotherapy and has been the subject of much recent research [331]. The principal example of drugs acting to

improve tumor immunogenicity are the checkpoint inhibitors, which act by preventing the tumor-induced deactivation of cytotoxic T lymphocytes by binding to and inhibiting the programmed death ligand and/or receptor (PD-1, PD-L1) and CTLA4 [332].

Checkpoint inhibitors have revolutionized therapy for a number of different types of cancer, the importance of which was recognized by the Nobel Committee when it awarded the 2018 Nobel Prize in Medicine to their inventors, Drs. James Allison and Tasuku Honjo, and the success of these drugs has placed increased emphasis on the host immune response to cancer as a therapeutic target [332].

A number of pro-inflammatory cytokines have been investigated for their potential use as therapeutic agents, the most well-studied of which is the T cell growth factor IL-2 [333]. IL-2, among other functions, stimulates the growth and proliferation of both CD8 and CD4 cells, assisting in the reversal of cancer-associated deactivation of these cells [334]. Clinical research into IL-2 therapy culminated in the FDA approval of the first cytokine-based therapy, aldesleukin, for the treatment of metastatic melanoma and renal cell carcinoma [335, 336]. Another widely studied cytokine, interferon alpha (IFN $\alpha$ ), has been approved for use as an immunotherapeutic agent against leukemia and melanoma under the trade name Roferon-A [337]. However, there are several major hurdles to the regular therapeutic use of cytokines as immunotherapies, the first of which is that cytokines typically exhibit an extremely short half-life, necessitating frequent high-dosing that can induce significant toxicities to the patient [338]. Furthermore, the diversity of cytokine functions dictates that under certain situations cytokines can be tumorigenic, which in turn requires very careful management during treatment. For instance, IL-2 is known to also induce the proliferation of T regulatory cells, which are

generally considered to be anti-inflammatory and pro-tumorigenic [339]. The major strategy that has emerged to limit systemic toxicity and improve cytokine targeting to tumor sites is through fusion of the cytokine to mAbs targeting tumor-associated antigens (TAAs) [340]. These so-called immunocytokines more efficiently concentrate the cytokines to the tumor microenvironment, allowing for improved interaction with immune cells and enhancing the conversion of “cold” tumors to “hot” ones. A number of TAA targets have been preclinically and clinically evaluated including GD2, TnC-A1, CD20, EpCAM, fibronectin extra-domain A and B (EDA and EDB), fibroblast activation protein (FAP), and histone H1 [341-347]. Furthermore, in addition to IL-2 fusions, which are by far the most frequently used, a number of other important cytokines have been fused to TAA-targeting mAbs including IL-12, IL-15, TNF, IFN $\alpha$ , and GM-CSF [348-352]. Though many of these have shown efficacy in phase II trials, only the anti-EDB-IL2 and anti-EDB-TNF fusions have progressed to phase III for malignant melanoma (NCT02938299 and NCT03567889).

The selectivity of the Avaren lectin for cancer-associated high-mannose glycans led us to hypothesize that AvFc-cytokine fusions may function similarly to mAb-based immunocytokines, and that such a fusion may offer significant benefit in OVCA, which is generally considered to be a poorly immunogenic cancer [300]. To this end we have recently proposed and received pilot funding for a project investigating fusion of Avaren and AvFc to TNF $\alpha$  and IL-2, respectively, for the treatment of OVCA (summarized in Figure 41). In this study we will create translational fusions of Avaren to TNF $\alpha$  and AvFc to IL-2 and express them in our plant-based transient over-expression platform in *N. benthamiana*. After confirming their producibility, proper structure, and bioactivity using

*in vitro* bioassays we plan to evaluate their activity using an orthotopic murine OVCA challenge model using ID8-luciferase cells, which are injected intraperitoneally to induce ascites and tumor formation (see Chapter 6). We predict that administration of these “lectikines” will result in a decreased tumor burden over time and greater survival by increasing the immunogenicity of the tumors. In particular, for the IL-2 fusion, we expect to see increases in CD8 and CD4 T cell populations in addition to NK cells, all of which respond to IL-2 stimulation and exhibit natural anticancer activity. Furthermore, TNF fusions (which form trimeric structures) suppress tumor growth both by binding and inducing apoptosis through TNF receptors as well as by recruiting macrophages and neutrophils. These lectikines could also be compared in the OVCA challenge model to the parent AvFc molecule, exploring cotreatment as a means to further increase any antitumor activity by the induction of ADCC. If successful, these studies will demonstrate the versatility of high-mannose glycan-targeting as a therapeutic strategy and open the door to further preclinical development of AvFc as an anticancer drug.

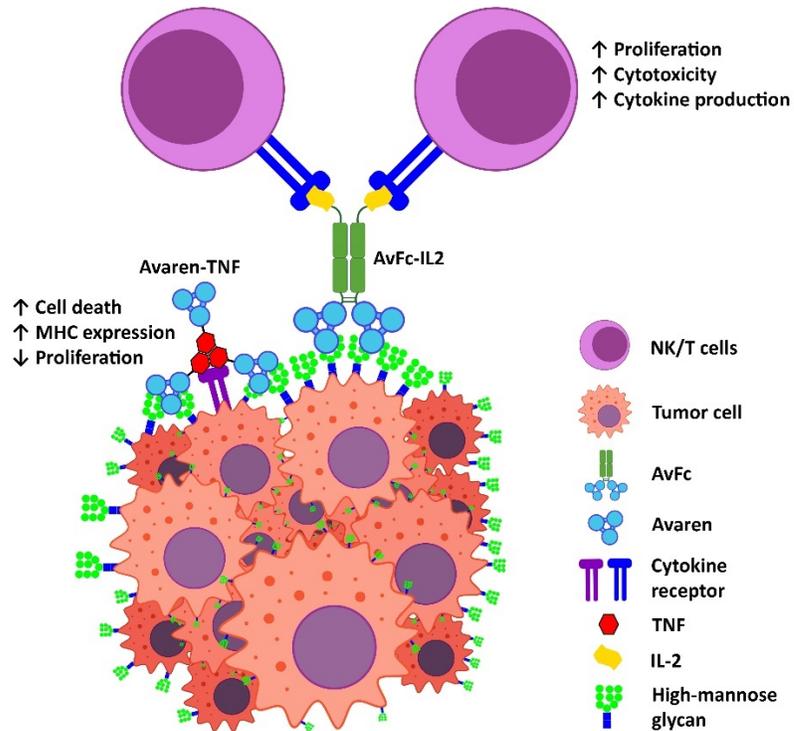


**Figure 41. Summary of lectikine approaches using AvFc- or Avaren-cytokine fusions.**

The goal of lectikine therapy is to improve the immunogenicity of the tumor while decreasing systemic toxicity resulting from off-target effects. Avaren-TNF fusions form a multimeric structure through the trimerization of TNF. Binding of TNF to its receptor and Avaren to the cancer cell surface is hypothesized to induce cell death by apoptosis and recruitment of immune cells such as macrophages and neutrophils. AvFc-IL2 fusions, on the other hand, bind to the target cell and form a complex with IL-2R-bearing cells (T cells, NK cells) inducing their activation and proliferation. We hypothesize that this will improve the immunogenicity of the tumor by converting inactivated or silenced T and NK cells to an activated form capable of inducing cytotoxicity.

### 7.3: Receptor targeting activities and their contribution to the mechanism of action

In the studies described in Chapter 6, we identified a number of potential binding partners for AvFc on the surface of OVCA cells using a proteomics approach with whole-cell lysates (Table 8). We have also performed similar analyses to identify binding partners on the surface of blood cancer and lung cancer cells (Table 9). We previously reported the validation of AvFc's recognition and inhibition of EGFR and IGF1R on the surface of A549 and H460 cells, which may contribute to its molecular mechanism of action in those models [105]. Further studies should be conducted to evaluate the impact of binding to other receptors on AvFc's mechanism of action and to validate these interactions in OVCA cell lines and primary cells using co-immunoprecipitation or the proximity ligation assay.

One of the major proteins identified in the proteomics analyses was integrin  $\alpha 5$ . Integrins are the principal receptors that are used by animal cells to bind to the extracellular matrix and direct movement and adhesion, in addition to facilitating some cell-to-cell communications and providing a link between the extracellular environment and the actin cytoskeleton of the cells [353]. All integrins form highly glycosylated heterodimers on the cell surface, which consist of an  $\alpha$  and a  $\beta$  subunit, and their expression is regulated from within the cell based on extracellular conditions. Cancers often manipulate expression of integrins to promote invasion and metastasis to secondary sites, and as such expression of certain integrins like integrin  $\alpha 5$  can be prognostic of lung, breast, colon, ovarian, and brain tumors [354-358]. Integrin  $\alpha 5$  (ITGA5) primarily forms a heterodimer with the  $\beta 1$  (ITGB1) subunit ( $\alpha 5\beta 1$ ) to recognize fibronectin, a major component of the extracellular matrix, to which binding facilitates cell migration

and invasion [353]. Antibodies targeting the  $\alpha 5\beta 1$  receptor, such as Pfizer's PF-04605412, have not seen tremendous clinical efficacy due in large part to the severity of infusion-related reactions [359]. However, clinical trials with other antibodies such as volociximab have not resulted in such toxicity [360]. Thus, the  $\alpha 5$  subunit may still be considered a druggable target, one that can potentially be recognized and inhibited by AvFc, however significant hurdles remain as integrins are commonly expressed on the surface of normal cells leading to adverse effects. The presence of high-mannose glycans on this could possibly provide a mechanism by which cancer-associated integrins are selectively targeted, limiting off-target effects.

Another protein potentially recognized by AvFc is plexin-B2. Plexin-B2 belongs to a family of plexin proteins that act as receptors for the semaphorin-family of signaling proteins, which primarily function in the guidance of axon development in the nervous system but also play roles in angiogenesis and immune cell trafficking [361, 362]. More recently, the plexin/semaphorin axis has been implicated in tumorigenesis and tumor metastasis, though the exact mechanisms have not been clearly identified, as the large number of semaphorins and plexin receptors also have complex interactions with not just the tumors but with cells in the environment [363, 364]. Semaphorin/plexin signaling, among other pro-survival functions, regulates the expression of integrins not through direct kinase activity but through activation or inhibition of plexin-associated receptor-type and nonreceptor-type tyrosine kinases [364, 365]. Disruption of this axis by inhibition of plexin-B2 has been shown to decrease proliferation and invasion of OVCA cells [366], chemosensitize prostate cancer cells [367], and decrease invasion of glioblastoma cells [368]. Semaphorin/plexin signaling is also important in trafficking and

migration of immune cells, though any potential relationship between this and other functions in cancer have yet to be elucidated [369]. Taken together, the evidence suggests that plexin-B2 expression may be important in tumor development and that binding and inhibition of it by AvFc may contribute to the lectibody's anti-cancer activity, though this hypothesis has yet to be tested.

The transferrin receptor TFR1 is a well-established target for cancer immunotherapy not only because iron plays a crucial role in physiological processes but because targeting TFR1 can result in the effective endocytosis of antibody-drug or transferrin-drug conjugates [370, 371]. TFR1 forms a disulfide-bond-linked homodimer at the cell surface with each of the monomers displaying several N-glycans [372]. Binding of the receptor to the iron transporter transferrin results in the endocytosis of the receptor-ligand complexes, bringing iron into the cell where it is used in the formation of heme- and iron-containing proteins that participate in oxygen transport, energy metabolism, DNA synthesis, and hormone synthesis, among others [370]. TFR1 is abnormally expressed in many cancers including liver, breast, lung, and colon [373-376]. As such, many groups have explored targeting TFR1 as a method to both disrupt iron metabolism and direct the internalization of cytotoxic drugs [371]. Both of these functions are potentially relevant to the development of AvFc as a therapeutic and should be explored further following formal validation of the interaction beyond proteomics. First, AvFc could bind to and inhibit iron transfer by selectively blocking cancer-associated (high-mannose glycan-bearing) TFR1. Secondly, AvFc-drug conjugates could theoretically be generated that utilize this pathway to internalize the drug leading to increased anti-tumor activity.

#### 7.4: Further assessment of the immunogenicity and immunotoxicity of Avaren-Fc

As discussed in Chapter 5 (5.2.7 and 5.3), AvFc is a non-native protein to both humans and mice and as such may be immunogenic and generate an ADA response upon administration. Indeed, we reported in Figure 23 that mice generate high-titers of ADAs to AvFc after repeated intraperitoneal administration of AvFc at 25 mg/kg, though these serum antibodies did not neutralize the activity of the drug within the B16F10 flank tumor model. Instead, a slight but non-significant enhancement effect was seen (Figure 23). Whether or not this is due to the animals being in a state of general inflammation due to repeated administration of AvFc (and is therefore not specific to AvFc) or if this is due to an enhancement of ADCC activity by ADAs is not clear, and repetitions of this study should include a group of animals that receives an irrelevant antigen during the pre-treatment phase and a group of animals with extended time between the last pretreatment dose and the first treatment to determine the specific impact of ADAs or inflammation. Interestingly, 6 of the 10 animals in the group that received AvFc pretreatment developed symptoms consistent with a hypersensitive or anaphylactic reaction within an hour of the first administration of AvFc in the treatment phase of the study (day 26), including labored breathing, hunching of the back, closed eyes, and lack of responsiveness to touch [297, 298]. While this condition abated within 5 hours and was not observed again after subsequent doses, the possibility of AvFc inducing such a toxic response is important to investigate further.

Adverse drug reactions (ADRs) to biologics can be classified into 5 types according to a scheme devised by Pichler et al., which is summarized in Table 10 [377]. Type alpha ADRs consist primarily of infusion reactions that result in cytokine release

syndrome or cytokine storm, or ADRs resulting from cytokine therapy. The severity of these reactions can range from minor gastrointestinal symptoms, fever, or edema to major respiratory distress syndrome, cardiovascular shock, and multi-organ failure [378]. Most often, these side effects occur during the first infusion and are dose and infusion-rate dependent [379]. Type beta ADRs are the immediate or delayed hypersensitivity reactions and will be discussed further below. Type gamma ADRs comprise drug-induced immunosuppression, opportunistic infections, cytokine imbalances, autoimmunities, and atopy. In some cases, drug-induced immunosuppression is a result of the intended mechanism of action of the drug (such as infliximab), however these treatments can result in the development of opportunistic infections such as tuberculosis, fungal infections, or herpes zoster [377]. Additionally, biologic drug administration can lead to autoimmune-like reactions including Guillain-Barré syndrome, vasculitis, psoriasis, and sclerosis [380]. Type delta ADRs occur when the drug or antibodies generated against a drug cross-react with antigen on normal host cells. A common example of this type of ADR is the development of acneiform eruptions in the skin of patients treated with cetuximab, due to the expression of EGFR on normal tissues [381]. Type delta reactions will likely be critical to examine during the preclinical investigation of AvFc, as high-mannose glycans can be found, albeit rarely, on normal tissues which may lead to off-target binding and toxicity. Off-target binding by AvFc can be assessed using tissue cross-reactivity assays, wherein *ex vivo* immunohistochemical staining of panels of frozen human or mouse tissues is performed with AvFc. While these studies cannot conclusively predict toxicity or efficacy in a tissue, their results are typically included in the Investigational New Drug (IND) application submitted to the FDA and

can direct further animal toxicity studies by shifting focus to particular organs or tissues [382]. Lastly, type epsilon ADRs are ambiguous and cover drug-mediated impairment of physiological functions that don't fit into other categories. Examples of these types of ADRs include heart failure induced by anti-TNF agents and neuropsychiatric/retinopathic effects caused by IFN $\alpha$  [383-385]. In the case of AvFc, the rapid onset of symptoms suggests either a type alpha ADR due to cytokine release in the peritoneal cavity (the site of drug administration) or a hypersensitivity reaction related to the presence of ADAs.

<b>Type alpha</b>	<b>Type beta</b>	<b>Type gamma</b>	<b>Type delta</b>	<b>Type epsilon</b>
Immunostimulation, high cytokine or cytokine release syndrome	Hypersensitivity	Immune or cytokine imbalance syndromes	Cross-reactivity	Non-immunological side effects
	Gell and Coombs type I-IV	Immunodeficiency		
		Autoimmunity		
		Allergy/atopic disorders		

**Table 10. Pichler classification of adverse reactions to biologics.**

In this system, ADRs are classified according to the underlying mechanism of action.

Type alpha ADRs comprise those induced by cytokine therapy or those induced by drugs that cause the sudden release of cytokines. Type beta ADRs consist of the classical hypersensitivities as defined by Gell and Coombs. Type gamma ADRs consist of drug-induced immunosuppression, autoimmunity, or allergies (to non-drug antigens). Type delta ADRs consist of toxicities that come about as a result of off-target binding of the drug to unintended tissues. Type epsilon ADRs are those that do not have an immunological mechanism.

Hypersensitivity reactions (HSRs), more commonly referred to as “allergies”, are undesirable reactions of the immune system to antigens, including innocuous antigens such as plant pollens, or therapeutic drugs. Antigens that cause such a reaction are referred to as allergens, regardless of their composition. These types of reactions can have a wide variety of physiological consequences ranging from simple discomfort, such as the congestion and itchiness associated with seasonal allergies, to far more serious systemic disease or anaphylaxis, often popularly associated with things like bee stings or food allergies. Reactions against drugs can also result in significant toxicity, which can limit the therapeutic benefits and options for patients who develop them. While the outward signs and symptoms of HSRs vary tremendously, they are generally divided into 4 groups based on the criteria established by Gell and Coombs, which considers the underlying immune mediators and effectors. The 4 classes in this system are thus defined as: IgE-mediated (type I), IgG-mediated (type II), immune complex-mediated (type III), and cell-mediated hypersensitivities (type IV) [386]. Most biologic drug hypersensitivities belong to classes I, III, and IV, and have been particularly well documented in monoclonal antibody therapies to cancer, where their development can result in significant toxicities resulting in the cessation of therapy [387, 388].

Type I HSRs are mediated by IgE-type antibodies, with FcεRI-bearing cells such as mast cells and basophils being the primary cellular effectors [386]. IgE is generated following the initial exposure to the allergen, or sensitization, when allergen-specific Th2 T helper cells secrete cytokines such as IL-4, IL-5, and IL-10 that cause B cells to undergo isotype switching from IgM to IgE [389]. Circulating IgE antibodies then bind to FcεRs on the surface of mast cells, which are rapidly activated following reintroduction

of the allergen to the body through subsequent exposure and cross-linking of the surface-bound IgE antibodies [390]. Activated mast cells degranulate, releasing histamine,  $\beta$ -hexoseaminidase, and other immune mediators (such as prostaglandins) that recruit other immune cells (primarily basophils and eosinophils) and cause the symptoms commonly associated with allergies including urticaria, pruritis, pain, edema, and congestion [390]. This activation of preformed IgE/Fc $\epsilon$ R complexes can happen within minutes of the secondary exposure to the allergen, and as such type I HSRs are considered immediate or rapid-onset hypersensitivities [388]. Severe type I HSRs can also result in anaphylaxis, which is a rapid systemic immune response caused by the massive production of pro-inflammatory mediators by mast cells and basophils following exposure to an allergen and can be fatal [391]. Type I HSRs are relatively common and have been well documented in patients receiving monoclonal antibody therapy with cetuximab or rituximab [392, 393].

Type II and III HSRs often occur simultaneously and are both mediated primarily by IgG-type antibodies but can also be mediated by IgM and to a lesser extent IgA [390]. In a type II HSR, antibodies targeting haptens composed of drug-modified cellular or extracellular matrix antigens result in the destruction of cells and damage to tissues by complement activation, phagocytosis, and ADCC [380]. These reactions are commonly observed in patients with penicillin and cephalosporin allergies, which are antibiotic compounds that fairly readily form haptens in the body [394]. Type II reactions are generally less relevant for biologics, however, as their administration does not routinely result in the formation of such autoantibodies [388]. Instead, biologics are more likely to induce type III HSRs, which result from the formation of large antibody-antigen

complexes that deposit in tissues and induce chronic inflammation via complement and activation of pro-inflammatory macrophages, damaging the surrounding cells and structures [380, 390]. The resulting symptoms are determined not by the antigen but by the site of deposition, which often occurs in small arteries, the renal glomeruli, and the synovial joints as they are too large to effectively clear from the circulation by phagocytosis [395]. Type III HSRs are often indistinguishable from autoimmune reactions. Examples of the prototypical conditions caused by type III HSRs include anemia, leukopenia, thrombocytopenia, pneumonitis, vasculitis, lupus-like reactions, or glomerulonephritis, and such reactions have been reported in patients receiving infliximab, etanercept, and adalimumab [395-398].

Lastly, type IV HSRs are cell-mediated, not antibody mediated, and are driven primarily by anti-allergen helper and cytotoxic T cell responses [379]. In this case, damage to tissues is caused directly by sensitized cytotoxic CD8<sup>+</sup> T cells or by T cell-mediated activation of macrophages, eosinophils, and neutrophils [390]. This type of HSR is likely involved in the pathogenesis of some autoimmune diseases including multiple sclerosis and type 1 diabetes [390]. In the context of drug administration, type IV HSRs manifest primarily as severe skin reactions but can also cause significant systemic disease in the form of Drug Reaction with Eosinophilia and Systemic Symptoms (DRESS) syndrome, Stevens-Johnsons syndrome (SJS), and toxic epidermal necrolysis (TEN), which occurs when cytotoxic CD8 T cells induce apoptosis and necrosis of keratinocytes [396]. Unlike type I, type II, III, and IV HSRs are delayed reactions, often occurring days after the exposure [386].

The acute reaction to AvFc by pretreated animals and subsequent resolution of the symptoms over time resembles a drug-induced HSR or anaphylaxis, likely of type I due to the time of onset, however this study was not designed to assess such an unexpected adverse event. Further studies need to be conducted to A) determine whether or not the reaction is repeatable and B) what the cause of the reaction was and whether or not it can be mitigated. To answer these questions, the study outlined in section 5.2.7 should be repeated in both healthy animals as well as in animals bearing B16F10 tumors, as it is possible that the presence of tumors in the animals contributed to the condition. If a similar adverse reaction is consistently observed after the first treatment dose on day 26 in pretreated animals, then further investigation into the nature of the reaction is warranted, as this would suggest a possible HSR.

Studies concerning the immunogenicity and immunotoxicity of biologic drugs are described in several FDA guidance documents, importantly in “Immunogenicity Assessment for Therapeutic Protein Products”, “Nonclinical Safety Evaluation of the Immunotoxic Potential of Drugs and Biologics”, and ICH S6 “Preclinical Safety Evaluation of Biotechnology-Derived Pharmaceuticals”. It is generally acknowledged that immunogenicity or immunotoxicity in animals is not predictive of either in humans, and the FDA does not recommend running a routine battery of tests for biotechnology-derived pharmaceuticals in the absence of a particular pathology. However, in instances where there is a particular immunotoxicological concern (such as was observed for AvFc) then *in vitro* and *in vivo* studies may provide valuable information and contribute to the overall risk assessment of the drug. In our case, it may be necessary to determine whether or not the acute reaction observed was due to one of the above-mentioned HSRs (Type I-

IV), anaphylaxis, or another immune-related reaction such as massive cytokine release, the latter of which can easily be assessed with a serum ELISPOT assay or multiplex Luminex assays to measure pro-inflammatory cytokines. In the event anaphylaxis is suspected, a scoring system can be used to gauge the severity of the reaction such as that developed by Li et al. [298], where 0 = no symptoms; 1 = scratching around the nose and head; 2 = puffiness around eyes and mouth, closed eyes; 3 = wheezing, labored breathing, cyanosis around mouth and tail; 4 = no activity after prodding, tremors or convulsions. Anaphylaxis would likely be evaluated concurrently while performing experiments to assess the type of HSR being induced.

For type I HSRs, one of the most important endpoints is the presence of anti-drug IgE in the serum, which can be measured using a simple ELISA, though this is not conclusive in and of itself. A number of further studies should be conducted to evaluate the risk of an IgE-mediated HSR including the mast cell activation test (MAT), the passive cutaneous anaphylaxis assay (PCA), the active cutaneous anaphylaxis assay (ACA), and the active systemic anaphylaxis assay (ASA). The MAT makes use of cultured primary mast cells (human or mouse) that would be sensitized with serum from animals exposed to AvFc followed by the addition of AvFc [399]. As a positive control, sensitized mast cells can be incubated with a goat anti-IgE antibody which will cross-link the bound IgE leading to degranulation. Negative controls can include serum from unexposed animals as well as coincubation with an unrelated antigen apart from AvFc. Mast cell activation is measured by flow cytometry with CD117, CD107a, CD63, and FcεR1a antibodies, while secretion of inflammatory mediators such as β-hexosaminidase and prostaglandin D<sub>2</sub> can be measured by ELISA. Dose-dependent

activation of mast cells by AvFc/IgE complexes would be indicated by the increase in CD107a and CD63 expression as well as by the increase in  $\beta$ -hexoseaminidase and prostaglandin D<sub>2</sub> levels. This assay can be performed in tandem with the PCA, ACA, or ASA, any of which would provide strong evidence for a drug-induced type I HSR. In the PCA, serum from animals exposed to AvFc is injected dermally into the ear followed by intravenous administration of AvFc and Evans Blue dye [400]. Changes in vascular permeability as a result of the HSR can be measured by the increase or decrease in Evans Blue dye in the ear. The ACA, which is a variation of the PCA, uses a similar protocol except the animals to be tested are exposed to the drug themselves (actively immunized) as opposed to simply injecting serum from other exposed animals into the ear [401]. The last test, the ASA test, simply extends the analysis of the animal to the development of anaphylaxis and can be performed simultaneously with the ACA or PCA [402]. Combined, these assays can help determine whether or not IgE is present and whether or not that IgE leads to an immunotoxicity, though these studies are not conclusive by themselves.

No standard non-clinical methods exist to predict type II and III HSRs [403]. In the case of drug-induced anemia (which can be detected through routine complete blood counts), a positive direct Coombs test can be indicative of a type II or III immunopathy targeting red blood cells [404]. In this test, erythrocytes taken from the exposed mice are incubated with anti-mouse antibodies, which will cause agglutination of the cells if they are coated with drug-induced anti-erythrocyte antibodies. In the event tissue damage is suspected, IHC can be performed to determine the presence of antibody or complement proteins in the tissues, which may suggest immune complex deposition [405].

Lastly, Type IV HSRs are cell-mediated and primarily manifest in the skin, making them a particular concern for topically applied compounds. While biologics are not typically applied in such a manner, even systemically administered drugs can be assessed for their potential ability to elicit a type IV HSR using established skin sensitization/challenge models. The most commonly used assays to do this are the Buehler Assay and the guinea pig maximization test (GPMT), both of which assess the ability of a drug to induce a skin reaction weeks after the initial subdermal exposure in guinea pigs [406]. The local lymph node assay (LLNA) in BALB/c mice can also be used to assess potential contact allergens and involves removal of the draining lymph nodes nearest to the site of drug administration and assessment of lymphocyte proliferation in response to drug administration after dermal sensitization [407].

In summary, the preclinical development of AvFc will require further study of the impact of immunogenicity to the drug, especially in light of the ADR observed in the pretreatment study described in Chapter 5.2.7. The rapid onset of the reaction indicates that it is likely due to a type alpha or beta reaction, and the assays described above can be used to determine whether or not AvFc administration is likely to lead to an HSR or cytokine release and can help determine the immunological mechanism behind the reaction.

## 7.5: Conclusion

In conclusion, we have demonstrated that AvFc binds to cancer cells through the recognition of cancer-associated high-mannose glycans, which are aberrantly overexpressed on the surface of cells as they undergo the transformation to malignancy.

AvFc appears to primarily exert its anti-cancer activity by binding to the cancer cell surface and inducing Fc-mediated effector functions, most importantly antibody-dependent cell-mediated cytotoxicity. However, much work remains to demonstrate its *in vivo* activity using more clinically relevant patient-derived xenograft models as well as to perform IND-enabling preclinical toxicological assessments that will enable future clinical evaluation of the drug candidate. In addition, it is possible that interaction with and inhibition of cell-surface receptors may contribute to its overall mechanism of action in certain models, and validation of the binding interactions elucidated in the proteomics analyses will be critical for understanding its activity in the future. Lastly, it will be critical to further understand the immunological mechanism of action of AvFc, in particular by examining its impact on the makeup of the tumor immune microenvironment and its ability to activate primary NK and myeloid cells. Overall, the data presented herein justify AvFc's continued development as a first-in-class cancer therapeutic that targets a novel cancer-associated glycobiomarker.

## REFERENCES

1. Stanley, P., N. Taniguchi, and M. Aebi, *N-glycans*. Essentials of Glycobiology [Internet]. 3rd edition, 2017.
  2. Reily, C., et al., *Glycosylation in health and disease*. Nat Rev Nephrol, 2019.
  3. Lairson, L., et al., *Glycosyltransferases: structures, functions, and mechanisms*. Annu. Rev. Biochem., 2008. **77**: p. 521-555.
  4. Brockhausen, I. and P. Stanley, *O-GalNAc Glycans*, in *Essentials of Glycobiology*, A. Varki, et al., Editors. 2015, Cold Spring Harbor Laboratory Press
- Copyright 2015-2017 by The Consortium of Glycobiology Editors, La Jolla, California. All rights reserved.: Cold Spring Harbor (NY). p. 113-23.
5. Bennett, E.P., et al., *Control of mucin-type O-glycosylation: a classification of the polypeptide GalNAc-transferase gene family*. Glycobiology, 2012. **22**(6): p. 736-56.
  6. Jensen, P.H., D. Kolarich, and N.H. Packer, *Mucin-type O-glycosylation--putting the pieces together*. Febs j, 2010. **277**(1): p. 81-94.
  7. Fukuda, M., *Roles of mucin-type O-glycans in cell adhesion*. Biochimica et Biophysica Acta (BBA)-General Subjects, 2002. **1573**(3): p. 394-405.
  8. Carlow, D.A., et al., *PSGL-1 function in immunity and steady state homeostasis*. Immunological reviews, 2009. **230**(1): p. 75-96.
  9. Wright, R.D. and D. Cooper, *Glycobiology of leukocyte trafficking in inflammation*. Glycobiology, 2014. **24**(12): p. 1242-1251.
  10. Daniels, G., *Human blood groups*. 2008: John Wiley & Sons.
  11. Topaz, O., et al., *Mutations in GALNT3, encoding a protein involved in O-linked glycosylation, cause familial tumoral calcinosis*. Nature genetics, 2004. **36**(6): p. 579-581.
  12. Khetarpal, S.A., et al., *Loss of function of GALNT2 lowers high-density lipoproteins in humans, nonhuman primates, and rodents*. Cell metabolism, 2016. **24**(2): p. 234-245.
  13. Pinho, S.S. and C.A. Reis, *Glycosylation in cancer: mechanisms and clinical implications*. Nature Reviews Cancer, 2015. **15**(9): p. 540-555.
  14. Loke, I., et al., *Emerging roles of protein mannosylation in inflammation and infection*. Molecular aspects of medicine, 2016. **51**: p. 31-55.
  15. Waechter, C.J. and W.J. Lennarz, *The role of polyprenol-linked sugars in glycoprotein synthesis*. Annu Rev Biochem, 1976. **45**: p. 95-112.
  16. Snider, M.D., L.A. Sultzman, and P.W. Robbins, *Transmembrane location of oligosaccharide-lipid synthesis in microsomal vesicles*. Cell, 1980. **21**(2): p. 385-92.

17. Schenk, B., F. Fernandez, and C.J. Waechter, *The ins(ide) and out(side) of dolichyl phosphate biosynthesis and recycling in the endoplasmic reticulum*. Glycobiology, 2001. **11**(5): p. 61r-70r.
18. Williams, D.B., *Beyond lectins: the calnexin/calreticulin chaperone system of the endoplasmic reticulum*. Journal of cell science, 2006. **119**(4): p. 615-623.
19. Ellgaard, L. and E.-M. Frickel, *Calnexin, calreticulin, and ERp57*. Cell biochemistry and biophysics, 2003. **39**(3): p. 223-247.
20. Oda, Y., et al., *EDEM as an acceptor of terminally misfolded glycoproteins released from calnexin*. Science, 2003. **299**(5611): p. 1394-1397.
21. Roth, J. and C. Zuber, *Quality control of glycoprotein folding and ERAD: the role of N-glycan handling, EDEM1 and OS-9*. Histochemistry and cell biology, 2017. **147**(2): p. 269-284.
22. Caramelo, J.J. and A.J. Parodi, *Getting in and out from calnexin/calreticulin cycles*. Journal of Biological Chemistry, 2008. **283**(16): p. 10221-10225.
23. Gonzalez, D.S., et al., *Identification, expression, and characterization of a cDNA encoding human endoplasmic reticulum mannosidase I, the enzyme that catalyzes the first mannose trimming step in mammalian Asn-linked oligosaccharide biosynthesis*. Journal of Biological Chemistry, 1999. **274**(30): p. 21375-21386.
24. Herscovics, A., *Importance of glycosidases in mammalian glycoprotein biosynthesis*. Biochim Biophys Acta, 1999. **1473**(1): p. 96-107.
25. Schachter, H., *The joys of HexNAc. The synthesis and function of N- and O-glycan branches*. Glycoconj J, 2000. **17**(7-9): p. 465-83.
26. Gomord, V., et al., *Plant-specific glycosylation patterns in the context of therapeutic protein production*. Plant biotechnology journal, 2010. **8**(5): p. 564-587.
27. Wilson, J.R., D. Williams, and H. Schachter, *The control of glycoprotein synthesis: N-acetylglucosamine linkage to a mannose residue as a signal for the attachment of l-fucose to the asparagine-linked N-acetylglucosamine residue of glycopeptide from  $\alpha$ 1-acid glycoprotein*. Biochemical and biophysical research communications, 1976. **72**(3): p. 909-916.
28. Shaaltiel, Y. and Y. Tekoah, *Plant specific N-glycans do not have proven adverse effects in humans*. Nature Biotechnology, 2016. **34**(7): p. 706-708.
29. Prescott, V.E. and S.P. Hogan, *Genetically modified plants and food hypersensitivity diseases: usage and implications of experimental models for risk assessment*. Pharmacology & therapeutics, 2006. **111**(2): p. 374-383.
30. Fischöder, T., et al., *Enzymatic synthesis of N-acetyllactosamine (LacNAc) type I oligomers and characterization as multivalent galectin ligands*. Molecules, 2017. **22**(8): p. 1320.
31. Schauer, R., *Sialic acids as regulators of molecular and cellular interactions*. Curr Opin Struct Biol, 2009. **19**(5): p. 507-14.
32. Varki, A., R.L. Schnaar, and R. Schauer, *Sialic acids and other nonulosonic acids*. Essentials of Glycobiology [Internet]. 3rd edition, 2017.
33. Mühlhoff, M., M. Eckhardt, and R. Gerardy-Schahn, *Polysialic acid: three-dimensional structure, biosynthesis and function*. Current opinion in structural biology, 1998. **8**(5): p. 558-564.

34. Hildebrandt, H., et al., *Dissecting polysialic acid and NCAM functions in brain development*. Journal of neurochemistry, 2007. **103**: p. 56-64.
35. Stencel-Baerenwald, J.E., et al., *The sweet spot: defining virus-sialic acid interactions*. Nat Rev Microbiol, 2014. **12**(11): p. 739-49.
36. Vigerust, D.J. and V.L. Shepherd, *Virus glycosylation: role in virulence and immune interactions*. Trends in Microbiology, 2007. **15**(5): p. 211-218.
37. Kreisman, L.S. and B.A. Cobb, *Infection, inflammation and host carbohydrates: a Glyco-Evasion Hypothesis*. Glycobiology, 2012. **22**(8): p. 1019-1030.
38. Mir-Shekari, S.Y., et al., *The Glycosylation of the Influenza A Virus Hemagglutinin by Mammalian Cells: A SITE-SPECIFIC STUDY* &. Journal of Biological Chemistry, 1997. **272**(7): p. 4027-4036.
39. Bonomelli, C., et al., *The glycan shield of HIV is predominantly oligomannose independently of production system or viral clade*. PloS one, 2011. **6**(8): p. e23521.
40. Iacob, R.E., et al., *Mass spectrometric characterization of glycosylation of hepatitis C virus E2 envelope glycoprotein reveals extended microheterogeneity of N-glycans*. Journal of the American Society for Mass Spectrometry, 2008. **19**(3): p. 428-444.
41. Jeffers, S.A., E.M. Hemmila, and K.V. Holmes, *Human coronavirus 229E can use CD209L (L-SIGN) to enter cells*, in *The Nidoviruses*. 2006, Springer. p. 265-269.
42. Ritchie, G., et al., *Identification of N-linked carbohydrates from severe acute respiratory syndrome (SARS) spike glycoprotein*. Virology, 2010. **399**(2): p. 257-269.
43. Watanabe, Y., et al., *Vulnerabilities in coronavirus glycan shields despite extensive glycosylation*. Nature Communications, 2020. **11**(1): p. 2688.
44. Li, J., et al., *The glycosylation site in the envelope protein of West Nile virus (Sarafenid) plays an important role in replication and maturation processes*. Journal of general virology, 2006. **87**(3): p. 613-622.
45. Watanabe, Y., et al., *Structure of the Lassa virus glycan shield provides a model for immunological resistance*. Proceedings of the National Academy of Sciences, 2018. **115**(28): p. 7320-7325.
46. Lin, G., et al., *Differential N-linked glycosylation of human immunodeficiency virus and Ebola virus envelope glycoproteins modulates interactions with DC-SIGN and DC-SIGNR*. Journal of virology, 2003. **77**(2): p. 1337-1346.
47. Balachandran, N. and L.M. Hutt-Fletcher, *Synthesis and processing of glycoprotein gG of herpes simplex virus type 2*. Journal of Virology, 1985. **54**(3): p. 825-832.
48. Rachmilewitz, J., *Glycosylation: An intrinsic sign of "danger"*. Self/nonsself, 2010. **1**(3): p. 250-254.
49. Giron, L.B., et al., *Interferon- $\alpha$  alters host glycosylation machinery during treated HIV infection*. EBioMedicine, 2020. **59**: p. 102945.
50. Heindel, D.W., et al., *Glycomic analysis of host response reveals high mannose as a key mediator of influenza severity*. Proceedings of the National Academy of Sciences, 2020. **117**(43): p. 26926-26935.

51. Pritchard, L.K., et al., *Structural constraints determine the glycosylation of HIV-1 envelope trimers*. Cell reports, 2015. **11**(10): p. 1604-1613.
52. Davis, C.W., et al., *West Nile virus discriminates between DC-SIGN and DC-SIGNR for cellular attachment and infection*. J Virol, 2006. **80**(3): p. 1290-301.
53. Mitchell, C.A., K. Ramessar, and B.R. O'Keefe, *Antiviral lectins: Selective inhibitors of viral entry*. Antiviral research, 2017. **142**: p. 37-54.
54. Haynes, B.F., D.R. Burton, and J.R. Mascola, *Multiple roles for HIV broadly neutralizing antibodies*. Science translational medicine, 2019. **11**(516).
55. Hakomori, S.-i. and R. Kannagi, *Glycosphingolipids as tumor-associated and differentiation markers*. 1983, Oxford University Press.
56. Hatano, K., et al., *Expression of gangliosides, GD1a, and sialyl paragloboside is regulated by NF- $\kappa$ B-dependent transcriptional control of  $\alpha$ 2, 3-sialyltransferase I, II, and VI in human castration-resistant prostate cancer cells*. International journal of cancer, 2011. **129**(8): p. 1838-1847.
57. Pinho, S.S., et al., *Loss and recovery of Mgat3 and GnT-III Mediated E-cadherin N-glycosylation is a mechanism involved in epithelial-mesenchymal-epithelial transitions*. PloS one, 2012. **7**(3): p. e33191.
58. Kumamoto, K., et al., *Increased expression of UDP-galactose transporter messenger RNA in human colon cancer tissues and its implication in synthesis of Thomsen-Friedenreich antigen and sialyl Lewis A/X determinants*. Cancer research, 2001. **61**(11): p. 4620-4627.
59. Kellokumpu, S., R. Sormunen, and I. Kellokumpu, *Abnormal glycosylation and altered Golgi structure in colorectal cancer: dependence on intra-Golgi pH*. FEBS letters, 2002. **516**(1-3): p. 217-224.
60. Dennis, J.W., et al., *Beta 1-6 branching of Asn-linked oligosaccharides is directly associated with metastasis*. Science, 1987. **236**(4801): p. 582-585.
61. Potapenko, I.O., et al., *Glycan gene expression signatures in normal and malignant breast tissue; possible role in diagnosis and progression*. Molecular oncology, 2010. **4**(2): p. 98-118.
62. Liu, Y.-C., et al., *Sialylation and fucosylation of epidermal growth factor receptor suppress its dimerization and activation in lung cancer cells*. Proceedings of the National Academy of Sciences, 2011. **108**(28): p. 11332-11337.
63. Hutchinson, W.L., et al., *Fucosyltransferases: differential plasma and tissue alterations in hepatocellular carcinoma and cirrhosis*. Hepatology, 1991. **13**(4): p. 683-688.
64. Sato, Y., et al., *Early recognition of hepatocellular carcinoma based on altered profiles of alpha-fetoprotein*. New England Journal of Medicine, 1993. **328**(25): p. 1802-1806.
65. Croci, D.O., et al., *Glycosylation-dependent lectin-receptor interactions preserve angiogenesis in anti-VEGF refractory tumors*. Cell, 2014. **156**(4): p. 744-758.
66. Seberger, P.J. and W.G. Chaney, *Control of metastasis by Asn-linked,  $\beta$ 1-6 branched oligosaccharides in mouse mammary cancer cells*. Glycobiology, 1999. **9**(3): p. 235-241.
67. Demetriou, M., et al., *Reduced contact-inhibition and substratum adhesion in epithelial cells expressing GlcNAc-transferase V*. The Journal of cell biology, 1995. **130**(2): p. 383-392.

68. Granovsky, M., et al., *Suppression of tumor growth and metastasis in Mgat5-deficient mice*. *Nature medicine*, 2000. **6**(3): p. 306-312.
69. Pinho, S.S., et al., *E-cadherin and adherens-junctions stability in gastric carcinoma: functional implications of glycosyltransferases involving N-glycan branching biosynthesis, N-acetylglucosaminyltransferases III and V*. *Biochimica et Biophysica Acta (BBA)-General Subjects*, 2013. **1830**(3): p. 2690-2700.
70. Yoshimura, M., et al., *Suppression of lung metastasis of B16 mouse melanoma by N-acetylglucosaminyltransferase III gene transfection*. *Proceedings of the National Academy of Sciences*, 1995. **92**(19): p. 8754-8758.
71. Xu, Q., et al., *Roles of N-acetylglucosaminyltransferase III in epithelial-to-mesenchymal transition induced by transforming growth factor  $\beta$ 1 (TGF- $\beta$ 1) in epithelial cell lines*. *Journal of Biological Chemistry*, 2012. **287**(20): p. 16563-16574.
72. De Leoz, M.L.A., et al., *High-mannose glycans are elevated during breast cancer progression*. *Molecular & Cellular Proteomics*, 2011. **10**(1).
73. Boyaval, F., et al., *N-glycomic signature of stage II colorectal cancer and its association with the tumor microenvironment*. *Molecular & Cellular Proteomics*, 2021. **20**.
74. Sethi, M.K., W.S. Hancock, and S. Fanayan, *Identifying N-glycan biomarkers in colorectal cancer by mass spectrometry*. *Accounts of chemical research*, 2016. **49**(10): p. 2099-2106.
75. Chik, J.H., et al., *Comprehensive glycomics comparison between colon cancer cell cultures and tumours: implications for biomarker studies*. *Journal of proteomics*, 2014. **108**: p. 146-162.
76. Takayama, H., et al., *Altered glycosylation associated with dedifferentiation of hepatocellular carcinoma: a lectin microarray-based study*. *BMC cancer*, 2020. **20**(1): p. 1-8.
77. Powers, T.W., et al., *Two-dimensional N-glycan distribution mapping of hepatocellular carcinoma tissues by MALDI-imaging mass spectrometry*. *Biomolecules*, 2015. **5**(4): p. 2554-2572.
78. Park, D.D., et al., *Metastasis of cholangiocarcinoma is promoted by extended high-mannose glycans*. *Proceedings of the National Academy of Sciences*, 2020. **117**(14): p. 7633-7644.
79. Ruhaak, L.R., et al., *Differential N-glycosylation patterns in lung adenocarcinoma tissue*. *Journal of proteome research*, 2015. **14**(11): p. 4538-4549.
80. Park, H.-M., et al., *Mass spectrometry-based N-linked glycomic profiling as a means for tracking pancreatic cancer metastasis*. *Carbohydrate research*, 2015. **413**: p. 5-11.
81. Chen, H., et al., *Mass spectrometric profiling reveals association of N-glycan patterns with epithelial ovarian cancer progression*. *Tumor Biology*, 2017. **39**(7): p. 1010428317716249.
82. Everest-Dass, A.V., et al., *N-glycan MALDI imaging mass spectrometry on formalin-fixed paraffin-embedded tissue enables the delineation of ovarian cancer tissues*. *Molecular & Cellular Proteomics*, 2016. **15**(9): p. 3003-3016.

83. Munkley, J., I.G. Mills, and D.J. Elliott, *The role of glycans in the development and progression of prostate cancer*. Nature Reviews Urology, 2016. **13**(6): p. 324-333.
84. Möglinger, U., et al., *Alterations of the human skin N-and O-glycome in basal cell carcinoma and squamous cell carcinoma*. Frontiers in oncology, 2018. **8**: p. 70.
85. An, H.J., et al., *Extensive determination of glycan heterogeneity reveals an unusual abundance of high mannose glycans in enriched plasma membranes of human embryonic stem cells*. Molecular & Cellular Proteomics, 2012. **11**(4).
86. Bhat, G., et al., *Shifted Golgi targeting of glycosyltransferases and  $\alpha$ -mannosidase IA from giantin to GM130-GRASP65 results in formation of high mannose N-glycans in aggressive prostate cancer cells*. Biochimica et Biophysica Acta (BBA) - General Subjects, 2017. **1861**(11, Part A): p. 2891-2901.
87. Cheng, P.-W., S. Davidson, and G. Bhat, *Markers of malignant prostate cancer cells: Golgi localization of  $\alpha$ -mannosidase IA at GM130-GRASP65 site and appearance of high mannose N-glycans on cell surface*. Biochemical and biophysical research communications, 2020. **527**(2): p. 406-410.
88. Phoomak, C., et al., *O-GlcNAcylation mediates metastasis of cholangiocarcinoma through FOXO3 and MAN1A1*. Oncogene, 2018. **37**(42): p. 5648-5665.
89. Park, D., et al., *Characteristic changes in cell surface glycosylation accompany intestinal epithelial cell (IEC) differentiation: high mannose structures dominate the cell surface glycome of undifferentiated enterocytes*. Molecular & Cellular Proteomics, 2015. **14**(11): p. 2910-2921.
90. Nicholson, R.I., J.M.W. Gee, and M.E. Harper, *EGFR and cancer prognosis*. European journal of cancer, 2001. **37**: p. 9-15.
91. Johns, T.G., et al., *The antitumor monoclonal antibody 806 recognizes a high-mannose form of the EGF receptor that reaches the cell surface when cells over-express the receptor*. The FASEB journal, 2005. **19**(7): p. 1-18.
92. Alonso-Garcia, V., et al., *High Mannose N-Glycans Promote Migration of Bone-Marrow-Derived Mesenchymal Stromal Cells*. International journal of molecular sciences, 2020. **21**(19): p. 7194.
93. Polonskaya, Z., et al., *High-affinity anti-glycan antibodies: challenges and strategies*. Current Opinion in Immunology, 2019. **59**: p. 65-71.
94. Ploessl, C., et al., *Dinutuximab: an anti-GD2 monoclonal antibody for high-risk neuroblastoma*. Annals of Pharmacotherapy, 2016. **50**(5): p. 416-422.
95. Newsom-Davis, T.E., et al., *Enhanced immune recognition of cryptic glycan markers in human tumors*. Cancer research, 2009. **69**(5): p. 2018-2025.
96. Dan, X., W. Liu, and T.B. Ng, *Development and applications of lectins as biological tools in biomedical research*. Medicinal research reviews, 2016. **36**(2): p. 221-247.
97. Yau, T., et al., *Lectins with potential for anti-cancer therapy*. Molecules, 2015. **20**(3): p. 3791-3810.
98. Hamorsky, K.T., et al., *Engineering of a lectibody targeting high-mannose-type glycans of the HIV envelope*. Molecular Therapy, 2019. **27**(11): p. 2038-2052.
99. Kulkarni, G. and C. McCulloch, *Concanavalin A induced apoptosis in fibroblasts: the role of cell surface carbohydrates in lectin mediated cytotoxicity*. Journal of cellular physiology, 1995. **165**(1): p. 119-133.

100. Chiba, H., et al., *Actinohivin, a novel anti-HIV protein from an actinomycete that inhibits syncytium formation: isolation, characterization, and biological activities*. Biochemical and biophysical research communications, 2001. **282**(2): p. 595-601.
101. Zhang, F., et al., *The Characteristic Structure of Anti-HIV Actinohivin in Complex with Three HMTG D1 Chains of HIV-gp120*. Chembiochem, 2014. **15**(18): p. 2766-2773.
102. Matoba, N., et al., *HIV-1 neutralization profile and plant-based recombinant expression of actinohivin, an Env glycan-specific lectin devoid of T-cell mitogenic activity*. PLoS One, 2010. **5**(6): p. e11143.
103. Suzuki, K., et al., *Peculiarity in crystal packing of anti-HIV lectin actinohivin in complex with  $\alpha$  (1–2) mannanose*. Acta Crystallographica Section D: Biological Crystallography, 2013. **69**(9): p. 1818-1825.
104. Hoque, M.M., et al., *Structural insights into the specific anti-HIV property of actinohivin: structure of its complex with the  $\alpha$ (1-2)mannobiose moiety of gp120*. Acta crystallographica. Section D, Biological crystallography, 2012. **68**(Pt 12): p. 1671-1679.
105. Oh, Y.J., et al., *Antitumor activity of a lectibody targeting cancer-associated high-mannose glycans*. bioRxiv, 2021.
106. Afshar-Kharghan, V., *The role of the complement system in cancer*. The Journal of clinical investigation, 2017. **127**(3): p. 780-789.
107. Bonavita, E., et al., *PTX3 is an extrinsic oncosuppressor regulating complement-dependent inflammation in cancer*. Cell, 2015. **160**(4): p. 700-714.
108. Fishelson, Z., et al., *Obstacles to cancer immunotherapy: expression of membrane complement regulatory proteins (mCRPs) in tumors*. Mol Immunol, 2003. **40**(2-4): p. 109-23.
109. Cao, Q., S.M. McIsaac, and A.W. Stadnyk, *Human colonic epithelial cells detect and respond to C5a via apically expressed C5aR through the ERK pathway*. Am J Physiol Cell Physiol, 2012. **302**(12): p. C1731-40.
110. Cho, M.S., et al., *Complement Component 3 Is Regulated by TWIST1 and Mediates Epithelial-Mesenchymal Transition*. J Immunol, 2016. **196**(3): p. 1412-8.
111. Wang, S.Y., et al., *Depletion of the C3 component of complement enhances the ability of rituximab-coated target cells to activate human NK cells and improves the efficacy of monoclonal antibody therapy in an in vivo model*. Blood, 2009. **114**(26): p. 5322-30.
112. Wang, S.Y., et al., *NK-cell activation and antibody-dependent cellular cytotoxicity induced by rituximab-coated target cells is inhibited by the C3b component of complement*. Blood, 2008. **111**(3): p. 1456-63.
113. Nimmerjahn, F., S. Gordan, and A. Lux, *Fc $\gamma$ R dependent mechanisms of cytotoxic, agonistic, and neutralizing antibody activities*. Trends in immunology, 2015. **36**(6): p. 325-336.
114. van Egmond, M. and J.E. Bakema. *Neutrophils as effector cells for antibody-based immunotherapy of cancer*. in *Seminars in cancer biology*. 2013. Elsevier.

115. Flannagan, R.S., V. Jaumouillé, and S. Grinstein, *The cell biology of phagocytosis*. Annual Review of Pathology: Mechanisms of Disease, 2012. **7**: p. 61-98.
116. Overdijk, M.B., et al. *Antibody-mediated phagocytosis contributes to the anti-tumor activity of the therapeutic antibody daratumumab in lymphoma and multiple myeloma*. in *MAbs*. 2015. Taylor & Francis.
117. Braster, R., T. O'toole, and M. Van Egmond, *Myeloid cells as effector cells for monoclonal antibody therapy of cancer*. Methods, 2014. **65**(1): p. 28-37.
118. Abès, R., et al., *Long-lasting antitumor protection by anti-CD20 antibody through cellular immune response*. Blood, The Journal of the American Society of Hematology, 2010. **116**(6): p. 926-934.
119. Gül, N. and M. van Egmond, *Antibody-Dependent Phagocytosis of Tumor Cells by Macrophages: A Potent Effector Mechanism of Monoclonal Antibody Therapy of Cancer*. Cancer Research, 2015. **75**(23): p. 5008-5013.
120. Jung, S.T., et al., *Effective phagocytosis of low Her2 tumor cell lines with engineered, aglycosylated IgG displaying high FcγRIIIa affinity and selectivity*. ACS chemical biology, 2013. **8**(2): p. 368-375.
121. Cartron, G., et al., *Therapeutic activity of humanized anti-CD20 monoclonal antibody and polymorphism in IgG Fc receptor FcγRIIIa gene*. Blood, The Journal of the American Society of Hematology, 2002. **99**(3): p. 754-758.
122. Weng, W.-K. and R. Levy, *Two immunoglobulin G fragment C receptor polymorphisms independently predict response to rituximab in patients with follicular lymphoma*. Journal of clinical oncology, 2003. **21**(21): p. 3940-3947.
123. Gómez Román, V.R., J.C. Murray, and L.M. Weiner, *Chapter 1 - Antibody-Dependent Cellular Cytotoxicity (ADCC)*, in *Antibody Fc*, M.E. Ackerman and F. Nimmerjahn, Editors. 2014, Academic Press: Boston. p. 1-27.
124. Shields, R.L., et al., *High resolution mapping of the binding site on human IgG1 for FcγRI, FcγRII, FcγRIII, and FcRn and design of IgG1 variants with improved binding to the FcγR*. Journal of Biological Chemistry, 2001. **276**(9): p. 6591-6604.
125. Shinkawa, T., et al., *The absence of fucose but not the presence of galactose or bisecting N-acetylglucosamine of human IgG1 complex-type oligosaccharides shows the critical role of enhancing antibody-dependent cellular cytotoxicity*. Journal of Biological Chemistry, 2003. **278**(5): p. 3466-3473.
126. Sondermann, P., et al., *The 3.2-Å crystal structure of the human IgG1 Fc fragment–FcγRIII complex*. Nature, 2000. **406**(6793): p. 267-273.
127. Dashivets, T., et al., *Multi-angle effector function analysis of human monoclonal IgG glycovariants*. PloS one, 2015. **10**(12): p. e0143520.
128. Ahmed, A.A., et al., *Structural characterization of GASDALIE Fc bound to the activating Fc receptor FcγRIIIa*. Journal of structural biology, 2016. **194**(1): p. 78-89.
129. Edwards, J.M., et al., *Enhancement of antibody-dependent cellular cytotoxicity and phagocytosis in anti-HIV-1 bovine chimeric broadly-neutralizing antibodies*. Journal of Virology, 2021: p. JVI. 00219-21.

130. Ackerman, M.E., et al., *Natural variation in Fc glycosylation of HIV-specific antibodies impacts antiviral activity*. The Journal of clinical investigation, 2013. **123**(5): p. 2183-2192.
131. Yamane-Ohnuki, N., et al., *Establishment of FUT8 knockout Chinese hamster ovary cells: an ideal host cell line for producing completely defucosylated antibodies with enhanced antibody-dependent cellular cytotoxicity*. Biotechnology and bioengineering, 2004. **87**(5): p. 614-622.
132. Hanania, U., et al., *Establishment of a tobacco BY2 cell line devoid of plant-specific xylose and fucose as a platform for the production of biotherapeutic proteins*. Plant biotechnology journal, 2017. **15**(9): p. 1120-1129.
133. Strasser, R., et al., *Generation of glyco-engineered Nicotiana benthamiana for the production of monoclonal antibodies with a homogeneous human-like N-glycan structure*. Plant Biotechnology Journal, 2008. **6**(4): p. 392-402.
134. Dent, M. and N. Matoba, *Cancer biologics made in plants*. Current opinion in biotechnology, 2020. **61**: p. 82-88.
135. Lindsley, C.W., *New 2016 data and statistics for global pharmaceutical products and projections through 2017*. 2017, ACS Publications.
136. Raedler, L.A., *Zarxio (filgrastim-sndz): first biosimilar approved in the United States*. American health & drug benefits, 2016. **9**(Spec Feature): p. 150.
137. Verch, T., V. Yusibov, and H. Koprowski, *Expression and assembly of a full-length monoclonal antibody in plants using a plant virus vector*. Journal of Immunological Methods, 1998. **220**(1): p. 69-75.
138. Pujol, M., et al., *Fighting cancer with plant-expressed pharmaceuticals*. Trends in Biotechnology, 2007. **25**(10): p. 455-459.
139. Sims, R.B., *Development of sipuleucel-T: autologous cellular immunotherapy for the treatment of metastatic castrate resistant prostate cancer*. Vaccine, 2012. **30**(29): p. 4394-4397.
140. Kang, Y.J., et al., *Expression of a human prostatic acid phosphatase (PAP)-IgM Fc fusion protein in plants using in vitro tissue subculture*. Frontiers in plant science, 2017. **8**: p. 274.
141. Fu, Y.Y., et al., *Human colorectal cancer antigen GA733-2-Fc fused to endoplasmic reticulum retention motif KDEL enhances its immunotherapeutic effects*. J Cancer Res Ther, 2018. **14**(Supplement): p. S748-S757.
142. Tuse, D., et al., *Clinical Safety and Immunogenicity of Tumor-Targeted, Plant-Made Id-KLH Conjugate Vaccines for Follicular Lymphoma*. Biomed Res Int, 2015. **2015**: p. 648143.
143. McCormick, A., et al., *Plant-produced idiotypic vaccines for the treatment of non-Hodgkin's lymphoma: safety and immunogenicity in a phase I clinical study*. Proceedings of the National Academy of Sciences, 2008. **105**(29): p. 10131-10136.
144. Bendandi, M., et al., *Rapid, high-yield production in plants of individualized idiotypic vaccines for non-Hodgkin's lymphoma*. Annals of Oncology, 2010. **21**(12): p. 2420-2427.
145. Plummer, M., et al., *Global burden of cancers attributable to infections in 2012: a synthetic analysis*. Lancet Glob Health, 2016. **4**(9): p. e609-16.

146. Chabeda, A., et al., *Therapeutic vaccines for high-risk HPV-associated diseases*. Papillomavirus Research, 2018. **5**: p. 46-58.
147. Yanez, R.J.R., et al., *Expression optimization of a cell membrane-penetrating human papillomavirus type 16 therapeutic vaccine candidate in Nicotiana benthamiana*. PLoS One, 2017. **12**(8): p. e0183177.
148. Yanez, R.J.R., et al., *LALF32-51 -E7, a HPV-16 therapeutic vaccine candidate, forms protein body-like structures when expressed in Nicotiana benthamiana leaves*. Plant Biotechnol J, 2018. **16**(2): p. 628-637.
149. McCormick, A.A., et al., *TMV-peptide fusion vaccines induce cell-mediated immune responses and tumor protection in two murine models*. Vaccine, 2006. **24**(40-41): p. 6414-23.
150. Murray, A.A., et al., *In Situ Vaccination with Cowpea vs Tobacco Mosaic Virus against Melanoma*. Mol Pharm, 2018. **15**(9): p. 3700-3716.
151. Shukla, S., et al., *Plant viral nanoparticles-based HER2 vaccine: Immune response influenced by differential transport, localization and cellular interactions of particulate carriers*. Biomaterials, 2017. **121**: p. 15-27.
152. Czapar, A.E., et al., *Slow-Release Formulation of Cowpea Mosaic Virus for In Situ Vaccine Delivery to Treat Ovarian Cancer*. Adv Sci (Weinh), 2018. **5**(5): p. 1700991.
153. Wang, C., S.N. Fiering, and N.F. Steinmetz, *Cowpea mosaic virus promotes anti-tumor activity and immune memory in a mouse ovarian tumor model*. Advanced therapeutics, 2019. **2**(5): p. 1900003.
154. Kerstetter-Fogle, A., et al., *Plant Virus-Like Particle In Situ Vaccine for Intracranial Glioma Immunotherapy*. Cancers (Basel), 2019. **11**(4).
155. Wang, C. and N.F. Steinmetz, *CD47 Blockade and Cowpea Mosaic Virus Nanoparticle In Situ Vaccination Triggers Phagocytosis and Tumor Killing*. Adv Healthc Mater, 2019. **8**(8): p. e1801288.
156. Lee, K.L., et al., *Combination of plant virus nanoparticle-based in situ vaccination with chemotherapy potentiates antitumor response*. Nano letters, 2017. **17**(7): p. 4019-4028.
157. Beihaghi, M., et al., *Transient expression of CCL21as recombinant protein in tomato*. Biotechnology reports, 2018. **17**: p. 10-15.
158. McLean, M.D., *Trastuzumab Made in Plants Using vivoXPRESS® Platform Technology*. 2017.
159. Song, I., et al., *Endoplasmic reticulum retention motif fused to recombinant anti-cancer monoclonal antibody (mAb) CO17-1A affects mAb expression and plant stress response*. PloS one, 2018. **13**(9): p. e0198978.
160. Jin, N., et al., *Low binding affinity and reduced complement-dependent cell death efficacy of ofatumumab produced using a plant system (Nicotiana benthamiana L.)*. Protein expression and purification, 2019.
161. Kommineni, V., et al., *In Vivo Glycan Engineering via the Mannosidase I Inhibitor (Kifunensine) Improves Efficacy of Rituximab Manufactured in Nicotiana benthamiana Plants*. Int J Mol Sci, 2019. **20**(1).
162. Dong, Y., et al., *Seed-specific expression and analysis of recombinant anti-HER2 single-chain variable fragment (scFv-Fc) in Arabidopsis thaliana*. Protein Expr Purif, 2017. **133**: p. 187-192.

163. Liu, S.D., et al., *Afucosylated antibodies increase activation of FcγRIIIa-dependent signaling components to intensify processes promoting ADCC*. *Cancer immunology research*, 2015. **3**(2): p. 173-183.
164. Marusic, C., et al., *N-glycan engineering of a plant-produced anti-CD20-hIL-2 immunocytokine significantly enhances its effector functions*. *Biotechnology and bioengineering*, 2018. **115**(3): p. 565-576.
165. Pitek, A., et al., *Cancer Theranostic Applications of Albumin-Coated Tobacco Mosaic Virus Nanoparticles*. *ACS applied materials & interfaces*, 2018. **10**(46): p. 39468-39477.
166. Gulati, N.M., et al., *Cryo-electron tomography investigation of serum albumin-camouflaged tobacco mosaic virus nanoparticles*. *Nanoscale*, 2017. **9**(10): p. 3408-3415.
167. Hu, H., et al., *Dysprosium-modified tobacco mosaic virus nanoparticles for ultra-high-field magnetic resonance and near-infrared fluorescence imaging of prostate cancer*. *ACS nano*, 2017. **11**(9): p. 9249-9258.
168. Kernan, D.L., et al., *Featured Article: Delivery of chemotherapeutic vcMMAE using tobacco mosaic virus nanoparticles*. *Experimental Biology and Medicine*, 2017. **242**(14): p. 1405-1411.
169. Franke, C.E., et al., *Tobacco Mosaic Virus-Delivered Cisplatin Restores Efficacy in Platinum-Resistant Ovarian Cancer Cells*. *Molecular pharmaceutics*, 2017. **15**(8): p. 2922-2931.
170. Marin-Caba, L., et al., *Tobacco Mosaic Virus-Functionalized Mesoporous Silica Nanoparticles, a Wool-Ball-like Nanostructure for Drug Delivery*. *Langmuir*, 2019. **35**(1): p. 203-211.
171. Le, D.H., et al., *Potato virus X, a filamentous plant viral nanoparticle for doxorubicin delivery in cancer therapy*. *Nanoscale*, 2017. **9**(6): p. 2348-2357.
172. Le, D.H.T., U. Commandeur, and N.F. Steinmetz, *Presentation and Delivery of Tumor Necrosis Factor-Related Apoptosis-Inducing Ligand via Elongated Plant Viral Nanoparticle Enhances Antitumor Efficacy*. *ACS Nano*, 2019. **13**(2): p. 2501-2510.
173. Le, D.H., et al., *Biodistribution of Filamentous Plant Virus Nanoparticles: Pepino Mosaic Virus versus Potato Virus X*. *Biomacromolecules*, 2018. **20**(1): p. 469-477.
174. Madden, A.J., et al., *Pharmacokinetics and efficacy of doxorubicin-loaded plant virus nanoparticles in preclinical models of cancer*. *Nanomedicine*, 2017. **12**(20): p. 2519-2532.
175. Alemzadeh, E., et al., *Enhanced anti-tumor efficacy and reduced cardiotoxicity of doxorubicin delivered in a novel plant virus nanoparticle*. *Colloids Surf B Biointerfaces*, 2019. **174**: p. 80-86.
176. Alemzadeh, E., K. Izadpanah, and F. Ahmadi, *Generation of recombinant protein shells of Johnson grass chlorotic stripe mosaic virus in tobacco plants and their use as drug carrier*. *Journal of virological methods*, 2017. **248**: p. 148-153.
177. Oronsky, B., et al., *A brief review of the management of platinum-resistant-platinum-refractory ovarian cancer*. *Med Oncol*, 2017. **34**(6): p. 103.

178. Varrot, A., S.M. Basheer, and A. Imberty, *Fungal lectins: structure, function and potential applications*. Current Opinion in Structural Biology, 2013. **23**(5): p. 678-685.
179. Bhutia, S.K., et al., *Plant lectins in cancer therapeutics: Targeting apoptosis and autophagy-dependent cell death*. Pharmacol Res, 2019. **144**: p. 8-18.
180. Pfüller, U., *Chemical Constituents of European Mistletoe (Viscum album L.) Isolation and Characterisation of the Main Relevant Ingredients: Lectins, Viscotoxins, Oligo-/polysaccharides, Flavonoides, Alkaloids*, in *Mistletoe*. 2000, CRC Press. p. 117-138.
181. Muthing, J., et al., *Mistletoe lectin I is a sialic acid-specific lectin with strict preference to gangliosides and glycoproteins with terminal Neu5Ac alpha 2-6Gal beta 1-4GlcNAc residues*. Biochemistry, 2004. **43**(11): p. 2996-3007.
182. Freuding, M., et al., *Mistletoe in oncological treatment: a systematic review : Part 2: quality of life and toxicity of cancer treatment*. J Cancer Res Clin Oncol, 2019. **145**(4): p. 927-939.
183. Freuding, M., et al., *Mistletoe in oncological treatment: a systematic review : Part 1: survival and safety*. J Cancer Res Clin Oncol, 2019. **145**(3): p. 695-707.
184. Thies, A., et al., *Low-dose mistletoe lectin-I reduces melanoma growth and spread in a scid mouse xenograft model*. British Journal Of Cancer, 2007. **98**: p. 106.
185. Gengenbach, B.B., et al., *Comparison of microbial and transient expression (tobacco plants and plant-cell packs) for the production and purification of the anti-cancer mistletoe lectin viscumin*. Biotechnology and bioengineering, 2019.
186. Baldauf, K., et al., *Oral administration of a recombinant cholera toxin B subunit promotes mucosal healing in the colon*. Mucosal immunology, 2017. **10**(4): p. 887.
187. Axelrad, J.E., S. Lichtiger, and V. Yajnik, *Inflammatory bowel disease and cancer: The role of inflammation, immunosuppression, and cancer treatment*. World J Gastroenterol, 2016. **22**(20): p. 4794-801.
188. Chang, M., et al., *Intestinal and Extraintestinal Cancers Associated With Inflammatory Bowel Disease*. Clin Colorectal Cancer, 2018. **17**(1): p. e29-e37.
189. Oliveira-Ferrer, L., K. Legler, and K. Milde-Langosch, *Role of protein glycosylation in cancer metastasis*. Semin Cancer Biol, 2017.
190. Loke, I., et al., *Emerging roles of protein mannosylation in inflammation and infection*. Mol Aspects Med, 2016. **51**: p. 31-55.
191. Ruhaak, L.R., S. Miyamoto, and C.B. Lebrilla, *Developments in the identification of glycan biomarkers for the detection of cancer*. Molecular & Cellular Proteomics, 2013. **12**(4): p. 846-855.
192. Seber Kasinger, L.E., et al., *A novel anti-HIV-1 bispecific bNAb-lectin fusion protein engineered in a plant-based transient expression system*. Plant Biotechnol J, 2019. **17**(8): p. 1646-1656.
193. Oliveira-Ferrer, L., K. Legler, and K. Milde-Langosch, *Role of protein glycosylation in cancer metastasis*. Semin Cancer Biol, 2017. **44**: p. 141-152.
194. Tuse, D., *Safety of plant-made pharmaceuticals: product development and regulatory considerations based on case studies of two autologous human cancer vaccines*. Hum Vaccin, 2011. **7**(3): p. 322-30.

195. Ma, J.K., et al., *Regulatory approval and a first-in-human phase I clinical trial of a monoclonal antibody produced in transgenic tobacco plants*. *Plant Biotechnol J*, 2015. **13**(8): p. 1106-20.
196. Pillet, S., et al., *A plant-derived quadrivalent virus like particle influenza vaccine induces cross-reactive antibody and T cell response in healthy adults*. *Clin Immunol*, 2016. **168**: p. 72-87.
197. Chichester, J.A., et al., *Safety and immunogenicity of a plant-produced Pfs25 virus-like particle as a transmission blocking vaccine against malaria: A Phase I dose-escalation study in healthy adults*. *Vaccine*, 2018. **36**(39): p. 5865-5871.
198. Leuzinger, K., et al., *Efficient agroinfiltration of plants for high-level transient expression of recombinant proteins*. *Journal of visualized experiments: JoVE*, 2013(77).
199. Wakita, T., et al., *Production of infectious hepatitis C virus in tissue culture from a cloned viral genome*. *Nature medicine*, 2005. **11**(7): p. 791-796.
200. Maurin, G., et al., *Identification of interactions in the E1E2 heterodimer of hepatitis C virus important for cell entry*. *Journal of Biological Chemistry*, 2011. **286**(27): p. 23865-23876.
201. Scheel, T.K., et al., *Development of JFH1-based cell culture systems for hepatitis C virus genotype 4a and evidence for cross-genotype neutralization*. *Proceedings of the National Academy of Sciences*, 2008. **105**(3): p. 997-1002.
202. Jensen, T.B., et al., *Highly efficient JFH1-based cell-culture system for hepatitis C virus genotype 5a: failure of homologous neutralizing-antibody treatment to control infection*. *The Journal of infectious diseases*, 2008. **198**(12): p. 1756-1765.
203. Gottwein, J.M., et al., *Development and characterization of hepatitis C virus genotype 1-7 cell culture systems: role of CD81 and scavenger receptor class B type I and effect of antiviral drugs*. *Hepatology*, 2009. **49**(2): p. 364-377.
204. Voisset, C. and J. Dubuisson, *Functional hepatitis C virus envelope glycoproteins*. *Biology of the Cell*, 2004. **96**(6): p. 413-413.
205. Joyce, A.P., et al., *One mouse, one pharmacokinetic profile: quantitative whole blood serial sampling for biotherapeutics*. *Pharmaceutical research*, 2014. **31**(7): p. 1823-1833.
206. Zhang, Y., et al., *PKSolver: An add-in program for pharmacokinetic and pharmacodynamic data analysis in Microsoft Excel*. *Computer methods and programs in biomedicine*, 2010. **99**(3): p. 306-314.
207. Tateno, C. and Y. Kojima, *Characterization and applications of chimeric mice with humanized livers for preclinical drug development*. *Lab Anim Res*, 2020. **36**: p. 2.
208. Ji, C., et al., *Prevention of hepatitis C virus infection and spread in human liver chimeric mice by an anti-CD81 monoclonal antibody*. *Hepatology*, 2015. **61**(4): p. 1136-1144.
209. Takeuchi, T., et al., *Real-time detection system for quantification of hepatitis C virus genome*. *Gastroenterology*, 1999. **116**(3): p. 636-42.
210. Rieger, A.M., et al., *Modified annexin V/propidium iodide apoptosis assay for accurate assessment of cell death*. *JoVE (Journal of Visualized Experiments)*, 2011(50): p. e2597.

211. Dent, M., et al., *Safety and Efficacy of Avaren-Fc Lectibody Targeting HCV High-Mannose Glycans in a Human Liver Chimeric Mouse Model*. Cellular and molecular gastroenterology and hepatology, 2021. **11**(1): p. 185-198.
212. Penin, F., et al., *Structural biology of hepatitis C virus*. Hepatology, 2004. **39**(1): p. 5-19.
213. Blach, S., et al., *Global prevalence and genotype distribution of hepatitis C virus infection in 2015: a modelling study*. The Lancet Gastroenterology & Hepatology, 2017. **2**(3): p. 161-176.
214. Zibbell, J.E., et al., *Increases in Acute Hepatitis C Virus Infection Related to a Growing Opioid Epidemic and Associated Injection Drug Use, United States, 2004 to 2014*. American Journal of Public Health, 2018. **108**(2): p. 175-181.
215. Zibbell, J.E., et al., *Increases in hepatitis C virus infection related to injection drug use among persons aged ≤ 30 years—Kentucky, Tennessee, Virginia, and West Virginia, 2006–2012*. MMWR. Morbidity and mortality weekly report, 2015. **64**(17): p. 453.
216. Manns, M.P., et al., *Hepatitis C virus infection*. Nature Reviews Disease Primers, 2017. **3**: p. 17006.
217. Negro, F., et al., *Extrahepatic morbidity and mortality of chronic hepatitis C*. Gastroenterology, 2015. **149**(6): p. 1345-1360.
218. Manns, M.P., et al., *Peginterferon alfa-2b plus ribavirin compared with interferon alfa-2b plus ribavirin for initial treatment of chronic hepatitis C: a randomised trial*. The Lancet, 2001. **358**(9286): p. 958-965.
219. Jacobson, I.M., et al., *Telaprevir for previously untreated chronic hepatitis C virus infection*. New England Journal of Medicine, 2011. **364**(25): p. 2405-2416.
220. Poordad, F., et al., *Boceprevir for untreated chronic HCV genotype 1 infection*. New England Journal of Medicine, 2011. **364**(13): p. 1195-1206.
221. Asselah, T., et al., *Efficacy of Glecaprevir/Pibrentasvir for 8 or 12 Weeks in Patients With Hepatitis C Virus Genotype 2, 4, 5, or 6 Infection Without Cirrhosis*. Clinical Gastroenterology and Hepatology, 2018. **16**(3): p. 417-426.
222. Afdhal, N., et al., *Ledipasvir and sofosbuvir for untreated HCV genotype 1 infection*. New England Journal of Medicine, 2014. **370**(20): p. 1889-1898.
223. Feld, J.J., et al., *Sustained virologic response of 100% in HCV genotype 1b patients with cirrhosis receiving ombitasvir/paritaprevir/r and dasabuvir for 12 weeks*. Journal of hepatology, 2016. **64**(2): p. 301-307.
224. Zeuzem, S., et al., *Grazoprevir–elbasvir combination therapy for treatment-naive cirrhotic and noncirrhotic patients with chronic hepatitis C virus genotype 1, 4, or 6 infection: a randomized trial*. Annals of internal medicine, 2015. **163**(1): p. 1-13.
225. Fernández-Carrillo, C., et al., *Treatment of Hepatitis C Virus in Patients with Advanced Cirrhosis: Always Justified? Analysis of the Hepa-C Registry*. Journal of Hepatology, 2016. **64**(2): p. S133.
226. Belli, L.S., et al., *Delisting of liver transplant candidates with chronic hepatitis C after viral eradication: A European study*. Journal of hepatology, 2016. **65**(3): p. 524-531.

227. Jothimani, D., S. Govil, and M. Rela, *Management of post liver transplantation recurrent hepatitis C infection with directly acting antiviral drugs: a review*. Hepatol Int, 2016. **10**(5): p. 749-61.
228. Hughes, M.G., Jr., et al., *Rate of hepatitis C viral clearance by human livers in human patients: Liver transplantation modeling primary infection and implications for studying entry inhibition*. PLoS One, 2017. **12**(7): p. e0180719.
229. Felmler, D.J., et al., *New perspectives for preventing hepatitis C virus liver graft infection*. Lancet Infect Dis, 2016. **16**(6): p. 735-45.
230. Colpitts, C.C. and T.F. Baumert, *Hepatitis C virus cell entry: a target for novel antiviral strategies to address limitations of direct acting antivirals*. Hepatol Int, 2016. **10**(5): p. 741-8.
231. Walls, A.C., et al., *Glycan shield and epitope masking of a coronavirus spike protein observed by cryo-electron microscopy*. Nature Structural & Molecular Biology, 2016. **23**(10): p. 899-905.
232. Leonard, C.K., et al., *Assignment of intrachain disulfide bonds and characterization of potential glycosylation sites of the type 1 recombinant human immunodeficiency virus envelope glycoprotein (gp120) expressed in Chinese hamster ovary cells*. J Biol Chem, 1990. **265**(18): p. 10373-82.
233. Suga, A., M. Nagae, and Y. Yamaguchi, *Analysis of protein landscapes around N-glycosylation sites from the PDB repository for understanding the structural basis of N-glycoprotein processing and maturation*. Glycobiology, 2018. **28**(10): p. 774-785.
234. Hamorsky, K.T., et al., *Efficient single tobamoviral vector-based bioproduction of broadly neutralizing anti-HIV-1 monoclonal antibody VRC01 in Nicotiana benthamiana plants and utility of VRC01 in combination microbicides*. Antimicrobial agents and chemotherapy, 2013. **57**(5): p. 2076-86.
235. Goffard, A., et al., *Role of N-Linked Glycans in the Functions of Hepatitis C Virus Envelope Glycoproteins*. Journal of Virology, 2005. **79**(13): p. 8400-8409.
236. Meuleman, P., et al., *Griffithsin has antiviral activity against hepatitis C virus*. Antimicrobial agents and chemotherapy, 2011: p. AAC. 00633-11.
237. Helle, F., et al., *Cyanovirin-N inhibits hepatitis C virus entry by binding to envelope protein glycans*. Journal of Biological Chemistry, 2006. **281**(35): p. 25177-25183.
238. Freedman, H., et al., *Computational Prediction of the Heterodimeric and Higher-Order Structure of gpE1/gpE2 Envelope Glycoproteins Encoded by Hepatitis C Virus*. J Virol, 2017. **91**(8).
239. Cholankeril, G. and A. Ahmed, *Alcoholic liver disease replaces hepatitis C virus infection as the leading indication for liver transplantation in the United States*. Clinical Gastroenterology and Hepatology, 2018. **16**(8): p. 1356-1358.
240. Wali, M., et al., *Advancing donor liver age and rapid fibrosis progression following transplantation for hepatitis C*. Gut, 2002. **51**(2): p. 248-252.
241. Colpitts, C.C., R.T. Chung, and T.F. Baumert, *Entry inhibitors: a perspective for prevention of hepatitis C virus infection in organ transplantation*. ACS infectious diseases, 2017. **3**(9): p. 620-623.
242. Baumert, T.F., et al., *Hepatitis C-related hepatocellular carcinoma in the era of new generation antivirals*. BMC medicine, 2017. **15**(1): p. 52.

243. Colpitts, C. and T. Baumert, *Addressing the challenges of hepatitis C virus resistance and treatment failure*. 2016, Multidisciplinary Digital Publishing Institute.
244. Colpitts, C.C., P.L. Tsai, and M.B. Zeisel, *Hepatitis C Virus Entry: An Intriguingly Complex and Highly Regulated Process*. *Int J Mol Sci*, 2020. **21**(6).
245. Terrault, N., et al., *LP17 : Novel approach for the prevention of recurrent hepatitis C in liver transplant recipients: Preliminary results from ongoing phase III trial with civalir*. *Journal of Hepatology*, 2015. **62**: p. S271-S272.
246. Smith, H.L., et al., *Prevention of allograft HCV recurrence with peri-transplant human monoclonal antibody MBL-HCV1 combined with a single oral direct-acting antiviral: A proof-of-concept study*. *Journal of Viral Hepatitis*, 2017. **24**(3): p. 197-206.
247. Helle, F., et al., *The Neutralizing Activity of Anti-Hepatitis C Virus Antibodies Is Modulated by Specific Glycans on the E2 Envelope Protein*. *Journal of Virology*, 2007. **81**(15): p. 8101-8111.
248. Pantua, H., et al., *Glycan shifting on hepatitis C virus (HCV) E2 glycoprotein is a mechanism for escape from broadly neutralizing antibodies*. *Journal of molecular biology*, 2013. **425**(11): p. 1899-1914.
249. Balzarini, J., *Targeting the glycans of glycoproteins: a novel paradigm for antiviral therapy*. *Nat Rev Microbiol*, 2007. **5**(8): p. 583-97.
250. Peters, L. and M.B. Klein, *Epidemiology of hepatitis C virus in HIV-infected patients*. *Curr Opin HIV AIDS*, 2015. **10**(5): p. 297-302.
251. Schranz, A.J., et al., *Challenges Facing a Rural Opioid Epidemic: Treatment and Prevention of HIV and Hepatitis C*. *Curr HIV/AIDS Rep*, 2018. **15**(3): p. 245-254.
252. Ruck, J.M. and D.L. Segev, *Expanding deceased donor kidney transplantation: medical risk, infectious risk, hepatitis C virus, and HIV*. *Curr Opin Nephrol Hypertens*, 2018. **27**(6): p. 445-453.
253. Bodzin, A.S. and T.B. Baker, *Liver Transplantation Today: Where We Are Now and Where We Are Going*. *Liver Transpl*, 2018. **24**(10): p. 1470-1475.
254. Mancardi, D. and M. Daéron, *Fc Receptors in Immune Responses*. *Reference Module in Biomedical Sciences*, 2014: p. B978-0-12-801238-3.00119-7.
255. Vidarsson, G., G. Dekkers, and T. Rispen, *IgG subclasses and allotypes: from structure to effector functions*. *Front Immunol*, 2014. **5**: p. 520.
256. Weiner, G.J., *Rituximab: Mechanism of Action*. *Seminars in Hematology*, 2010. **47**(2): p. 115-123.
257. Zahavi, D., et al., *Enhancing antibody-dependent cell-mediated cytotoxicity: a strategy for improving antibody-based immunotherapy*. *Antibody Therapeutics*, 2018. **1**(1): p. 7-12.
258. Ochoa, M.C., et al., *Antibody-dependent cell cytotoxicity: immunotherapy strategies enhancing effector NK cells*. *Immunol Cell Biol*, 2017. **95**(4): p. 347-355.
259. Jennewein, M.F. and G. Alter, *The immunoregulatory roles of antibody glycosylation*. *Trends in immunology*, 2017. **38**(5): p. 358-372.

260. Smith, P., et al., *Mouse model recapitulating human Fcγ receptor structural and functional diversity*. Proceedings of the National Academy of Sciences, 2012. **109**(16): p. 6181-6186.
261. DiLillo, D.J. and J.V. Ravetch, *Differential Fc-receptor engagement drives an anti-tumor vaccinal effect*. Cell, 2015. **161**(5): p. 1035-1045.
262. Wang, L.-X., et al., *Glycoengineering of antibodies for modulating functions*. Annual review of biochemistry, 2019. **88**: p. 433-459.
263. Kommineni, V., et al., *In vivo glycan engineering via the mannosidase I inhibitor (Kifunensine) improves efficacy of rituximab manufactured in Nicotiana benthamiana plants*. International journal of molecular sciences, 2019. **20**(1): p. 194.
264. Roychowdhury, S., et al., *Hydroponic treatment of Nicotiana benthamiana with kifunensine modifies the N-glycans of recombinant glycoprotein antigens to predominantly Man9 high-mannose type upon transient overexpression*. Frontiers in plant science, 2018. **9**: p. 62.
265. Schähns, M., et al., *Production of a monoclonal antibody in plants with a humanized N-glycosylation pattern*. Plant Biotechnology Journal, 2007. **5**(5): p. 657-663.
266. Shields, R.L., et al., *Lack of fucose on human IgG1 N-linked oligosaccharide improves binding to human FcγRIII and antibody-dependent cellular toxicity*. Journal of Biological Chemistry, 2002. **277**(30): p. 26733-26740.
267. Jansing, J., et al., *CRISPR/Cas9-mediated knockout of six glycosyltransferase genes in Nicotiana benthamiana for the production of recombinant proteins lacking β-1,2-xylose and core α-1,3-fucose*. Plant Biotechnology Journal, 2019. **17**(2): p. 350-361.
268. Weterings, K. and G. Van Eldik, *Nicotiana benthamiana plants deficient in fucosyltransferase activity*. 2019, Google Patents.
269. Lai, H., et al., *Structural and functional characterization of an anti-West Nile virus monoclonal antibody and its single-chain variant produced in glycoengineered plants*. Plant Biotechnology Journal, 2014. **12**(8): p. 1098-1107.
270. Hurtado, J., et al., *In vitro and in vivo efficacy of anti-chikungunya virus monoclonal antibodies produced in wild-type and glycoengineered Nicotiana benthamiana plants*. Plant Biotechnology Journal, 2020. **18**(1): p. 266-273.
271. Loos, A., et al., *Expression and glycoengineering of functionally active heteromultimeric IgM in plants*. Proceedings of the National Academy of Sciences, 2014. **111**(17): p. 6263-6268.
272. Tsekoa, T.L., et al., *Efficient in vitro and in vivo activity of glyco-engineered plant-produced rabies monoclonal antibodies E559 and 62-71-3*. PloS one, 2016. **11**(7): p. e0159313.
273. Forthal, D.N., et al., *Fc-Glycosylation Influences Fcγ Receptor Binding and Cell-Mediated Anti-HIV Activity of Monoclonal Antibody 2G12*. The Journal of Immunology, 2010. **185**(11): p. 6876-6882.
274. Bridgwater, C., et al., *89Zr-labeled anti-PD-L1 antibody fragment for evaluating in vivo PD-L1 levels in melanoma mouse model*. Cancer biotherapy & radiopharmaceuticals, 2020. **35**(8): p. 549-557.

275. Arntzen, C., *Plant-made pharmaceuticals: from 'Edible Vaccines' to Ebola therapeutics*. *Plant biotechnology journal*, 2015. **13**(8): p. 1013-1016.
276. Ward, B.J., et al., *Efficacy, immunogenicity, and safety of a plant-derived, quadrivalent, virus-like particle influenza vaccine in adults (18–64 years) and older adults (≥65 years): two multicentre, randomised phase 3 trials*. *The Lancet*, 2020. **396**(10261): p. 1491-1503.
277. Casacuberta, J.M., et al., *Biotechnological uses of RNAi in plants: risk assessment considerations*. *Trends in Biotechnology*, 2015. **33**(3): p. 145-147.
278. Khan, Z., et al., *Use of TALEs and TALEN technology for genetic improvement of plants*. *Plant molecular biology reporter*, 2017. **35**(1): p. 1-19.
279. Petolino, J.F., *Genome editing in plants via designed zinc finger nucleases*. In *Vitro Cellular & Developmental Biology-Plant*, 2015. **51**(1): p. 1-8.
280. Feng, Z., et al., *Efficient genome editing in plants using a CRISPR/Cas system*. *Cell research*, 2013. **23**(10): p. 1229-1232.
281. Nimmerjahn, F. and J.V. Ravetch, *Divergent immunoglobulin g subclass activity through selective Fc receptor binding*. *Science*, 2005. **310**(5753): p. 1510-1512.
282. He, J., et al., *Generation and analysis of novel plant-derived antibody-based therapeutic molecules against West Nile virus*. *PLoS One*, 2014. **9**(3): p. e93541.
283. Lee, J.-H., et al., *Intracellular reprogramming of expression, glycosylation, and function of a plant-derived antiviral therapeutic monoclonal antibody*. *PloS one*, 2013. **8**(8): p. e68772.
284. Bardor, M., et al., *Monoclonal C5-1 antibody produced in transgenic alfalfa plants exhibits a N-glycosylation that is homogenous and suitable for glyco-engineering into human-compatible structures*. *Plant biotechnology journal*, 2003. **1**(6): p. 451-462.
285. Triguero, A., et al., *Plant-derived mouse IgG monoclonal antibody fused to KDEL endoplasmic reticulum-retention signal is N-glycosylated homogeneously throughout the plant with mostly high-mannose-type N-glycans*. *Plant Biotechnology Journal*, 2005. **3**(4): p. 449-457.
286. Feige, M.J., et al., *An Unfolded CHI Domain Controls the Assembly and Secretion of IgG Antibodies*. *Molecular Cell*, 2009. **34**(5): p. 569-579.
287. Lynaugh, H., H. Li, and B. Gong, *Rapid Fc glycosylation analysis of Fc fusions with IdeS and liquid chromatography mass spectrometry*. *mAbs*, 2013. **5**(5): p. 641-645.
288. Jones, A.J., et al., *Selective clearance of glycoforms of a complex glycoprotein pharmaceutical caused by terminal N-acetylglucosamine is similar in humans and cynomolgus monkeys*. *Glycobiology*, 2007. **17**(5): p. 529-540.
289. Keck, R., et al., *Characterization of a complex glycoprotein whose variable metabolic clearance in humans is dependent on terminal N-acetylglucosamine content*. *Biologicals*, 2008. **36**(1): p. 49-60.
290. Schriebl, K., et al., *Biochemical characterization of rhEpo-Fc fusion protein expressed in CHO cells*. *Protein expression and purification*, 2006. **49**(2): p. 265-275.
291. Bongers, J., et al., *Characterization of glycosylation sites for a recombinant IgG1 monoclonal antibody and a CTLA4-Ig fusion protein by liquid chromatography–*

- mass spectrometry peptide mapping*. Journal of Chromatography A, 2011. **1218**(45): p. 8140-8149.
292. Lu, Z., et al., *Expression of GA733-Fc Fusion Protein as a Vaccine Candidate for Colorectal Cancer in Transgenic Plants*. Journal of Biomedicine and Biotechnology, 2012. **2012**: p. 364240.
  293. Nagels, B., et al., *Biologically active, magnICON®-expressed EPO-Fc from stably transformed Nicotiana benthamiana plants presenting tetra-antennary N-glycan structures*. Journal of Biotechnology, 2012. **160**(3): p. 242-250.
  294. Goetze, A.M., et al., *High-mannose glycans on the Fc region of therapeutic IgG antibodies increase serum clearance in humans*. Glycobiology, 2011. **21**(7): p. 949-959.
  295. Mackness, B.C., et al. *Antibody Fc engineering for enhanced neonatal Fc receptor binding and prolonged circulation half-life*. in *MAbs*. 2019. Taylor & Francis.
  296. Chirmule, N., V. Jawa, and B. Meibohm, *Immunogenicity to therapeutic proteins: impact on PK/PD and efficacy*. The AAPS journal, 2012. **14**(2): p. 296-302.
  297. Manzano-Szalai, K., et al., *Anaphylaxis Imaging: Non-Invasive Measurement of Surface Body Temperature and Physical Activity in Small Animals*. PloS one, 2016. **11**(3): p. e0150819-e0150819.
  298. Li, X.-m., et al., *A murine model of IgE-mediated cow's milk hypersensitivity*. Journal of Allergy and Clinical Immunology, 1999. **103**(2): p. 206-214.
  299. Binnewies, M., et al., *Understanding the tumor immune microenvironment (TIME) for effective therapy*. Nature medicine, 2018. **24**(5): p. 541-550.
  300. Ning, F., C.B. Cole, and C.M. Annunziata, *Driving immune responses in the ovarian tumor microenvironment*. Frontiers in Oncology, 2021. **10**: p. 3060.
  301. Hinshaw, D.C. and L.A. Shevde, *The Tumor Microenvironment Innately Modulates Cancer Progression*. Cancer Res, 2019. **79**(18): p. 4557-4566.
  302. Saleh, R. and E. Elkord. *Acquired resistance to cancer immunotherapy: Role of tumor-mediated immunosuppression*. in *Seminars in cancer biology*. 2020. Elsevier.
  303. Pitt, J.M., et al., *Targeting the tumor microenvironment: removing obstruction to anticancer immune responses and immunotherapy*. Ann Oncol, 2016. **27**(8): p. 1482-92.
  304. Abdou, Y., et al., *Mechanism-based treatment of cancer with immune checkpoint inhibitor therapies*. British journal of clinical pharmacology, 2020. **86**(9): p. 1690-1702.
  305. Vermaelen, K., *Vaccine Strategies to Improve Anti-cancer Cellular Immune Responses*. Front Immunol, 2019. **10**: p. 8.
  306. Murer, P. and D. Neri, *Antibody-cytokine fusion proteins: A novel class of biopharmaceuticals for the therapy of cancer and of chronic inflammation*. N Biotechnol, 2019. **52**: p. 42-53.
  307. Shukla, S., et al., *Antibody response against cowpea mosaic viral nanoparticles improves in situ vaccine efficacy in ovarian cancer*. ACS nano, 2020. **14**(3): p. 2994-3003.

308. Bharat, A., A.C. McQuattie-Pimentel, and G.R.S. Budinger, *Non-classical monocytes in tissue injury and cancer*. *Oncotarget*, 2017. **8**(63): p. 106171-106172.
309. Mukherjee, R., et al., *Non-Classical monocytes display inflammatory features: Validation in Sepsis and Systemic Lupus Erythematosus*. *Scientific Reports*, 2015. **5**(1): p. 13886.
310. Thomas, G.D., et al., *Deleting an Nr4a1 super-enhancer subdomain ablates Ly6Clow monocytes while preserving macrophage gene function*. *Immunity*, 2016. **45**(5): p. 975-987.
311. Hanna, R.N., et al., *Patrolling monocytes control tumor metastasis to the lung*. *Science*, 2015. **350**(6263): p. 985-990.
312. Kamen, L., et al., *A novel method for determining antibody-dependent cellular phagocytosis*. *Journal of Immunological Methods*, 2019. **468**: p. 55-60.
313. Lengyel, E., *Ovarian cancer development and metastasis*. *The American journal of pathology*, 2010. **177**(3): p. 1053-1064.
314. Surveillance Research Program National Cancer Institute. *SEER\*Explorer: An interactive website for SEER cancer statistics [Internet]*. [cited 2020 April 2]; Available from: <https://seer.cancer.gov/explorer/>.
315. Lheureux, S., et al., *Epithelial ovarian cancer*. *The Lancet*, 2019. **393**(10177): p. 1240-1253.
316. Moore, K., et al., *Maintenance olaparib in patients with newly diagnosed advanced ovarian cancer*. *New England Journal of Medicine*, 2018. **379**(26): p. 2495-2505.
317. Coleman, R.L., et al., *Bevacizumab and paclitaxel–carboplatin chemotherapy and secondary cytoreduction in recurrent, platinum-sensitive ovarian cancer (NRG Oncology/Gynecologic Oncology Group study GOG-0213): a multicentre, open-label, randomised, phase 3 trial*. *The Lancet Oncology*, 2017. **18**(6): p. 779-791.
318. Mirza, M.R., et al., *Niraparib maintenance therapy in platinum-sensitive, recurrent ovarian cancer*. *New England Journal of Medicine*, 2016. **375**(22): p. 2154-2164.
319. Aghajanian, C., et al., *OCEANS: a randomized, double-blind, placebo-controlled phase III trial of chemotherapy with or without bevacizumab in patients with platinum-sensitive recurrent epithelial ovarian, primary peritoneal, or fallopian tube cancer*. *Journal of clinical oncology*, 2012. **30**(17): p. 2039.
320. Coleman, R.L., et al., *Rucaparib maintenance treatment for recurrent ovarian carcinoma after response to platinum therapy (ARIEL3): a randomised, double-blind, placebo-controlled, phase 3 trial*. *The Lancet*, 2017. **390**(10106): p. 1949-1961.
321. Hamanishi, J., et al., *Safety and antitumor activity of anti–PD-1 antibody, nivolumab, in patients with platinum-resistant ovarian cancer*. *Journal of Clinical Oncology*, 2015. **33**(34): p. 4015-4022.
322. Colombo, I., et al., *Immunologic and genomic characterization of high grade serous ovarian cancer (HGSOC) in patients (pts) treated with pembrolizumab (Pembro) in the phase II INSPIRE trial*. 2017, American Society of Clinical Oncology.

323. Pearce, O.M., *Cancer glycan epitopes: biosynthesis, structure and function*. Glycobiology, 2018. **28**(9): p. 670-696.
324. Oliveira-Ferrer, L., K. Legler, and K. Milde-Langosch. *Role of protein glycosylation in cancer metastasis*. in *Seminars in cancer biology*. 2017. Elsevier.
325. Zhang, X., et al., *Discovery of specific metastasis-related N-glycan alterations in epithelial ovarian cancer based on quantitative glycomics*. PLoS One, 2014. **9**(2): p. e87978.
326. Anugraham, M., et al., *Specific glycosylation of membrane proteins in epithelial ovarian cancer cell lines: glycan structures reflect gene expression and DNA methylation status*. Molecular & Cellular Proteomics, 2014. **13**(9): p. 2213-2232.
327. Wei, H., et al., *Combinatorial PD-1 blockade and CD137 activation has therapeutic efficacy in murine cancer models and synergizes with cisplatin*. PloS one, 2013. **8**(12): p. e84927-e84927.
328. Guo, Z., et al., *PD-1 blockade and OX40 triggering synergistically protects against tumor growth in a murine model of ovarian cancer*. PloS one, 2014. **9**(2).
329. Baert, T., et al., *The dark side of ID8-Luc2: pitfalls for luciferase tagged murine models for ovarian cancer*. Journal for immunotherapy of cancer, 2015. **3**(1): p. 1-5.
330. Uhrberg, M., *The CD107 mobilization assay: viable isolation and immunotherapeutic potential of tumor-cytolytic NK cells*. Leukemia, 2005. **19**(5): p. 707-709.
331. Fouad, Y.A. and C. Aanei, *Revisiting the hallmarks of cancer*. American journal of cancer research, 2017. **7**(5): p. 1016-1036.
332. Hargadon, K.M., C.E. Johnson, and C.J. Williams, *Immune checkpoint blockade therapy for cancer: an overview of FDA-approved immune checkpoint inhibitors*. International immunopharmacology, 2018. **62**: p. 29-39.
333. Rosenberg, S.A., *IL-2: the first effective immunotherapy for human cancer*. The Journal of Immunology, 2014. **192**(12): p. 5451-5458.
334. Jiang, T., C. Zhou, and S. Ren, *Role of IL-2 in cancer immunotherapy*. Oncoimmunology, 2016. **5**(6): p. e1163462.
335. Amaria, R.N., et al., *Update on use of aldesleukin for treatment of high-risk metastatic melanoma*. ImmunoTargets and therapy, 2015. **4**: p. 79.
336. McDermott, D., et al., *The high-dose aldesleukin (HD IL-2) "SELECT" trial in patients with metastatic renal cell carcinoma (mRCC)*. Journal of Clinical Oncology, 2010. **28**(15\_suppl): p. 4514-4514.
337. Taguchi, T., *Clinical studies of recombinant interferon alfa-2a (Roferon®-A) in cancer patients*. Cancer, 1986. **57**(S8): p. 1705-1708.
338. Baldo, B.A., *Side effects of cytokines approved for therapy*. Drug safety, 2014. **37**(11): p. 921-943.
339. Barron, L., et al., *Cutting edge: Mechanisms of IL-2-dependent maintenance of functional regulatory T cells*. The Journal of Immunology, 2010. **185**(11): p. 6426-6430.
340. Neri, D. and P.M. Sondel, *Immunocytokines for cancer treatment: past, present and future*. Current Opinion in Immunology, 2016. **40**: p. 96-102.
341. Weiss, T., et al., *Immunocytokines are a promising immunotherapeutic approach against glioblastoma*. Science Translational Medicine, 2020. **12**(564).

342. Catania, C., et al., *The tumor-targeting immunocytokine F16-IL2 in combination with doxorubicin: dose escalation in patients with advanced solid tumors and expansion into patients with metastatic breast cancer*. *Cell adhesion & migration*, 2015. **9**(1-2): p. 14-21.
343. Lansigan, F., et al., *Di-Leu16-IL2, an anti-CD20-interleukin-2 immunocytokine, is safe and active in patients with relapsed and refractory B-cell lymphoma: a report of maximum tolerated dose, optimal biologic dose, and recommended phase 2 dose*. *Blood*, 2016. **128**(22): p. 620.
344. Connor, J.P., et al., *A phase 1b study of humanized KS-interleukin-2 (huKS-IL2) immunocytokine with cyclophosphamide in patients with EpCAM-positive advanced solid tumors*. *BMC cancer*, 2013. **13**(1): p. 1-12.
345. Weide, B., et al., *A phase II study of the L19IL2 immunocytokine in combination with dacarbazine in advanced metastatic melanoma patients*. *Cancer Immunology, Immunotherapy*, 2019. **68**(9): p. 1547-1559.
346. Soerensen, M.M., et al., *Safety, PK/PD, and anti-tumor activity of RO6874281, an engineered variant of interleukin-2 (IL-2v) targeted to tumor-associated fibroblasts via binding to fibroblast activation protein (FAP)*. 2018, American Society of Clinical Oncology.
347. Strauss, J., et al., *First-in-human phase I trial of a tumor-targeted cytokine (NHS-IL12) in subjects with metastatic solid tumors*. *Clinical Cancer Research*, 2019. **25**(1): p. 99-109.
348. Hemmerle, T. and D. Neri, *The antibody-based targeted delivery of interleukin-4 and 12 to the tumor neovasculature eradicates tumors in three mouse models of cancer*. *International journal of cancer*, 2014. **134**(2): p. 467-477.
349. Vincent, M., et al. *Highly potent anti-CD20-RLI immunocytokine targeting established human B lymphoma in SCID mouse*. in *MAbs*. 2014. Taylor & Francis.
350. Ziffels, B., et al., *Antibody-based delivery of cytokine payloads to carbonic anhydrase IX leads to cancer cures in immunocompetent tumor-bearing mice*. *Molecular cancer therapeutics*, 2019. **18**(9): p. 1544-1554.
351. Xuan, C., et al., *Targeted delivery of interferon-alpha via fusion to anti-CD20 results in potent antitumor activity against B-cell lymphoma*. *Blood, The Journal of the American Society of Hematology*, 2010. **115**(14): p. 2864-2871.
352. Kaspar, M., E. Trachsel, and D. Neri, *The antibody-mediated targeted delivery of interleukin-15 and GM-CSF to the tumor neovasculature inhibits tumor growth and metastasis*. *Cancer research*, 2007. **67**(10): p. 4940-4948.
353. Desgrosellier, J.S. and D.A. Cheresh, *Integrins in cancer: biological implications and therapeutic opportunities*. *Nature Reviews Cancer*, 2010. **10**(1): p. 9-22.
354. Zheng, W., C. Jiang, and R. Li, *Integrin and gene network analysis reveals that ITGA5 and ITGB1 are prognostic in non-small-cell lung cancer*. *OncoTargets and therapy*, 2016. **9**: p. 2317.
355. Pantano, F., et al., *Integrin alpha5 in human breast cancer is a mediator of bone metastasis and a therapeutic target for the treatment of osteolytic lesions*. *Oncogene*, 2021. **40**(7): p. 1284-1299.

356. Pelillo, C., et al., *Colorectal cancer metastases settle in the hepatic microenvironment through  $\alpha 5\beta 1$  integrin*. Journal of cellular biochemistry, 2015. **116**(10): p. 2385-2396.
357. Murillo, C.A., P.G. Rychahou, and B.M. Evers, *Inhibition of  $\alpha 5$  integrin decreases PI3K activation and cell adhesion of human colon cancers*. Surgery, 2004. **136**(2): p. 143-149.
358. Schaffner, F., A.M. Ray, and M. Dontenwill, *Integrin  $\alpha 5\beta 1$ , the Fibronectin Receptor, as a Pertinent Therapeutic Target in Solid Tumors*. Cancers, 2013. **5**(1): p. 27-47.
359. Mateo, J., et al., *A first-in-human study of the anti- $\alpha 5\beta 1$  integrin monoclonal antibody PF-04605412 administered intravenously to patients with advanced solid tumors*. Cancer chemotherapy and pharmacology, 2014. **74**(5): p. 1039-1046.
360. Besse, B., et al., *Phase Ib safety and pharmacokinetic study of volociximab, an anti- $\alpha 5\beta 1$  integrin antibody, in combination with carboplatin and paclitaxel in advanced non-small-cell lung cancer*. Annals of oncology, 2013. **24**(1): p. 90-96.
361. Fujisawa, H., *Discovery of semaphorin receptors, neuropilin and plexin, and their functions in neural development*. Journal of neurobiology, 2004. **59**(1): p. 24-33.
362. Basile, J.R., et al., *Class IV semaphorins promote angiogenesis by stimulating Rho-initiated pathways through plexin-B*. Cancer research, 2004. **64**(15): p. 5212-5224.
363. Casazza, A., et al., *Sema3E–Plexin D1 signaling drives human cancer cell invasiveness and metastatic spreading in mice*. The Journal of clinical investigation, 2010. **120**(8): p. 2684-2698.
364. Capparuccia, L. and L. Tamagnone, *Semaphorin signaling in cancer cells and in cells of the tumor microenvironment—two sides of a coin*. Journal of cell science, 2009. **122**(11): p. 1723-1736.
365. Casazza, A., P. Fazzari, and L. Tamagnone, *Semaphorin signals in cell adhesion and cell migration: functional role and molecular mechanisms*. Semaphorins: Receptor and Intracellular Signaling Mechanisms, 2007: p. 90-108.
366. Xiang, G. and Y. Cheng, *MiR-126-3p inhibits ovarian cancer proliferation and invasion via targeting PLXNB2*. Reproductive biology, 2018. **18**(3): p. 218-224.
367. Li, S., et al., *Chemosensitization of prostate cancer stem cells in mice by angiogenin and plexin-B2 inhibitors*. Communications biology, 2020. **3**(1): p. 1-18.
368. Le, A.P., et al., *Plexin-B2 promotes invasive growth of malignant glioma*. Oncotarget, 2015. **6**(9): p. 7293.
369. Takamatsu, H. and A. Kumanogoh, *Diverse roles for semaphorin–plexin signaling in the immune system*. Trends in Immunology, 2012. **33**(3): p. 127-135.
370. Shen, Y., et al., *Transferrin receptor 1 in cancer: a new sight for cancer therapy*. Am J Cancer Res, 2018. **8**(6): p. 916-931.
371. Tortorella, S. and T.C. Karagiannis, *Transferrin Receptor-Mediated Endocytosis: A Useful Target for Cancer Therapy*. The Journal of Membrane Biology, 2014. **247**(4): p. 291-307.
372. Cheng, Y., et al., *Structure of the human transferrin receptor-transferrin complex*. Cell, 2004. **116**(4): p. 565-576.

373. Horniblow, R.D., et al., *BRAF mutations are associated with increased iron regulatory protein-2 expression in colorectal tumorigenesis*. *Cancer Sci*, 2017. **108**(6): p. 1135-1143.
374. Wang, B., et al., *EGFR regulates iron homeostasis to promote cancer growth through redistribution of transferrin receptor 1*. *Cancer Lett*, 2016. **381**(2): p. 331-40.
375. Kindrat, I., et al., *MicroRNA-152-mediated dysregulation of hepatic transferrin receptor 1 in liver carcinogenesis*. *Oncotarget*, 2016. **7**(2): p. 1276-87.
376. Rychtarcikova, Z., et al., *Tumor-initiating cells of breast and prostate origin show alterations in the expression of genes related to iron metabolism*. *Oncotarget*, 2017. **8**(4): p. 6376-6398.
377. Pichler, W.J. and P. Campi, *Adverse side effects to biological agents*. *Drug hypersensitivity*, 2007: p. 151-165.
378. Shimabukuro-Vornhagen, A., et al., *Cytokine release syndrome*. *Journal for immunotherapy of cancer*, 2018. **6**(1): p. 1-14.
379. Gülsen, A., B. Wedi, and U. Jappe, *Hypersensitivity reactions to biologics (part II): classifications and current diagnostic and treatment approaches*. *Allergo Journal International*, 2020. **29**(5): p. 139-154.
380. Pichler, W.J., D.J. Naisbitt, and B.K. Park, *Immune pathomechanism of drug hypersensitivity reactions*. *Journal of Allergy and Clinical Immunology*, 2011. **127**(3, Supplement): p. S74-S81.
381. Pérez-Soler, R. and L. Saltz, *Cutaneous adverse effects with HER1/EGFR-targeted agents: is there a silver lining?* *Journal of Clinical Oncology*, 2005. **23**(22): p. 5235-5246.
382. Leach, M.W., et al., *Use of Tissue Cross-reactivity Studies in the Development of Antibody-based Biopharmaceuticals: History, Experience, Methodology, and Future Directions*. *Toxicologic Pathology*, 2010. **38**(7): p. 1138-1166.
383. Sinagra, E., et al., *Heart failure and anti tumor necrosis factor-alpha in systemic chronic inflammatory diseases*. *European journal of internal medicine*, 2013. **24**(5): p. 385-392.
384. Al-Huthail, Y.R., *Neuropsychiatric side-effects of interferon alfa therapy for hepatitis C and their management: a review*. *Saudi Journal of Gastroenterology*, 2006. **12**(2): p. 59.
385. Mathur, G., D.V. Singh, and A. Singal, *Unusual course of interferon-related retinopathy in chronic hepatitis C*. *Oman journal of ophthalmology*, 2016. **9**(3): p. 189.
386. Chen, C.-B., et al., *An Updated Review of the Molecular Mechanisms in Drug Hypersensitivity*. *Journal of Immunology Research*, 2018. **2018**: p. 6431694.
387. Isabwe, G.A.C., et al., *Hypersensitivity reactions to therapeutic monoclonal antibodies: Phenotypes and endotypes*. *Journal of Allergy and Clinical Immunology*, 2018. **142**(1): p. 159-170.e2.
388. Leach, M.W., et al., *Immunogenicity/Hypersensitivity of Biologics*. *Toxicologic Pathology*, 2013. **42**(1): p. 293-300.
389. Looney, T.J., et al., *Human B-cell isotype switching origins of IgE*. *Journal of Allergy and Clinical Immunology*, 2016. **137**(2): p. 579-586.e7.

390. Uzzaman, A. and S.H. Cho. *Classification of hypersensitivity reactions*. in *Allergy Asthma Proc*. 2012.
391. Finkelman, F.D., *Anaphylaxis: Lessons from mouse models*. *Journal of Allergy and Clinical Immunology*, 2007. **120**(3): p. 506-515.
392. Levin, A.S., et al., *Reactions to rituximab in an outpatient infusion center: a 5-year review*. *The Journal of Allergy and Clinical Immunology: In Practice*, 2017. **5**(1): p. 107-113. e1.
393. Arnold, D.F. and S.A. Misbah, *Cetuximab-induced anaphylaxis and IgE specific for galactose-alpha-1, 3-galactose*. *The New England journal of medicine*, 2008. **358**(25): p. 2735; author reply 2735-6.
394. Maker, J.H., et al., *Antibiotic hypersensitivity mechanisms*. *Pharmacy*, 2019. **7**(3): p. 122.
395. Demoly, P., et al., *International Consensus on drug allergy*. *Allergy*, 2014. **69**(4): p. 420-437.
396. Dispenza, M.C., *Classification of hypersensitivity reactions*. *Allergy Asthma Proc*, 2019. **40**(6): p. 470-473.
397. O'Meara, S., K.S. Nanda, and A.C. Moss, *Antibodies to infliximab and risk of infusion reactions in patients with inflammatory bowel disease: a systematic review and meta-analysis*. *Inflammatory bowel diseases*, 2014. **20**(1): p. 1-6.
398. Bavbek, S., et al., *Rapid subcutaneous desensitization for the management of local and systemic hypersensitivity reactions to etanercept and adalimumab in 12 patients*. *The Journal of Allergy and Clinical Immunology: In Practice*, 2015. **3**(4): p. 629-632.
399. Bahri, R., et al., *Mast cell activation test in the diagnosis of allergic disease and anaphylaxis*. *The Journal of allergy and clinical immunology*, 2018. **142**(2): p. 485-496.e16.
400. Bryce, P.J., et al., *Humanized mouse model of mast cell-mediated passive cutaneous anaphylaxis and passive systemic anaphylaxis*. *Journal of Allergy and Clinical Immunology*, 2016. **138**(3): p. 769-779.
401. Inagaki, N., et al., *Active cutaneous anaphylaxis (ACA) in the mouse ear*. *Jpn J Pharmacol*, 1992. **59**(2): p. 201-8.
402. Doyle, E., J. Trosien, and M. Metz, *Protocols for the induction and evaluation of systemic anaphylaxis in mice*, in *Mouse Models of Allergic Disease*. 2013, Springer. p. 133-138.
403. Park, B.K., *Role of drug disposition in drug hypersensitivity: a chemical molecular, and clinical perspective*. *Chem Res Toxicol*, 1998. **11**: p. 969-988.
404. Verdier, F., C. Patriarca, and J. Descotes, *Autoantibodies in conventional toxicity testing*. *Toxicology*, 1997. **119**(1): p. 51-58.
405. Andrews, A., et al., *Immune complex vasculitis with secondary ulcerative dermatitis in aged C57BL/6NNia mice*. *Veterinary pathology*, 1994. **31**(3): p. 293-300.
406. Botham, P., et al., *Skin sensitization—a critical review of predictive test methods in animals and man*. *Food and Chemical Toxicology*, 1991. **29**(4): p. 275-286.
407. de Silva, O., et al., *Local lymph node assay: study of the in vitro proliferation and control of the specificity of the response by FACScan analysis*. *Toxicol In Vitro*, 1993. **7**(4): p. 299-303.

## CURRICULUM VITAE

NAME: Matthew William Dent

ADDRESS: Clinical and Translational Research Building  
505 South Hancock Street Lab 442  
Louisville, Kentucky 40202

DOB: September 6, 1991

EDUCATION AND TRAINING: B.S. Molecular Biosciences and Biotechnology  
Arizona State University  
2010-2014

M.Sc. Plant Genetics and Crop Improvement  
University of East Anglia  
2014-2015

M.S. Pharmacology and Toxicology  
University of Louisville  
2016-2019

AWARDS: Provost's Scholarship Award, 2010-2014

B.S. awarded Magna Cum Laude, 2014

ASU Sun Award, 2014

1st place at Research!Louisville, Poster Competition,  
Category: Master's Basic Science Graduate Student

OVSOT Summer Conference 2019: Best oral presentation

PUBLICATIONS: Leuzinger, K., **Dent, M.\***, et al., Efficient agroinfiltration of  
plants for high-level transient expression of recombinant  
proteins. Journal of Visualized Experiments, 2013(77).  
\* Co-first author

Chen, Q., et al., Agroinfiltration as an effective and scalable  
strategy of gene delivery for production of pharmaceutical  
proteins. Adv Tech Biol Med, 2013. 1(1).

Chen, Q., et al. (2016). Transient protein expression by agroinfiltration in lettuce. *Recombinant proteins from plants*, Humana Press, New York, NY: 55-67.

**Dent, M.**, et al., Plant-produced anti-dengue virus monoclonal antibodies exhibit reduced antibody-dependent enhancement of infection activity. *Journal of General Virology*, 2016. 97(12): p. 3280-3290.

Yang, M., **Dent, M.\***, et al., Immunization of Zika virus envelope protein domain III induces specific and neutralizing immune responses against Zika virus. *Vaccine*, 2017. 35(33): p. 4287-4294.

\* Co-first author

Chen, Q., et al., *Molecular Pharming: Plant-Made Vaccines*. *Molecular Pharming*, 2018: p. 231-273.

Kasinger, L., **Dent, M.\***, et al. (2019). A Novel Anti-HIV-1 Bispecific bNAb-Lectin Fusion Protein Engineered in a Plant-based Transient Expression System. *Plant Biotech Journal*.

\* Co-first author

Hamorsky, K.T., Kouokam, J.C., **Dent, M.\***, et al. (2019). Engineering of a Lectibody Targeting High-Mannose-Type Glycans of the HIV Envelope. *Molecular Therapy*.

\* Co-first author

**Dent, M.**, & Matoba, N. (2020). Cancer biologics made in plants. *Current opinion in biotechnology*, 61, 82-88.

**Dent, M.**, Hamorsky, K., Vausselin, T., Dubuisson, J., Miyata, Y., Morikawa, Y., & Matoba, N. (2021). Safety and Efficacy of Avaron-Fc Lectibody Targeting HCV High-Mannose Glycans in a Human Liver Chimeric Mouse Model. *Cellular and molecular gastroenterology and hepatology*, 11(1), 185-198.

Oh, Y. J., **Dent, M.**, Freels, A. R., Zhou, Q., Lebrilla, C. B., Merchant, M. L., & Matoba, N. (2021). Antitumor activity of a lectibody targeting cancer-associated high-mannose glycans. *bioRxiv*.

**Dent, M.,** Mayer, K., Guo, H., Steinkellner, H., Kajiura, H., Kazuhito, F., Matoba, N. (2021). Impact of glycoengineering and immunogenicity on the anti-cancer activity of a novel lectin-Fc fusion protein. Article in preparation.

NATIONAL/  
INTERNATIONAL  
PRESENTATIONS:

“Enhancing the tobacco chassis: applications of Cas9-based genome editing technologies to heterologous protein production in plants” – Poster given at Plant Based Vaccines, Antibodies, and Biologics in Lausanne, Switzerland (June 2015)

“Pharmacology and Toxicology of a Novel Oligomannose-binding Lectin-Fc Fusion Protein” – Presentation at Ohio Valley Society of Toxicology meeting at Purdue University, Lafayette, IN (June 2019). **First prize for best oral presentation.**

“Toxicity of a novel lectin-Fc fusion protein in a human liver chimeric mouse model of hepatitis C infection”- Oral presentation at Ohio Valley Society of Toxicology meeting at Purdue University, Lafayette, IN (November 2020)

“Development of a novel lectin-Fc fusion targeting cancer-associated oligomannose glycans” – Poster presentation at PepTalk conference (January 2021).

“Impact of glycoengineering and immunogenicity on the anti-cancer activity of a novel lectin-Fc fusion protein” – Oral presentation at PMP Asia conference (November 2021).

MENTORING

Have mentored 4 rotation students, 2 R25 students, and multiple undergraduates and high school students in my time at U of L. I was also responsible for teaching younger undergraduates at ASU.